ELUCIDATING THE ROLE OF SINE NON-CODING RNAS IN AMYLOID BETA PATHOLOGY

YUBO CHENG
Master of Science, **University at Buffalo SUNY, 2017**

A thesis submitted
in partial fulfilment of the requirements for the degree of

DOCTOR OF PHILOSOPHY

in

BIOMOLECULAR SCIENCE

Department of Chemistry and Biochemistry
University of Lethbridge
LETHBRIDGE, ALBERTA, CANADA

ELUCIDATING THE ROLE OF SINE NON-CODING RNAS IN AMYLOID BETA PATHOLOGY

YUBO CHENG

Date of Defence: May 26, 2021

Dr. A. Zovoilis Dr. T. Patel Thesis Co-Supervisors	Associate Professor Assistant Professor	Ph.D. Ph.D.
Dr. S. Wetmore Thesis Examination Committee Member	Professor	Ph.D.
Dr. M. Mohajerani Thesis Examination Committee Member	Associate Professor	Ph.D.
Dr. S. Wiseman Internal External Examiner Department of Biological Sciences Faculty of Arts & Science	Associate Professor	Ph.D.
Dr. P. Bose External Examiner University of Calgary Calgary, Alberta	Assistant Professor	Ph.D.
Dr. M. Gerken Chair, Thesis Examination Committee	Professor	Ph.D.

DEDICATION

I would like to dedicate this thesis to my family.

ABSTRACT

Despite recent advances in our understanding of gene expression networks in Alzheimer's disease (AD), the molecular mechanisms of its pathogenesis still remain unclear. Previous studies have shown that mechanisms involving non protein-coding RNAs transcribed by Short Interspersed Nuclear Element (SINE) are key in maintaining transcriptional homeostasis in cells. RNAs from SINE B2 repeats in mouse and SINE Alu repeats in human, control gene expressions through binding and inhibition of RNA Polymerase II. Here, an integrative RNA genomics and bioinformatics approach is applied to investigate the connection between SINE RNAs, amyloid beta neuro-toxicity and dementia both in mouse models of AD and brains of AD patients. Our data shows that processing of SINE RNAs is abnormally increased in response to amyloid beta toxicity, and is connected with deregulation of gene expression during amyloid beta pathology and AD.

PREFACE

Chapter 2 and 3 have been published in peer-reviewed journals.

Chapter 2 was published in eLife journal: Cheng, Y., Saville, L., Gollen, B., Isaac, C., Belay, A., Mehla, J., Patel, K., Thakor, N., Mohajerani, M., Zovoilis, A. (2020). Increased processing of SINE B2 ncRNAs unveils a novel type of transcriptome deregulation in amyloid beta neuropathology. elife, 9. doi:10.7554/eLife.61265.

Chapter 3 was published in Embo Reports. Cheng, Y., Saville, L., Gollen, B., Veronesi, A. A., Mohajerani, M., Joseph, J. T., & Zovoilis, A. (2021). Increased Alu RNA processing in Alzheimer brains is linked to gene expression changes. Embo Reports, e52255. doi:10.15252/embr.202052255.

For these two chapters, I accomplished data curation, establishment and testing of the analysis pipelines, validation, investigation, formal bioinformatics analysis, statistical analysis, data visualization and writing of the manuscript; Dr. Athan Zovoilis contributed to conception and design, establishment and testing of data generation and analysis pipelines, data interpretation, data visualization, writing of the manuscript, and overall supervision; Luke Saville contributed to testing of the next-generation-sequencing and in vitro assay pipelines, library construction, RT-qPCRs, in vitro assays, data visualization; Babita Gollen and Chris Isaac contributed to establishment and testing of the next-generation-sequencing pipelines, library construction.

ACKNOWLEDGMENT

I would like to thank my supervisor Dr. Athan Zovoilis for all the help and guidance, Luke Saville, Babita Gollen and Chris Isaac for wet lab experiments, and other Zovoilis members for their support, as well as my committee members: Dr. Trushar Patel, Dr. Stacey Wetmore, and Dr. Majid Mohajerani for their advices and comments. I also would like to thank all collaborators: Mohajerani lab, Calgary Brain Bank, and ROSMAP study from AMP-AD Knowledge Portal. Finally, I would like to thank the support from Alberta Innovates – Technology Futures (AITF) Doctoral Graduate Student Scholarship.

TABLE OF CONTENTS

LIST OF TABLES

LIST OF FIGURES

LIST OF ABBREVIATIONS

AD	Alzheimer's Disease
APOE	Apolipoprotein E
APP	Amyloid Precursor Protein
CBB	Calgary Brain Bank
FPKM	Fragments Per Kilobase of transcript per Million
HSF1	Heat Shock Factor 1
HT22	Mouse Hippocampal Neuron Cell Line
LINE	Long Interspersed Nuclear Element
ncRNA	non-coding RNA
SINE	Small Interspersed Nuclear Element
SRG	Stress Response Gene
TPM	Transcripts Per Million
TSS	Transcriptional Start Site
WT	Wild Type

Chapter 1: Introduction

As the human life span increases, the number of people suffering from aging associated diseases, such as cancer and Alzheimer's diseases (AD) are expected to rise. This will generate a wave of new cases in the upcoming years throughout the world (Cornutiu, 2015). However, the molecular mechanisms underlying the pathogenesis of these diseases remain elusive. Here the association between Alzheimer's diseases and non-coding RNAs is investigated within both mouse model and human brains.

Alzheimer's disease

Alzheimer's disease (AD) is the main cause of dementia, and it is a neurodegenerative disease that is characterized by slowly progressing loss of memory and other cognitive functions (Scheltens et al., 2016). AD is identified by the aggregation and deposition of misfolded proteins, in particular aggregated amyloid beta peptide in the form of extracellular neuritic plaques, and hyperphosphorlylated tau protein in the form of intracellular neurofibrillary tangles (NFTs) (Bertram, Lill, & Tanzi, 2010). Common clinical signs and symptoms of AD patients include memory impairment and executive dysfunction which interfere with daily life activities (Scheltens et al., 2016).

AD is probably caused by interactions among multiple genetic, epigenetic, and environmental factors and pathways. Many risk factors might play a role in developing AD, including diabetes, obesity, physical and mental inactivity, depression, smoking, low educational attainment, and diet (Huang & Mucke, 2012; Scheltens et al., 2016).

Genetically, AD is usually divided into two forms: familial cases with Mendelian inheritance of predominantly early-onset (< 60 years, early-onset familial AD), and sporadic

cases with less apparent or no familial aggregation and usually of later onset age (≥ 60 years, late-onset AD) (Bertram et al., 2010). Early-onset familial AD (autosomal dominant hereditary) is mainly caused by mutations in three genes: amyloid precursor protein (APP), presenilin 1 (PSEN1) and presenilin 2 (PSEN2) (Bertram et al., 2010; Huang & Mucke, 2012). Late-onset (> 60 years) familial and sporadic AD account for most AD cases, and Apolipoprotein E4 (APOE4) is the most important genetic risk factor for late-onset AD (Genin et al., 2011).

Epigenetic mechanisms may also associate with AD pathogenesis, including epigenetic dysregulation, abnormal DNA methylation, histone modification, etc. (reviewed in (Huang & Mucke, 2012)). Beside genetic and epigenetic factors, aging is the most important known nongenetic risk factor for late-onset AD, also environmental risk factors may involve into AD pathogenesis, such as head injury, low educational levels, hyperlipidemia, hypertension, diabetes, obesity, hearing loss, physical and mental inactivity, depression, smoking (reviewed in (Huang & Mucke, 2012; Scheltens et al., 2016)).

Many potential mechanisms can be linked to AD pathogenesis: amyloid beta production, amyloid beta aggregation, amyloid beta clearance, tau phosphorylation, synaptic transmission, inflammation, cerebrovascular events, and so on. Studies showed that aberrant neural network activity, dysfunction and loss of synapses, and degeneration of specific neuronal populations are the main substrates of cognitive decline in AD (reviewed in (Huang & Mucke, 2012)). APP is the precursor of the amyloid beta peptides and APP mutations affect amyloid beta cleavage and aggregation. The peptides are derived from APP, which is cleaved by beta secretase and gamma secretase to yield amyloid beta. Amyloid beta is thought to be the main cause of AD (reviewed in (Huang & Mucke, 2012; Scheltens et al., 2016)). AD is associated not only with the abnormal accumulation of amyloid plaques, but also with that of NFTs. NFTs form intracellularly and are

made up primarily of aggregated tau bearing abnormal posttranslational modifications, including increased phosphorylation and acetylation (Huang & Mucke, 2012; Scheltens et al., 2016).

SINE RNAs

Until recently, research of aging associated diseases has mainly focused on the less than 3% of the human genome that encodes for proteins. With the advances in next generation sequencing technology, the massive sequencing of RNAs from the brain and other tissues revealed that the vast majority of the non-coding genome is transcribed into non-coding RNAs (ncRNAs), RNAs produced by the non-protein coding part of the genome. Among them are small non-coding RNAs such as microRNAs (miRNAs) and promoter associated RNAs (PARs) that have been shown to be connected with dementia and other diseases (Zovoilis et al., 2011; Zovoilis et al., 2014). The rest of the non-coding genome consists largely of repetitive DNA elements (~50% of noncoding sequences) with Short Interspersed Nuclear Elements (SINEs), a class of non-autonomous retrotransposons, being among the most frequent repeat elements. For the past few decades, these elements have been considered "junk DNA" or transcriptional noise without any functional importance.

Retrotransposons are the dominant repetitive transposable elements in the mammalian genome (Natt & Thorsell, 2016). SINE RNAs are non-coding RNAs generated by SINEs, which consist of 100 to 500 base pairs, and contribute more than 50% of the genomes (de Koning, Gu, Castoe, Batzer, & Pollock, 2011; Tatosyan & Kramerov, 2016). Most likely, SINEs originated from one of the three types of cellular RNAs synthesized by RNA Polymerase III: tRNA, 7SL RNA, or 5S rRNA, through the intermediate stage of RNA retropseudogenes. SINEs are

abundant both in intergenic regions and within genes, and particularly ample in introns (Kramerov & Vassetzky, 2011).

SINE B2 repetitive elements, one of the most frequent in mouse (Kramerov & Vassetzky, 2011), are retrotransposons present in hundreds of thousands of copies. The most successful SINE retroelement in the human genome, SINE Alu, accounts for more than 10% of the human genome, and has an amplification rate of one new insertion per 20 human births leading to the current one million transcripts in the genome (Deininger, 2011; Walters, Kugel, & Goodrich, 2009). While most of retrotransposons are inactive through epigenetic regulatory mechanisms, Alu, together with some other retroelements such as L1 (a LINE element) can be active (Mu, Ahmad, & Hur, 2016; Platt, Vandewege, & Ray, 2018). For a long time, most SINEs have been regarded as genomic parasites, a part of the non-coding genome with no apparent function (Karijolich, Zhao, Alla, & Glaunsinger, 2017). More recently, it was shown that SINE genomic elements contribute to genomic diversity through their integration into multiple genomic sites, by providing novel splicing sites, promoter elements, enhancers and transcription factor binding sites or disrupting existing ones (Kaaij, Mohn, van der Weide, de Wit, & Buhler, 2019; Zhang, Gingeras, & Weng, 2019).

Not much is known about the role of the non-coding RNAs transcribed by SINE genomic elements themselves. Two of the most frequent subclasses of SINEs, the B2 and Alu retrotransposons, are present in millions of copies in mouse and human, respectively, and are either transcribed by RNA Polymerase III independently or by RNA Polymerase II as parts of naïve transcripts in which they are embedded (Yakovchuk, Goodrich, & Kugel, 2009).

SINE RNAs and cellular stress

RNAs from these SINE elements have been known for years to be up-regulated during response to various types of cellular stress. In particular, levels of RNAs transcribed from SINEs such as B1 and B2 (mouse), Alu (human), PRE-1 (swine), Bm 1 (silkworm) and C (rabbit) have been reported to increase during heat shock (Funkhouser et al., 2017; Tatosyan & Kramerov, 2016). Studies have also shown that during response to cellular stress, SINE B2 RNAs suppress the transcription of a number of housekeeping genes through binding of RNA Polymerase II (RNA Pol II), potentially facilitating the redirection of cell resources to pro-survival pathways (Yakovchuk et al., 2009).

In a recent study, a heat-shock model was used to study the stress response and it showed a central regulatory role for EZH2 and B2 transcript. For heat shock up-regulated genes, in unstressed cells, B2 RNA binds target genes, serves as a Pol II speed bump, and reduces gene expression. Upon stress, EZH2 is recruited and triggers B2 degradation, thereby enabling more transcriptional elongation, and B2 cleavage induces high level Pol II activity. In contrast, heat shock down-regulated genes bind B2 after stress induction and are reduced in expression (Zovoilis, Cifuentes-Rojas, Chu, Hernandez, & Lee, 2016). B2 and Alu SINE retrotransposons have been shown to be self-cleaving ribozymes that function as ribo-switches which control gene expression during cellular stress, and their activities can be accelerated by an epigenetic factor (Hernandez et al., 2020).

Stress response genes in mouse hippocampus

Stress response genes (SRGs) are genes that are activated transiently upon cellular stress and rapidly in response to a wide variety of cellular stimuli. SRGs is involved a standing response mechanism that is activated at the transcription level in the first round of response to

stimuli, before any new proteins are synthesized. The expression of some of these genes was identified to be associated with learning and memory (Gallo, Katche, Morici, Medina, & Weisstaub, 2018).

Previous works have shown that learning impairment in dementia is connected with hippocampus–specific changes of gene expression including SRGs and microRNAs in mouse and human brain (Peleg et al., 2010; Zovoilis et al., 2011). Transcriptional activation of these genes serves as the response to a learning or stress stimulus but these genes are also known to protect cells from the flux of misfolded proteins when cells are exposed to cellular stress (Kikis, Gidalevitz, & Morimoto, 2010). SRGs activation is followed by activation of apoptotic genes such as p53, which in the case of a prolonged exposure to the environmental stimulus or irreparable cellular damage can lead to cell death (Ron & Walter, 2007; Westerheide & Morimoto, 2005). Thus, fine tuning of SRGs expression appears to be an additional layer of the regulation of gene expression that may play a role in neurodegeneration.

Rational and Aims

The findings about the role of B2 RNAs in the regulation of gene expression lead another possibility to investigate AD molecular pathogenesis. A list of protein coding genes to be associated with learning and memory in mouse hippocampus were identified in two previous papers (Peleg et al., 2010; Zovoilis et al., 2011). These studies also revealed a genome-wide deregulation of gene expression of these genes in the hippocampus during amyloid beta pathology; however, the underlying mechanisms remained elusive. The findings mentioned above about the role of SINE RNAs in regulation of gene expression provided new tools to understand these mechanisms and investigate AD molecular pathogenesis. In particular, the

number of the genes and gene pathways recognized to be de-regulated in mouse models of AD and cognitive impairment in previous studies (Peleg et al., 2010; Zovoilis et al., 2011) were also found to be direct targets of SINE B2 RNAs (Zovoilis et al., 2016), raising the possibility that AD may be connected with SINE RNA deregulation. The current thesis builds on this hypothesis and aims:

- Aim 1: To understand whether SINE RNAs may be one of the missing links in the pathways connecting amyloid beta toxicity with transcriptome changes in mouse hippocampus during amyloid pathology.
- Aim 2: To investigate whether there is a similar role for SINE RNAs in AD pathogenesis in the human brain.

  This thesis addresses aim 1 in chapter two and aim 2 in chapter three.

References

Bertram, L., Lill, C. M., & Tanzi, R. E. (2010). The genetics of Alzheimer disease: back to the future. *Neuron, 68*(2), 270-281. doi:10.1016/j.neuron.2010.10.013

Cornutiu, G. (2015). The Epidemiological Scale of Alzheimer's Disease. *J Clin Med Res, 7*(9), 657-666. doi:10.14740/jocmr2106w

de Koning, A. P. J., Gu, W. J., Castoe, T. A., Batzer, M. A., & Pollock, D. D. (2011). Repetitive Elements May Comprise Over Two-Thirds of the Human Genome. *Plos Genetics, 7*(12). doi:ARTN e100238410.1371/journal.pgen.1002384

Deininger, P. (2011). Alu elements: know the SINEs. *Genome Biology, 12*(12). doi:ARTN 23610.1186/gb-2011-12-12-236

Funkhouser, S. A., Steibel, J. P., Bates, R. O., Raney, N. E., Schenk, D., & Ernst, C. W. (2017). Evidence for transcriptome-wide RNA editing among Sus scrofa PRE-1 SINE elements. *Bmc Genomics, 18*(1), 360. doi:10.1186/s12864-017-3766-7

Gallo, F. T., Katche, C., Morici, J. F., Medina, J. H., & Weisstaub, N. V. (2018). Immediate Early Genes, Memory and Psychiatric Disorders: Focus on c-Fos, Egr1 and Arc. *Front Behav Neurosci, 12*, 79. doi:10.3389/fnbeh.2018.00079

Genin, E., Hannequin, D., Wallon, D., Sleegers, K., Hiltunen, M., Combarros, O., . . . Campion, D. (2011). APOE and Alzheimer disease: a major gene with semi-dominant inheritance. *Molecular Psychiatry, 16*(9), 903-907. doi:10.1038/mp.2011.52

Hernandez, A. J., Zovoilis, A., Cifuentes-Rojas, C., Han, L., Bujisic, B., & Lee, J. T. (2020). B2 and ALU retrotransposons are self-cleaving ribozymes whose activity is enhanced by EZH2. *Proceedings of the National Academy of Sciences of the United States of America, 117*(1), 415-425. doi:10.1073/pnas.1917190117

Huang, Y., & Mucke, L. (2012). Alzheimer mechanisms and therapeutic strategies. *Cell, 148*(6), 1204-1222. doi:10.1016/j.cell.2012.02.040

Kaaij, L. J. T., Mohn, F., van der Weide, R. H., de Wit, E., & Buhler, M. (2019). The ChAHP Complex Counteracts Chromatin Looping at CTCF Sites that Emerged from SINE Expansions in Mouse. *Cell, 178*(6), 1437-1451 e1414. doi:10.1016/j.cell.2019.08.007

Karijolich, J., Zhao, Y., Alla, R., & Glaunsinger, B. (2017). Genome-wide mapping of infection-induced SINE RNAs reveals a role in selective mRNA export. *Nucleic Acids Research, 45*(10), 6194-6208. doi:10.1093/nar/gkx180

Kikis, E. A., Gidalevitz, T., & Morimoto, R. I. (2010). Protein Homeostasis in Models of Aging and Age-Related Conformational Disease. *Protein Metabolism and Homeostasis in Aging, 694*, 138-159. doi:Book_Doi 10.1007/978-1-4419-7002-2

Kramerov, D. A., & Vassetzky, N. S. (2011). SINEs. *Wiley Interdisciplinary Reviews-Rna, 2*(6), 772-786. doi:10.1002/wrna.91

Mu, X., Ahmad, S., & Hur, S. (2016). Endogenous Retroelements and the Host Innate Immune Sensors. *Adv Immunol, 132*, 47-69. doi:10.1016/bs.ai.2016.07.001

Natt, D., & Thorsell, A. (2016). Stress-induced transposon reactivation: a mediator or an estimator of allostatic load? *Environ Epigenet, 2*(3), dvw015. doi:10.1093/eep/dvw015

Peleg, S., Sananbenesi, F., Zovoilis, A., Burkhardt, S., Bahari-Javan, S., Agis-Balboa, R. C., . . . Fischer, A. (2010). Altered Histone Acetylation Is Associated with Age-Dependent Memory Impairment in Mice. *Science, 328*(5979), 753-756. doi:10.1126/science.1186088

Platt, R. N., 2nd, Vandewege, M. W., & Ray, D. A. (2018). Mammalian transposable elements and their impacts on genome evolution. *Chromosome Research, 26*(1-2), 25-43. doi:10.1007/s10577-017-9570-z

Ron, D., & Walter, P. (2007). Signal integration in the endoplasmic reticulum unfolded protein response. *Nature Reviews Molecular Cell Biology, 8*(7), 519-529. doi:10.1038/nrm2199

Scheltens, P., Blennow, K., Breteler, M. M., de Strooper, B., Frisoni, G. B., Salloway, S., & Van der Flier, W. M. (2016). Alzheimer's disease. *Lancet, 388*(10043), 505-517. doi:10.1016/S0140-6736(15)01124-1

Tatosyan, K. A., & Kramerov, D. A. (2016). Heat shock increases lifetime of a small RNA and induces its accumulation in cells. *Gene, 587*(1), 33-41. doi:10.1016/j.gene.2016.04.025

Walters, R. D., Kugel, J. F., & Goodrich, J. A. (2009). InvAluable Junk: The Cellular Impact and Function of Alu and B2 RNAs. *Iubmb Life, 61*(8), 831-837. doi:10.1002/iub.227

Westerheide, S. D., & Morimoto, R. I. (2005). Heat shock response modulators as therapeutic tools for diseases of protein conformation. *Journal of Biological Chemistry, 280*(39), 33097-33100. doi:10.1074/jbc.R500010200

Yakovchuk, P., Goodrich, J. A., & Kugel, J. F. (2009). B2 RNA and Alu RNA repress transcription by disrupting contacts between RNA polymerase II and promoter DNA within assembled complexes. *Proceedings of the National Academy of Sciences of the United States of America, 106*(14), 5569-5574. doi:10.1073/pnas.0810738106

Zhang, X. O., Gingeras, T. R., & Weng, Z. (2019). Genome-wide analysis of polymerase III-transcribed Alu elements suggests cell-type-specific enhancer function. *Genome Research, 29*(9), 1402-1414. doi:10.1101/gr.249789.119

Zovoilis, A., Agbemenyah, H. Y., Agis-Balboa, R. C., Stilling, R. M., Edbauer, D., Rao, P., . . . Fischer, A. (2011). microRNA-34c is a novel target to treat dementias. *Embo Journal, 30*(20), 4299-4308. doi:10.1038/emboj.2011.327

Zovoilis, A., Cifuentes-Rojas, C., Chu, H. P., Hernandez, A. J., & Lee, J. T. (2016). Destabilization of B2 RNA by EZH2 Activates the Stress Response. *Cell, 167*(7), 1788-1802 e1713. doi:10.1016/j.cell.2016.11.041

Zovoilis, A., Mungall, A. J., Moore, R., Varhol, R., Chu, A., Wong, T. N., . . . Jones, S. J. M. (2014). The expression level of small non-coding RNAs derived from the first exon of protein-coding genes is predictive of cancer status. *Embo Reports, 15*(4), 402-410. doi:10.1002/embr.201337950

Chapter 2: Increased processing of SINE B2 ncRNAs unveils a novel type of transcriptome deregulation in amyloid beta neuropathology

Abstract

The functional importance of many non-coding RNAs (ncRNAs) generated by repetitive elements and their connection with pathologic processes remains elusive. B2 RNAs, a class of ncRNAs of the B2 family of SINE repeats, mediate through their processing the transcriptional activation of various genes in response to stress. Here we show that this response is dysfunctional during amyloid beta toxicity and pathology in the mouse hippocampus due to increased levels of B2 RNA processing, leading to constitutively elevated B2 RNA target gene expression and high Trp53 levels. Evidence indicates that Hsf1, a master regulator of stress response, mediates B2 RNA processing in hippocampal cells, and is activated during amyloid toxicity, accelerating the processing of SINE RNAs and gene hyper-activation. Our study reveals that in mouse, SINE RNAs constitute a novel pathway deregulated in amyloid beta pathology, with potential implications for similar cases in the human brain, such as Alzheimer's disease (AD).

Introduction

Amyloid pathology, and particularly, amyloid beta peptides and their aggregated forms have been connected with AD pathogenesis (Bloom, 2014) as well as with neurotoxicity in mouse models of amyloid pathology (Ittner et al., 2010). Nevertheless, the transcriptome changes involved in cell stress response to amyloid toxicity in brains with extensive amyloid beta pathology are still not entirely clear. The hippocampus is a primary target of amyloid pathology in humans. In healthy hippocampi, among the genes that have been implicated in transcriptome-

environment interactions are stress response genes (SRGs) (Gallo, Katche, Morici, Medina, & Weisstaub, 2018). These genes have been initially described in other biological contexts, such as thermal and oxidative stress, as pro-survival genes activated early after the application of a stress stimulus, such as heat shock, that help the cell overcome the stress condition (Mahat, Salamanca, Duarte, Danko, & Lis, 2016). However, in addition to the cellular response to stress, many SRGs were shown to have a central role in the function of the mouse hippocampus, by mediating cell signaling and genome-environment interactions. In particular, we and others have shown that in the healthy hippocampus during neural response to environmental stimuli, SRGs, such as those of the MAPK pathway, are transiently activated during various hippocampal processes including learning and response to cellular stress (Peleg et al., 2010; Sananbenesi, Fischer, Schrick, Spiess, & Radulovic, 2003; Yutsudo et al., 2013). Activation of SRGs is followed by a transient upregulation of the pro-apoptotic factor Trp53 and, subsequently, of a pro-apoptotic miRNA, Mir34c, which are transiently induced by and as a response to the activation of pro-survival SRGs (Yamakuchi & Lowenstein, 2009; Zovoilis et al., 2011). Trp53 activates the expression of genes engaged in promoting cell death in response to multiple forms of cellular stress including Mir34c (Yamakuchi & Lowenstein, 2009). This miRNA acts transiently as a guard and fine tuner of the expression of many SRGs by targeting them, thus, creating a negative feedback regulatory loop that keeps SRG expression in healthy cells under strict control. This facilitates the return to the pro-stimulation state in approximately 3 hours after the application of the stimulus (Zovoilis et al., 2011). In contrast, hippocampi of mouse models of amyloid pathology and post-mortem brains of human patients of AD are characterized by abnormally high Mir34c levels that subsequently can lead to prolonged high Trp53 levels and neural death (Yamakuchi & Lowenstein, 2009; Zovoilis et al., 2011). Given that many SRGs are upstream regulators of

Trp53-Mir34c activation (Gao et al., 2010), high Trp53 and Mir34c levels in amyloid pathology implied a possible transcriptome deregulation of the pathways that involve SRGs but whether such a deregulation exists, and which is the mechanism underlying this, it remained unknown. Interestingly, in a recent publication, we showed that expression of a number of SRGs were regulated by a class of non-protein coding (non-coding) RNAs called B2 SINE RNAs (Zovoilis, Cifuentes-Rojas, Chu, Hernandez, & Lee, 2016), raising the possibility that these non-coding RNAs may be a missing link in the pathways connecting amyloid beta toxicity with transcriptome changes in mouse hippocampus during amyloid pathology.

It was recently shown that SINE B2 RNAs mediate cellular response to stress through the regulation of pro-survival stress response genes by acting as transcriptional switches. In particular, in the pro-cellular stress state SINE B2 RNAs bind RNA Pol II at several SRGs and suppress their transcription. In this way, stalled or delayed RNA Pol II remains poised for a fast activation and ramp up of transcription when needed. Upon application of a stress stimulus, SINE B2 RNAs, which have a self-cleavage activity that is accelerated by their interaction with a protein (Ezh2) (Hernandez et al., 2020), are processed into unstable fragments that lack the ability to bind and suppress RNA Pol II. This event releases the delayed or stalled RNA Pol II and enables fast transcriptional activation of stress response genes (Zovoilis et al., 2016).

The above findings have revealed a novel role in cellular function for processing of SINE B2 RNAs (hereafter referred simply as B2 RNAs) through the activation of a number of SRGs regulated by them (hereafter called B2-SRGs). However, an association of the processing and destabilization of B2 RNAs with any pathological cellular process remains unknown. Here, given the importance of SRGs in hippocampal neuronal function, we examine whether this newly described B2 RNA-SRG regulatory mechanism is linked with pathological processes,

focusing on transcriptome response to amyloid beta toxicity and pathology. To this end, we investigate whether B2-SRGs are indeed deregulated during amyloid pathology, which would imply a role for B2 RNAs in this condition and we examine whether amyloid toxicity is connected with changes in B2 RNA processing. Subsequently, we investigate the further upstream molecular mechanisms underlying any potential deregulation of B2 RNA processing in response to amyloid toxicity in hippocampal neural cells.

Methods

For the tissue enrichment and GO term analysis of B2 RNA regulated SRGs (B2-SRGs) (Table 2.1), we used the DAVID function annotation platform (DAVID 6.8, February 2020) with default parameters (EASE score 0.1, max. 1000 entries), and a reporting EASE score threshold of 0.05 and p-adjusted values calculated based on the Benjamini method (Huang, Sherman, & Lempicki, 2009a, 2009b). For both GO Biological process and Cellular Compartment we selected the BP- or CC-direct options.

For the analysis of the short-RNA-seq and long-RNA-seq data, initially FastQC (Babraham Bioinformatics, https://www.bioinformatics.babraham.ac.uk/projects/fastqc/) was run for quality control of generated reads in fastq format. Subsequently, standard Illumina adaptor sequences were trimmed off using cutadapt-1.18 (https://doi.org/10.14806/ej.17.1.200). Short-RNA-seq reads were mapped to mouse reference genome (UCSC mm10) (November 2017) using bwa-0.7.17 in single end mode with default aln parameters (Li & Durbin, 2009). Long-RNA-seq reads for each sample were mapped to reference genome ensembl GRCm38 (November 2018) primary assembly using hisat2-2.1.0, in single end mode, with the following parameters: Report alignments tailored for transcript assemblers including StringTie, searches

for at most 1 distinct, primary alignment for each read (Kim, Paggi, Park, Bennett, & Salzberg, 2019). SAM format files generated from mapping were converted to BAM format files using samtools-1.6 (Li et al., 2009), and to files in BED format with bamToBed utility from BEDTools-2.26.0 (Quinlan & Hall, 2010).

Models of distribution of 5' end read fragments within the B2 loci (B2_Mm1a, B2_Mm1t and B2_Mm2) were performed using an in house python script. In brief, the script constructs a read accumulation metagene model around a hypothetical set of genomic points, in our case the start site for all B2 elements (TSS), in which the numbers of reads (or read 5' ends) around each different TSS were calculated and attributed to defined points in the model. B2 element coordinates are based on the UCSC genome browser RepeatMasker track (as of November 2018). To calculate the B2 processing ratio, Babraham NGS analysis suite Seqmonk 1.38.2 (https://www.bioinformatics.babraham.ac.uk/projects/seqmonk/) was used to obtain number of long reads overlapping with B2 loci (B2_Mm1a, B2_Mm1t and B2_Mm2), as well as the number of reads overlapping with tRNA loci from -5 to 15 bp. Processing ratio for each sample was calculated by processed B2 count obtained from the in house python scripts normalized by tRNA from -5 to 15 bp and small reads fastq read count, as well as B2 count and long reads fastq read count: [Small fragments (position 95-110) / [tRNAs / small RNA fastq]] / [B2 RNA / long RNA fastq]. The full length of B2 consensus sequence is 188nt and this is the one we use for the in vitro experiments. However, structure of the RNA has been resolved only for the 155nt (Espinoza, Goodrich, & Kugel, 2007), and this is the structure currently used in our figures. For the mapping of short fragments, we have used the same range tested in our previous study (Zovoilis et al., 2016) to maintain consistency of the results. The reason why this 120nt threshold was selected in the Cell paper was to exclude artifacts from short RNAs mapping partially in our

metagene as well as downstream of those B2 elements that are shorter from the consensus sequence.

In long-RNA-seq, FPKM (Fragments Per Kilobase of transcript per Million) and TPM (Transcripts Per Million) for genes were generated using StringTie-1.3.4d (Pertea et al., 2015) with the following annotation: ensembl GRCm38 patch 94 gff3 file, and parameters limiting the processing of read alignments to only estimate and output the assembled transcripts matching the reference transcripts given in annotation and excluding non-regular chromosomes. Because TPM already includes scaling of the data it is unsuitable for the averaging of the gene expression levels of multiple genes (B2-SRGs) used in the boxplots of Figure 2.2. This does not apply in case of single genes as in Figure 2.2C (Trp53) or in the heatmap of the same figure, where each gene is presented in a separate row, and for which TPM values are used. For data visualization, statistics and differential expression analysis we employed R (version 3.4.3) (https://www.R-project.org/) and the package DESeq2 (Love, Huber, & Anders, 2014). Differential expression analysis was implemented on transcript count data for 6-month old mice between APP and wild type. Boxplots central line represents median and t-test was applied on the group numbers mentioned in the text. PCA plots for samples used and read count correlation matrix between 6-month old mice samples are presented in Figure 2.12.

For Hsf1 metagene analysis, we used peak.txt files of Hsf1 peaks for ChIP-seq from (Mahat et al., 2016). Peaks were analyzed with Seqmonk around Transcription start sites of genes (TSS) based on the Eponine annotation (Down & Hubbard, 2002), and filtered based on their overlap with B2 RNA regulated genes (Zovoilis et al., 2016). Also, B2 RNA binding (CHART-seq) peaks were analyzed with Seqmonk around TSS (Eponine), then filtered by

overlapping with learning associated SRGs or all genes (Peleg et al., 2010). Relative density metagene plots of the distribution of the above peaks were generated using Seqmonk.

Results

B2 RNA regulated SRGs (B2-SRGs) are enriched in neural functions

In a previous study, we have identified genomic locations that are subject to regulation by SINE B2 non-coding RNAs during response to thermal stress (heat shock) through binding and suppression of transcription by the RNA Pol II at the pre-stimulus state. Upon induction of cellular stress through the application of a stimulus, SRGs in these locations become activated through B2 processing and release of RNA Pol II suppression (Figure 2.1A) (Zovoilis et al., 2016). A list of B2 RNA regulated SRGs (B2-SRGs) at these locations is available in Table 2.1. Response to thermal stress (heat shock) has been used for years as a basic study model of cellular response to stress. Proteins and gene pathways initially identified in heat shock have been subsequently shown to play identical pro-survival roles in other biological systems. Thus, we questioned whether there are other known cellular functions, beyond response to heat shock, that are connected with B2-SRGs.

As shown in Figure 2.1B, after performing a tissue enrichment analysis to identify tissue terms that are over-represented in the list of our SRGs, we found a significant enrichment of neural tissue terms compared to other tissues in our list. Similarly, during Gene Ontology term enrichment analysis, cellular compartments closely related to neural functions top the list of enriched terms in these genes, including among the first 10 entries terms such as synapse, postsynaptic density and membrane, dendrites, neural projections and pre-synaptic membrane (Figure 2.1C). Most importantly, after performing the same analysis for Biological Processes GO

terms, B2-SRGs were found to be enriched considerably in neural function related terms. GO terms, such as learning, nervous system development, synaptic transmission, synapse receptor localization and neurotransmitter transport were among the first 10 entries with the highest adjusted p value scores enriched in B2-SRGs (Figure 2.1D).

Among the biological processes potentially affected by B2 RNAs that were identified above was learning. We and others have already shown that learning processes in the mouse hippocampus are connected with the transient activation of a number of learning associated genes and pathways, including many known SRGs (Peleg et al., 2010). For this reason, we examined whether any learning associated genes are among the binding targets of B2 RNAs. To this end, we compared the distribution of B2 RNA binding sites in the genome between learning associated genes and all genes. Indeed, as shown in Figure 2.1E, B2 RNA binding sites were found to be enriched in learning associated genes compared to other genes. In particular, based on learning associated genes previously identified in mouse hippocampus (Peleg et al., 2010), among the B2-SRGs (1684 genes), 102 genes (Figure 2.1E, Table 2.2) are associated with learning. In addition, biological process terms enriched in B2-SRGs included, among others, pathways implicated with response to cellular stress in neural cells, and various genes implicated with synaptic function (Figure 2.1E).

This data suggests that B2-SRGs could potentially affect a wide spectrum of functions beyond heat shock including response to cellular stress in neural cells, synaptic function, and learning. All these biological processes are heavily impaired in AD. Given the role of hippocampus as a primary target of amyloid pathology in AD, we decided to expand our investigation towards the potential role of B2-SRGs regulation in this pathological process. We have previously shown that in hippocampus the pro-apoptotic miRNA Mir34c, which is induced

among others by Trp53 and controls it in a negative feedback loop manner (Yamakuchi & Lowenstein, 2009), targets many learning associated genes in order to help to restore their expression and Trp53 expression levels after application of a stimulus (Figure 2.1F) (Yamakuchi & Lowenstein, 2009; Zovoilis et al., 2011). In both mouse models of amyloid beta pathology and AD patient brains, we found persistently high levels of Mir34c. High Mir34c levels in hippocampi with amyloid pathology are indicative of a transcriptome-wide deregulation of Trp53 and associated genes, as many of these genes are either direct or indirect upstream regulators of Mir34c (Figure 2.1F) (Rokavec, Li, Jiang, & Hermeking, 2014). Since, as shown above, B2-SRGs include many learning genes as well as other genes involved in neural function, we questioned whether such transcriptome changes in response to amyloid pathology involve B2-SRGs.

A number of B2-SRGs get hyper-activated during the neurodegeneration phase of amyloid pathology

To test whether B2-SRGs are indeed de-regulated in amyloid pathology, we employed a transgenic mouse model of amyloid pathology, $APP^{NL\text{-}G\text{-}F}$ (Saito et al., 2014), and the respective wild type control (C57BL/6J). The same animal cohorts that were previously characterized through a battery of immunohistochemistry (IHC) and behavioral tests (Mehla et al., 2019) were used to isolate whole hippocampi for the transcriptome analysis conducted in the current study. Figure 2.2A depicts our experimental design while Figure 2.2B depicts the amyloid plaque deposition in the brains. The behavioral tests in these mouse cohorts are presented in our previous study (Mehla et al., 2019).

We have focused on three different mouse ages that correspond to different phases of amyloid beta pathology and represent the: i) pre-symptomatic stage with undetectable (very low) amyloid plaque load (3 months - 3m, Figure 2.2B left panels), ii) stage of symptom manifestation (6 months - 6m) that coincides with the active neurodegeneration phase and appearance of amyloid plaques (Figure 2.2B, middle-panels), and iii) terminal stage of the pathology (12 months - 12m, Figure 2.2B right panels) when mice have already acquired the extensive brain atrophy due to neural cell death. Whole hippocampi from mice of these three groups were isolated and the extracted RNA was subjected to next-generation sequencing. We performed directional RNA sequencing for these samples and subsequently quantified gene expression levels. Sequenced samples depicted high expression levels for known hippocampal markers such as Gad1, Gad2, Slc17a7 and Mbp (Figure 2.3).

In accordance with increased cell death during the active neurodegeneration phase at 6 months, levels of Trp53 were elevated in APP mice of this age compared to controls of the same age (t-test, $p < 0.05$, $n = 3$/group) (Figure 2.2C). Differential expression analysis at this time point revealed a number of genes that are up-regulated in 6-month old APP mice (Table 2.3), including 72 B2-SRGs among them (Table 2.4), of which 13 are learning associated (Table 2.5). These 72 B2-SRGs were enriched in neural function related terms, such as neural development, learning, synapse function and calcium signaling (Table 2.6). Consistent with a hypothesis of a transcriptome-wide deregulation that involves B2-SRGs, levels of the 72 B2-SRGs were found to be strongly up-regulated during the active phase of neurodegeneration at 6 months (Figure 2.2D-F). In particular, in healthy hippocampi (WT control mice), levels of these genes are normally down-regulated in 6m and 12m old mice compared to 3m old mice ($p = 0.02$ and $p = 0.05$, respectively) (Figure 2.2E). This is in accordance with the higher level of neural synaptic

activity and plasticity that younger mice have (Lilja et al., 2013). In contrast, levels of B2-SRGs in APP mice remain abnormally high in 6m old APP mice compared to the 6m old control mice ($p < 0.05$) (Figure 2.2E and 2.2F). A validation of our RNA-seq data through RT-qPCR for selected genes that we identified by RNA-seq to be up-regulated in 6m old APP mice, is presented in Figure 2.4. In Figure 2.2, we only tested the expression of those B2-SRGs that overlapped with the up-regulated genes revealed by DESeq in 6-month old APP mice. When expression dynamics for all B2-SRGs are tested (Figure 2.5DE), these are similar to the ones observed for genes in Figure 2.2, while such dynamics are not observed when a random set of non B2 RNA regulated genes is tested (Figure 2.5BC). Thus, as explained in Figure 2.5, it cannot be excluded that our findings may extend to additional B2-SRGs beyond the 72 identified through our differential gene expression analysis.

These findings show a transcriptome wide hyper-activation of certain B2-SRGs during the active neurodegeneration phase of amyloid pathology.

B2 RNA processing ratio increases during the neurodegeneration phase of in vivo amyloid pathology

Given the role of B2 RNAs in the regulation of SRGs, we hypothesized that the observed hyper-activation of B2-SRGs in the hippocampus of 6m old APP mice may reflect a similar upstream deregulation at the level of the B2 RNAs.

To test this, we employed a customized version of RNA sequencing and analysis used in our previous study (Zovoilis et al., 2016) that allows for enrichment and sequencing of the short SINE RNA fragments (< 100nt) produced by B2 RNA processing (short-RNA-seq). In contrast to standard long-RNA-seq protocols that include RNA fragmentation, thus, may introduce bias,

this approach circumvents this problem. Moreover, the long-RNA-seq protocols exclude short RNA fragments of < 100nt making the identification of B2 short fragments challenging. After short-RNA-seq (Figure 2.6A), mapping of the 5'ends of the sequenced fragments across the B2 loci enables the determination of processing points at B2 RNA (depicted as "X" in Figure 2.6A), including those at the critical RNA Pol II binding region (depicted as a rectangle in Figure 2.6A). Figure 2.6B depicts an example of these fragments from one of the samples. As shown in Figure 2.6A, B2 RNA is extensively processed in hippocampi with amyloid pathology. In particular, this data revealed an increased number of B2 RNA fragments in 6m old APP mice compared to controls (Figure 2.6A), a difference that cannot be explained by full length B2 RNA levels between these groups of mice using long-RNA-seq (Figure 2.6C).

This data suggests that the processing ratio of B2 RNAs may be higher in APP mice of this age. To estimate this ratio, we used the short RNA-seq data in combination with standard long-RNA-seq. As in our previous study, for normalization of short RNA 5'end values we used a class of short RNAs that is not affected by B2 RNAs, the RNA Pol III-transcribed tRNAs and estimated the levels of B2 RNA processing fragments (Figure 2.6E). Moreover, the absolute numbers of fragmented B2 RNA may vary according to the underlying expression of full length B2 RNA transcripts. Therefore, in order to factor in any differences in the amount of fragments due to basal expression levels of the full length B2 RNA, full length B2 RNA levels were calculated by the directional long-RNA-seq (Figure 2.6F). The long-RNA-seq approach excludes short fragments, and subsequently, B2 RNA fragment values from short RNA-seq were normalized to the levels of the full length B2 RNAs to calculate the processing ratio. Consistent with our hypothesis and Figure 2.6A findings, 6m old APP mice were found to have substantially increased ratio of B2 RNA processing compared to control mice of the same age

(Figure 2.6G) ($p < 0.05$, n = 3/group). This increase was observed only in the 6 month old mice (Figure 2.6G, Figure 2.7) and coincides with the increase in Trp53 levels and B2-SRGs levels observed in this age.

Thus, APP mice at the active neuro-degeneration phase are characterized by higher destabilization and processing ratio of B2 RNAs, consistent with the observed increase in B2 RNA regulated SRG levels in these same animals.

Hsf1 mediates increased B2 RNA processing in response to amyloid beta toxicity

We then focused on the molecular mechanism underlying the increased B2 RNA processing during response to amyloid toxicity. When we had previously examined the mechanism of B2 RNA processing in non-neural cells (NIH/3T3 cells during heat shock), a member of the PRC2 protein complex, Ezh2, was reported as being responsible for the B2 RNA accelerated destabilization and processing during response to stress (Zovoilis et al., 2016). However, as shown in Figure 2.9 A-B, scant expression levels of Ezh2 levels in neural cells indicate that Ezh2 is not a key factor in B2 RNA processing in brain. Thus, the factors that may mediate destabilization for B2 RNAs during stress in neural cells remain elusive.

In our earlier study that described the induction of B2 RNA processing by Ezh2, it remained unclear how Ezh2 exerted its impact on B2 RNAs, since Ezh2 lacked any known RNAse activity (Zovoilis et al., 2016). However, in subsequent experiments (Hernandez et al., 2020) we showed that instability is in fact inherent to the B2 RNA molecule while interaction with Ezh2 only accelerates this destabilization and Ezh2 does not cleave B2 RNA by itself. This finding suggests that other proteins may have a similar effect on B2 RNA stability. Therefore,

we started searching for stress related candidate proteins that could affect the B2 RNA processing.

We showed before that, during response to stress in NIH/3T3 cells, B2 RNA binding is enriched near stalled RNA polymerase genomic sites. These areas are known to be highly enriched in binding sites of various stress related proteins, among which Hsf1, a master regulator of stress response for various types of cellular stress (Pandey, Mandal, Jha, & Mukerji, 2011). Hsf1 has been previously connected with activation of SRGs through both transcriptional factor (TF) activities as well as other yet unknown TF-independent processes (Inouye et al., 2007). Interestingly, when we examined the proximity of Hsf1 binding sites, identified by the Lis lab (Mahat et al., 2016), to genes with B2 RNA binding sites (Table 2.1) (Zovoilis et al., 2016), we found that increased number of Hsf1 binding sites were found near B2-SRGs (Figure 2.9 C) and were further enriched after application of a heat-shock stimulus (KS-test < 0.05). Moreover, as shown in Figure 2.9 A-B, in contrast to Ezh2, Hsf1 is expressed in neural tissues and especially in hippocampus. These findings provided an indication that Hsf1 may be implicated in B2 RNA biology and that it is also expressed in neural cells, which urged us to test further its expression pattern in our biological context. Hsf1 levels were found to be up-regulated in APP 6m old mice compared to control group of the same age ($p < 0.05$, $n = 3$/group) (Figure 2.10) in the RNA-seq data, a result confirmed also through RT-qPCR. As mentioned above, at the same time, 6m old APP mice have increased B2 RNA processing ratio. Thus, this data suggests that Hsf1 may be a good candidate for accelerating B2 RNA processing in the context of amyloid pathology.

The increased levels of Hsf1/B2 RNA processing in APP 6m old mice raised the question whether response to amyloid toxicity in hippocampal cells is connected with an Hsf1-mediated increase in B2 RNA processing. In order to test this, we employed a hippocampal cell culture

model using the a HT-22 cell line, which has been used extensively in the past as hippocampal cell stress model (Davis & Maher, 1994; J. Liu, Li, & Suo, 2009). We incubated these cells with amyloid beta peptides (1-42 aa) and compared their transcriptome to the one of cells incubated with an inverted sequence control peptide (R, reverse 42-1) (Figure 2.11A). Incubation of these cells with 1-42 amyloid beta peptides results in upregulation of a number of genes (Table 2.7), 25 of which are also found up-regulated in amyloid beta pathology (6m old APP mice) (Table 2.8). The increase in expression levels of genes associated with amyloid pathology (Figure 2.11B and C) suggests that this cellular model simulates to a certain extend the amyloid toxicity effect on the transcriptome of hippocampal cells and their response to cellular stress. However, as any cell culture system, it has limitations regarding tissue level functions such as learning.

Genes up-regulated in our amyloid toxicity model included 25 B2-SRGs (Table 2.9). When testing for enriched terms in these 25 genes, biological processes related to apoptosis, such as regulation of apoptotic process and programmed cell death were at the top of the list (Table 2.10) and included, among others, genes such as Fosb and Mitf that have been connected with Alzheimer's disease (Gupta, Gupta, & Haberman, 1986; Sole-Domenech, Cruz, Capetillo-Zarate, & Maxfield, 2016). Validation of our RNA-seq data in HT-22 cells through RT-qPCR for selected B2-SRGs identified to be up-regulated in 42 vs. R is presented in Figure 2.11D. In the same figure we also present the expression levels of these genes during recovery, 24h after application of the amyloid beta toxicity stimulus, confirming the return to pre-stimulus levels and the specificity of the treatment with amyloid beta peptides (Figure 2.11D).

Out of the 25 genes that are up-regulated in both mice and our cell culture system, six are B2-SRGs (4932438A13Rik, Fosb, Pag1, Ptprs, Sema5a, and Sgms1) and include a well-known immediate early gene (Fosb), genes associated with sensitivity to amyloid toxicity (Pag1,

Sema5a, Sgms1, Fosb) (Hadar et al., 2016; Lin, Lesnick, Maraganore, & Isacson, 2009), as well as genes associated with Trp53 (Ptprs, Fosb) (S. Liu et al., 2018; Motiwala & Jacob, 2006).

We then questioned whether by inducing an artificial degradation of B2 RNA, we would be able to induce expression of B2-SRGs in our model system of HT22 cells in the absence of any stimulus such as amyloid beta. To achieve this, we employed a similar approach and the same LNAs against B2 RNA that we used in our previous study (NIH/3T3, heat shock). Application of the LNA against B2 (Figure 2.13A) was able to reduce levels of B2 RNA compared to the control LNA (Figure 2.13B). Similar to NIH/3T3 cells, targeting of the B2 RNA in HT22 cells, resulted in the increase of the expression levels of selected B2-SRGs that are up-regulated in amyloid beta pathology (see Figure 2.4 the first 10 genes and Figure 2.11D). The increase in gene expression occurred in the absence of the stress stimulus, in this case amyloid beta, suggesting that these genes are under the suppressive control of B2 RNAs in HT22 cells (Figure 2.13C). At the same time, B2 RNA destabilization did not affect expression of 5 non B2-SRGs that were used as negative controls, including example genes, such as Adcy1 and Kalrn, that are nevertheless up-regulated in amyloid beta pathology (Figure 2.4, the last two genes)

Subsequently, in order to test the impact of amyloid toxicity to Hsf1-mediated B2 RNA processing we treated HT22 cells with either an LNA against Hsf1 or a scramble LNA (control) followed by incubation with the 1-42 peptides, that subject the cells to amyloid toxicity stress, or the respective control peptide (Figure 2.14A, same experimental design and cells as in Figure 2.11). As shown in Figure 2.14B, treatment with the anti-Hsf1 LNA suppressed any increase in Hsf1 levels between 42-anti-Hsf1 and R-anti-Hsf1 cells, while this increase is observed between non Hsf1 LNA treated cells upon application of the amyloid beta peptides (42-ctrl vs R-ctrl). As observed in the APP mice, amyloid beta peptides resulted in increased B2 RNA processing only

in cells without Hsf1 knock down, suggesting that it is the toxicity of these peptides that induces the SINE B2 RNA transcriptome changes (Figure 2.14C, Figure 2.15). In contrast, under anti-Hsf1 LNA, application of the 1-42 peptides was unable to increase B2 RNA processing in the cells compared to the control cells (Figure 2.14C). A similar effect was observed in B2-SRGs that are up-regulated during amyloid toxicity (Table 2.9, Figure 2.14D-F). A selected number of genes was also tested with RT-qPCR to confirm the patterns observed in the RNA-seq data (Figure 2.14E). As in case of amyloid pathology, it cannot be excluded that our findings may extend to additional B2-SRGs (Figure 2.16).

These results suggest that amyloid beta toxicity induces B2 RNA processing also in vitro and Hsf1 comprises a necessary component in the upstream activation pathway of B2 RNA processing and, thus, of the genes regulated by B2 RNA.

Discussion

Fewer than five ribozymes have been identified in mammals, including our previous work on RNAs made from two retrotransposon families, murine SINE B2 RNAs and human SINE Alu RNAs, which are self-cleaving RNAs (Hernandez et al., 2020). We previously showed that cleavage in SINE B2 RNAs controls response to cellular stress through activation of stress response genes in heat shock. However, no connection between this novel molecular mechanism and pathologic processes was until now known. Moreover, since B2 RNAs are intrinsically reactive, and contact with Ezh2 only accelerates cleavage, it remained plausible that other stress-related proteins may also have a similar effect on accelerating B2 RNA processing, which would link this ribozyme-like property to stress response through pathways other than Ezh2. This is

especially relevant in mouse tissues, such as the brain, where Ezh2 expression is limited, an expression pattern observed also in human (Human Protein Atlas) (Uhlen et al., 2015).

Here, we unveil increased processing of SINE B2 RNAs as a novel type of transcriptome de-regulation underlying amyloid beta neuro-pathology. Our data provides a new link in the murine hippocampal pathways connecting amyloid beta toxicity with transcriptome changes in SRGs through processing of B2 RNAs. In particular, the B2 RNA processing ratio increases upon progression of amyloid pathology both in mouse hippocampus and a hippocampal cell culture model, and B2-SRGs become hyper-activated. Consistent with the spatial proximity between B2-SRGs and Hsf1 binding sites, Hsf1 proved to be key for mediating B2 RNA processing in response to amyloid toxicity. This correlation is observed throughout all sequencing experiments performed in this study (Figure 2.15). Our work assigns to Hsf1 a new function that is independent of its long-established transcription factor function and includes the interaction with and processing of SINE B2 RNAs. The high levels of Hsf1 trigger a downstream cascade of events which are orchestrated into a cell-wide, SRG-mediated response to stress conditions. This axis is mediated by the ability of B2 RNA to get processed and, thus, act as a molecular switch. While healthy cells and animals are able to restore the expression levels of Hsf1, SRGs and their regulating B2 RNAs upon removal of the stress-generating stimulus, the amyloid beta load in our biological models acts as a continuous stimulus that causes the Hsf1 - B2 RNA - SRG axis to “lock” into an activated mode. Upregulation of SRGs results in increased Trp53 levels that induce neuronal cell death (Figure 2.17).

Stress response genes, that constitute the basis of response to heat shock, have been shown in various studies from us and others to play a critical role also in hippocampal function (Peleg et al., 2010; Zovoilis et al., 2011). Thus, our findings here on a potential role of B2 RNAs

in the context of neural response to stress constitute a natural continuation of our previous study in heat shock (Zovoilis et al., 2016). The fact that B2-SRGs identified in our previous study were found in the current study to be highly enriched in neuronal tissue related biological processes terms and compartments was what has compelled us to investigate further a potential role of B2 RNAs in neural tissue associated pathologies.

In this study, we employed a mouse model of amyloid pathology in order to test the impact of increased amyloid beta load on B2 RNA processing in vivo. This mouse model has the NL-G-F mutations in the amyloid precursor protein knocked-in to a C57BL genomic background, with each mutation contributing to an increased severity and speed manifestation of the disease (Mehla et al., 2019). The combined effect of the APP^{NL-G-F} mutations results in mice that experience rapid onset of AD-like symptoms at approximately 6 months (Mehla et al., 2019). This is exactly the time point that we observed the massive hyper-activation of B2 RNA SRGs, Trp53 and B2 RNA processing, suggesting that these changes constitute a molecular signature for the active neurodegenerative phase months, before the end state of 12 months that the mice develop terminal AD-like pathology and symptoms.

Interestingly, symptoms and molecular changes are not observed in younger APP mice suggesting the existence of a yet unknown protective mechanism against increased neuronal activity of SRGs in 3m old APP mice. This may be attributed to the increased neuronal plasticity observed in younger brains (Lilja et al., 2013), which suggest that mechanisms in the younger brain may exist for counter-acting this excessive activity. In particular, stress response genes such as Fosb have been shown to participate in specification of cell type-specific activity-dependent gene programs early in development (Yap & Greenberg, 2018). In contrast, during aging, B2-SRG activity in WT mice ramps down, which is not the case in APP mice (Figure

2.2), explaining at the molecular level the increased Trp53 levels and subsequent activation of cell death (Figure 2.1F). Our findings for B2 RNA SRG upregulation and B2 RNA increased processing coincide with the active neurodegeneration phase of amyloid pathology but in later stages the effect is not that prominent. This suggests that the initial active phase differs from the terminal stage regarding role of B2 RNA. As in the terminal stage a large number of cells have already died, B2 processing activation appears to be more connected with the initial response of cells to amyloid toxicity.

The B2 RNA-mediated regulation of gene expression during stress identified in one biological context may be relevant to a broad range of cellular types and disease pathophysiology. In the current study, to identify examples of genes that are subject to B2 RNA regulation in hippocampus molecular pathology we utilized the gene list of B2-SRGs identified in our previous study in heat shock. Of the previously identified 1684 B2-SRGs, we found here 72 genes that are deregulated specifically during the active neurodegeneration phase in hippocampal cells. However, this does not exclude the possibility that beyond these 72 genes, B2 RNA processing may also affect expression of additional B2 SRGs that are associated with other hippocampal functions that are independent of amyloid beta pathology. To get a better insight into this possibility, we tested the correlation between the gene expression of other B2-SRGs and the B2 RNA processing ratio, independently of amyloid beta status. In particular, for each of these genes we have calculated the Pearson correlation coefficient between gene expression levels and B2 RNA processing ratio in the hippocampal samples of the current study. As shown in Figure 2.15E, we have been able to calculate a statistically significant correlation coefficient for at least 659 genes (the rest where either not sufficiently expressed in all samples or returned a p value > 0.05). From these 659 genes, expression of 344 genes (52.2%) showed a strong

correlation with B2 RNA processing ratio ($r \geq 0.5$), while an additional 75 genes (11.3%) showed a weak correlation ($0.5 > r \geq 0.25$), and only 240 genes (36.4%) had an $r < 0.25$ and no correlation. This data suggests that for a large number of the B2-SRGs previously identified in the context of heat shock, correlation between gene expression and B2 RNA processing ratio holds true also in the context of hippocampal cells.

During our amyloid toxicity experiments, cells inoculated with the reverse peptide and the anti-Hsf1 LNA did not show any reduction in Hsf1 levels in contrast to those inoculated with amyloid beta (Figure 2.14B). This could be attributed to compensation during non-stress conditions. In contrast, under stress conditions, when Hsf1 is heavily used due to stress response, cellular needs surpass the available Hsf1 transcripts that are continuously depleted by the LNA. This is also in agreement with levels of B2-SRGs in this condition (Figure 2.14E), which are minimal in both R-ctrl and R-anti-Hsf1 conditions and only get activated during stress response to the amyloid beta in the 42-ctrl condition.

Our study leaves a number of open questions. Particularly, our study raises the question whether a similar mode of regulation of SRGs by SINE RNAs may exist also in human and which SINE RNAs could play such a role. Similar to B2 RNA, such SINE RNAs would be able to bind and inhibit RNA Pol II, and would be subject to a similar RNA processing mechanism enabling the release of RNA Pol II. A number of studies have described that in human, repetitive SINE RNAs of the Alu family are also up-regulated during cellular stress and can bind RNA Pol II inhibiting the transcription of target genes (Yakovchuk, Goodrich, & Kugel, 2009). Alu RNAs are widely regarded as the equivalent in human of B2 RNA. Most importantly, as we showed before, human Alu RNAs, alike B2 RNAs, are self-cleaving RNAs and can become destabilized in vitro (Hernandez et al., 2020). It remains unknown whether SINE RNAs and Hsf1 play a

similar role in amyloid pathology in the case of humans and whether we can extrapolate the generated conclusions in murine models to deduce that SINE RNAs are key components of the pathophysiological mechanisms underlying debilitating diseases such as AD. One major limitation compared to human pathophysiology is that the phenotype of amyloid pathology is not observed in mice even during aging. Nonetheless, a stress-central role of Alu RNAs, the human counterpart of B2 RNAs is plausible and, thus, future studies need to elucidate whether Alu RNA processing is also hyperactivated in the brain of patients with amyloid pathology in the context of AD.

Moreover, in the RNA-seq data one cannot distinguish between Pol III transcribed B2 RNA and Pol II transcribed B2 RNA (typically embedded within introns and UTRs of mRNAs). To get an indication whether such transcripts may contribute to our data we have separated the B2 elements against which we map the RNA fragments into two categories, those that fall within exonic/genic regions and those outside these regions (Figure 2.8). Although B2 RNAs are produced by multiple copies in the genome, each copy does harbor multiple SNPs, insertions and deletions, which means that each B2 RNA fragment is mapped to a specific set of B2 elements and not to all of them. Thus, despite multiple mapping of the reads, a level of spatial specificity is maintained. If the B2 RNAs we map were coming exclusively from either only Pol III B2 elements or mRNA embedded B2 elements, we would expect at least some difference in the distribution of fragments between B2 elements of these two categories, as the second one overlaps with mRNAs. However, as shown in Figure 2.8, the fact that distribution models are very similar between the two categories supports the hypothesis that both types of B2 elements may contribute to B2 RNA processing. Thus, it cannot be excluded whether the regulatory role of B2 RNAs may extend from Pol III transcribed B2 RNAs into B2 RNAs embedded into

mRNAs (likely nascent ones) that may be also under the same endogenous ribozyme activity of this sequence, may suppress Pol II and get processed in response to stimuli.

Our results suggest that B2 RNA regulation is a new process implicated in response to stress in amyloid pathology but it is definitely not the only one. Since B2-SRGs are highly interconnected and interweaved into various pathways, the impact of SRG hyperactivation by B2 RNA processing may extend to pathways that lie downstream of SRGs and affect various gene programs without binding directly B2 RNA. However, here it should be noted that high levels of Hsf1 are certainly expected to affect transcription also through Hsf1's conventional transcriptional factor function while there are still many SRGs that are not directly regulated by B2 RNA. Thus, B2 RNA processing described here does not constitute the only one but just one of the parameters in the equation of SRG regulation. It remains unclear which is the interplay between Hsf1 traditional transcription factor activities and its ability to affect B2 RNA processing and whether there is any overlap or synergies. For example, it remains unclear what percentage of activated genes are activated though Hsf1 DNA binding and what through binding of B2 RNA and subsequent release of suppressed Pol II activity.

Given how easily B2 RNA is processed in the presence of certain proteins, Hsf1 may be only one of the factors accelerating B2 processing in mouse hippocampus as we are just beginning to understand the implications of this form of SINE RNA regulation in cells. A broader role of SINE RNA processing in brain physiology and pathophysiology constitutes, thus, a significant possibility that could further revise our understanding of these RNAs as something more than just transcriptional noise.

References

Bloom, G. S. (2014). Amyloid-beta and tau: the trigger and bullet in Alzheimer disease pathogenesis. *JAMA Neurol, 71*(4), 505-508. doi:10.1001/jamaneurol.2013.5847

Davis, J. B., & Maher, P. (1994). Protein kinase C activation inhibits glutamate-induced cytotoxicity in a neuronal cell line. *Brain Res, 652*(1), 169-173. doi:10.1016/0006-8993(94)90334-4

Down, T. A., & Hubbard, T. J. P. (2002). Computational detection and location of transcription start sites in mammalian genomic DNA. *Genome Research, 12*(3), 458-461. doi:10.1101/gr.216102

Espinoza, C. A., Goodrich, J. A., & Kugel, J. F. (2007). Characterization of the structure, function, and mechanism of B2 RNA, an ncRNA repressor of RNA polymerase II transcription. *Rna, 13*(4), 583-596. doi:10.1261/rna.310307

Gallo, F. T., Katche, C., Morici, J. F., Medina, J. H., & Weisstaub, N. V. (2018). Immediate Early Genes, Memory and Psychiatric Disorders: Focus on c-Fos, Egr1 and Arc. *Front Behav Neurosci, 12*, 79. doi:10.3389/fnbeh.2018.00079

Gao, J., Wang, W. Y., Mao, Y. W., Graff, J., Guan, J. S., Pan, L., . . . Tsai, L. H. (2010). A novel pathway regulates memory and plasticity via SIRT1 and miR-134. *Nature, 466*(7310), 1105-U1120. doi:10.1038/nature09271

Gupta, M. A., Gupta, A. K., & Haberman, H. F. (1986). Psychotropic drugs in dermatology. A review and guidelines for use. *J Am Acad Dermatol, 14*(4), 633-645. doi:10.1016/s0190-9622(86)70081-9

Hadar, A., Milanesi, E., Squassina, A., Niola, P., Chillotti, C., Pasmanik-Chor, M., . . . Gurwitz, D. (2016). RGS2 expression predicts amyloid-beta sensitivity, MCI and Alzheimer's disease: genome-wide transcriptomic profiling and bioinformatics data mining. *Transl Psychiatry, 6*(10), e909. doi:10.1038/tp.2016.179

Hernandez, A. J., Zovoilis, A., Cifuentes-Rojas, C., Han, L., Bujisic, B., & Lee, J. T. (2020). B2 and ALU retrotransposons are self-cleaving ribozymes whose activity is enhanced by EZH2. *Proceedings of the National Academy of Sciences of the United States of America, 117*(1), 415-425. doi:10.1073/pnas.1917190117

Huang, D. W., Sherman, B. T., & Lempicki, R. A. (2009a). Bioinformatics enrichment tools: paths toward the comprehensive functional analysis of large gene lists. *Nucleic Acids Research, 37*(1), 1-13. doi:10.1093/nar/gkn923

Huang, D. W., Sherman, B. T., & Lempicki, R. A. (2009b). Systematic and integrative analysis of large gene lists using DAVID bioinformatics resources. *Nature Protocols, 4*(1), 44-57. doi:10.1038/nprot.2008.211

Inouye, S., Fujimoto, M., Nakamura, T., Takaki, E., Hayashida, N., Hai, T., & Nakai, A. (2007). Heat shock transcription factor 1 opens chromatin structure of interleukin-6 promoter to facilitate binding of an activator or a repressor. *J Biol Chem, 282*(45), 33210-33217. doi:10.1074/jbc.M704471200

Ittner, L. M., Ke, Y. D., Delerue, F., Bi, M., Gladbach, A., van Eersel, J., . . . Gotz, J. (2010). Dendritic function of tau mediates amyloid-beta toxicity in Alzheimer's disease mouse models. *Cell, 142*(3), 387-397. doi:10.1016/j.cell.2010.06.036

Kim, D., Paggi, J. M., Park, C., Bennett, C., & Salzberg, S. L. (2019). Graph-based genome alignment and genotyping with HISAT2 and HISAT-genotype. *Nature Biotechnology, 37*(8), 907-+. doi:10.1038/s41587-019-0201-4

Li, H., & Durbin, R. (2009). Fast and accurate short read alignment with Burrows-Wheeler transform. *Bioinformatics, 25*(14), 1754-1760. doi:10.1093/bioinformatics/btp324

Li, H., Handsaker, B., Wysoker, A., Fennell, T., Ruan, J., Homer, N., . . . Proc, G. P. D. (2009). The Sequence Alignment/Map format and SAMtools. *Bioinformatics, 25*(16), 2078-2079. doi:10.1093/bioinformatics/btp352

Lilja, A. M., Rojdner, J., Mustafiz, T., Thome, C. M., Storelli, E., Gonzalez, D., . . . Marutle, A. (2013). Age-Dependent Neuroplasticity Mechanisms in Alzheimer Tg2576 Mice Following Modulation of Brain Amyloid-beta Levels. *Plos One, 8*(3). doi:ARTN e5875210.1371/journal.pone.0058752

Lin, L., Lesnick, T. G., Maraganore, D. M., & Isacson, O. (2009). Axon guidance and synaptic maintenance: preclinical markers for neurodegenerative disease and therapeutics. *Trends Neurosci, 32*(3), 142-149. doi:10.1016/j.tins.2008.11.006

Liu, J., Li, L., & Suo, W. Z. (2009). HT22 hippocampal neuronal cell line possesses functional cholinergic properties. *Life Sci, 84*(9-10), 267-271. doi:10.1016/j.lfs.2008.12.008

Liu, S., Yao, X., Zhang, D., Sheng, J., Wen, X., Wang, Q., . . . Zhang, X. (2018). Analysis of Transcription Factor-Related Regulatory Networks Based on Bioinformatics Analysis and Validation in Hepatocellular Carcinoma. *Biomed Res Int, 2018*, 1431396. doi:10.1155/2018/1431396

Love, M. I., Huber, W., & Anders, S. (2014). Moderated estimation of fold change and dispersion for RNA-seq data with DESeq2. *Genome Biology, 15*(12). doi:ARTN 55010.1186/s13059-014-0550-8

Mahat, D. B., Salamanca, H. H., Duarte, F. M., Danko, C. G., & Lis, J. T. (2016). Mammalian Heat Shock Response and Mechanisms Underlying Its Genome-wide Transcriptional Regulation. *Mol Cell, 62*(1), 63-78. doi:10.1016/j.molcel.2016.02.025

Mehla, J., Lacoursiere, S. G., Lapointe, V., McNaughton, B. L., Sutherland, R. J., McDonald, R. J., & Mohajerani, M. H. (2019). Age-dependent behavioral and biochemical characterization of single APP knock-in mouse (APP(NL-G-F/NL-G-F)) model of Alzheimer's disease. *Neurobiology of Aging, 75*, 25-37. doi:10.1016/j.neurobiolaging.2018.10.026

Motiwala, T., & Jacob, S. T. (2006). Role of protein tyrosine phosphatases in cancer. *Prog Nucleic Acid Res Mol Biol, 81*, 297-329. doi:10.1016/S0079-6603(06)81008-1

Pandey, R., Mandal, A. K., Jha, V., & Mukerji, M. (2011). Heat shock factor binding in Alu repeats expands its involvement in stress through an antisense mechanism. *Genome Biol, 12*(11), R117. doi:10.1186/gb-2011-12-11-r117

Peleg, S., Sananbenesi, F., Zovoilis, A., Burkhardt, S., Bahari-Javan, S., Agis-Balboa, R. C., . . . Fischer, A. (2010). Altered Histone Acetylation Is Associated with Age-Dependent Memory Impairment in Mice. *Science, 328*(5979), 753-756. doi:10.1126/science.1186088

Pertea, M., Pertea, G. M., Antonescu, C. M., Chang, T. C., Mendell, J. T., & Salzberg, S. L. (2015). StringTie enables improved reconstruction of a transcriptome from RNA-seq reads. *Nature Biotechnology, 33*(3), 290-+. doi:10.1038/nbt.3122

Ponicsan, S. L., Kugel, J. F., & Goodrich, J. A. (2010). Genomic gems: SINE RNAs regulate mRNA production. *Current Opinion in Genetics & Development, 20*(2), 149-155. doi:10.1016/j.gde.2010.01.004

Ponicsan, S. L., Kugel, J. F., & Goodrich, J. A. (2015). Repression of RNA Polymerase II Transcription by B2 RNA Depends on a Specific Pattern of Structural Regions in the RNA. *Noncoding RNA, 1*, 4-16. doi:10.3390/ncrna1010004

Quinlan, A. R., & Hall, I. M. (2010). BEDTools: a flexible suite of utilities for comparing genomic features. *Bioinformatics, 26*(6), 841-842. doi:10.1093/bioinformatics/btq033

Rokavec, M., Li, H. H., Jiang, L. C., & Hermeking, H. (2014). The p53/miR-34 axis in development and disease. *Journal of Molecular Cell Biology, 6*(3), 214-230. doi:10.1093/jmcb/mju003

Saito, T., Matsuba, Y., Mihira, N., Takano, J., Nilsson, P., Itohara, S., . . . Saido, T. C. (2014). Single App knock-in mouse models of Alzheimer's disease. *Nature Neuroscience, 17*(5), 661-+. doi:10.1038/nn.3697

Sananbenesi, F., Fischer, A., Schrick, C., Spiess, J., & Radulovic, J. (2003). Mitogen-activated protein kinase signaling in the hippocampus and its modulation by corticotropin-releasing factor receptor 2: A possible link between stress and fear memory. *Journal of Neuroscience, 23*(36), 11436-11443. Retrieved from <Go to ISI>://WOS:000187232800018

Sole-Domenech, S., Cruz, D. L., Capetillo-Zarate, E., & Maxfield, F. R. (2016). The endocytic pathway in microglia during health, aging and Alzheimer's disease. *Ageing Res Rev, 32*, 89-103. doi:10.1016/j.arr.2016.07.002

Uhlen, M., Fagerberg, L., Hallstrom, B. M., Lindskog, C., Oksvold, P., Mardinoglu, A., . . . Ponten, F. (2015). Proteomics. Tissue-based map of the human proteome. *Science, 347*(6220), 1260419. doi:10.1126/science.1260419

Yakovchuk, P., Goodrich, J. A., & Kugel, J. F. (2009). B2 RNA and Alu RNA repress transcription by disrupting contacts between RNA polymerase II and promoter DNA within assembled complexes. *Proceedings of the National Academy of Sciences of the United States of America, 106*(14), 5569-5574. doi:10.1073/pnas.0810738106

Yamakuchi, M., & Lowenstein, C. J. (2009). MiR-34, SIRT1 and p53 The feedback loop. *Cell Cycle, 8*(5), 712-715. doi:DOI 10.4161/cc.8.5.7753

Yap, E. L., & Greenberg, M. E. (2018). Activity-Regulated Transcription: Bridging the Gap between Neural Activity and Behavior. *Neuron, 100*(2), 330-348. doi:10.1016/j.neuron.2018.10.013

Yutsudo, N., Kamada, T., Kajitani, K., Nomaru, H., Katogi, A., Ohnishi, Y. H., . . . Nakabeppu, Y. (2013). fosB-Null Mice Display Impaired Adult Hippocampal Neurogenesis and Spontaneous Epilepsy with Depressive Behavior. *Neuropsychopharmacology, 38*(5), 895-906. doi:10.1038/npp.2012.260

Zovoilis, A., Agbemenyah, H. Y., Agis-Balboa, R. C., Stilling, R. M., Edbauer, D., Rao, P., . . . Fischer, A. (2011). microRNA-34c is a novel target to treat dementias. *Embo Journal, 30*(20), 4299-4308. doi:10.1038/emboj.2011.327

Zovoilis, A., Cifuentes-Rojas, C., Chu, H. P., Hernandez, A. J., & Lee, J. T. (2016). Destabilization of B2 RNA by EZH2 Activates the Stress Response. *Cell, 167*(7), 1788-1802 e1713. doi:10.1016/j.cell.2016.11.041

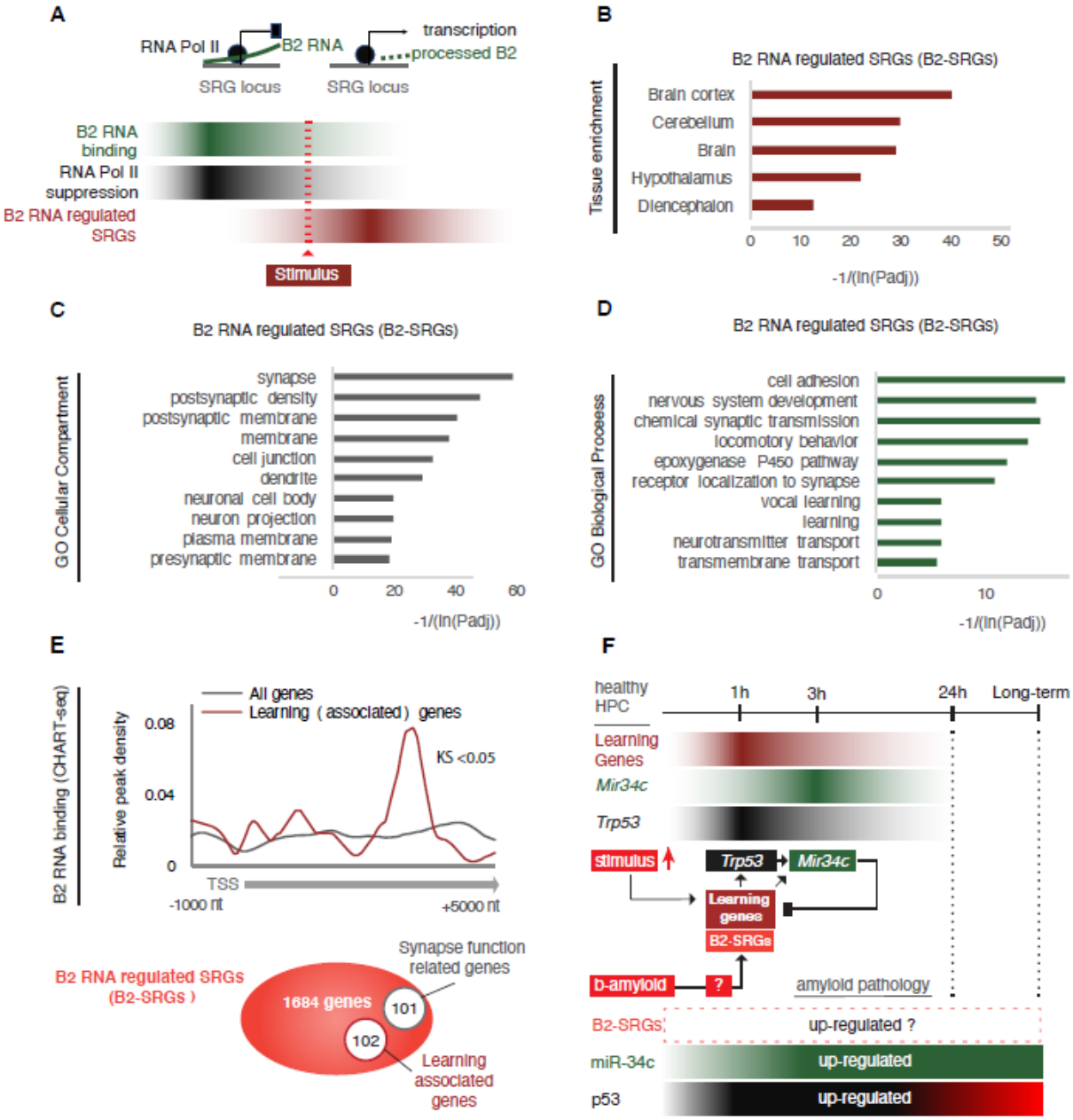

Figure 2.1. B2-SRGs are enriched in neural functions.

(A) Regulation mode of SRGs by B2 RNA processing based on previous works (Ponicsan, Kugel, & Goodrich, 2010; Yakovchuk et al., 2009; Zovoilis et al., 2016). Color intensity represents higher B2 RNA binding (green), Pol II suppression (black) or SRG expression (red).

(B) Tissue enrichment analysis of B2-SRGs listed in Table 2.1 based on the DAVID functional annotation platform (Huang et al., 2009a, 2009b). The adjusted p-values of top 5 ranking terms are plotted as a function with higher scores representing lower adjusted p-values (higher statistical significance) ranging from padj 1.92E-04 for "Diencephalon" to padj 8.91E-13 for "Brain Cortex".

(C) Gene ontology (GO) analysis (DAVID) of B2 RNA regulated genes on the basis of cellular compartments. The adjusted p-values of top 10 ranking terms are plotted as a function with higher scores representing lower adjusted p-values ranging from 2.23E-06 for “Presynaptic membrane” to 1.88E-18 for “Synapse”.

(D) GO analysis (DAVID) of B2 RNA regulated genes on the basis of biological processes. As above, adjusted p-values of top ranking terms are plotted as a function, with higher scores representing lower adjusted p-values ranging from 0.02 for “Transmembrane transport” to 5.44E-06 for “Cell adhesion”.

(E) Upper panel: Metagene analysis of distribution of genomic B2 RNA binding sites across the start of genes from (Zovoilis et al., 2016), comparing learning associated genes from (Peleg et al., 2010) with all genes (Kolmogorov Smirnov test, KS < 0.05). TSS represents the Transcription Start Site of these genes. Lower panel: Representation of the number of B2-SRGs that are i) learning associated based on (Peleg et al., 2010) (Table 2.2), ii) synapse function related based on GO term enrichment.

(F) Regulatory loop of learning genes-Trp53-Mir34c in mouse hippocampus based on (Peleg et al., 2010; Yamakuchi & Lowenstein, 2009; Zovoilis et al., 2011). A potential role of B2 SRGs, that include many learning genes, in affecting this loop in amyloid pathology remained unknown after these studies (noted with a question mark in the figure).

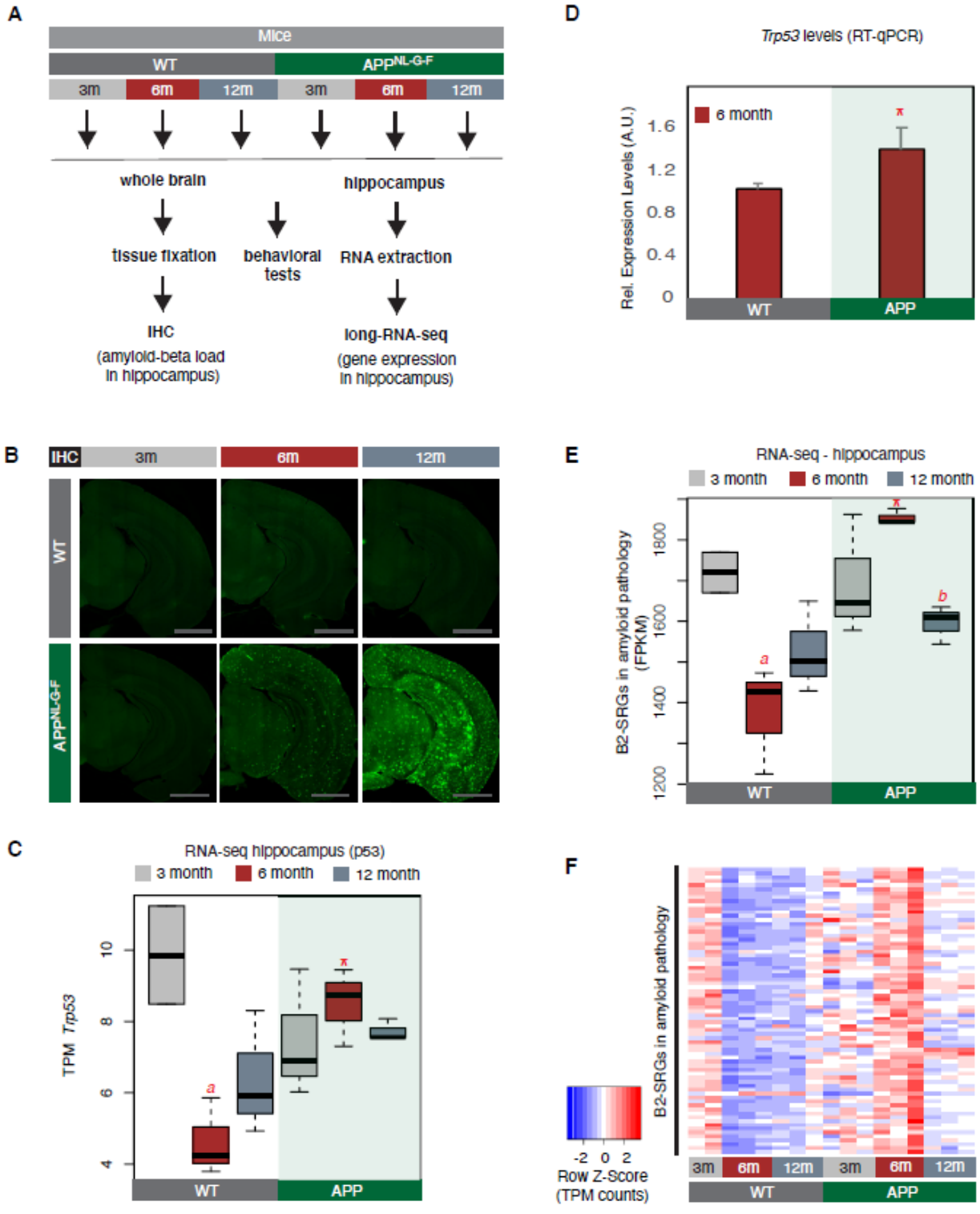

Figure 2.2. A number of B2-SRGs are hyper-activated in amyloid pathology.

(A) Experimental design for study of B2-SRGs in the hippocampus of the amyloid pathology mouse model (APP) and the respective wild type (WT) control.

(B) Immunohistochemistry for identifying amyloid-beta load in the brain sections of mice from the same cohort as in (A) (image credit: Mehla and colleagues, adapted from previously published figure (Mehla et al., 2019)). Higher fluorescence intensity corresponds to higher amyloid load in APP mice from 6m old onwards.

(C) Expression levels of the pro-apoptotic gene Trp53 (official symbol Trp53) as defined by long-RNA-seq. Trp53 transcripts per million reads (TPM) from the APP mice compared to WT, grouped by age. Boxplot depicts distribution of expression levels of Trp53 gene among different age groups of mice (WT: wild type, APP: mice with amyloid pathology). Black line denotes median. Statistical significance (p value threshold 0.05) for the comparison between 6m old APP and 6m old WT ($p = 0.01$) (depicted as asterisk, unpaired, non-directional t-test, n = 3/group) and the comparison between 3m old WT (n = 2) and 6m old WT (n = 3) ($p = 0.04$) (depicted as a). No significance for the rest of the comparisons between APP and WT in the other two age groups, or between other different ages within the same group (APP or WT).

(D) Expression levels of the pro-apoptotic gene Trp53 (official symbol Trp53) in 6 month old mice as defined by RT-qPCR. Statistical significance (p value threshold 0.05) for 6m old APP greater than 6m old WT (depicted as asterisk, unpaired directional t-test, n = 3/group, error bars represent standard deviation from the mean).

(E) Expression levels as defined by long-RNA-seq of B2-SRGs that are up-regulated in amyloid pathology (72 genes, Table 2.4). Boxplot depicts distribution of expression levels (in FPKM / Fragments per Kilobase per Million) of B2-SRGs among different age groups of wild type and APP mice. Statistical significance (p value threshold 0.05) for the comparison between 6m old APP and 6m old WT ($p = 0.02$) (depicted as asterisk, unpaired, non-directional t-test, n = 3/group), for the comparison between 3m old WT (n = 2) and 6m old WT (n = 3) ($p = 0.03$) (depicted as a) and for the comparison between 6m old APP and 12m old APP ($p = 0.005$) (depicted as b). No significance for the rest of the comparisons between APP and WT in the other two age groups, or between other different ages within the same group (APP or WT).

(F) Gene expression levels of B2-SRGs that are up-regulated in amyloid pathology (72 genes, Table 2.4) show strong association with amyloid pathology status in the hippocampus of APP and WT mice of different ages. Heatmap depicts gene expression with rows representing B2 RNA regulated genes and columns representing mouse samples. Expression values are normalized per row and correspond to TPM values. Red color represents higher expression.

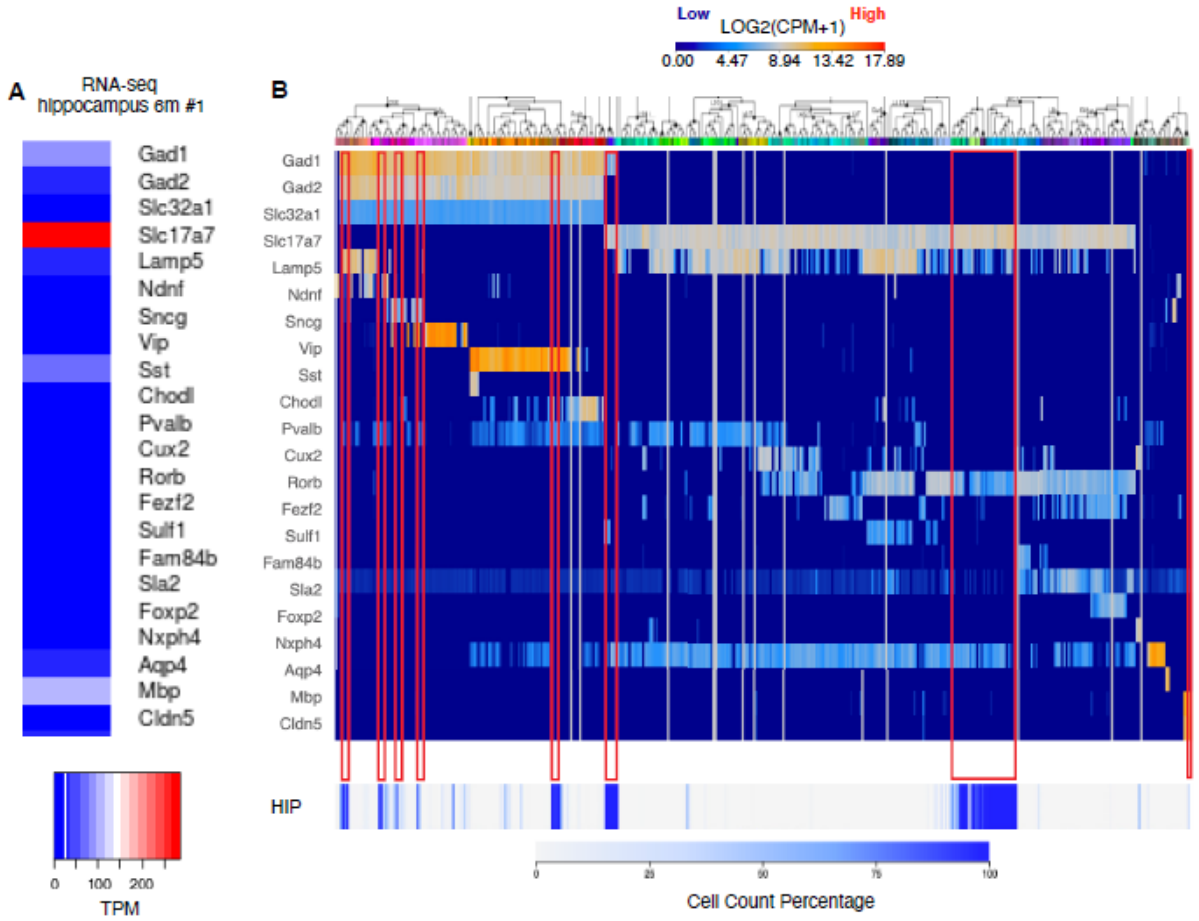

Figure 2.3. Expression of known hippocampal markers in our RNA-seq data of mice hippocampi.

(A-B) Expression levels comparison between RNA-seq data from WT 6m old mouse hippocampus used in our study (panel A) and RNA-seq data from the Allen Brain Atlas (Panel B). Comparison is done for the standard panel genes of reference genes used by Allen Brain Atlas. Every column in panel B represents a different cell type in brain with cell types belonging to hippocampus corresponding to increased density (cell count percentage) at the lower part of panel B labelled as HIP. Red rectangles mark the most prominent cell types that are enriched in Hippocampus. For panels B: Image credit: Allen Institute. © [2015] Allen Institute for Brain Science. [Allen Mouse Brain Atlas]. Available from: [https://portal.brain-map.org/atlases-and-data/rnaseq#Mouse_Cortex_and_Hip].

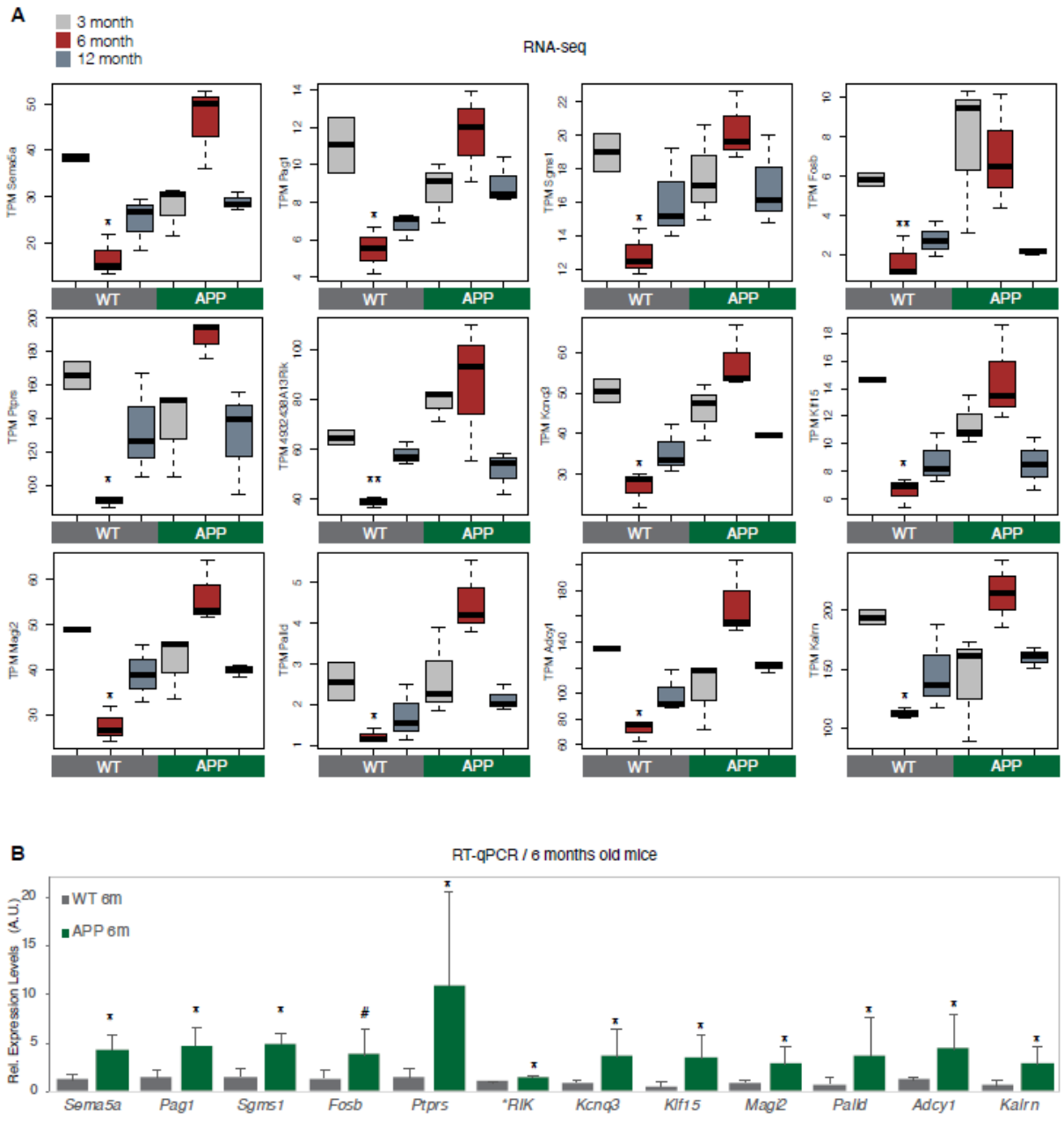

Figure 2.4. Validation of RNA-seq data in WT and APP mice by RT-qPCR.

(A) Expression levels calculated through RNA-seq for the selected genes to be tested through RT-qPCR in (B). These are 12 from the genes that were found to be up-regulated in APP 6 month old mice compared to WT mice of the same age (Table 2.3). The selected subset includes both B2-SRGs (first 10 boxplots) that are part of the 72 B2-SRGs up-regulated in APP mice (Table 2.4) but also two non B2-SRGs (last two plots; Adcy1 and Kalrn) that are used later as negative controls (see Figure 2.13C). Values are based on TPM counts of long-RNA-seq data. One asterisk marks statistical significance ($p < 0.05$) for the comparison between 6-month old APP and 6m old WT (n = 3/group, unpaired non-directional t-test), while two asterisks marks

statistical significance only for 6-month old APP greater than 6m old WT (n = 3/group, unpaired directional t-test). All the other comparisons between groups and different ages are non-significant.

(B) Confirmation through RT-qPCR of the expression differences between 6 m old WT and APP mice. Statistical significance (p value threshold 0.05), is depicted as asterisk, for expression in 6m old APP mice greater than the expression in 6m old WT mice (unpaired directional t-test, n numbers as in (A), error bars represent standard deviation from the mean). # represents a p = 0.08 for the same comparison and test. * RIK stands for 4932438A13Rik.

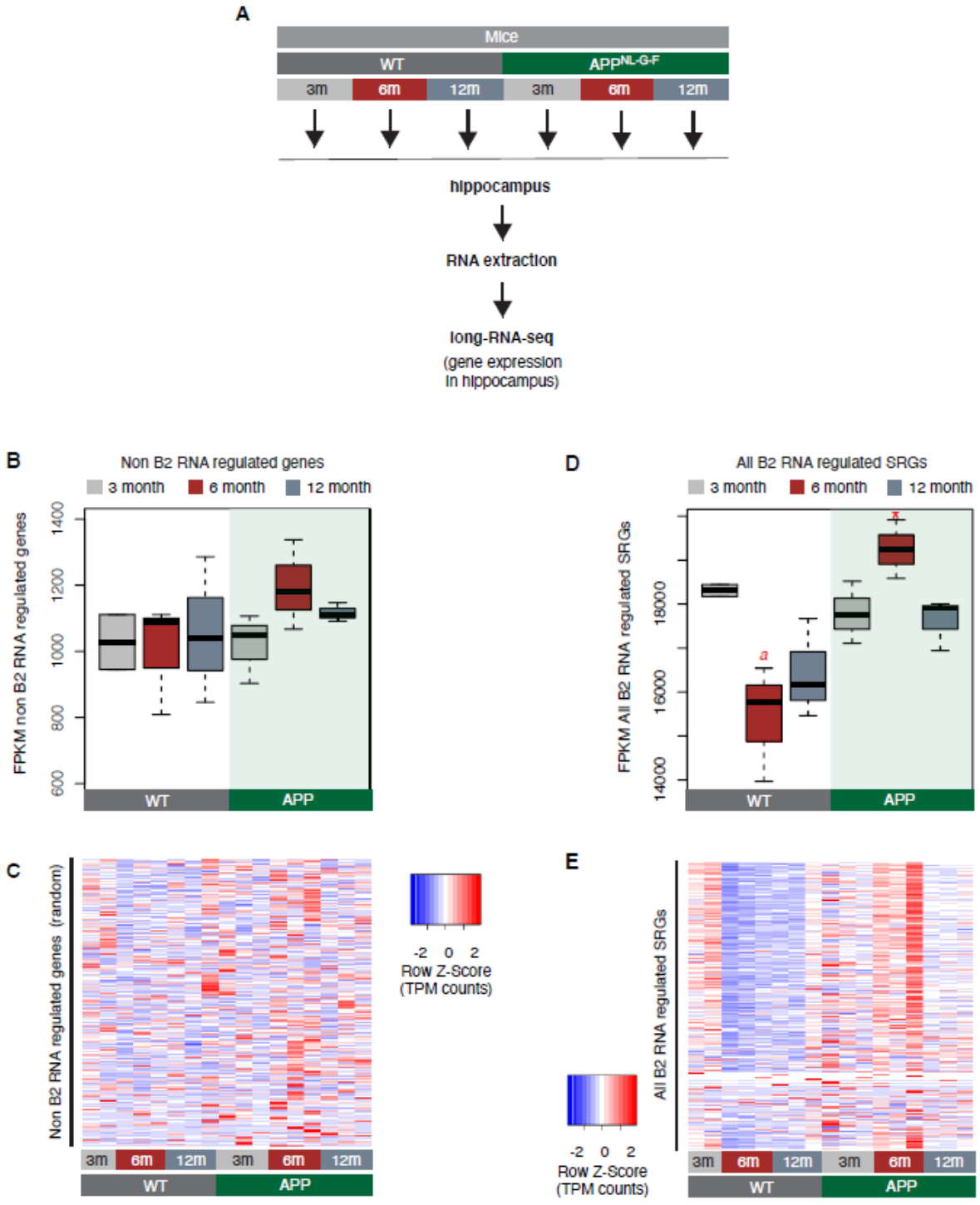

Figure 2.5. Expression levels of all B2-SRGs in amyloid pathology.

(A) Experimental design for study of B2-SRGs in the hippocampus of the amyloid pathology mouse model (APP) and the respective wild type (WT) control.

(B) Expression levels of non B2 RNA regulated genes as defined by long-RNA-seq. Boxplot depicts distribution of expression levels (in FPKM / Fragments per Kilobase per Million) among different age groups of wild type and APP mice. Not significant difference between 6m old APP and 6m old WT.

(C) Gene expression levels (defined by long-RNA-seq) of a random set of genes not associated with B2 RNAs show weak or no association with amyloid pathology status in the hippocampus of APP and WT mice of different ages. Heatmap depicts gene expression with rows representing 1385 non B2 RNA regulated genes (Table 2.12) and columns representing the different mouse samples. Expression values are normalized per row and correspond to TPM values.

(D) Expression levels of B2-SRGs (1684 genes, Table 2.1) as defined by long-RNA-seq. Boxplot depicts distribution of expression levels (in FPKM / Fragments per Kilobase per Million) of B2 RNA regulated genes among different age groups of wild type and APP mice. Statistical significance (p value threshold 0.05) for the comparison between 6m old APP and 6m old WT ($p = 0.02$) (depicted as asterisk, unpaired, non-directional t-test, n = 3/group) and the comparison between 3m old WT and 6m old WT ($p = 0.05$) (depicted as a). No significance for the rest of the comparisons between APP and WT in the other two age groups, or between other different ages within the same group (APP or WT).

(E) Gene expression levels of B2-SRGs (1684 genes, Table 2.1) show strong association with amyloid pathology status in the hippocampus of APP and WT mice of different ages. Heatmap depicts gene expression with rows representing B2 RNA regulated genes and columns representing mouse samples. Expression values are normalized per row and correspond to TPM values. Red color represents higher expression.

(Note) When expression dynamics for all B2-SRGs are tested, these are similar to the ones observed for genes in Figure 2.2, while this pattern in B2 RNA regulated SRG expression was not observed when a random set of genes is tested. Thus, it cannot be excluded that the expression pattern observed in genes of Figure 2.2 may extend to additional B2-SRGs described in our previous work that have been filtered out by DEseq. This could be attributed to our current sequencing depth and the large dynamic range of some of them as shown in panel E, but also due to genome wide mRNA expression level changes in our system that are not taken into account by DEseq's conservative hypothesis that expression levels of most genes remain unchanged. This is relevant in our case given the ability of full length B2 RNAs (which are elevated in our system) to suppress global gene expression and thus, it may have resulted in a number of genes being filtered out during DESeq correction for multiple testing.

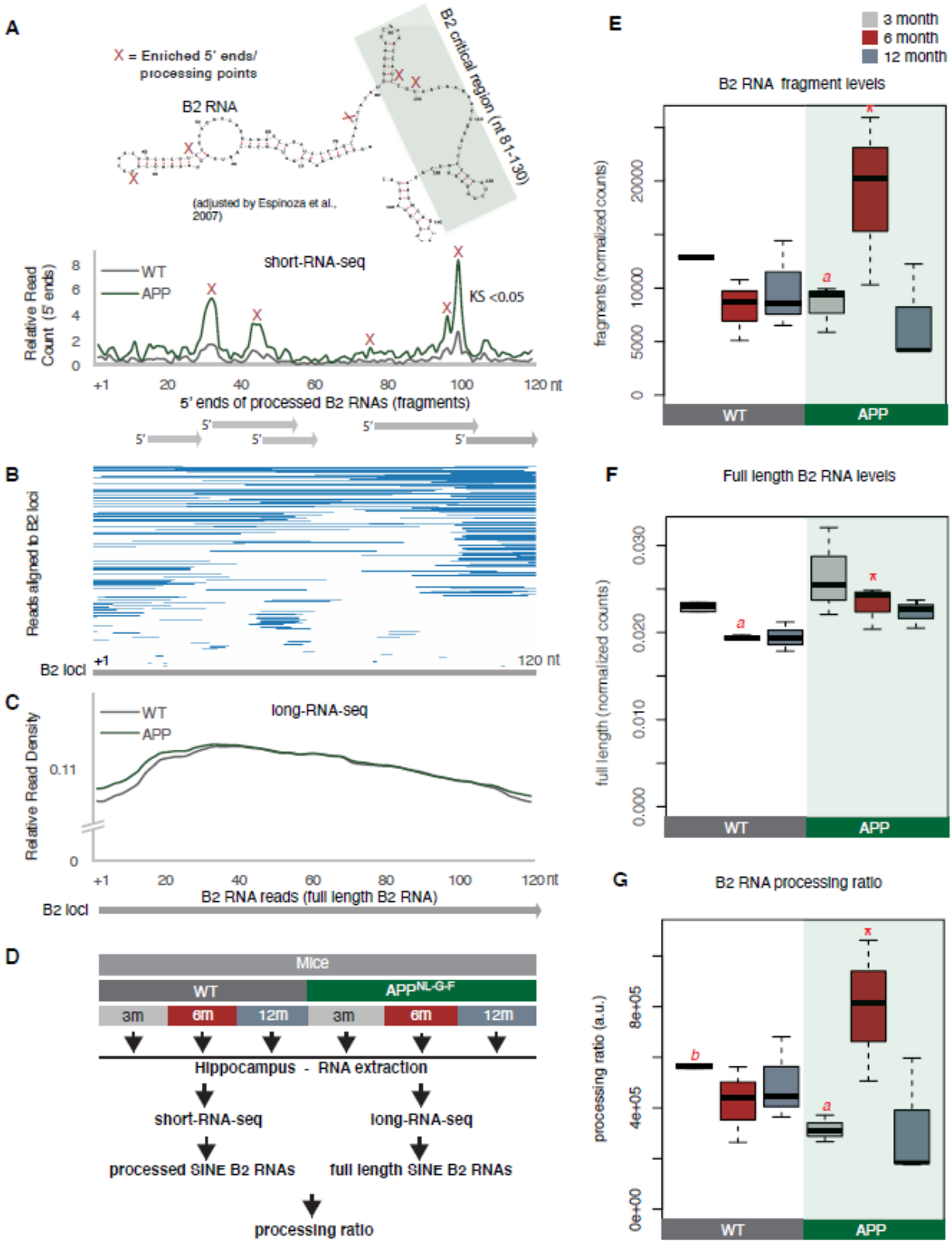

Figure 2.6. B2 RNA processing ratio is increased in 6m old APP mice.

(A) Plotting of the position of the first base (5’ end) of B2 RNA fragments across the B2 loci to depict increased levels of B2 RNA fragments in 6m old APP mice. Upper panel: Secondary structure and processing points of B2 RNA. Secondary structure of B2 RNA adapted from Espinosa and colleagues (Espinoza et al., 2007). As in our previous study (Zovoilis et al., 2016), we depict the B2 RNA processing points based on short RNA-seq data and mapping of the 5’ends of B2 RNA fragments. X marks which cleavage sites of B2 RNA in the upper panel correspond to enriched processing points (the peaks of 5’end fragments distribution) at the lower panel. The green rectangle depicts the critical region that binds and suppresses RNA Pol II (Espinoza et al., 2007; Ponicsan et al., 2010; Ponicsan, Kugel, & Goodrich, 2015; Yakovchuk et al., 2009) that may be affected by such processing points. Lower panel: Distribution of the 5’ends of B2 RNA fragments across the B2 RNA loci based on mapped short RNA-seq from the hippocampi of 6m old APP and WT mice. The x axis represents a metagene combining all B2 RNA loci aligned at the start site of their consensus sequence (position +1) and the y axis shows the relative 5’ end count for B2 RNA fragments aligning to any position downstream of position +1. Figure depicts the difference between B2 RNA fragment distribution of 6m old APP mice (higher peaks) vs 6m old WT mice (lower peaks) (Kolmogorov Smirnov test, KS < 0.05).

(B) Alignment of short-RNA seq reads mapped against the multiple B2 loci. Only B2 loci with at least one read are depicted. Short RNA-seq reads from one of the 6m old APP mice, whose 5’ends are plotted at (A) lower panel are used here as an example of the length and position of fragments across B2 loci.

(C) Metagene analysis of long-RNA-seq reads of mice across B2 RNA loci that is enriched in full length B2 RNAs but not in B2 RNA fragments. Comparative analysis shows low difference in relative read density of full length B2 RNAs between WT and 6m old APP. X axis as in A. Y axis corresponds to read coverage across the B2 loci.

(D) Experimental design for estimation of B2 RNA processing ratio based on short and long-RNA seq data for all APP mice and controls.

(E) Boxplot depicts distribution of levels of processed SINE B2 RNA fragments among different age groups of mice between wild type and APP. Statistical significance (p value threshold 0.05) only for 6m old APP greater than 3m old APP ($p = 0.04$), 12m old APP ($p = 0.04$) and 6m old WT ($p = 0.04$) (depicted as asterisk, n = 3/group, unpaired directional t-test). All the other comparisons between groups and different ages non-significant except 3m old WT less than 3m old APP ($p = 0.03$) (depicted as a).

(F) Boxplot depicts distribution of levels of full length SINE B2 RNAs among different age groups of mice between wild type and APP. Statistical significance (p value threshold 0.05) for the comparison between 6m old APP and 6m old WT ($p = 0.05$) (depicted as asterisk, n = 3/group, non-directional unpaired t-test) and for the comparison between 3m old WT (n = 2) and 6m old WT (n = 3) ($p = 0.004$) (depicted as a). All the other comparisons between groups and different ages are non-significant.

(G) Boxplot depicts distribution of SINE B2 RNA processing ratio among different age groups of mice between wild type and APP. Statistical significance (p value threshold 0.05) for the

comparison between 3m APP and 6m old APP ($p = 0.04$) (depicted as a, n = 3/group, non-directional unpaired t-test), for the comparison between 3m old WT (n = 2) and 3m old APP (n = 3) ($p = 0.008$) (depicted as b) and for 6m old APP greater than 6m old WT ($p = 0.05$) (depicted as asterisk, n = 3/group). All the other comparisons between groups and different ages are non-significant.

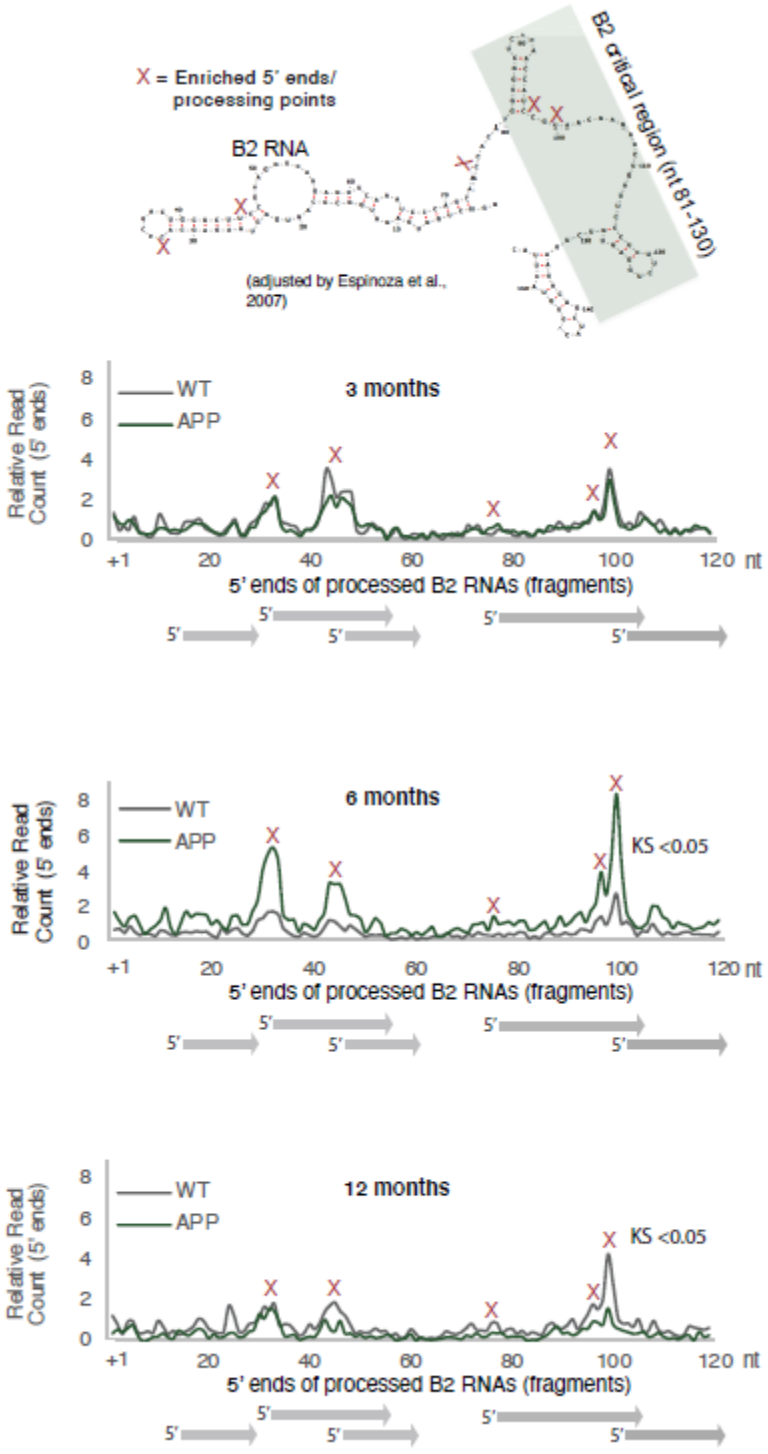

Figure 2.7. Plotting of the position of the first base (5' end) of B2 RNA fragments across the B2 loci to compare levels of B2 RNA fragments between APP and WT mice in the three different age groups.

This figure relates to Figure 2.6A. Upper panel: As in Figure 2.6A. Secondary structure and processing points of B2 RNA. Secondary structure of B2 RNA adapted from Espinosa and colleagues (Espinoza et al., 2007). Lower panels: Distribution of the 5'ends of B2 RNA fragments across the B2 RNA loci based on mapped short RNA-seq from the hippocampi of 3m, 6m and 12m old APP and WT mice. The x axis represents a metagene combining all B2 RNA loci aligned at the start site of their consensus sequence (position +1) and the y axis shows the relative 5' end count for B2 RNA fragments aligning to any position downstream of position +1. Figure depicts the difference between B2 RNA fragment distribution of 6m old APP mice (higher peaks) vs 6m old WT mice (lower peaks) (Kolmogorov Smirnov test, KS<0.05) and the reverse difference of 6m old APP mice (higher peaks) vs 6m old WT mice (lower peaks) (Kolmogorov Smirnov test, KS < 0.05).

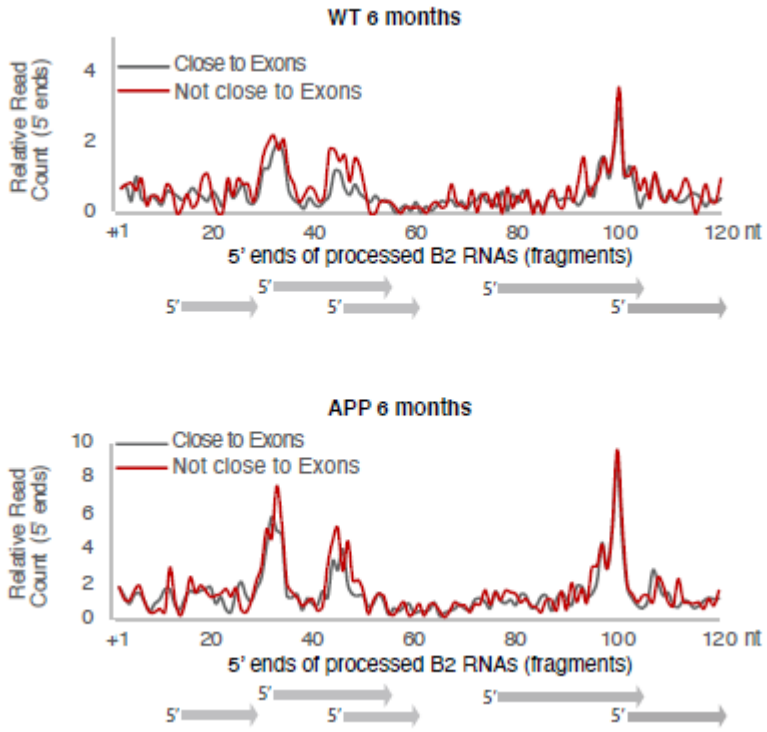

Figure 2.8. Plotting of the position of the first base (5' end) of B2 RNA fragments across the B2 loci to compare levels of B2 RNA fragments in 6 month old mice between B2 elements that overlap exonic/genic regions and those that do not.

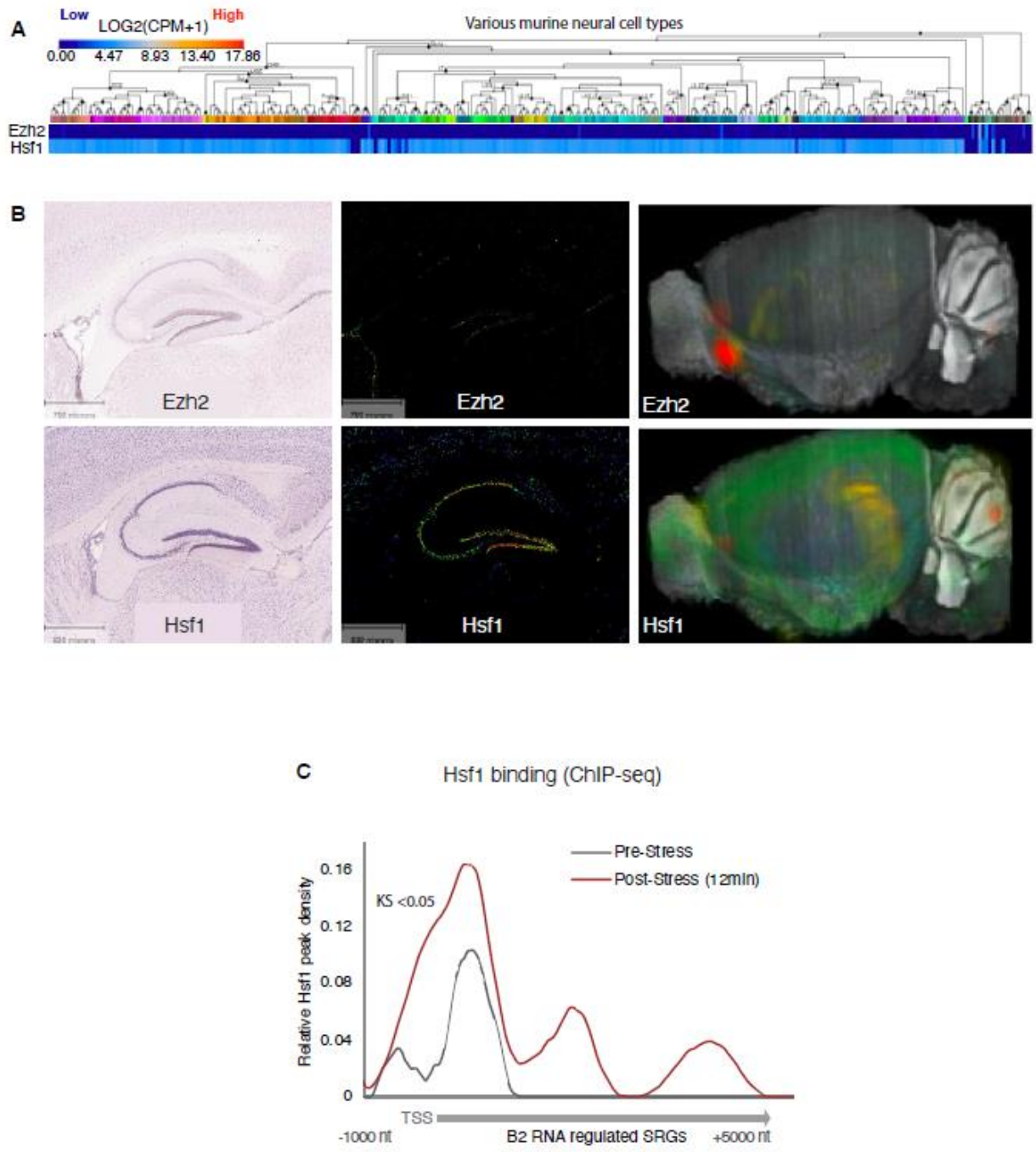

Figure 2.9. Expression of Hsf1 in neural tissues.

(A) Mouse cortex and hippocampus gene expression levels for Ezh2 and Hsf1 depicted in the Allen Brain Atlas Transcriptomics explorer showing limited expression of Ezh2 across multiple neural tissues compared to Hsf1. Levels are per cell type based on RNA-seq data. Image credit: Allen Institute. © [2015] Allen Institute for Brain Science. [Allen Mouse Brain Atlas]. Available from: [https://portal.brain-map.org/atlases-and-data/rnaseq#Mouse_Cortex_and_Hip].

(B) In situ hybridization brain image data with cellular-level resolution for Ezh2 (upper panel) and Hsf1 (lower panel) depicting low expression levels for Ezh2. Left panel, ISH images, middle panel, gene expression images, right panel, expression in 3D reconstructed whole mouse brain. Image credit: Allen Institute. © [2007] Allen Institute for Brain Science. [Allen Mouse Brain Atlas]. Available from: [https://mouse.brain-map.org/experiment/show/100142521 for Eh2 and https://mouse.brain-map.org/experiment/show/68196972 for Hsf1].

(C) Metagene analysis of increase in Hsf1 binding (ChIP-seq data) across the start of B2 RNA regulated genes (Table 2.1) between pre-stress and 12-minutes post-stress (KS < 0.05). ChIP-deq data are from Mahat and colleagues (Mahat et al., 2016). TSS represents the Transcription Start Site of these genes. This figure provides the rational why we started investigating Hsf1 as a candidate with a potential relation to B2 Biology and a potential effect on B2 RNA processing.

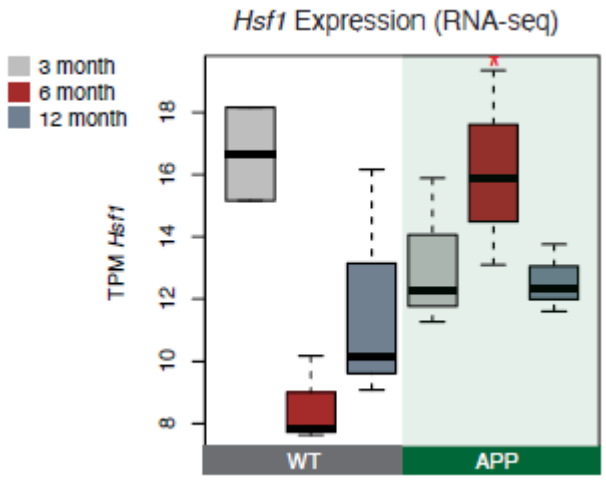

Figure 2.10. Hsf1 is up-regulated in 6m old APP mice.

Boxplot depicts distribution of expression levels of Hsf1 gene among different age groups of mice between wild type and APP. Values are based on TPM counts of long-RNA-seq data. Statistical significance (p value threshold 0.05) for the comparison between 6-month old APP and 6m old WT ($p = 0.03$) ($n = 3$/group, unpaired non-directional t-test). All the other comparisons between groups and different ages are non-significant.

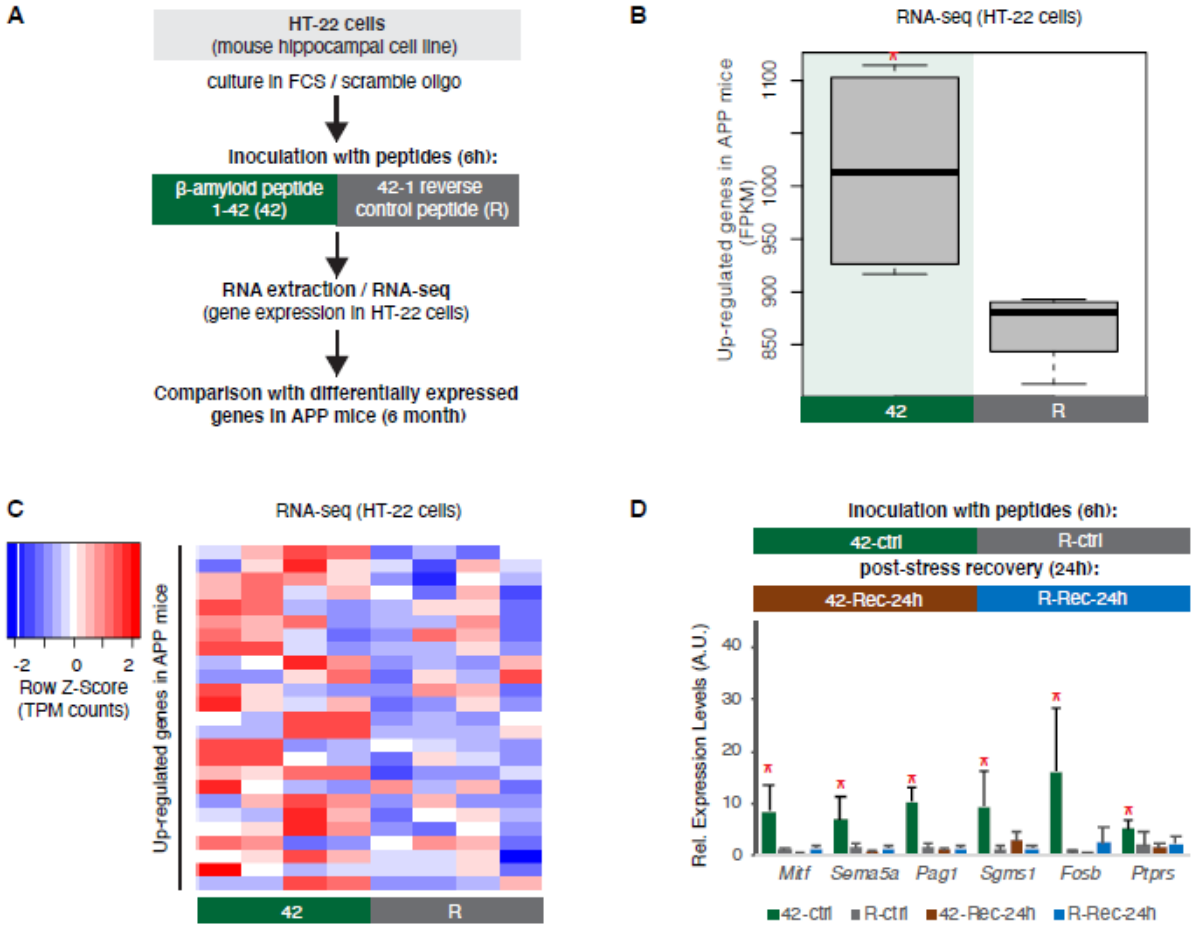

Figure 2.11. A hippocampal cell culture assay for tracking effects of amyloid beta toxicity on B2 RNA stability.

(A) Experimental design for the amyloid toxicity cell culture assay employing HT-22 cells. Cells culture media were supplemented with Fetal Calf Serum (FCS) and the scramble LNA described in Figure 2.14 to allow comparison with the LNA experiments.

(B) Expression levels as defined by long-RNA-seq of genes up-regulated in amyloid pathology (6-month old APP mice) that are also up-regulated in amyloid toxicity (25 genes, Table 2.8). Boxplot depicts distribution of expression levels (in FPKM / Fragments per Kilobase per Million) of these genes between the two conditions in HT-22 cells. p = 0.05 for the comparison between HT22 samples transfected with 1-42 (42) vs 42-1 reverse control peptide (R) (depicted as asterisk, unpaired non-directional t-test, n = 4/group).

(C) Heatmap showing gene expression changes during incubation with amyloid peptides in HT22 cells for genes that are also up-regulated in amyloid pathology (25 genes, Table 2.8) to test whether our cell culture system can simulate the transcriptome observed in amyloid pathology in vivo. Heatmap depicts increase in expression values calculated by long-RNA-seq (TPM values) in the HT22 samples transfected with 1-42 (42) vs 42-1 reverse control peptide (R) (heatmap

columns), for these genes (Table 2.8) (heatmap rows). TPM values are normalized per row. Red color represents higher expression.

(D) Upper panel: Experimental design for the amyloid toxicity assay and a control experiment testing recovery 24h after application of the stress stimulus to confirm return of gene expression levels to pre-stress levels. Lower panel: Confirmation through RT-qPCR of the expression differences of selected B2-SRGs identified in RNA-seq data to differ between HT22 cells transfected with 1-42 (42) and cells transfected with the 42-1 reverse control peptide (R) for 6 hours (Table 2.9). Statistical significance (p value threshold 0.05) is depicted as asterisk for expression in treated cells (42) greater than the expression in controls (R) (unpaired directional t-test, n = 4, error bars represent standard deviation from the mean). In the same graph, we include also expression levels of cells from the same experiment that were left to recover in standard medium without any peptides for 24h after the initial 6h application of the peptides (42-Rec and R-Rec). Expression levels in all genes tested returned to pre-stress levels. Asterisk depicts statistical significance as described above also for the comparison between 42-ctrl and 42-Rec-24h.

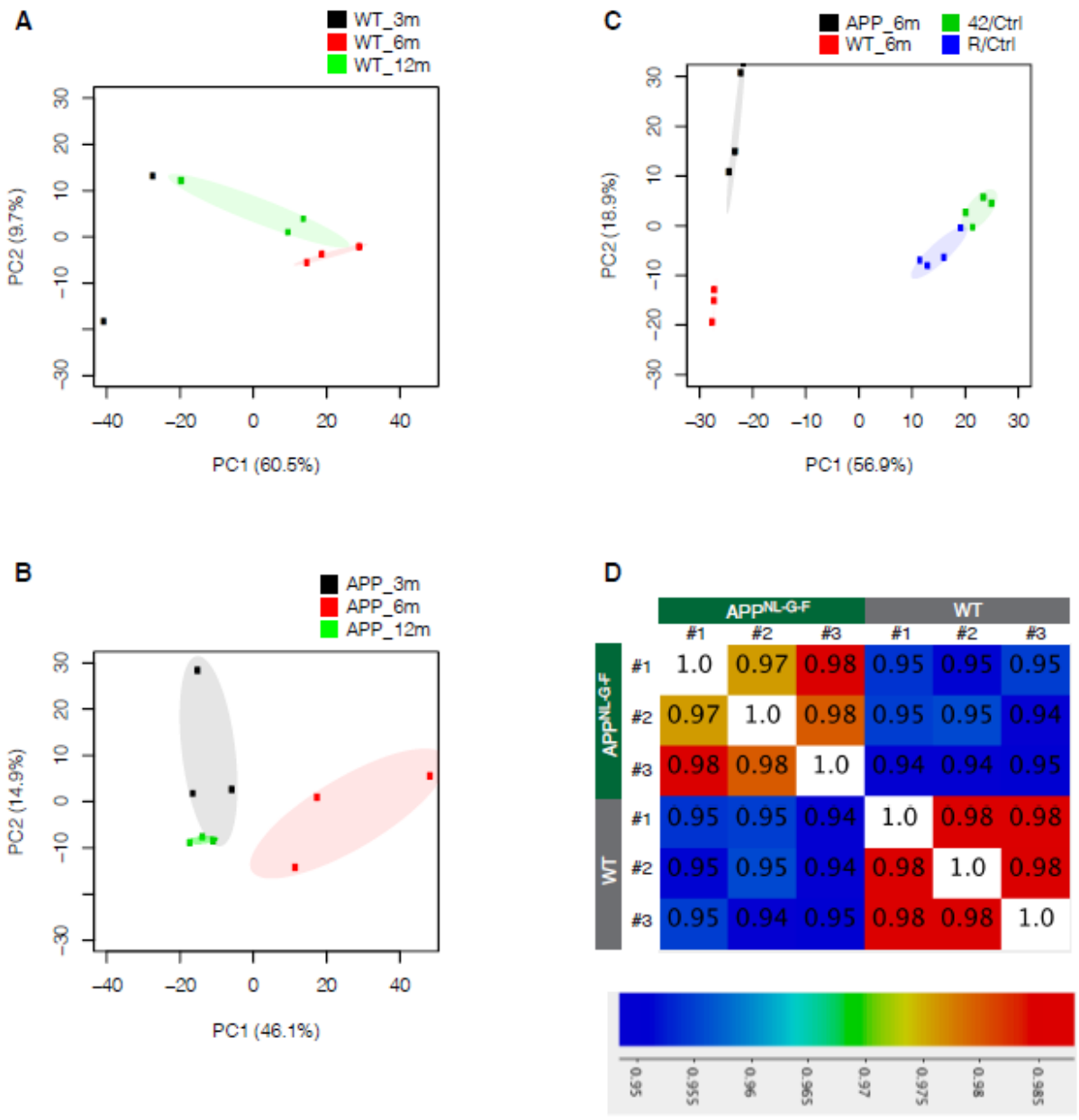

Figure 2.12. PCA plots and correlation matrix for sequenced samples in amyloid pathology and amyloid toxicity models. Plots are based on amyloid pathology genes (Table 2.3). Correlation matrix was constructed using Seqmonk for the reads per million per gene length counts.

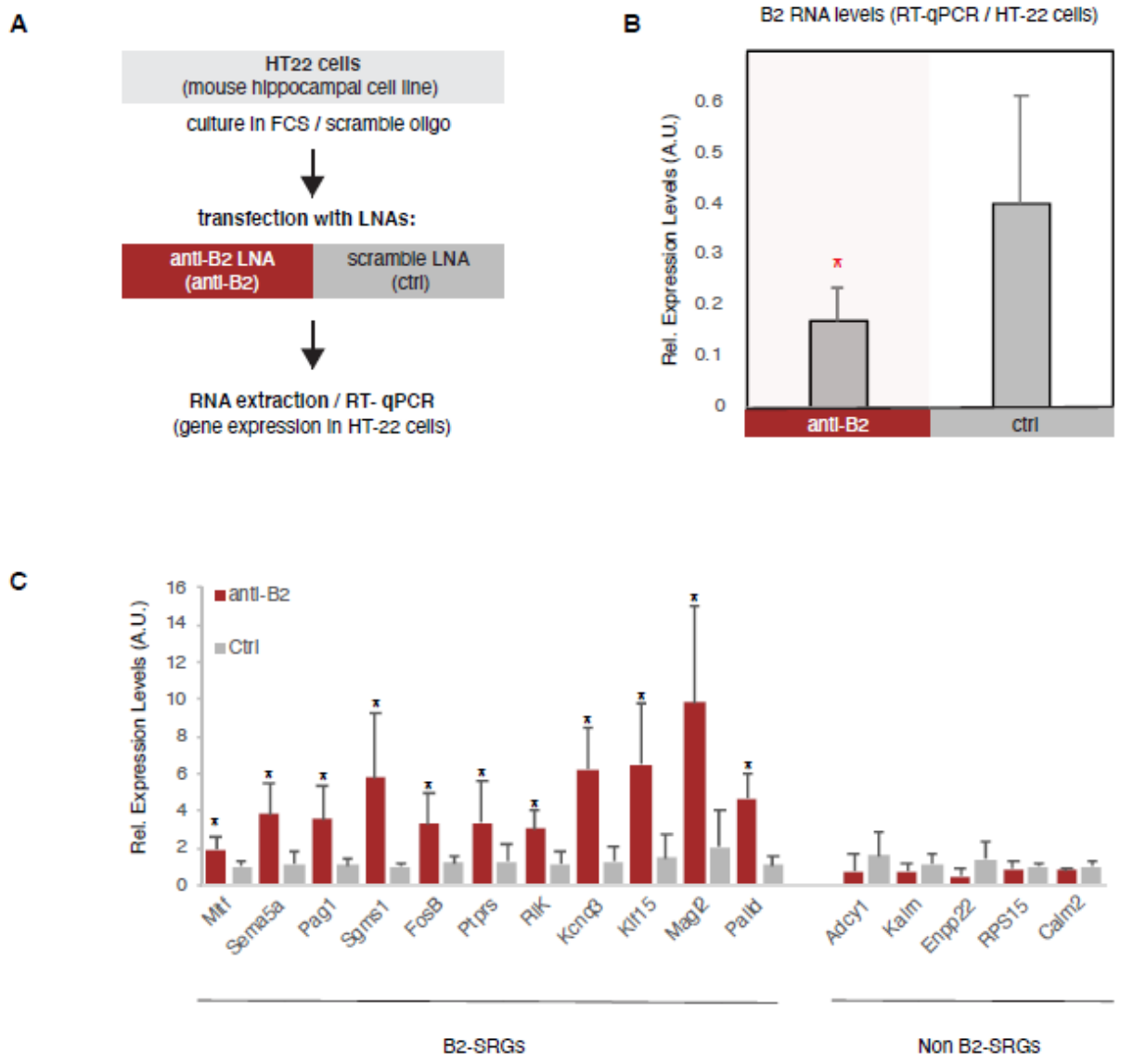

Figure 2.13. B2 RNA destabilization leads to increase in expression of B2-SRGs

(A) Experimental design for the B2 RNA knock-down cell culture assay employing HT-22 cells.

(B) Expression levels of full length B2 RNA (RT-qPCR) in the B2 RNA KD experiment. Statistical significance (p value threshold 0.05) for anti-B2 less than control (depicted as asterisk, n = 3, unpaired directional t-test, error bars represent standard deviation from the mean).

(C) Expression levels (RT-qPCR) of selected B2-SRGs (see Figure 2.4 and Figure 2.11D) and the respective negative controls during B2 RNA KD. Statistical significance (p value threshold 0.05) for anti-B2 greater than control (depicted as asterisk, n = 3/group, unpaired directional t-test, error bars represent standard deviation from the mean). Negative controls include five non-B2 SRGs that show no statistically significant difference between the two conditions.

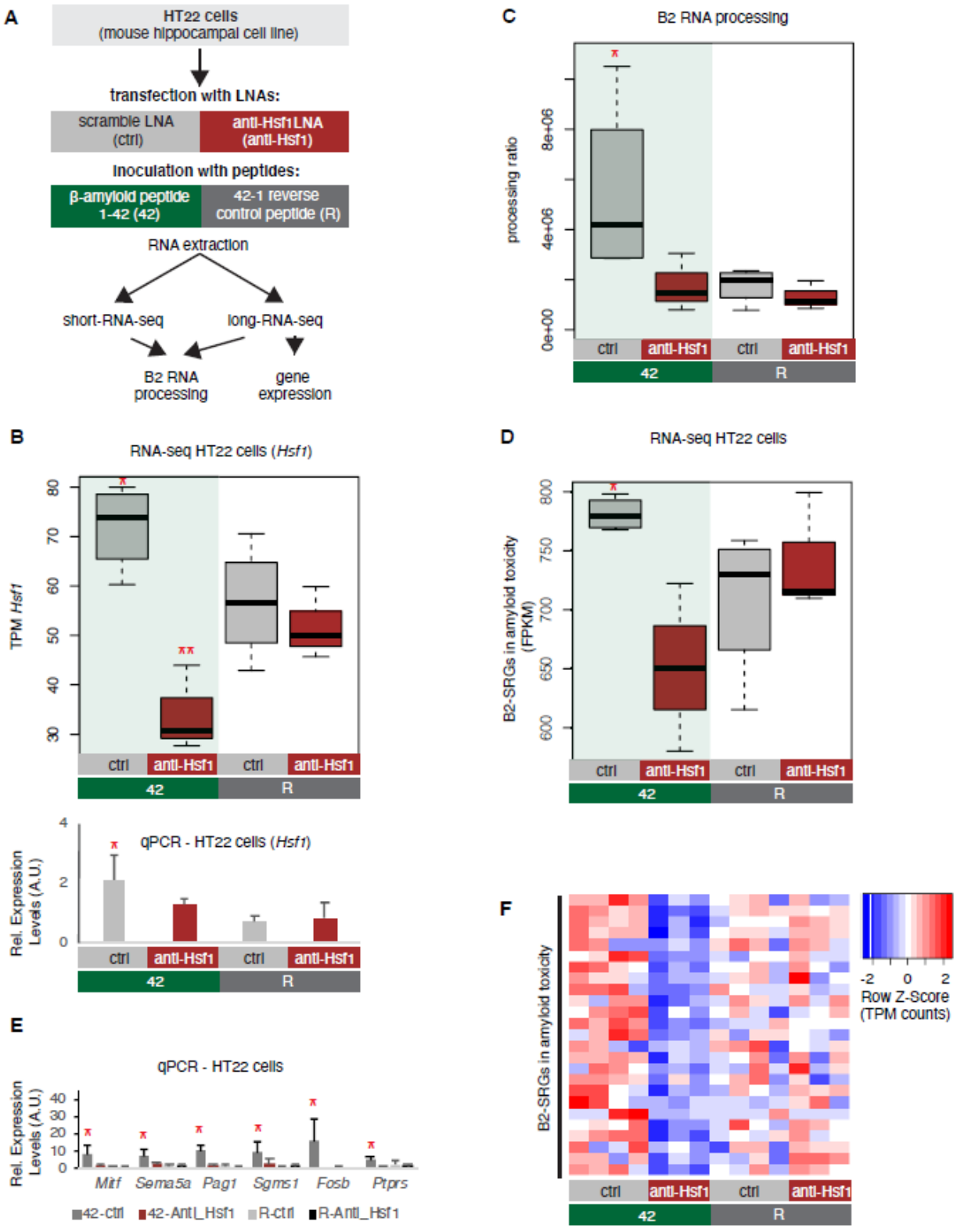

Figure 2.14. Hsf1 mediates B2 RNA processing in amyloid toxicity.

(A) Experimental design of the combined Hsf1 Knock Down – amyloid toxicity assay in HT22 cells followed by short and long RNA-seq.

(B) Expression levels of Hsf1 as defined by long-RNA-seq (upper panel) and RT-qPCR (lower panel). Boxplots compare Hsf1 expression (TPM values) during incubation with the scramble LNA, and anti-Hsf1 specific LNA, incubated with either the 42 or R amyloid peptides. Statistical significance (p value threshold 0.05) for the comparison between 42/ctrl (n = 4) and 42/anti-Hsf1 (n = 3), unpaired non-directional t-test) and for 42/ctrl (n = 4) greater than R/ctrl (n = 4) (both depicted as one asterisk), while two asterisks represent $p < 0.05$ between 42/anti-Hsf1 and the other three groups.

(C) B2 RNA processing ratio based on a combination of short and long-RNA-seq. Boxplot depicts distribution of total SINE B2 RNA processing ratio among different groups of HT22 cells between 42 and R. Statistical significance (p value threshold 0.05) for 42/ctrl greater than R/ctrl ($p = 0.04$, n = 4/group, unpaired directional t-test, depicted as asterisk). No significant difference was observed between 42/anti-Hsf1 and R/anti-Hsf1 (n = 3/group) and between R/anti-Hsf1 and R/ctrl.

(D) B2-SRGs expression levels in amyloid beta toxicity based on long-RNA-seq data (FPKM values) for genes of Table 2.9 (25 genes). Boxplot depicts distribution of expression levels in HT22 cells between 42 and R. $p = 0.05$ for 42/ctrl greater than R/ctrl (n = 4/group, unpaired directional t-test, depicted as asterisk). No significant difference was observed between 42/anti-Hsf1 and R/anti-Hsf1 (NS, n = 3/group) and between R/anti-Hsf1 and R/ctrl.

(E) Expression levels of selected B2-SRGs in the four conditions tested in our amyloid toxicity model though RT-qPCR. Statistical significance (p value threshold 0.05) for 42/ctrl greater than R/ctrl, unpaired directional t-test, n numbers as in subfigure B, with $p < 0.05$ depicted as asterisk, (error bars represent standard deviation from the mean). Samples and values depicted for non-Hsf1 LNA treated samples are the same as in Figure 2.11D and are used as controls as these samples were treated with a scramble LNA to allow comparison with the Hsf1 LNA treated samples.

(F) Gene expression levels (long-RNA-seq) of B2-SRGs that are up-regulated in amyloid toxicity (Table 2.9, 25 genes) show strong association with Hsf1 treatment during response to amyloid toxicity in HT22 cells. Heatmap depicts gene expression with rows as B2-SRGs in amyloid toxicity (Table 2.9) and columns as different HT22 cell treatments. TPM values are normalized per row. Red color represents higher expression.

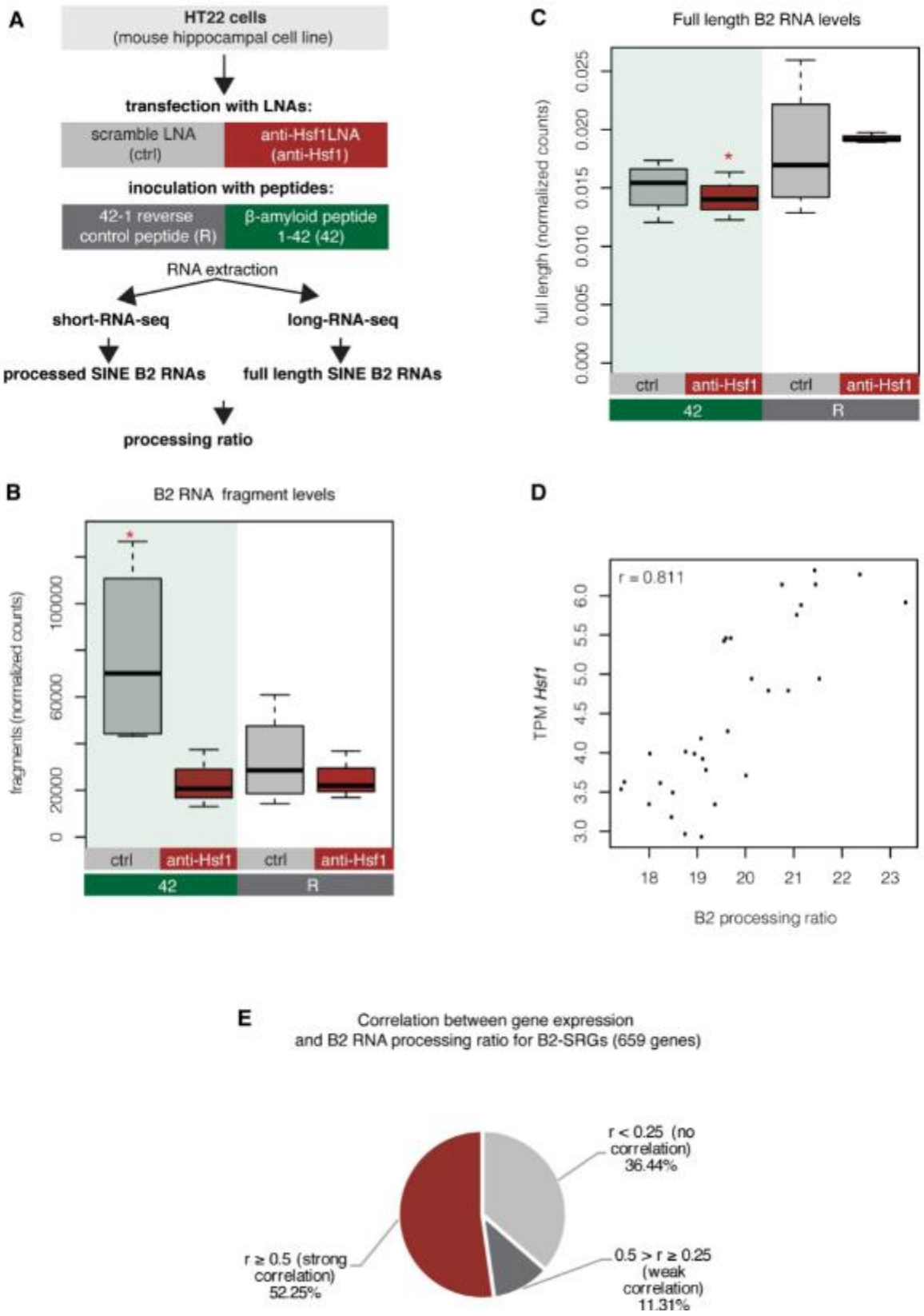

Figure 2.15. B2 RNA levels in HT22 cells and relationship with Hsf1 levels.

(A) Experimental design for estimation of B2 RNA processing ratio based on short and long-RNA seq data in our HT22 amyloid toxicity model.

(B) Boxplot depicts distribution of levels of processed SINE B2 RNA fragments among different conditions. Statistical significance (p value threshold 0.05) for 42/ctrl greater than R/ctrl ($p = 0.03$) ($n = 4$/group, unpaired directional t-test, depicted as asterisk). No significant difference was observed between 42/anti-Hsf1 and R/anti-Hsf1 (NS, $n = 3$/group) and between R/anti-Hsf1 and R/ctrl.

(C) Boxplot depicts distribution of levels of full length SINE B2 RNAs among different conditions. Statistical significance (p value threshold 0.05) for the comparison between 42-anti-Hsf1 and R-anti-Hsf1 ($p = 0.04$) (depicted as asterisk, $n = 3$/group, unpaired non-directional t-test). No significant difference was observed for the other comparisons.

(D) Correlation plot for the relationship between Hsf1 levels and processing ratio in all samples sequenced in the current study (Pearson correlation, r: correlation co-efficient, $p < 0.001$).

(E) Correlation between B2-SRGs expression and B2 RNA processing ratio calculated based on RNA-seq data and short-RNA-seq data from hippocampal samples in the current study. Only B2-SRGs, independently from amyloid beta status, that had read coverage across all samples were considered. For every gene a correlation coefficient was calculated (Pearson correlation) together with the respective p-value. Genes with a correlation p value less than 0.05 were considered in the subsequent analysis (659 genes) that classified them into three categories based on r: i) no correlation ($r < 0.25$); ii) weak correlation ($r = 0.25$ or $r < 0.05$), and iii) strong correlation ($r = 0.5$ or $r > 0.05$). The pie diagram represents the percentage of each category. The exact r and p values of these genes are listed in Table 2.11.

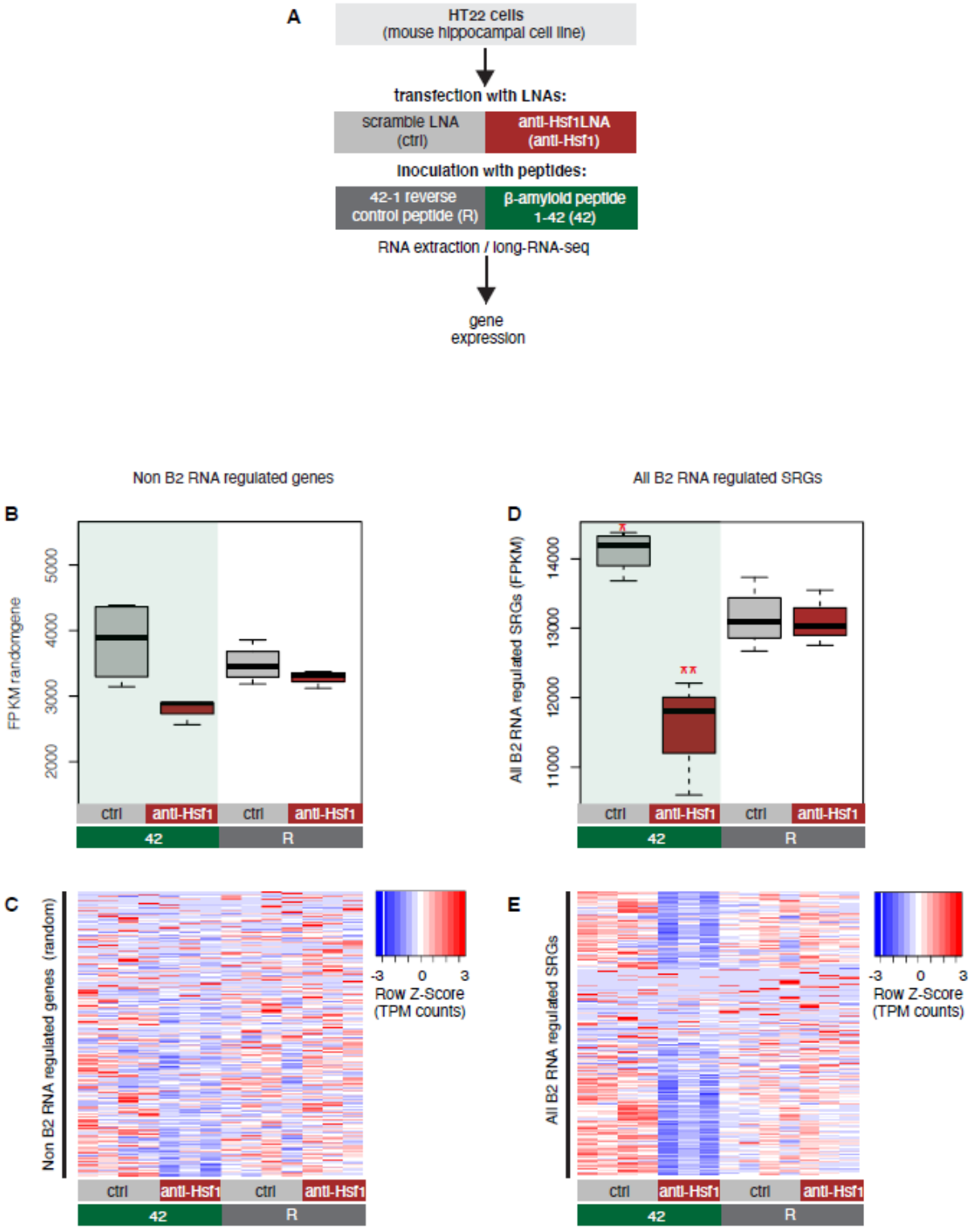

Figure 2.16. Expression levels of all B2-SRGs in amyloid beta toxicity.

(A) Experimental design of the combined Hsf1 Knock Down – amyloid toxicity assay in HT22 cells followed by short and long RNA-seq.

(B) Expression levels of non B2 RNA regulated genes as defined by long-RNA-seq. Boxplot depicts distribution of expression levels (in FPKM / Fragments per Kilobase per Million) among different groups of HT22 cells.

(C) Gene expression levels (defined by long-RNA-seq) of a random set of genes not associated with B2 RNAs (Table 2.12) show weak or no association with Hsf1 treatment during response to amyloid toxicity in HT22 cells. Heatmap depicts gene expression with rows as random genes (non B2 RNA regulated) and columns corresponding to the different HT22 cell treatments. Expression values are normalized per row and correspond to TPM values, with red color represents higher expression.

(D) B2 RNA regulated SRG expression levels based on long-RNA-seq data (FPKM values). Boxplot depicts distribution of expression levels of B2 RNA regulated genes among different groups of HT22 cells between 42 and R (1684 genes, Table 2.1). Statistical significance (p value threshold 0.05) for the comparison between 42/ctrl and R/ctrl ($p = 0.01$) ($n = 4$/group, unpaired directional t-test, depicted as one asterisk) and for 42/anti-Hsf1 less than R/anti-Hsf1 ($p = 0.03$) ($n = 3$/group, depicted as two asterisks, unpaired directional t-test).

(E) Gene expression levels (long-RNA-seq) of B2-SRGs (Table 2.1) show strong association with Hsf1 treatment during response to amyloid toxicity in HT22 cells. Heatmap depicts gene expression with rows as B2 RNA regulated genes (1684 genes, Table 2.1) and columns as different HT22 cell treatments. TPM values are normalized per row. Red color represents higher expression.

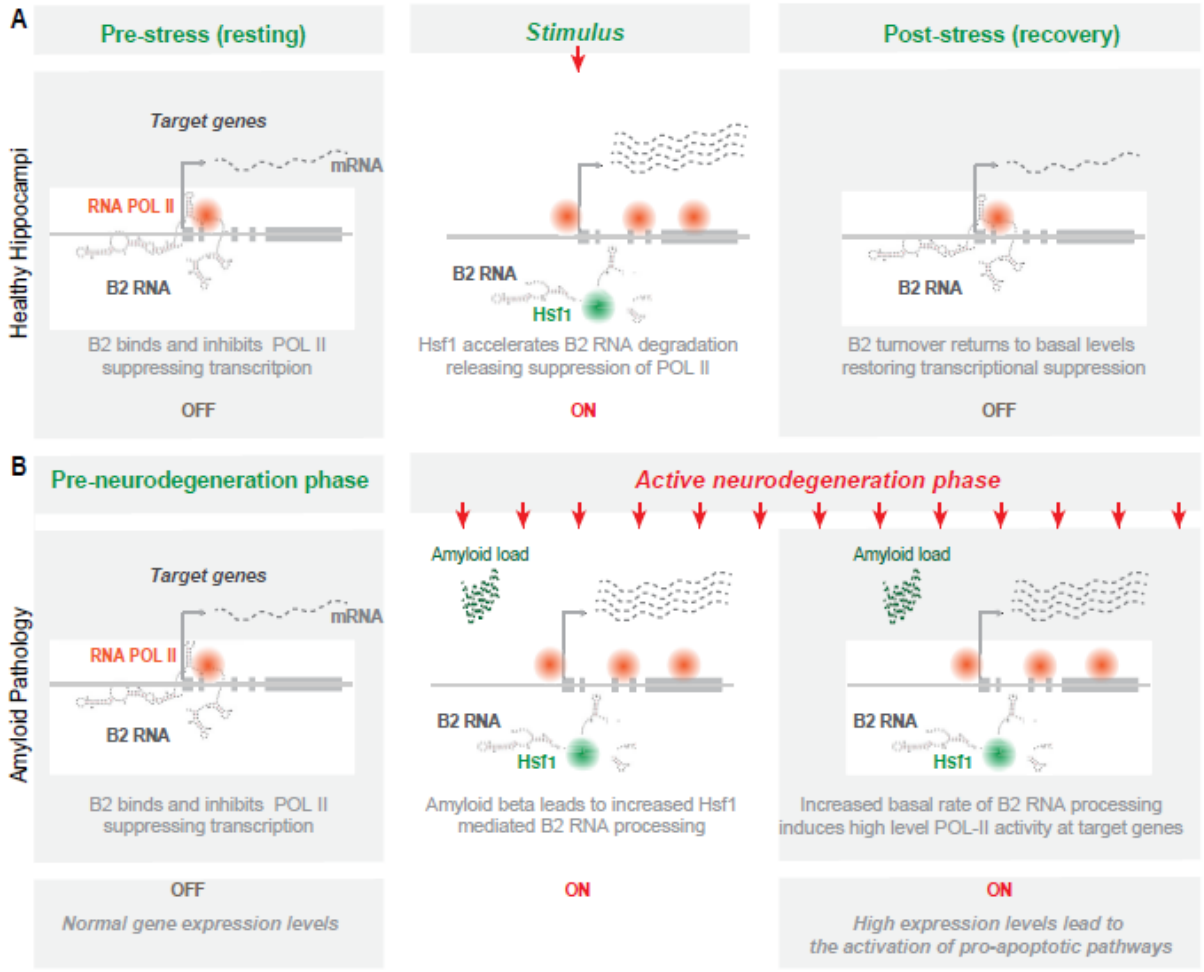

Figure 2.17. Representation of the role of B2 RNA processing in amyloid pathology.

Upon removal of the stress-generating stimulus, healthy cells restore the expression levels of Hsf1, specific B2 RNA regulated target genes and processing ratio of B2 RNAs returns to base levels. In contrast, in amyloid pathology, increased amyloid beta load acts as a continuous stimulus that causes the Hsf1 - B2 RNA – B2-SRG axis to “lock” into an activated mode. ON/OFF represent active and suppressed SRG transcription, respectively.

Chapter 3: Increased Alu RNA processing in Alzheimer brains is linked to gene expression changes

Abstract

Despite significant steps in our understanding of Alzheimer's Disease (AD), many of the molecular processes underlying its pathogenesis remain largely unknown. Here we focus on the role of non-coding RNAs produced by Small Interspersed Nuclear Elements (SINEs). RNAs from SINE B2 repeats in mouse and SINE Alu repeats in human, long regarded as "junk" DNA, control gene expression by binding RNA polymerase II and suppressing transcription. They also possess self-cleaving activity that is accelerated through their interaction with certain proteins disabling this suppression. Here we show that similar to mouse SINE RNAs, human Alu RNAs, are processed, and the processing rate is increased in brains of AD patients. This increased processing correlates with the activation of genes up-regulated in AD patients, while intact Alu RNA levels inversely correlate with the expression of genes down-regulated in AD. In vitro assays show that processing of Alu RNAs is accelerated by HSF1. Overall, our data show that RNAs from SINE elements in the human brain show a similar pattern of deregulation during amyloid beta pathology as in mouse.

Introduction

Amyloid pathology is a required feature of AD, where amyloid beta peptides and their aggregated forms have been associated with AD pathogenesis in brains of Alzheimer’s disease patients as well as neural cell toxicity in mouse models of amyloid pathology (Bloom, 2014; Gonzalez et al., 2018; Ittner et al., 2010; Mehla et al., 2019). However, despite the significant steps made in understanding AD pathogenesis during the last decades, diagnostic tests and

clinical trials for potential therapeutic factors in AD remain inconclusive, as AD remains a highly complex disease, with extreme heterogeneity and many of the molecular processes underlying its pathogenesis still elusive (Bertram, Lill, & Tanzi, 2010; Hane et al., 2017; Toledo, Shaw, & Trojanowski, 2013). Among such molecular mechanisms that have attracted only a little attention until now are transcriptome changes in a class of RNAs produced by retrotransposons called SINE RNAs.

Studies have revealed that levels of SINE B2 and Alu RNAs are elevated during response to stress to suppress transcription through their binding of RNA Polymerase II (Espinoza, Goodrich, & Kugel, 2007; Mariner et al., 2008; Ponicsan, Kugel, & Goodrich, 2010, 2015; Yakovchuk, Goodrich, & Kugel, 2009). This binding contributes to the genome wide transcriptional repression observed during cellular stress by suppressing housekeeping genes, potentially facilitating redistribution of energy resources of the cell to support survival (Mariner et al., 2008). Subsequently, we showed that SINE RNAs can also mediate cellular response to stress in a different way. In particular, we showed that SINE B2 RNAs in mouse show a protein-accelerated self-cleavage activity (Cheng et al., 2020; Hernandez et al., 2020; Zovoilis, Cifuentes-Rojas, Chu, Hernandez, & Lee, 2016), leading to their fragmentation and thus, interfering with their capability of binding to and suppressing RNA polymerase II. As a result, SINE RNAs in mouse act as transcriptional switches during response to stress stimuli by binding RNA Polymerase II at several stress response genes in the pre-cellular stress state and suppressing their transcription. Upon application of a stress stimulus, B2 RNAs are processed, leading to the release of the delayed or stalled RNA polymerase at stress response genes and, thus, their transcription (Zovoilis et al., 2016). Thus, SINE RNAs, based on their processing status, play an important role in stress response through either suppressing (as full length RNAs)

or activating (during processing) gene expression (Figure S3.1 provides a model combining what is known for this mode of regulation of gene expression in mouse).

Interestingly, in a recent study we have shown that this processing and destabilization of B2 RNAs is connected with a pathologic process in the cell, namely amyloid pathology in mouse neural cells (Cheng et al., 2020). In particular, increased amyloid beta load during the active neurodegenerative phase acts as a continuous stimulus that causes an increase in a key stress response factor, called Hsf1. Increased Hsf1 levels accelerate B2 RNA processing and lead the Hsf1 / B2 RNA / stress response genes axis to "lock" into an activated mode with accompanying high levels of pro cell death genes, such as p53 (Cheng et al., 2020).

The above findings have revealed a role for SINE RNA processing in amyloid beta pathology in mouse brain and raised the intriguing possibility that a similar mode of deregulation of SINE RNA processing may also exist in human brain. In humans, SINE Alu RNAs are also able to bind and inhibit RNA Pol II alike to B2 RNAs (Mariner et al., 2008). We have found that, in vitro, much alike B2 RNAs, Alu RNAs are also self-cleaving RNAs and can become destabilized (Hernandez et al., 2020). Thus, in vivo, SINE Alu RNAs in human brains could also be subject to a similar RNA processing as SINE B2 RNAs in mouse brains, assigning a broader role to SINE RNA processing in brain molecular physiology and AD pathogenesis. Here, we investigate this hypothesis by examining whether Alu RNAs are processed in human brains, whether their processing ratio is deregulated in brains of AD patients compared to healthy aging individuals, and the potential mechanisms underlying such a deregulation.

Methods

For Calgary Brain Bank (CBB) short RNA-seq data analysis, standard Illumina adaptor sequences were trimmed off using cutadapt-1.18 (https://doi.org/10.14806/ej.17.1.200). For the construction of the "ALUome" we retrieved Alu sequences for all identified Alu elements (within the range of 280-320 bp in order to exclude truncated forms) from UCSC hg38 Repeat Masker (August 2018) and subsequently collapsed sequences present in our list more than once into one unique representative sequence, resulting only in unique Alu sequences. Alu RNA sequences mapping within known exons, upstream/downstream 300 bp of exons, snoRNAs, microRNAs and tRNAs were filtered out (using as annotation: Hg38, UCSC NCBI RefSeq, sno/miRNA, tRNA Genes). Reads for each sample were mapped to the ALUome using bwa-0.7.17 (Li & Durbin, 2009) aln single end mode, with parameters: maximum edit distance: 0, maximum number of gap opens: 0, disallow a long deletion within bp towards the 3'-end: 100, disallow an indel within bp towards the ends: 100, maximum edit distance in the seed: 0, mismatch penalty: 4, gap open penalty: 22, gap extension penalty: 12. SAM format files generated from mapping were converted to BAM format files using samtools-1.6 (Li et al., 2009), and to files in BED format with bamToBed utility from BEDTools-2.26.0 (Quinlan & Hall, 2010). Then, start positions of reads mapping in the sense direction to each unique Alu of the ALUome were retrieved. For each sample, a matrix was generated with Alu sequneces as rows and counts of read starts for each Alu position as columns, normalized to FASTQ file reads (per 100 million reads). Sum of counts from position above 130 were calculated for each Alu and patient, then the respective count matrices were generated combining each Alu (rows) with the counts in the patients (columns) for position above 130. R (version 3.4.3) (https://www.R-project.org/) package DESeq2 (Love, Huber, & Anders, 2014) was applied to counts above 130 between AD and no AD patients to get differentially expressed processed Alus. To calculate the

Alu RNA processing ratio, Babraham NGS analysis suite Seqmonk 1.45.4 (https://www.bioinformatics.babraham.ac.uk/projects/seqmonk/) was used to obtain the number of reads overlapping with RNA 7SL as well as the read coverage per base along all Alu loci. Processing ratio for each sample was calculated by the processed Alu count obtained from mapping fragments to unique Alus normalized by the RNA 7SL counts and total Alu read coverage per base: [processed fragments (position above 130) / [Alu read coverage per base / RNA 7SL count]].

For ROSMAP study data, RNA-seq data from the AMP-AD Knowledge Portal (https://adknowledgeportal.synapse.org) for the MAP project (Synapse ID: syn3219045) (Bennett, Schneider, Arvanitakis, & Wilson, 2012) was acquired and paired end FASTQ files of each sample were converted from original data in BAM format using utility bam2fq in samtools-1.6. Then, sequencing data was mapped against the ALUome and analyzed generating Alu count matrices. For each sample, a matrix was generated with Alu sequences as rows and counts of read starts for each Alu position as columns, normalized to FASTQ file reads (per 100 million reads). Sum of counts from position 0 to 15 (full length Alu) and above 130 (processed Alus) were calculated for each Alu and patient, then the respective count matrices were generated combining each Alu (rows) with the counts in the patients (columns) for position 0 to 15 and above 130. To get differentially expressed processed Alus, the R package DESeq2 was applied to counts above 130 between no AD patients (with a final clinical consensus diagnosis of no cognitive impairment and a Braak stage: 0 - III) and AD (final clinical consensus diagnosis: Alzheimer's disease and no other cause of cognitive impairment, Braak stage: IV - VI). Processing ratio for each sample was calculated by dividing the processed Alu count obtained from mapping to unique Alus with the full length Alu level count mentioned above.

The decision for the selection of the appropriate method for estimating Alu RNA processing ratio in Short-RNA-seq and RNA-seq data was based on whether the applied RNA selection and library construction protocol maintains both fragments generated by the cut at XR1 (one overlapping with left arm and one overlapping right arm) or only the one at the right arm (Figure 3.1). As shown in Figure S3.10C, short-RNA seq maintains both fragments as depicted by the existence of two major 3'end densities, one around XR1 and one around the expected end of the full length Alu RNA. In contrast, RNA-seq of Poly-A RNA filters out the fragment overlapping the left arm, as now increased density is observed around XR1 position. This is in accordance with the poly A selection step used, which would select only the full length fragment and the processed fragment at the right arm. Thus, position 0-15 is expected in the standard RNA seq protocol to map only full length Alu reads, which is why the count at this position is used for the estimation of the processing ratio at Figure 3.4. In contrast, for short RNA-seq, the 0-15 position count number includes both full length and fragmented RNAs. Thus, for the estimation of the processing ratio in short-RNA-seq samples, we used the total Alu read coverage per base that is independent from the position of the mapping of the 5' end of the reads. As in our previous studies in mouse, the SINE RNA levels were normalized to a Pol III transcript (7SL RNA) to account for non-specific degradation by nucleases. As shown in Figure S3.10D, as expected, we observed no difference in 7SL levels between the two groups of patients, supporting the use for the per sample normalization.

Regarding gene expression analysis of MAP patients, reads for each sample were mapped to the reference genome acquired from ensemble (GRCh38 / November 2018, primary assembly) using hisat2-2.1.0, in single end mode, with the following parameters: Report alignments tailored for transcript assemblers including StringTie and searches for at most 1 distinct, primary

alignments for each read (Kim, Paggi, Park, Bennett, & Salzberg, 2019). SAM format files generated from mapping were converted to BAM format files using samtools-1.6, and to files in BED format with bamToBed utility from BEDTools-2.26.0. FPKM (Fragments Per Kilobase of transcript per Million) for genes were generated using StringTie-1.3.4d, with the following annotation: ensembl GRCh38 patch 94 gff3 file, and parameters: limits the processing of read alignments to only estimate and output the assembled transcripts matching the reference transcripts given in annotation and excluding non-regular chromosomes, then normalized gene FPKM with RN7SL2. R package DESeq2 was applied to gene counts to perform differential gene expression analysis between no AD and AD individuals (with padj < 0.05 used as thresholds for reporting). For data visualization, statistics and differential expression analysis we employed R (version 3.4.3) with r in scatterplots corresponding to Pearson correlation coefficient (https://www.R-project.org/). In the boxplots, the central band (the line that divides the box into 2 parts) represents the median of the data, the ends of the box show the upper (Q3) and lower (Q1) quartiles, the extreme line shows Q3+1.5xIQR to Q1-1.5xIQR (the highest and lowest value excluding potential outliers), while dots beyond the extreme line show potential outliers.

For the cellular deconvolution approach, we used the R (version 3.6.1) package MuSiC (Wang, Park, Susztak, Zhang, & Li, 2019). This was implemented to estimate cell type proportions from MAP project data based on the Allen Brain Map Anterior Cingulate Cortex (ACC) SMART-seq dataset (https://portal.brain-map.org/atlases-and-data/rnaseq/human-v1-acc-smart-seq).

Gene expression analysis of microglia RNA-seq data (Synapse ID: syn11468526) from ROSMAP study was also conducted with the same analysis pipeline as described for MAP patients above, and subsequently gene expression levels of the two datasets were compared.

Patients with available H3K9ac ChIP Seq data from ROSMAP study (Synapse ID: syn4896408) overlapping with tested MAP RNA Seq patients were identified, and filtered bam files against the provided peak file (H3K9acDomains.bed) were obtained with the intersectBed utility from BEDTools-2.26.0 (Quinlan & Hall, 2010). Then metagene plots of the filtered bam files for the different gene lists were generated using Seqmonk.

Results

Short-RNA sequencing identifies processing at the right arm of Alu RNAs in human hippocampus

Much alike SINE B2 RNAs, SINE Alu RNAs can bind RNA Polymerase II and suppress transcription. In the absence of an intact Alu RNA region binding Pol II, for example after fragmentation of the Alu RNA, this binding and suppression of Pol II cannot take place (Figure 3.1A) (Ponicsan et al., 2010; Yakovchuk et al., 2009). This is of particular interest, given that we have recently shown that Alu RNAs, as in the case of B2 RNAs, are self-cleaving RNAs (Hernandez et al., 2020). In mouse, we have shown that processing of SINE RNAs in both NIH/3T3 cells and mouse hippocampus takes place at a position within the RNA region that binds and suppresses RNA Polymerase II (Cheng et al., 2020). Interestingly, previous studies have identified a similar Pol II binding and suppression region also in Alu RNA. In particular, Alu RNA consists of two parts (arms) and the Alu RNA's 3' part (right arm), including the nucleotide bridge connecting the two arms, has been reported as the part of the Alu RNAs that is necessary for binding and suppression of RNA Polymerase II (Mariner et al., 2008). Thus, we questioned whether Alu RNAs are processed within their Pol II binding and repression region also in human brain.

To test this, we extracted RNA from post-mortem hippocampal tissues from 13 individuals with no clinical signs of Alzheimer's disease from the Calgary Brain Bank (CBB). We then employed an RNA sequencing approach that has been customized for the sequencing of SINE RNAs and their fragments (short-RNA-seq). This library construction approach reduces any potential bias introduced through RNA fragmentation, that is used in standard long RNA-seq protocols, which is optimal for the identification of short SINE Alu RNA fragments (< 200nt) that may be produced by Alu RNA processing. The version of short-RNA sequencing we have used for Alu RNAs is similar to the version used in our previous work for SINE B2 RNAs (Zovoilis et al., 2016), but modified to include also the full length Alu RNAs that are approximately 300 nt long.

In contrast to B2 elements studied before in inbred mouse models and cell lines, Alu elements show increased genomic sequence variability when tested at the population level, for example in humans. To account for this, after short-RNA-seq, we performed mapping of the sequenced reads not against the human reference genome but against a generated list of all unique Alu sequences that are available in the UCSC Genome Browser (genome.ucsc.edu) Repeat Masker track (repeatmasker.org). Sequenced reads were mapped against the generated unique "ALUome" with an aligner normally used for genomic mapping (no splicing or soft-clipping). Despite being computationally more intensive, this approach also helps to eliminate potential biases due to truncated Alu forms, Alu copy number variations, insertions and deletions that may exist in the genome of tested individuals as well as sequences that are generated through splicing and could intervene with the mapping process.

Subsequently, for every patient, an Alu metagene model was constructed, plotting cumulatively the distribution of the 5' ends of all sequenced RNAs aligning to the ALUome with

regard to their distance from the Alu elements' start. These 5'end read distribution models for each patient across the Alu metagene are presented one above the other in the form of a heatmap in Figure 3.1B. Increased color density in the heatmap represents increased number of 5'ends of sequenced reads mapping to specific positions in the Alu metagene, thus enabling the study of both full length Alu RNAs (mapping within the first 15 nt to account for the variability in sequence among Alus) and their fragments (mapping either at the Transcription Start Site – TSS or beyond) (Figure 3.1B). This approach enabled the determination in our short RNA sequencing data of three processing areas at Alu RNAs. These processing areas are highlighted in the previously described structure of the Alu consensus sequence (Hadjiargyrou & Delihas, 2013) depicted in Figure 3.1C and annotated as X L(eft arm)1, X R(ight arm)1 and XR2. The processing areas include two positions (XR1 and XR2) located within the right arm and the Pol II binding region (depicted as a rectangle in Figure 3.1C). Due to the very high prevalence of small insertions/deletions in the ALUome with regard to Alu consensus sequence, in the current study we opted for the definition of processing areas rather than processing points to present more accurately this level of sequence variability. The distances presented in Figure 3.1B correspond to the distance between the peaks of distributions around each high-density area, with the peak in the TSS region marking position 0 in the distance from TSS.

This data shows, that in human hippocampus, SINE Alu RNAs are processed within their Pol II binding and suppression region, suggesting that the mode of regulation of gene expression though SINE RNA processing previously described in mouse may extend also to human brain.

Alu RNA processing is accelerated in hippocampi of AD patients

We have previously shown that in the hippocampi of a mouse model of amyloid beta pathology, SINE B2 RNA processing is accelerated. We questioned whether a similar mode of de-regulation is present in humans. To this end, we employed post-mortem hippocampal tissue from a group of patients from the Calgary Brain Bank (CBB) clinically diagnosed with AD that was compared to the non-AD individuals tested above. Post mortem delay was comparable between the two groups. De-identified clinical and pathological data for the CBB patients used in the current study are deposited as meta-data in the controlled access next-generation sequencing repository.

In total, we performed short-RNA-seq in RNA from hippocampi from 24 patients, 13 with no clinical signs of AD and 11 diagnosed with AD (labeled as no AD and AD in Figure 3.2, respectively). RNAs were mapped against the ALUome as described above and 5' end counts of Alu RNA fragments mapping to the Pol II binding region of Alu RNA (right arm positions > 130nt from Alu start) were calculated. Subsequently, we identified Alu RNAs that are differentially processed in this region between AD and no AD patients (Figure 3.2A). Processing levels for these Alu RNAs for the two patient groups is presented as a heatmap in Figure 3.2B. As shown in Figure 3.2B, more than 80% of identified Alu RNAs are highly processed in hippocampi of AD patients, with these results being consistent within each group despite the expected variability and heterogeneity among individuals.

This data revealed an increased number of Alu RNA fragments in AD patients, suggesting that the processing of Alu RNAs may be higher in these patients. In order to factor in any differences in the number of fragments due to changes in total Alu RNA levels, counts of Alu RNA processing fragments were normalized to total read coverage per base across the full length Alu RNA sequence (from start to end) (Figure 3.2C). As in case of mouse short-RNA-seq

in our previous studies (Cheng et al., 2020; Zovoilis et al., 2016), in order to factor in any changes in these levels due to any SINE specific degradation of Alu RNAs, we normalized our data with a housekeeping Pol III non-coding RNA transcript (7SL RNA) the levels of which do not vary across AD and no AD patients (see methods). This approach enabled us to estimate the Alu RNA processing ratio in AD and no AD patients, confirming substantially higher levels of Alu RNA processing in AD patients compared to no AD (Figure 3.2D, left panel) ($p = 0.01$, $n = 11$ (AD) / 13 (no AD)), but not a change in total Alu RNA levels (Figure 3.2D, right panel).

Thus, hippocampi of AD patients are characterized by higher destabilization and processing ratios of Alu RNAs in the right arm including the RNA Pol II binding domain, consistent with the similar increased processing of B2 SINE RNAs previously described in the hippocampi of mouse models.

Standard RNA sequencing is able to detect the processing area in the right arm of Alu RNAs

Our strategy until now involved as a proof of principle the employment of short RNA sequencing as the method of choice for studying Alu RNA processing given its proven ability to detect SINE RNA fragments in mouse in the past. Our strategy also involved human hippocampi as the tissue of choice in order to maintain consistency with our previous SINE RNA studies data in mouse (Cheng et al., 2020) (Figure 3.3A). However, when it comes to large scale transcriptome studies in AD, this approach has a number of limitations. Firstly, short RNA-seq is not the first choice for study of mRNAs. In case of large transcriptome projects involving hundreds of patients compared to our small patient cohort, this approach would create the need for additional sequencing per sample, significantly increasing the cost. Moreover, a number of

large-scale RNA-seq projects in AD patients have been completed using standard RNA-seq with a focus on protein coding RNAs. These studies have already generated an immense amount of publicly available data not only in hippocampus but also in other brain regions that are affected during AD, such as cortex. Thus, despite the increased transcript noise that RNA fragmentation in standard RNA-seq may cause, we were compelled to test whether available large-scale standard RNA-seq projects could enable identification of SINE Alu RNA processing at least at the Pol II binding region of the Alu RNA right arm.

In particular, we questioned whether publicly available poly-A selection-based RNA sequencing approaches in AD patients would allow the identification of Alu RNA processing in the Alu right arm. This could be possible in human compared to mouse for a number of reasons. Firstly, Alu RNAs in human are much longer than B2 RNAs (300nt vs 180nt). With a processing area at 135 nt downstream of TSS, the resulting Alu RNA fragment size would fall within the range of most standard RNA-seq protocols in contrast to shorter SINE B2 RNA fragments in mouse. Secondly, despite being non-coding, SINE RNAs contain long 3' end adenosine stretches. This would enable their sequencing in most standard RNA-seq projects that use poly(A) adapters or selection strategies. In addition, due to the poly(A) tail selection, this approach would enable filtering out processed transcripts at TSS and counting only of full length Alu RNAs at this position in contrast to short RNA-seq which at TSS could include both types of transcripts.

To test this, we employed RNA-seq data from one of the largest transcriptome projects in AD completed until now, the Memory and Aging Project (MAP) study that is part of the ROSMAP study. MAP is a longitudinal, epidemiologic clinical-pathologic cohort study with an emphasis on decline in cognitive and motor function and risk of Alzheimer's disease that began

in 1997 and is run from Rush University (Bennett et al., 2012). The Broad Institute's Genomics Platform performed the RNA-seq (Mostafavi et al., 2018). The study employed poly(A) based RNA sequencing for the study of mRNAs and includes RNA sequencing data from the gray matter of the dorsolateral prefrontal cortex, accompanied with various clinical and demographic metadata including clinical diagnosis, Braak staging, ApoE genotype and age. Sequence data from this project was obtained from the AMP-AD Knowledge Portal (https://adknowledgeportal.synapse.org) and FASTQ files were reconstructed and then re-analyzed with the exact same pipelines used in our CBB patient cohort. In addition, given that this data offers the possibility to study also mRNA expression, we applied in parallel a typical mRNA analysis pipeline, involving mapping against the genome (with splicing), transcriptome assembly and quantification, in order to be able to associate our findings in SINE Alu RNAs with gene expression at a later stage (Figure 3.3A). Based on our preliminary quality control, we identified potential batch effects in samples sequenced within a specific time period (year 2013), and these samples were excluded from further analysis. In total data from 241 MAP patients were analyzed.

As shown in Figure 3.3B, mapping of the 5' ends of reads aligning to the ALUome across the Alu metagene confirmed that Alu RNAs can indeed be poly(A) selected and sequenced through this approach generating clear strong read distribution density at the TSS region at the beginning of the Alu elements. Most importantly, it revealed the exact same processing area (XR1 – 135nt downstream of TSS) we have been able to identify through short RNA-seq above, suggesting that generation of this fragment is one of the first steps of processing of the initial poly(A) full length Alu RNA. In contrast, both XL1 and XR2 areas identified in short RNA-seq were not prominent in standard RNA-seq, suggesting that these are processing fragments without

the 3’ poly(A) end, that can be recognised only with methods such as short-RNA-seq that detect both poly(A) and non-poly(A) fragments. The level of transcriptional noise expected due to library RNA fragmentation was low and amenable, with none of the other density areas competing the density at XR1. Moreover, identification of the XR1 processing area was consistent across all MAP patients tested (Figure 3.3B).

This data shows that study of Alu RNA processing is possible also when using standard RNA-seq techniques, expanding significantly our potential to investigate SINE RNAs in already completed large transcriptome studies in human brain.

Alu RNA processing is accelerated in the cortex of AD patients

As in the case of hippocampus, cortex regions are among the primary targets of amyloid pathology in AD. To this end, we investigated whether Alu RNA processing ratio is increased in the dorsolateral prefrontal cortex of AD MAP patients similarly to CBB hippocampal tissues. MAP includes patients with a wide range of clinical diagnosis, including no cognitive impairment (NCI), mild cognitive impairment (MCI) and AD, as well as of patients classified in all Braak stages (from 0 to VI). Similar to our CBB cohort, patients from the MAP cohort were separated into two categories, no AD and AD, based on clinical diagnosis and Braak staging (see methods).

As in the case of hippocampus, based on RNAs mapped against the ALUome, we calculated 5’ end counts of Alu RNA fragments mapping to the Pol II binding region of Alu RNA (right arm position > 130nt) of MAP patients. Subsequently, we identified Alu RNAs that are differentially processed in this region between AD and no AD patients (Figure 3.4A). Resembling our observations in the hippocampus, the vast majority of differentially processed

Alus (> 80%) depict increased processing levels in the dorsolateral prefrontal cortex of the AD patient group. These Alu RNAs are presented for all MAP AD and no AD patients in the heatmap of Figure 3.4B. In contrast to short RNA-seq, in standard RNA-seq, due to poly(A) selection, 5' end counts at TSS correspond only to full length Alu RNAs. Thus, we have been able to calculated the Alu processing ratio factoring in the full length Alu RNA levels as described in Figure 3.4C. As in case of hippocampal samples, the Alu RNA processing ratio is significantly elevated in the dorsolateral prefrontal cortices of AD patients (Figure 3.4D left panel) ($p < 0.001$, n = 67 (AD) / 51 (no AD)). Full length Alu RNA levels were also slightly increased, but not to the extent of the processing ratio (Figure 3.4D, right panel, $p = 0.005$).

We then questioned whether our results may be influenced by the patient's age. This is of particular interest given that aging constitutes one of the main risk factors for AD. As shown in Figure 3.4E and Figure 3.4F, increased Alu RNA processing ratio is a distinct characteristic of AD patients independently of their age, while no difference was observed regarding full length Alu RNA levels.

We then decided to investigate the association of Alu RNA processing ratio with additional clinical and molecular indicators of AD included in the dorsolateral prefrontal cortices of patients of the MAP study. In particular, the MAP patient cohort includes also a number of patients with clinical diagnosis or pathology data in-between the two categories of no AD and AD patients tested above (for example patients with MCI, and/or intermediate Braak stage). Thus, we questioned whether changes in the Alu RNA processing ratio can mirror differences in the clinical diagnosis and the Braak staging not only of AD and no AD patient categories but of all MAP patients, including those in the middle of the assessed clinical range. Indeed, as shown in Figure 3.5A and Figure 3.5B, processing ratios are gradually being elevated as we move from

low to higher severity cases both regarding clinical diagnosis and Braak staging. Moreover, the MAP study includes information about additional molecular genetics indicators, such as APOE genotypes. APOE gene is associated with the risk of developing late-onset Alzheimer's disease, with the variant APOE e4 (E4) conferring a higher risk (Genin et al., 2011; Green et al., 2009). Interestingly, as shown in Figure S3.2A, when all MAP patients are sorted based on their Alu RNA processing ratio (upper panel of Figure S3.2A), and the presence of the E4 variant in the genotype of each of them is plotted (lower panel of Figure S3.2A), we observed higher Alu RNA processing ratios in most patients with this variant.

The above data suggest that Alu RNA processing is increased also in the cortex of AD patients and it is associated with major clinical, genetic, and molecular pathology markers of AD.

Changes in Alu RNA processing ratio are associated with changes in P53 levels

Neural cell death leading to brain atrophy is a hallmark of AD disease. P53 (TP53) constitutes one of the major markers of cell death and P53 de-regulation has been connected with AD molecular pathology, soluble amyloid beta oligomers and tau hyperphosphorylation (reviewed at (Jazvinscak Jembrek, Slade, Hof, & Simic, 2018) and (Chang et al., 2012)). In our previous study in the mouse (Cheng et al., 2020), we found that SINE B2 RNA processing is associated with high P53 levels, likely as a result of consistently high levels of stress response genes upstream of P53 that are activated by increased B2 RNA processing. Since the MAP patient data included levels of mRNAs in these tissues, we questioned whether a similar association between P53 (TP53) levels and Alu RNA processing ratio exists also in humans. The scatterplot of Figure 3.5C depicts this relationship, revealing a moderately strong correlation

between P53 levels and Alu RNA processing ratio ($r = 0.65$, $p < 0.001$) in AD patients. This strong correlation was only observed with Alu RNA processing ratio (that is indicative of increased gene activation) and not with levels of full length Alu RNAs (Figure 3.5D) (that are indicative of suppression of gene expression). Similar results were observed, as shown in Figure S3.2B, when we investigated the relationship between P53 and Alu RNA processing ratio in all MAP patients, which confirmed the association between the expression levels of this gene and Alu RNA processing ($r = 0.58$, $p < 0.001$) but no association with the full length Alu RNA levels (Figure S3.2C).

This data raised the question whether gene expression of members of pathways that are upstream of P53 are also associated with Alu RNA processing ratio.

Changes in Alu RNA expression and processing are associated with changes in gene expression

As shown above, changes in the Alu RNA processing ratio correlate with P53 levels in MAP patients, which is consistent with our previous studies in mouse fibroblasts and neural cells that connected the activation of gene expression in pro-apoptotic/pro-survival pathways with SINE RNA processing (Cheng et al., 2020; Zovoilis et al., 2016). We decided to investigate the global gene expression in MAP AD patients and search for possible associations between SINE RNA processing ratio and transcriptome changes as it has been previously shown for mouse. To this end, we first analyzed the MAP mRNA data and identified genes that are differentially expressed between AD and no AD patients. These genes are divided into two lists including genes that are up-regulated in AD patients (up-regulated genes) and genes that are down-regulated in AD patients (down-regulated genes).

Should the mode of regulation for activated genes in human be the same as the one described in mouse (Figure S3.1), we would expect a strong positive correlation between high Alu processing ratio and gene expression of up-regulated genes (Figure 3.6A, left panel). In the same way, should the mode of regulation for suppressed genes be the same as the one previously described in mouse, we would expect a negative correlation between high full length (un-processed) Alu RNA levels and gene expression of down-regulated genes (Figure 3.6A, right panel). To test these two hypotheses, we sorted the patients based either on their Alu RNA processing ratio (Figure 3.6B, upper panel) or their full length Alu RNA levels (Figure 3.6C, upper panel), respectively, while in the lower panels we depicted gene expression levels of up- and down-regulated genes, for each of these patients sorted in the same order as the sorted processing ratio or full length levels (Figure 3.6B and Figure 3.6C lower panels, respectively).

As shown in Figure 3.6B, consistent with our hypothesis, increase of Alu RNA processing ratio correlates with gradual increase in the expression levels of up-regulated genes. In fact, gene expression levels of up-regulated genes are strongly correlated with Alu RNA processing ratio in AD patients (Figure 3.6D, $r = 0.88$, $p < 0.001$). No such correlation is observed between up-regulated genes and full length Alu RNA levels (Figure S3.3), in which sorting based on full length Alu RNA levels generates a rather random distribution of gene expression densities across patients. In contrast, as shown in Figure 3.6C and Figure 3.6E, full length Alu RNA levels correlate negatively with gene expression levels of down-regulated genes ($r = -0.42$, $p < 0.001$), in accordance with our hypothesis, while as shown in Figure S3.4, there is a much weaker correlation when the relationship of these genes with Alu RNA processing ratio is tested ($r = - 0.26$).

The changes in expression levels in AD relevant genes reported by RNA-seq correspond to final mRNA levels in the cell and not to the initial levels transcribed by Pol II. These initially transcribed levels may have been subject to a cascade of potential post transcriptional modifications and processing that may have affected stability and half-life of the mRNAs. Thus, final mRNA levels reported by RNA-seq may not correspond completely to the elongation activity of RNA Polymerase II at the chromatin level, for which we are mostly interested in the current study. To this end, we have also employed ChIP-seq data for Histone 3 Lysine 9 acetylation (H3K9ac) that are available for the same patients. H3K9ac is a chromatin mark for the switch of RNA Pol II from transcription initiation to elongation (Gates et al., 2017). Thus, testing this chromatin mark corresponds very well to RNA Pol II elongation activity. As shown in Figure S3.5, H3K9ac occupancy downstream of the transcription start site is significantly increased in AD patients for AD up-regulated genes compared to i) down-regulated genes (Figure S3.5A) or ii) a random set of non-AD differentiating genes (Figure S3.5B). This finding supports that there is an increase in Pol II elongation in AD up-regulated genes.

This data shows that transcriptome changes in SINE RNA are associated with transcriptome and chromatin-wide changes observed in brains of AD patients.

Targeting of Alu RNAs leads to activation of those AD up-regulated genes that are strongly associated with Alu RNA processing

We then questioned to what extend the observed transcriptome-wide changes in AD patients are connected with Alu RNAs ability to suppress transcription, which would justify the increase of expression of potential target genes in AD due to increased Alu RNA processing and alleviation of such suppression.

Despite the overall positive correlation between gene expression and Alu RNA processing ratio in AD patients described in Figure 3.6, it is unlikely that this correlation applies to all 2860 genes that were found to be up-regulated in AD and 627 of them have log2 fold change > 0.5 (Table 3.1). To clarify this point, we estimated the correlation coefficient (r) between gene expression and Alu RNA processing of each of these 2860 genes as well as for a random set of genes that are not differentially expressed in AD as reference. Subsequently, we classified tested genes in two main categories: one including results either non-significant (p value < 0.05) or with weak/no correlation (r less or equal to 0.5) and one including results that are both statistically significant and depict strong or very strong correlation (r more than 0.5). As shown in Figure 3.7A, in accordance with our findings in Figure 3.6, the vast majority of AD up-regulated genes (88%) were classified to the significant and strong correlation group compared to only 26% in the control set of genes.

Gene ontology and pathway analysis of the AD genes identified above to be strongly correlated with Alu RNA processing revealed a statistically significant enrichment (padj < 0.05) for terms directly related with response to cellular stress, cell proliferation, cell death, P53 function, and regulation of transcription and RNA Polymerase activity (Table 3.3). In particular, KEGG pathway analysis of these genes (Table 3.3) revealed enrichment of terms for a number of cell signaling pathways upstream of P53, originally described in cancer, but subsequently attributed also to regulation of learning and memory, chromatin and synaptic plasticity and AD pathogenesis in brain. Among these pathways are MAPK and PI3K-AKT signaling pathways (Figure S3.6) as well as the RAS and HIPPO signaling pathways (Figure S3.7). These results show that not only P53 but also members of upstream regulatory pathways of P53 are strongly associated with Alu RNA processing. Moreover, Gene Ontology term enrichment analysis of Alu

RNA processing correlated genes (Table 3.3) revealed among the top enrichment terms, multiple terms related with regulation of transcription from RNA polymerase II.

We then questioned whether by inducing an artificial degradation of Alu RNAs, we would be able to induce expression of these Alu RNA processing correlated genes in a neural cell culture model frequently used in AD molecular pathology experiments (SHSY5Y cells) (Jazvinscak Jembrek et al., 2018). To achieve this, we employed a similar approach that we used in our previous study in mouse (LNAs against SINE RNAs). Application of a set of LNAs against Alu RNAs was able to reduce levels of Alu RNAs compared to the control LNA (Figure 3.7B, Figure 3.7C). Similar to mouse neural cells and SINE B2 RNAs, targeting of the Alu RNAs in SHSY5Y cells, resulted in the increase of the expression levels of selected AD up-regulated genes that are strongly correlated with Alu RNA processing ratio and also of P53 levels (Figure 3.7D, Figure 3.7E). The increase in gene expression occurred in the absence of any stress stimulus, suggesting that these genes are under the suppressive control of Alu RNAs. At the same time, Alu RNA destabilization did not affect expression of 5 AD up-regulated genes with a weak or no correlation to Alu RNA processing that were used as negative controls.

HSF1 can accelerate Alu RNA processing in vitro

We have shown before, that SINE B2 and SINE Alu RNA processing can be attributed to an endogenous self-cleaving ability of these RNAs that is accelerated in the presence of a protein called Ezh2 in a ribo-switch manner (Hernandez et al., 2020). Subsequently, we expanded the list of B2 RNA processing accelerators to include a protein that is key in cellular response to stress called Heat Shock Factor (Hsf1) and we showed that increased SINE RNA processing during

amyloid beta toxicity in neural cells in mouse can be at least partially attributed to increased levels of Hsf1 (Cheng et al., 2020).

Thus, we questioned whether HSF1 in human is also a potential accelerator of SINE Alu RNA processing as it is for SINE B2 RNAs in mouse. To test this, we incubated the Alu RNA in the presence of the HSF1 protein in vitro under the same conditions used in our previous studies. Then we measured levels of the remaining full length Alu RNA over time in the presence and the absence of HSF1. As shown in Figure 3.8A, incubation of the full length Alu RNA in vitro led to processing and destabilization of the Alu RNA in the presence of HSF1. We then tested the impact on acceleration of Alu RNA processing by HSF1 in the case of heat denaturation of HSF1. As shown in Figure 3.8B, heat denaturation of HSF1 resulted in abrogation of its ability to accelerate Alu RNA processing (Figure 3.8B). Similar results were obtained with the incubation of Alu RNA with another RNA binding protein of similar size to HSF1, Poly A polymerase (HSF1 ~60KDa, Poly A polymerase ~56KDa) (Figure 3.8B). In order to take into account any RNA destabilization due to non-specific degradation, hydrolysis or Alu RNA endogenous self-cleavage, we also incubated Alu RNA in the absence of any HSF1 but in the same buffer and for the same time as the sample with the HSF1 protein, and we also used as controls other RNAs in parallel reactions. In the presence of HSF1 none of these RNAs depicted the destabilization observed in Alu RNAs (Figure 3.8C).

Then we purified the Alu RNA fragments derived in vitro from the incubation with HSF1 and subjected them to the same short RNA sequencing protocol we used for the post mortem samples in order to compare the Alu RNA fragmentation pattern in vitro with that in vivo. As shown in Figure 3.8D, we have been able to identify also in vitro the major cut at Alu RNA right arm we had observed in vivo. Interestingly, the position of the cut was slightly shifted for 11nt

towards the 5’ end, across the poly A bridge. This finding implies that the initial cut in vivo may be subsequently subjected to a yet unclear form of maturation that trims the 5’ end of the generated fragment. Alternatively, given the great genomic sequence diversity of Alu RNA elements among humans, we cannot exclude that the single Alu consensus sequence we used for the in vitro synthesis of the RNA may not correspond completely to the most frequently represented Alu RNAs in the samples we tested from the patients that may include deletions compared to this consensus. However, the lack of whole genome sequencing data from these patients makes clarifying this point challenging.

This data shows that B2 RNA and Alu RNA may share a common factor, HSF1, as a potential accelerator of their processing. To assess this potential in our context we tested the association of Alu RNA processing ratio with regard to HSF1 mRNA levels in the brains of MAP AD patients. Indeed, as shown in Figure 3.8E a strong correlation was found between them in AD patients ($r = 0.72$, $p < 0.001$). In contrast, when an association between HSF1 levels and full length Alu RNA levels was tested, no correlation was found (Figure 3.8F).

This data suggests that similarities observed between mice and humans in vitro, may also extend to SINE RNA processing in human brain.

Discussion

Elucidation of the molecular mechanisms underlying AD pathogenesis comprises an important part of efforts currently underway to understand better this debilitating disease. To this end, recent high throughput approaches and advances in our understanding of novel elements of human transcriptome’s architecture such as RNAs from SINE transposable elements may offer novel perspectives regarding molecular pathology of neurodegenerative diseases.

SINE Alu elements constitute a substantial part of the repetitive non-coding genome in human, being present in millions of copies in human DNA (Walters, Kugel, & Goodrich, 2009). Although SINE elements had been regarded for long as genetic parasites and part of "junk" DNA, numerous studies in recent years have started shedding light into their potential functions in increasing genomic regulatory capabilities through generation of new genomic regulatory sites (Deininger, 2011). However, little is known about the role in human health and disease of the non-coding RNAs generated by these SINE repeats. The identification, some years ago, of the critical ability of SINE B2 and SINE Alu RNAs to regulate transcription through suppression of RNA Polymerase II, both in human and mouse, opened a totally new avenue of possibilities regarding their potential role in cellular function as well as their potential involvement in molecular pathologies (Espinoza et al., 2007; Mariner et al., 2008; Ponicsan et al., 2010, 2015; Walters et al., 2009; Yakovchuk et al., 2009). Subsequently, our recent discovery of the SINE RNA ribozyme/riboswitch potential in response to cellular stress expanded further these possibilities (Hernandez et al., 2020; Zovoilis et al., 2016), and resulted in the identification of a connection between transcriptome deregulation observed in amyloid beta pathology in mouse brain and increased processing of SINE B2 RNAs accelerated by high Hsf1 levels (Cheng et al., 2020).

Here, we show that SINE Alu RNAs are processed also in human brains and reveal increased processing of SINE RNAs as a novel type of transcriptome de-regulation observed in AD (Figure 3.9). These findings allow us to extend to human AD patients our previous conclusions in murine models of AD and deduce that SINE RNAs may be important components of the molecular mechanisms underlying this disease. To this end, this is the first human disease

identified to be connected with the ribozyme-based processing of SINE RNAs and also with a ribozyme-based activity in human in general.

The hypothesis that transposable elements such as Alu elements may play a role in neurodegeneration is not new. Non-coding RNAs and transposable elements in the context of neurodegenerative diseases have been shown to play interesting roles in how neural cells regulate pro-survival and pro-death pathways. For example, tau has been shown to activate transposable elements in Alzheimer's Disease, while pathogenic tau-induced piRNA depletion has been shown to promote neuronal death through transposable element dysregulation in neurodegenerative tauopathies (Sun, Samimi, Gamez, Zare, & Frost, 2018). Moreover, a described protein-RNA interaction between the engrailed homeoprotein b and the LINE-1 retrotransposon has been shown to prevent neurodegeneration in adult dopaminergic neurons (de The et al., 2018). A potential connection of Alu elements with neurodegeneration has been documented in a number of reports and it is very well outlined in a review by Larsen and colleagues (Larsen et al., 2017) that points into the impact of insertions of Alu elements into genes such as TOMM40 that control mitochondrial function. In addition, more than 95% of Adenosine-to-Inosine RNA editing sites have been discovered within Alu regions (Huang et al., 2018) and it is now well established that the major targets for these modifications are Alu elements embedded in mRNAs, especially the retro-transposition-incompetent ones (Nakahama & Kawahara, 2020). In particular, RNA editing in protein coding genes has been shown to be connected with recoding (changes in the protein coding sequence) of protein coding RNAs associated with neurodegenerative diseases including Alzheimer’s disease (Annese et al., 2018; Kanata et al., 2019; Khermesh et al., 2016; Krestel & Meier, 2018; Larsen, Hunnicutt, Larsen, Yoder, & Saunders, 2018; Singh, 2012).

However, until now the role of Alu elements in neurodegeneration has been described mainly as a passive one, via disruption of genomic integrity though their integration into critical regions in the genome or as mediators of RNA editing of the mRNAs in which they are embedded. Here we present evidence about a more active role of SINEs in regulation of gene expression in neurodegenerative diseases, through an independent ribozyme related function of the transcripts generated by these elements. Moreover, a pioneering study by the Ambati lab (Kaneko et al., 2011), revealed a critical role of Alu RNAs in pathogenesis of macular degeneration, through cellular toxicity effects of Alu RNAs. Thus, in addition to the potential direct impact that Alu RNA processing can have on gene transcription through abolition of Pol II suppression, it is likely that increased Alu RNA processing we observe in AD patients may impact cells also in other ways such as through the generation of toxic Alu RNA species.

In this study we employed RNA-seq data from two different sequencing approaches, one customized for these RNAs (short-RNA-seq) and a standard one used in one of the larger transcriptome studies in AD, in order to test whether existing standard RNA seq datasets can be used to study Alu RNA processing beyond the more specific short-RNA-seq approach. Our findings indeed indicate that this data can be used in case of human for study of Alu RNA processing. Being able to use standard RNA seq to study Alu RNA processing has significant advantages with regards to the more specific short RNA seq approach given that existing publicly available data have been generated using standard protocols. Moreover, the list of Alu RNA sequences that were found to be differentially processed in hippocampus of CBB patients was different from that in the prefrontal cortex of MAP patients. This difference could be attributed to either the different tissue source (different transcription levels in different tissues) or to different demographics between the two patient cohorts (genetic variability/CNVs, SNPs,

insertions/deletions), or to a combination of both. Thus, despite the end result being the same (i.e. increased processing of Alu RNAs), the source of these RNAs remains a population of a quite diverse set of Alu genomic elements reflecting human genomic variability, which denotes the need for cost-effective ways to study Alu RNA processing in order to include large patient cohorts that are representative of such variability.

For our analysis we have used RNA-seq data from bulk tissue specimens. Despite their undisputable value, such type of data cannot directly distinguish between neuroglia and neurons. As shown in Figure S3.8, RNA-seq data used in this study express both markers that are predominantly neuronal (such as SLC17A7) and markers that are mainly non-neuronal (such as AQP4) in contrast to RNA-seq dataset from exclusively non-neuronal cells (Figure S3.8A-C). Application of a cellular deconvolution approach revealed that approx. 43% of the cells that contribute to the MAP RNA-seq data are neuronal cells (Figure S3.8D-E). Moreover, both neuronal and neuroglia cells express Alu RNAs (Figure S3.8F). This data excludes the possibility that our findings could be attributed exclusively to either neuronal or non-neuronal cells within this brain tissue, though the exact contribution of each cell type to our results remains unknown. The same applies to the observed correlation between P53 and Alu RNA processing ratio. It is currently unclear whether this is result of microgliosis, astrogliosis neuronal death or combination of these, since our RNA-seq is not single cell specific and all the identified pathways (Table 3.3, Figure S3.6 and Figure S3.7) are cellular stress response and signaling pathways that are universally expressed in all these cell types.

In our analysis we found no correlation between HSF1 levels and full length Alu RNAs. We have included the HSF1 vs. full-length plot in Figure 3.8 as a control to the HSF1 vs. processing ratio plot. In that way we wanted to exclude the possibility that Alu RNAs may be

under the direct transcriptional control of HSF1, which would confound our findings by causing an increase in the denominator of our estimated Alu RNA processing ratio. Our results show that HSF1 is unlikely to be an upstream direct regulator of Alu RNA transcription, as there is practically no correlation with Alu RNA full length levels, and that HSF1 rather exerts its action on Alu RNAs by increasing the proportion of fragmented Alu RNAs. As with many gene circuits and pathways involved in cellular response to stress, there are usually a number of compensatory cellular homeostasis mechanisms in place that through positive and negative feedbacks regulate RNA levels. In our case, it would be reasonable to expect that in vivo there are compensatory pathways that would respond to the reduction of Alu RNA levels by increased processing through an increase of Pol III Alu RNA transcription. This could even result in an increase of total Alu RNA levels after chronic exposure to such stimulus as observed in Figure 3.4D.

Due to the repetitive nature of Alu RNAs, it is currently difficult to make any direct conclusions regarding how many of the Alu sequences tested here originate from Pol III transcripts and how many from transcripts embedded into mRNAs (likely nascent ones). As shown in Figure S3.9, we tried to address this question indirectly by repeating our mapping against the genome, and separating the Alu elements, against which we map the RNA fragments, into two categories: i) Alu elements that fall within gene regions, and (ii) Alu elements outside of gene regions. Despite Alu multiple mapping, a level of information regarding genomic positions that generate Alu RNAs is expected to be maintained through this approach. Therefore, if the mapped Alu RNAs originated exclusively from either only Pol III Alu elements or mRNA embedded Alu elements, we would expect at least some difference in the distribution of fragments between Alu elements of these two categories, as the genic ones overlap with mRNAs. As shown in Figure S3.9, the fact that distribution models are very similar between the two

categories implies that both types of Alu elements may contribute to Alu RNA processing. However, given the limitations posed by the repetitive nature of Alu RNAs mentioned above, it remains difficult to provide an exact number regarding the portion of Alu RNA fragments produced by each category.

In the current study we have justified higher levels of Alu RNA fragments in AD patients as a result of higher processing and destabilization of Alu RNAs, using as reference the full length Alu RNA levels estimated through the Poly(A) selection based RNA-seq in MAP patients. However, it is important to note that acceleration of Alu self-cleavage is likely only one of the ways through which the cell may control Alu RNA levels. Other pathways may also be at play including nucleases or protection through A-I editing. In fact, the 11nt shift in the cutting point we observe in vivo compared to the in vitro processed RNA in Figure 3.8D implies an additional Alu RNA processing step in vivo beyond its self-cleaving activity. We are at the moment unaware of any nuclease defects in AD patients that may be specific to Alu RNA, but such a possibility can also not be excluded.

Our study leaves also some additional open questions. This study is the first to confirm an association between SINE RNA transcriptome and genome wide transcriptome changes in a human tissue. We also showed that in the context of a neural cell line, targeting SINE Alu RNAs in human elicits the up-regulation of various genes in agreement with what was previously described in mouse. However, it remains unclear whether this applies also in vivo since performing such studies in vivo is not possible.

Moreover, our data tested in human the potential role of HSF1 in SINE RNA processing previously observed in mouse only in vitro. Future studies should examine that impact also in cell systems that may resemble neural cells in human brain. Finally, it currently remains

unknown which other factors may be implicated in the increased processing of Alu RNAs in AD beyond HSF1. Elucidating the factors that are upstream of this process may provide additional insight regarding the mechanisms underlying molecular pathology of AD and help advance further our understanding of these RNAs as potential novel therapeutic targets and not just "junk DNA" products.

References

Annese, A., Manzari, C., Lionetti, C., Picardi, E., Horner, D. S., Chiara, M., . . . D'Erchia, A. M. (2018). Whole transcriptome profiling of Late-Onset Alzheimer's Disease patients provides insights into the molecular changes involved in the disease. *Scientific Reports, 8*. doi:ARTN 428210.1038/s41598-018-22701-2

Bennett, D. A., Schneider, J. A., Arvanitakis, Z., & Wilson, R. S. (2012). Overview and Findings from the Religious Orders Study. *Current Alzheimer Research, 9*(6), 628-645. Retrieved from <Go to ISI>://WOS:000308864500003

Bertram, L., Lill, C. M., & Tanzi, R. E. (2010). The genetics of Alzheimer disease: back to the future. *Neuron, 68*(2), 270-281. doi:10.1016/j.neuron.2010.10.013

Bloom, G. S. (2014). Amyloid-beta and tau: the trigger and bullet in Alzheimer disease pathogenesis. *JAMA Neurol, 71*(4), 505-508. doi:10.1001/jamaneurol.2013.5847

Chang, J. R., Ghafouri, M., Mukerjee, R., Bagashev, A., Chabrashvili, T., & Sawaya, B. E. (2012). Role of p53 in Neurodegenerative Diseases. *Neurodegenerative Diseases, 9*(2), 68-80. doi:10.1159/000329999

Cheng, Y., Saville, L., Gollen, B., Isaac, C., Belay, A., Mehla, J., . . . Zovoilis, A. (2020). Increased processing of SINE B2 ncRNAs unveils a novel type of transcriptome deregulation in amyloid beta neuropathology. *Elife, 9*. doi:10.7554/eLife.61265

de The, F. X. B., Rekaik, H., Peze-Heidsieck, E., Massiani-Beaudoin, O., Joshi, R. L., Fuchs, J., & Prochiantz, A. (2018). Engrailed homeoprotein blocks degeneration in adult dopaminergic neurons through LINE-1 repression. *Embo Journal, 37*(15). doi:ARTN e9737410.15252/embj.201797374

Deininger, P. (2011). Alu elements: know the SINEs. *Genome Biology, 12*(12). doi:ARTN 23610.1186/gb-2011-12-12-236

Espinoza, C. A., Goodrich, J. A., & Kugel, J. F. (2007). Characterization of the structure, function, and mechanism of B2 RNA, an ncRNA repressor of RNA polymerase II transcription. *Rna, 13*(4), 583-596. doi:10.1261/rna.310307

Gates, L. A., Shi, J. J., Rohira, A. D., Feng, Q., Zhu, B. K., Bedford, M. T., . . . O'Malley, B. W. (2017). Acetylation on histone H3 lysine 9 mediates a switch from transcription initiation

to elongation. *Journal of Biological Chemistry, 292*(35), 14456-14472. doi:10.1074/jbc.M117.802074

Genin, E., Hannequin, D., Wallon, D., Sleegers, K., Hiltunen, M., Combarros, O., . . . Campion, D. (2011). APOE and Alzheimer disease: a major gene with semi-dominant inheritance. *Molecular Psychiatry, 16*(9), 903-907. doi:10.1038/mp.2011.52

Gonzalez, C., Armijo, E., Bravo-Alegria, J., Becerra-Calixto, A., Mays, C. E., & Soto, C. (2018). Modeling amyloid beta and tau pathology in human cerebral organoids. *Molecular Psychiatry, 23*(12), 2363-2374. doi:10.1038/s41380-018-0229-8

Green, R. C., Roberts, J. S., Cupples, L. A., Relkin, N. R., Whitehouse, P. J., Brown, T., . . . Grp, R. S. (2009). Disclosure of APOE Genotype for Risk of Alzheimer's Disease. *New England Journal of Medicine, 361*(3), 245-254. doi:DOI 10.1056/NEJMoa0809578

Hadjiargyrou, M., & Delihas, N. (2013). The intertwining of transposable elements and non-coding RNAs. *Int J Mol Sci, 14*(7), 13307-13328. doi:10.3390/ijms140713307

Hane, F. T., Robinson, M., Lee, B. Y., Bai, O. W., Leonenko, Z., & Albert, M. S. (2017). Recent Progress in Alzheimer's Disease Research, Part 3: Diagnosis and Treatment. *Journal of Alzheimers Disease, 57*(3), 645-665. doi:10.3233/Jad-160907

Hernandez, A. J., Zovoilis, A., Cifuentes-Rojas, C., Han, L., Bujisic, B., & Lee, J. T. (2020). B2 and ALU retrotransposons are self-cleaving ribozymes whose activity is enhanced by EZH2. *Proceedings of the National Academy of Sciences of the United States of America, 117*(1), 415-425. doi:10.1073/pnas.1917190117

Hodge, R. D., Bakken, T. E., Miller, J. A., Smith, K. A., Barkan, E. R., Graybuck, L. T., . . . Lein, E. S. (2019). Conserved cell types with divergent features in human versus mouse cortex. *Nature, 573*(7772), 61-68. doi:10.1038/s41586-019-1506-7

Huang, Y. W., Cao, Y. Y., Li, J. R., Liu, Y. H., Zhong, W., Li, X., . . . Hao, P. (2018). A survey on cellular RNA editing activity in response to Candida albicans infections. *Bmc Genomics, 19*. doi:ARTN 4310.1186/s12864-017-4374-2

Ittner, L. M., Ke, Y. D., Delerue, F., Bi, M., Gladbach, A., van Eersel, J., . . . Gotz, J. (2010). Dendritic function of tau mediates amyloid-beta toxicity in Alzheimer's disease mouse models. *Cell, 142*(3), 387-397. doi:10.1016/j.cell.2010.06.036

Jazvinscak Jembrek, M., Slade, N., Hof, P. R., & Simic, G. (2018). The interactions of p53 with tau and Ass as potential therapeutic targets for Alzheimer's disease. *Prog Neurobiol, 168*, 104-127. doi:10.1016/j.pneurobio.2018.05.001

Kanata, E., Llorens, F., Dafou, D., Dimitriadis, A., Thune, K., Xanthopoulos, K., . . . Sklaviadis, T. (2019). RNA editing alterations define manifestation of prion diseases. *Proceedings of the National Academy of Sciences of the United States of America, 116*(39), 19727-19735. doi:10.1073/pnas.1803521116

Kaneko, H., Dridi, S., Tarallo, V., Gelfand, B. D., Fowler, B. J., Cho, W. G., . . . Ambati, J. (2011). DICER1 deficit induces Alu RNA toxicity in age-related macular degeneration. *Nature, 471*(7338), 325-+. doi:10.1038/nature09830

Khermesh, K., D'Erchia, A. M., Barak, M., Annese, A., Wachtel, C., Levanon, E. Y., . . . Eisenberg, E. (2016). Reduced levels of protein recoding by A-to-I RNA editing in Alzheimer's disease. *Rna, 22*(2), 290-302. doi:10.1261/rna.054627.115

Kim, D., Paggi, J. M., Park, C., Bennett, C., & Salzberg, S. L. (2019). Graph-based genome alignment and genotyping with HISAT2 and HISAT-genotype. *Nature Biotechnology, 37*(8), 907-+. doi:10.1038/s41587-019-0201-4

Krestel, H., & Meier, J. C. (2018). RNA Editing and Retrotransposons in Neurology. *Frontiers in Molecular Neuroscience, 11*. doi:ARTN 16310.3389/fnmol.2018.00163

Larsen, P. A., Hunnicutt, K. E., Larsen, R. J., Yoder, A. D., & Saunders, A. M. (2018). Warning SINEs: Alu elements, evolution of the human brain, and the spectrum of neurological disease. *Chromosome Research, 26*(1-2), 93-111. doi:10.1007/s10577-018-9573-4

Larsen, P. A., Lutz, M. W., Hunnicutt, K. E., Mihovilovic, M., Saunders, A. M., Yoder, A. D., & Roses, A. D. (2017). The Alu neurodegeneration hypothesis: A primate-specific mechanism for neuronal transcription noise, mitochondrial dysfunction, and manifestation of neurodegenerative disease. *Alzheimers & Dementia, 13*(7), 828-838. doi:10.1016/j.jalz.2017.01.017

Li, H., & Durbin, R. (2009). Fast and accurate short read alignment with Burrows-Wheeler transform. *Bioinformatics, 25*(14), 1754-1760. doi:10.1093/bioinformatics/btp324

Li, H., Handsaker, B., Wysoker, A., Fennell, T., Ruan, J., Homer, N., . . . Proc, G. P. D. (2009). The Sequence Alignment/Map format and SAMtools. *Bioinformatics, 25*(16), 2078-2079. doi:10.1093/bioinformatics/btp352

Love, M. I., Huber, W., & Anders, S. (2014). Moderated estimation of fold change and dispersion for RNA-seq data with DESeq2. *Genome Biology, 15*(12). doi:ARTN 55010.1186/s13059-014-0550-8

Mariner, P. D., Walters, R. D., Espinoza, C. A., Drullinger, L. F., Wagner, S. D., Kugel, J. F., & Goodrich, J. A. (2008). Human Alu RNA is a modular transacting repressor of mRNA transcription during heat shock. *Molecular Cell, 29*(4), 499-509. doi:10.1016/j.molcel.2007.12.013

Mehla, J., Lacoursiere, S. G., Lapointe, V., McNaughton, B. L., Sutherland, R. J., McDonald, R. J., & Mohajerani, M. H. (2019). Age-dependent behavioral and biochemical characterization of single APP knock-in mouse (APP(NL-G-F/NL-G-F)) model of Alzheimer's disease. *Neurobiology of Aging, 75*, 25-37. doi:10.1016/j.neurobiolaging.2018.10.026

Mostafavi, S., Gaiteri, C., Sullivan, S. E., White, C. C., Tasaki, S., Xu, J. S., . . . De Jager, P. L. (2018). A molecular network of the aging human brain provides insights into the pathology and cognitive decline of Alzheimer's disease. *Nature Neuroscience, 21*(6), 811-+. doi:10.1038/s41593-018-0154-9

Nakahama, T., & Kawahara, Y. (2020). Adenosine-to-inosine RNA editing in the immune system: friend or foe? *Cell Mol Life Sci, 77*(15), 2931-2948. doi:10.1007/s00018-020-03466-2

Ponicsan, S. L., Kugel, J. F., & Goodrich, J. A. (2010). Genomic gems: SINE RNAs regulate mRNA production. *Current Opinion in Genetics & Development, 20*(2), 149-155. doi:10.1016/j.gde.2010.01.004

Ponicsan, S. L., Kugel, J. F., & Goodrich, J. A. (2015). Repression of RNA Polymerase II Transcription by B2 RNA Depends on a Specific Pattern of Structural Regions in the RNA. *Noncoding RNA, 1*, 4-16. doi:10.3390/ncrna1010004

Quinlan, A. R., & Hall, I. M. (2010). BEDTools: a flexible suite of utilities for comparing genomic features. *Bioinformatics, 26*(6), 841-842. doi:10.1093/bioinformatics/btq033

Singh, M. (2012). Dysregulated A to I RNA editing and non-coding RNAs in neurodegeneration. *Front Genet, 3*, 326. doi:10.3389/fgene.2012.00326

Sun, W. Y., Samimi, H., Gamez, M., Zare, H., & Frost, B. (2018). Pathogenic tau-induced piRNA depletion promotes neuronal death through transposable element dysregulation in neurodegenerative tauopathies. *Nature Neuroscience, 21*(8), 1038-+. doi:10.1038/s41593-018-0194-1

Tasic, B., Yao, Z., Graybuck, L. T., Smith, K. A., Nguyen, T. N., Bertagnolli, D., . . . Zeng, H. (2018). Shared and distinct transcriptomic cell types across neocortical areas. *Nature, 563*(7729), 72-78. doi:10.1038/s41586-018-0654-5

Toledo, J. B., Shaw, L. M., & Trojanowski, J. Q. (2013). Plasma amyloid beta measurements - a desired but elusive Alzheimer's disease biomarker. *Alzheimers Research & Therapy, 5*(2). doi:ARTN 810.1186/alzrt162

Walters, R. D., Kugel, J. F., & Goodrich, J. A. (2009). InvAluable Junk: The Cellular Impact and Function of Alu and B2 RNAs. *Iubmb Life, 61*(8), 831-837. doi:10.1002/iub.227

Wang, X., Park, J., Susztak, K., Zhang, N. R., & Li, M. (2019). Bulk tissue cell type deconvolution with multi-subject single-cell expression reference. *Nat Commun, 10*(1), 380. doi:10.1038/s41467-018-08023-x

Yakovchuk, P., Goodrich, J. A., & Kugel, J. F. (2009). B2 RNA and Alu RNA repress transcription by disrupting contacts between RNA polymerase II and promoter DNA within assembled complexes. *Proceedings of the National Academy of Sciences of the United States of America, 106*(14), 5569-5574. doi:10.1073/pnas.0810738106

Zovoilis, A., Cifuentes-Rojas, C., Chu, H. P., Hernandez, A. J., & Lee, J. T. (2016). Destabilization of B2 RNA by EZH2 Activates the Stress Response. *Cell, 167*(7), 1788-1802 e1713. doi:10.1016/j.cell.2016.11.041

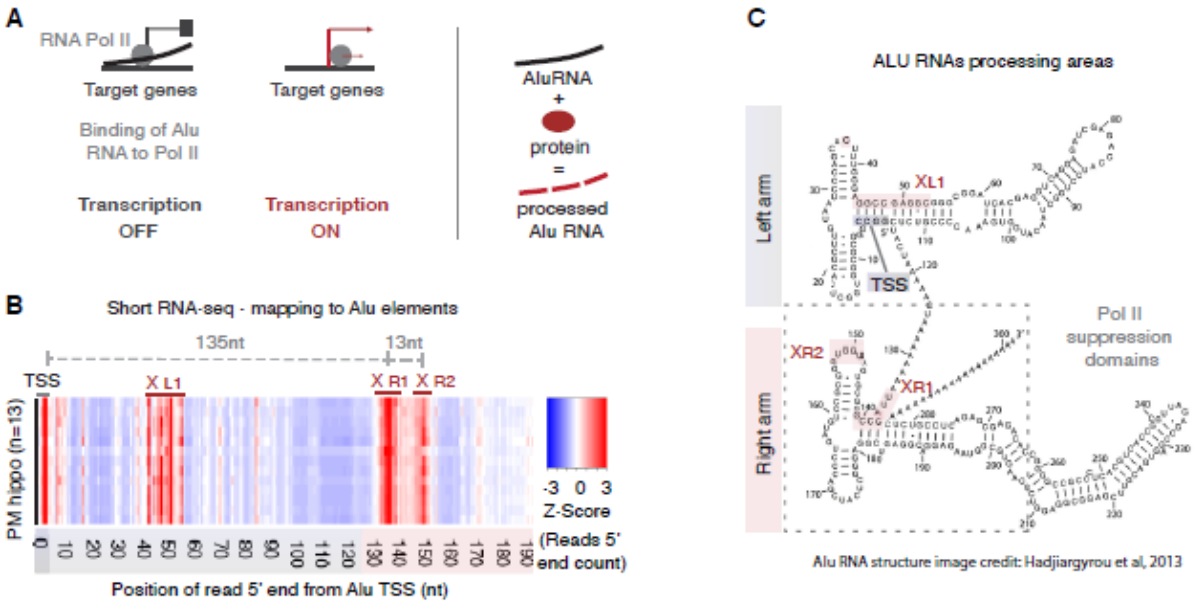

Figure 3.1. Processing areas of Alu RNAs in the human hippocampus as revealed by short-RNA-seq.

(A) Mode of regulation of transcription by Alu RNAs through suppression of RNA Polymerase II (left panel) and protein-accelerated self-cleaving processing properties of Alu RNAs (right panel) as described in previous studies (Hernandez et al., 2020; Mariner et al., 2008; Ponicsan et al., 2010; Yakovchuk et al., 2009).

(B) Plotting of the position of the 5'end of Alu RNA fragments across the Alu metagene to depict potential processing areas of Alu RNAs in all post-mortem hippocampal tissues (PM hippo) from patients from the CBB. Each row in the heatmap depicts the distribution of counts of the 5'ends of reads mapped across the Alu metagene for each patient. The x-axis represents a metagene combining all unique Alu RNA sequences (ALUome) aligned at the start site of their consensus sequence with numbers representing the distance from the Transcriptional Start Site (TSS) area. Heatmap density corresponds to normalized counts of the 5'end of the reads with red corresponding to higher density of these 5'ends at a specific position. XL1, XR1 and XR2 denote the Alu processing areas defined by the high-density areas in the heatmap at specific positions of the Alu metagene, with the middle letter corresponding to the arm of the Alu RNA (see Figure 3.1C, L=Left, R=Right), in which the area is located.

(C) Processing areas of Alu RNAs on the secondary Alu RNA structure. Secondary structure of Alu RNA adapted from Hadjiargyrou and colleagues (Hadjiargyrou & Delihas, 2013). As in our previous studies (Cheng et al., 2020; Zovoilis et al., 2016), we depict the SINE RNA processing areas (highlighted in pink) based on short RNA-seq data and mapping of the 5'ends of Alu RNA fragments. X mark the cleavage sites of Alu RNA that correspond to enriched processing areas (the high densities of 5'end fragments distribution) at the heatmap of Figure 3.1B. The rectangle depicts the critical region that binds and suppresses RNA Pol II based on (Mariner et al., 2008) that may be affected due to processing points.

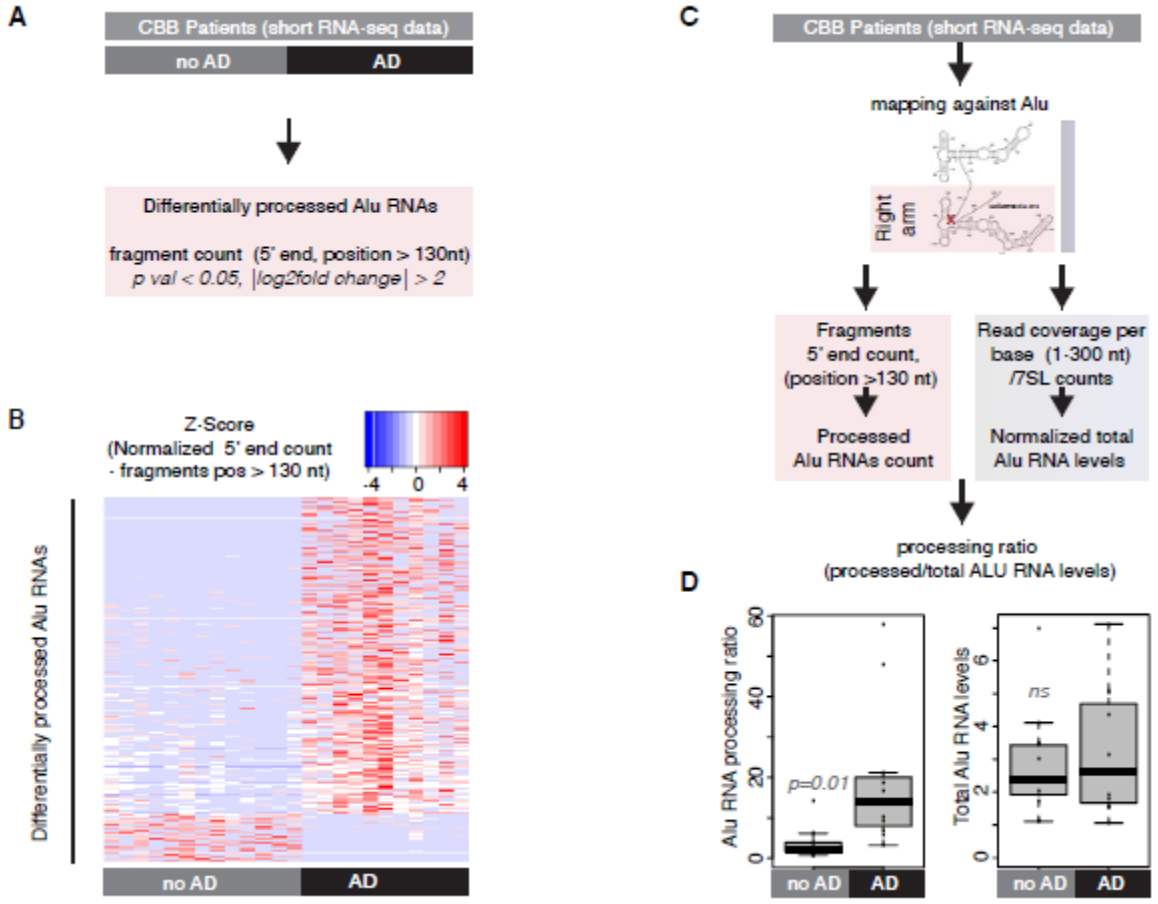

Figure 3.2. Alu RNA processing ratio is increased in the hippocampi of AD patients in CBB cohort.

(A) Analysis design for the identification of differentially processed Alu RNAs between no AD (n = 13) and AD (n = 11) patients of the CBB cohort using the DESeq2 R package. Statistical significance was estimated using the Wald significance tests within the DESeq2 package.

(B) Normalized counts of processed fragments mapping to the right arm of Alu RNAs that are differentially processed (rows) between AD and no AD for each CBB patient (columns). Red corresponds to higher normalized counts of processed Alu RNA fragments.

(C) Analysis design for calculation of the Alu RNA processing ratio in CBB patients short-RNA-seq data.

(D) Boxplots depict differences in hippocampi of AD and no AD patients regarding SINE Alu RNA processing ratio (left panel) (a p value of 0.05 was considered as threshold for statistical significance with p = 0.01, n = 24, unpaired non-directional t-test) and in total Alu RNA levels (right panel) (ns = not significant). In the boxplots, the central band (the line that divides the box into 2 parts) represents the median of the data, the ends of the box show the upper (Q3) and lower (Q1) quartiles, the extreme line shows Q3+1.5xIQR to Q1-1.5xIQR (the highest and

lowest value excluding potential outliers), while dots beyond the extreme line show potential outliers.

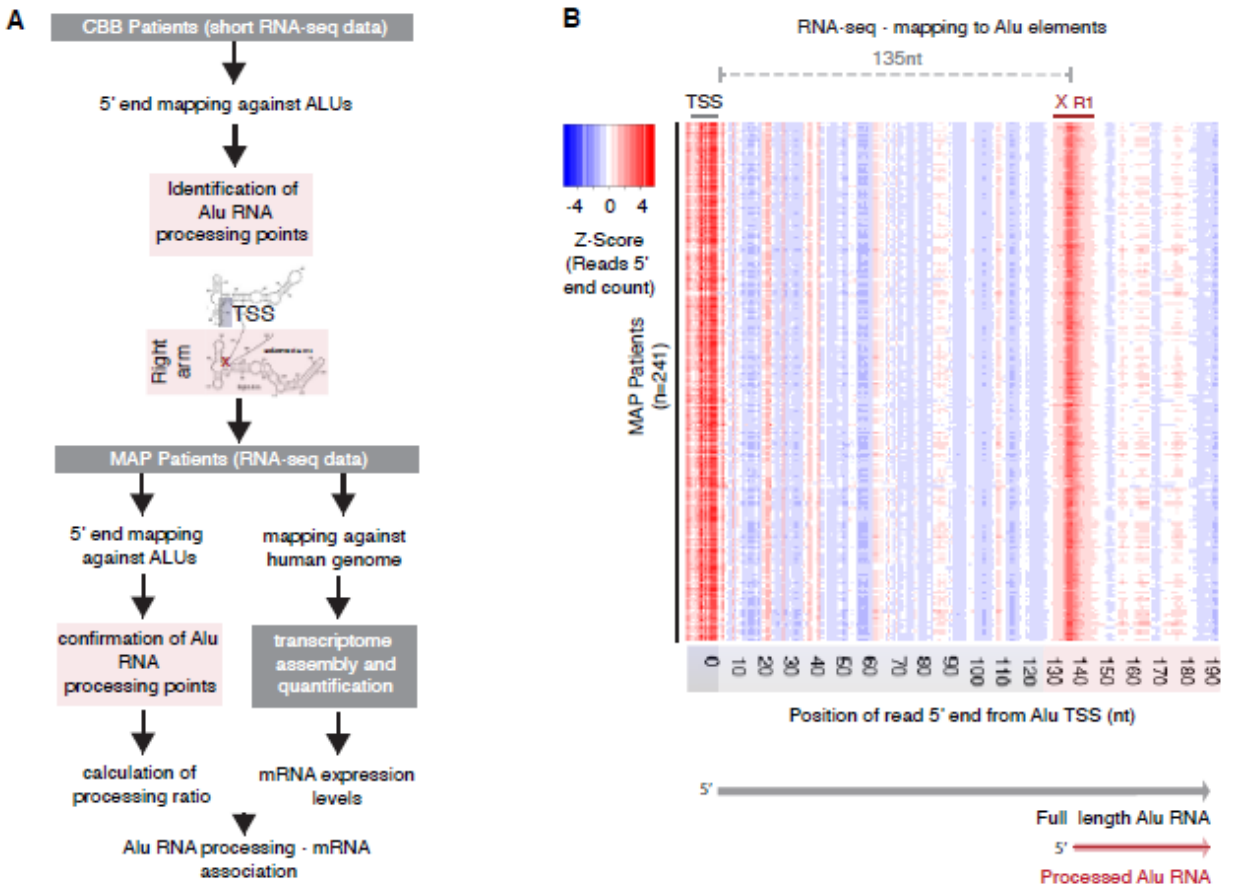

Figure 3.3. Processing areas of Alu RNAs in the human cortex as revealed by RNA-seq.

(A) Two-tier analysis strategy and design for the confirmation of processing areas in Alu RNAs in human brain combining different sequencing approaches and patient cohorts (CBB cohort, n = 24; MAP cohort, n = 241).

(B) Plotting of the position of the 5'end of Alu RNA fragments across the Alu metagene to depict potential processing areas of Alu RNAs in all post-mortem cortex tissues from patients from the MAP cohort. As in Figure 3.1B each row represents the distribution of normalized counts of the 5'ends of reads mapped across the Alu metagene for each patient. As in Figure 3.1B x-axis numbers represent the distance from the Transcriptional Start Site (TSS) area and heatmap density corresponds to normalized counts of the 5'end of the reads with red for higher density of these 5'ends at a specific position. XR1 as in Figure 3.1B.

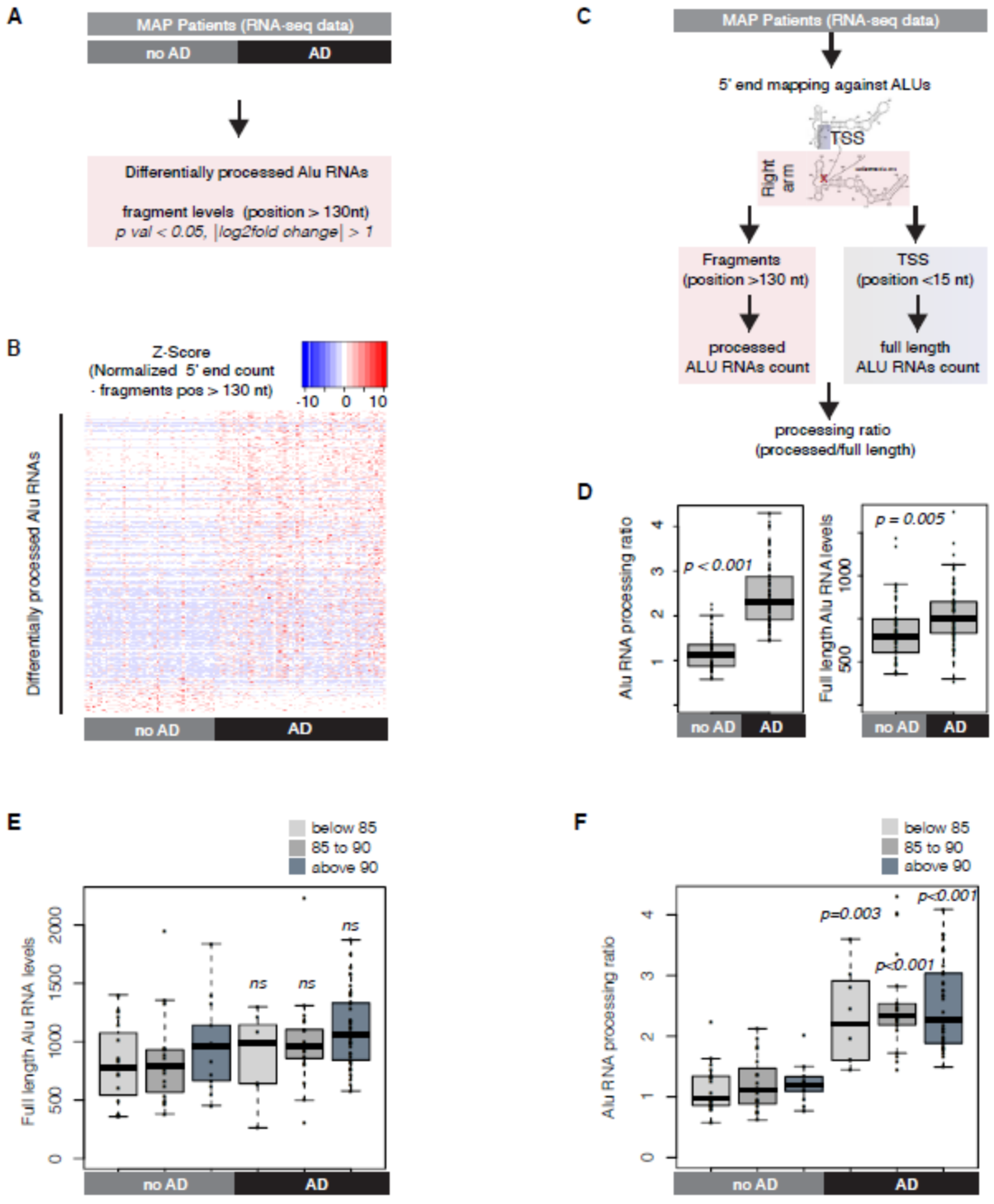

Figure 3.4. Alu RNA processing ratio is increased in the cortex of AD patients in the MAP cohort.

(A) Analysis design for the identification of differentially processed Alu RNAs between AD (n = 67) and no AD patients (n = 51) of the MAP cohort using the DESeq2 R package. Statistical significance was estimated using the Wald significance tests within the DESeq2 package.

(B) As in Figure 3.2B, normalized counts of processed fragments mapping to the right arm of Alu RNAs that are differentially processed (rows) between AD and no AD for each MAP patient (columns). Red corresponds to higher normalized counts of processed Alu RNA fragments.

(C) Analysis design for calculation of the Alu RNA processing ratio in MAP patients' RNA-seq data.

(D) Boxplots depict differences in cortex of AD and no AD patients regarding SINE Alu RNA processing ratio (left panel) (a p value of 0.05 was considered as threshold for statistical significance with $p < 0.001$, n = 118, unpaired non-directional t-test) and in full length Alu RNAs ($p = 0.005$).

(E) Boxplots depict full length Alu RNA levels in cortex of AD and no AD patients separated into three age groups. No significant difference observed between the different age groups of either AD or no AD patients or for the comparisons between no AD and AD of each age group (unpaired non-directional t-test, with $p < 0.05$ considered the threshold for statistical significance, n for no AD = 19 (below 85), 19 (between 85 to 90), 13 (above 90); n for AD = 8 (below 85), 21 (between 85 to 90), 38 (above 90)).

(F) Boxplots depict differences in SINE Alu RNA processing ratio in cortex of AD and no AD patients separated into three age groups. No significant difference observed between the different age groups of either AD or no AD patients. A p value 0.05 was considered as threshold for statistical significance for the comparisons between no AD and AD of each age group (unpaired non-directional t-test, with $p = 0.003$ for the comparison below 85, and $p < 0.001$ for the other two comparisons and n numbers as in (E)).

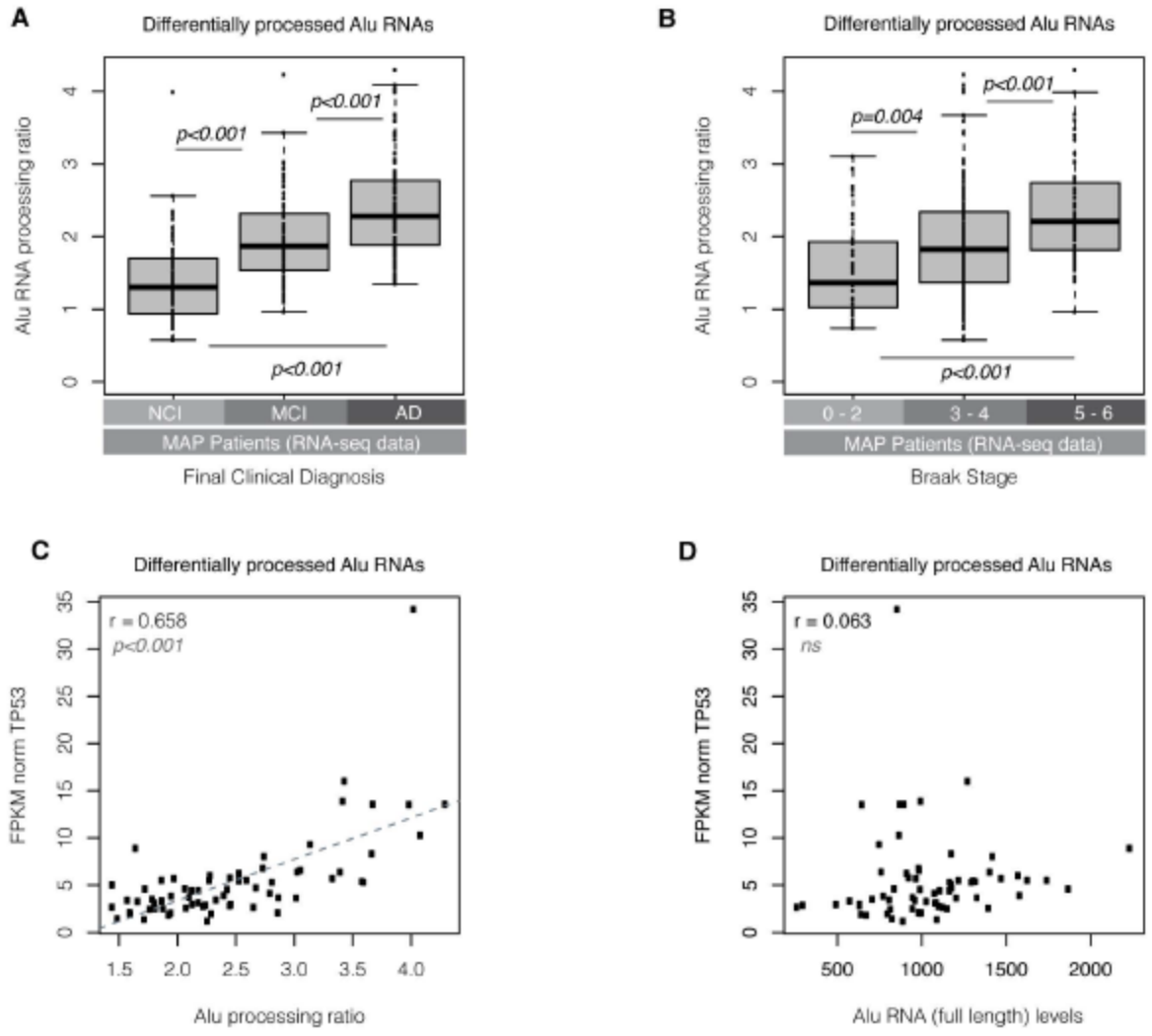

Figure 3.5. Alu RNA processing ratio is associated with clinical, pathology, genetic and molecular markers of AD in MAP patients.

(A) Boxplots depict differences in SINE Alu RNA processing ratio in all MAP patients with regard to final clinical diagnosis ($p < 0.01$ for the comparison between NCI and MCI, between NCI and AD, and between MCI and AD, unpaired, non-directional t-test). NCI = no cognitive impairment (n = 71), MCI = mild cognitive impairment (n = 67), AD = Alzheimer's disease (n = 87).

(B) Boxplots depict differences in SINE Alu RNA processing ratio in all MAP patients (n = 241) with regard to Braak stage classified into three categories ($p = 0.004$ for the comparison between 0-2 and 3-4, and $p < 0.001$ for the comparisons between 3-4 and 5-6 and between 0-2 and 5-6, unpaired, non-directional t-test, n = 39[0-2], n = 148[3-4] and n = 54[5-6]).

(C) Scatterplot depicting the positive correlation between TP53 expression values and Alu RNA processing ratio in AD patients ($r = 0.65$, $p < 0.001$). Statistical test is based on Pearson's product

moment correlation coefficient and follows a t distribution using the cor.test function in R package stats.

(D) Scatterplot depicting no correlation between TP53 expression values and full length Alu RNA levels in AD patients (r = 0.06, no correlation, ns = non-significant). Statistical test as in Figure 3.5C.

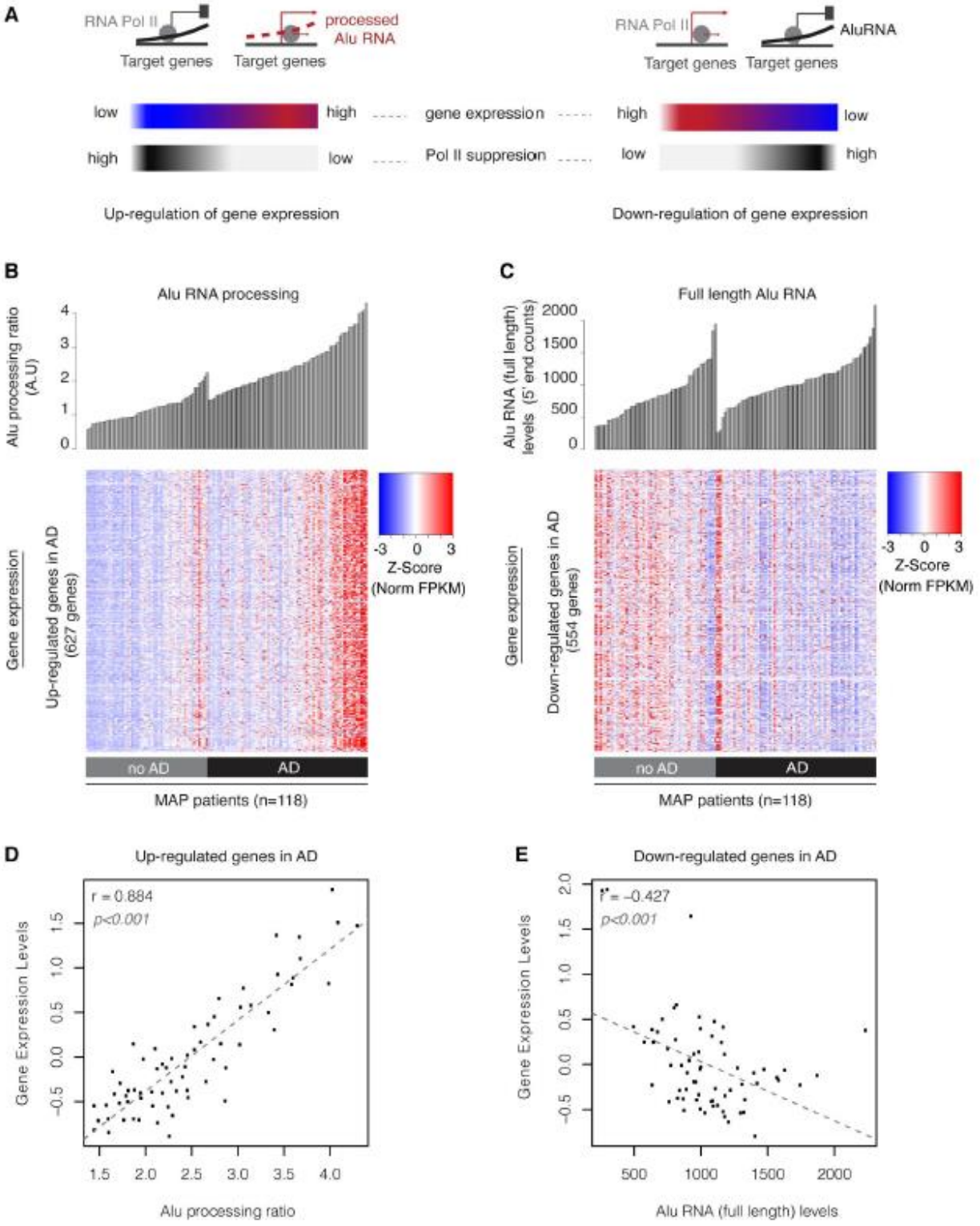

Figure 3.6. Alu RNA expression and processing levels are associated with transcriptome changes in the cortex of MAP patients.

(A) Graphical representation of the expected transcriptome changes with regard to Alu RNA expression and processing levels based on previous findings in mouse (Figure S3.1) and prior reports on the ability of Alu RNAs to control transcription (Mariner et al., 2008; Ponicsan et al., 2010; Yakovchuk et al., 2009) and become self-cleaved (Hernandez et al., 2020).

(B) Association between SINE Alu RNA ratio (upper panel) and gene expression levels (lower panel) of genes up-regulated in AD (Table 3.1). Every column in both panels corresponds to the same MAP patient of either the no AD or AD group. Patients in each group are sorted from left to right in an ascending order with regard to Alu RNA processing ratio. Every row in the heatmap corresponds to one gene, with color density representing normalized FPKM values from RNA-seq for this gene for each patient (columns) (red represents high and blue low expression levels).

(C) Association between full length Alu RNA levels (upper panel) and gene expression levels (lower panel) of genes down-regulated in AD (Table 3.2). Every column in both panels corresponds to the same MAP patient of either the no AD or AD group. Patients in each group are sorted from left to right in an ascending order with regard to full length Alu RNA levels. Every row in the heatmap corresponds to one gene, with color density representing normalized FPKM values from RNA-seq for this gene for each patient (columns) (red represents high and blue low expression levels).

(D) Scatterplot depicting the positive correlation between average gene expression values of up-regulated genes in Figure 3.6B and Alu RNA processing ratio in AD patients ($r = 0.88$, $p < 0.001$). Statistical test is based on Pearson's product moment correlation coefficient and follows a t distribution using the cor.test function in R package stats.

(E) Scatterplot depicting the negative correlation between average gene expression values of down-regulated genes in Figure 3.6C and full length Alu RNA levels in AD patients ($r = -0.42$, $p < 0.001$). Statistical test as in Figure 3.6D.

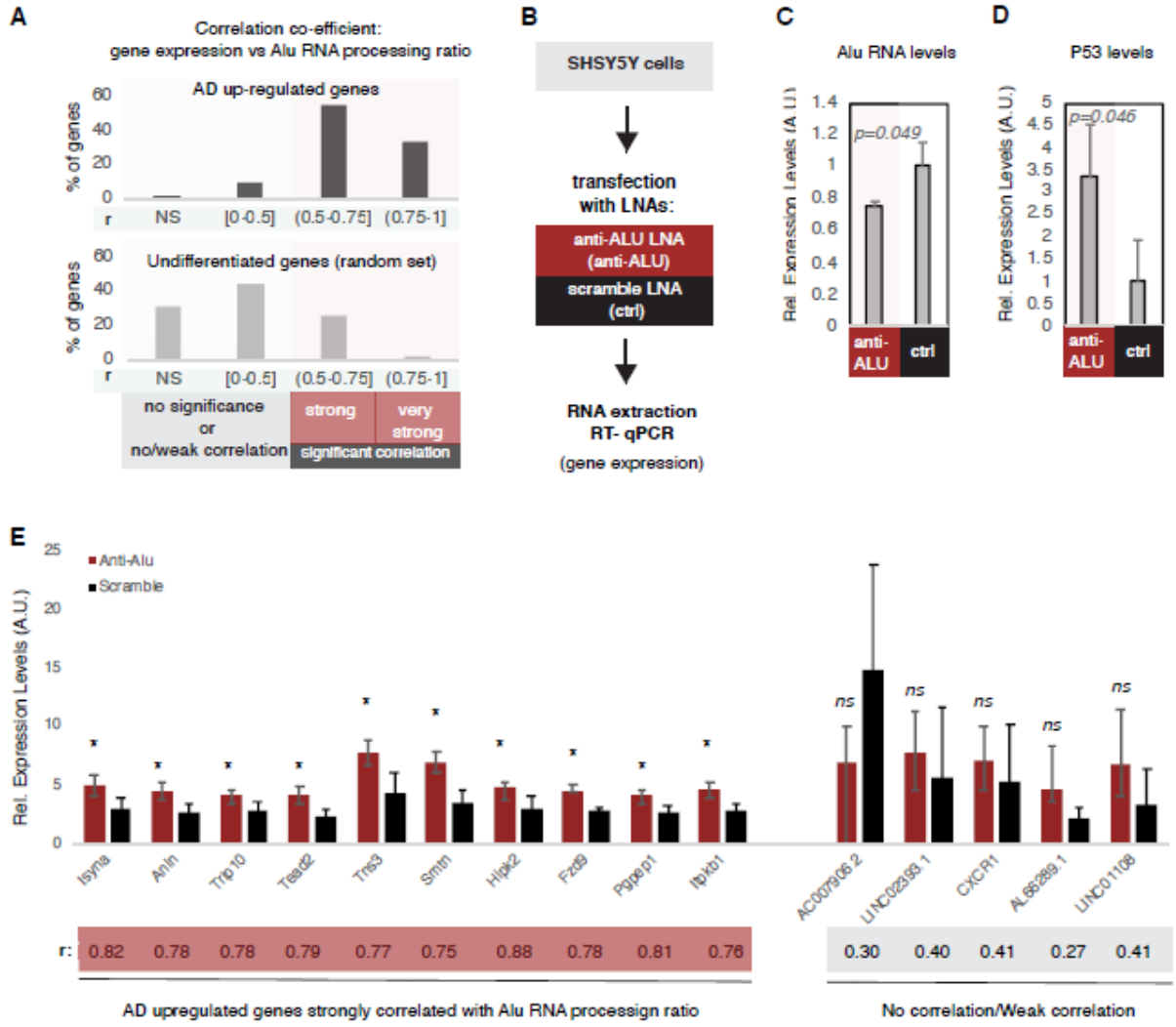

Figure 3.7. Alu RNA destabilization leads to increase in expression of Alu RNA processing correlated genes.

(A) Correlation between gene expression and Alu RNA processing ratio for AD up-regulated genes (upper panel) and a random set of non-differentially expressed genes (lower panel). For every gene a correlation coefficient was calculated (Pearson correlation) together with the respective p-value. Statistical test is based on Pearson's product moment correlation coefficient and follows a t distribution using the cor.test function in R package stats. Based on the r and p value genes were classified into four categories: i) NS, non-significant for p value > 0.05, ii) no correlation or weak correlation ($r \leq 0.05$), iii) significant ($p < 0.05$) and strong correlation ($0.5 < r \leq 0.75$) and iv) significant ($p < 0.05$) and very strong correlation ($0.75 < r$). The bar graphs represent the percentage of each category for each set of genes.

(B) Experimental design for targeting Alu RNAs in a cell culture assay employing SHSY5Y neural cells.

(C) Expression levels of full length Alu RNA (RT-qPCR) in the Alu RNA KD experiment. Statistical significance (p value threshold 0.05) for the comparison between anti-Alu LNA treated samples (anti-Alu) and samples treated with a scramble control LNA (ctrl) with $p = 0.049$ and $n = 3$, unpaired non-directional t-test. Error bars represent standard deviation from the mean.

(D) Expression levels of P53 (RT-qPCR) in the Alu RNA KD experiment. Statistical significance (p value threshold 0.05) for levels in anti-Alu LNA treated samples (anti-Alu) greater than samples treated with a scramble control LNA (ctrl) with $p = 0.046$ and $n = 3$, unpaired directional t-test. Error bars represent standard deviation from the mean.

(E) Expression levels (RT-qPCR) of selected genes from panel A that are either strongly correlated with Alu RNA processing (left, $r > 0.5$) or only weakly/not correlated (right, $r < 0.5$). Statistical significance (p value threshold 0.05) for anti-Alu greater than control (depicted as asterisk, $n = 3$/group, unpaired directional t-test, error bars represent standard deviation from the mean). Pearson correlation co-efficient for each gene is depicted below the name of each gene.

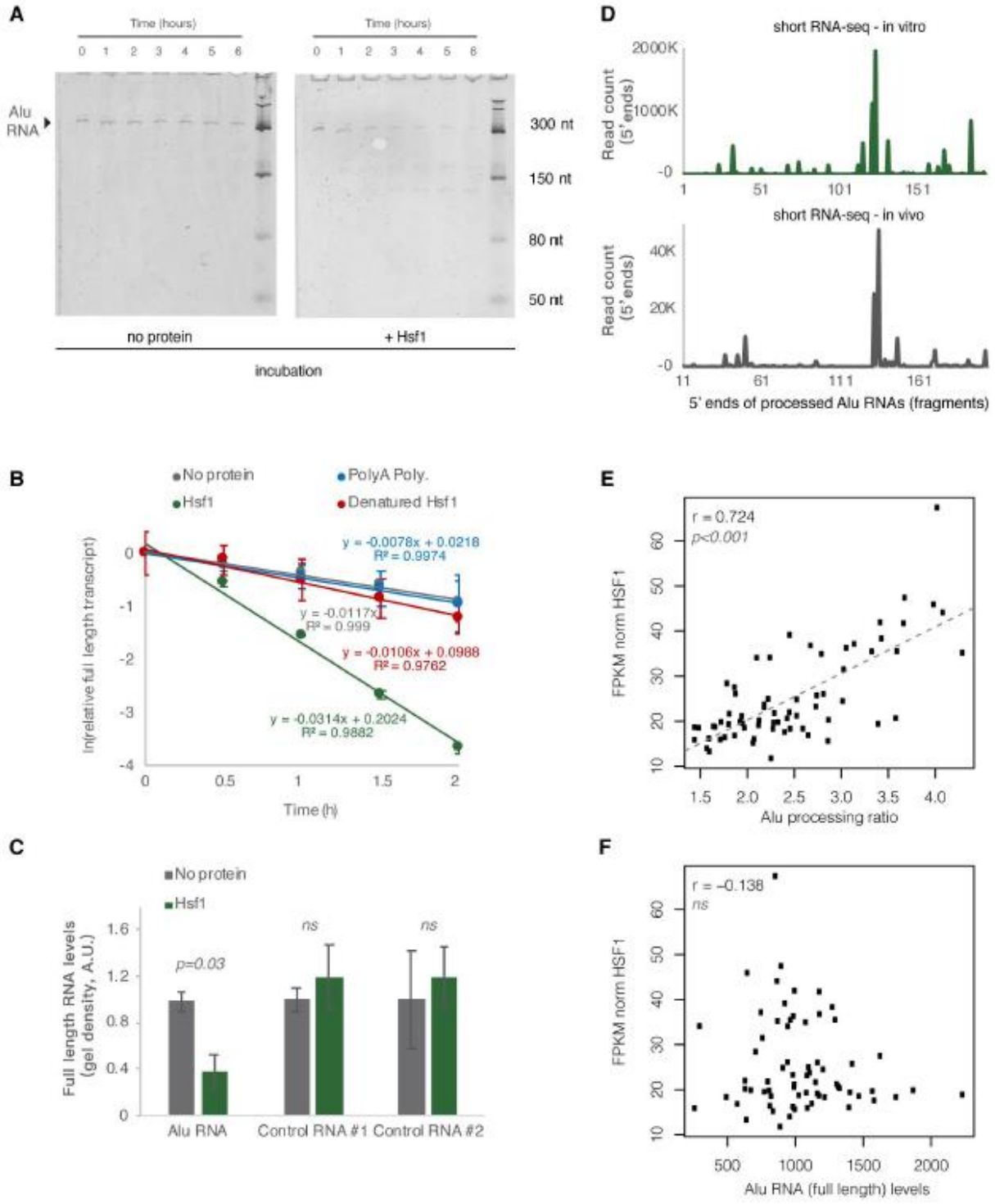

Figure 3.8. HSF1 accelerates Alu RNA processing in vitro.

(A) In vitro incubation of one of the Alu RNA consensus sequences for different incubation periods. In vitro transcribed Alu RNA (67nM) incubated at 37oC with 250nM HSF1 in the course of 6 hours with time intervals of 1 hour.

(B) Comparison among HSF1 (~60KDa), denatured HSF1, Poly A polymerase (~56KDa) and no protein (just TAP buffer) with regard to Alu RNA processing (estimating relative full length RNA remaining) (two replicates). For Figure 3.8. Relative full length RNA remaining was calculated using ImageJ area under the curve software over time. Error bars represent standard deviation from the mean.

(C) Comparison among Alu RNA (three replicates), and two control RNAs (two replicates) regarding the full-length RNA levels remaining after in vitro incubation for 90 minutes at 37C with HSF1. Sizes of control RNAs are control for RNA #1, 143nt and for control RNA #2, 432nt. Incubation in the absence of HSF1 but presence of the same buffer (TAP) was used as control to take into account any non HSF1 specific RNA destabilization due to non-specific degradation. Threshold for statistical significance was a p value of 0.05 with $p = 0.03$ (unpaired, non-directional t-test) for the comparison between HSF1 and no protein incubation ($n = 3$, for Alu RNA). The full gels are available as Source Data. For Figure 3.8. Error bars represent standard deviation from the mean.

(D) Plotting of the position of the first base (5’ end) of Alu RNA fragments across the Alu consensus sequence produced by Alu RNA that has been processed in vitro for 90 minutes at 37C in the presence of HSF1 (upper panel) and compared with one of the in vivo samples of Figure 3.1 (lower panel). The x axis represents an Alu RNA metagene aligned at the start site of the Alu consensus sequence and the y axis shows the 5’ end count for Alu RNA fragments aligning to any position downstream of position +1. The in vivo sample x axis depicts a 11nt sift compared to the in vitro one.

(E) Scatterplot depicting the positive correlation between HSF1 mRNA expression values and Alu RNA processing ratio in MAP AD patients ($r = 0.72$, $p < 0.001$). Statistical test is based on Pearson's product moment correlation coefficient and follows a t distribution using the cor.test function in R package stats.

(F) Scatterplot depicting lack of correlation between HSF1 mRNA expression values and full length Alu RNA levels in MAP AD patients (ns = non-significant, with p value 0.05 as the significance threshold). Statistical test as in Figure 3.8E.

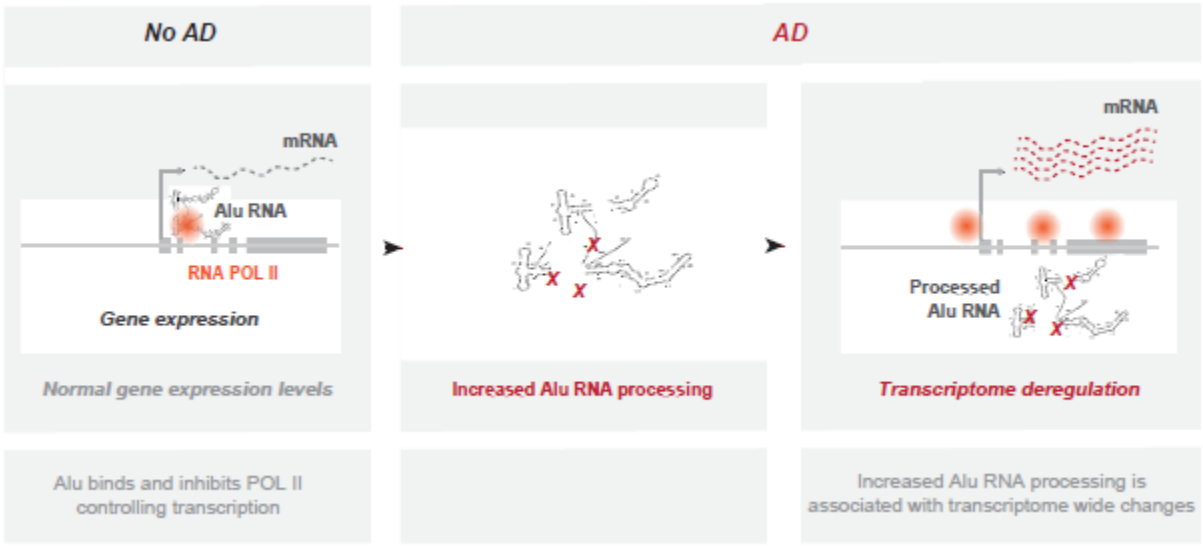

Figure 3.9. Representation of the observed changes in Alu RNA processing in AD.

In no AD brains, basal Alu RNA processing levels maintain control of gene transcription through regulation of RNA Pol II. In contrast, in AD pathology, various, yet unknown, factors lead to an increase in Alu RNA processing associated with transcriptome-wide de-regulation of gene expression.

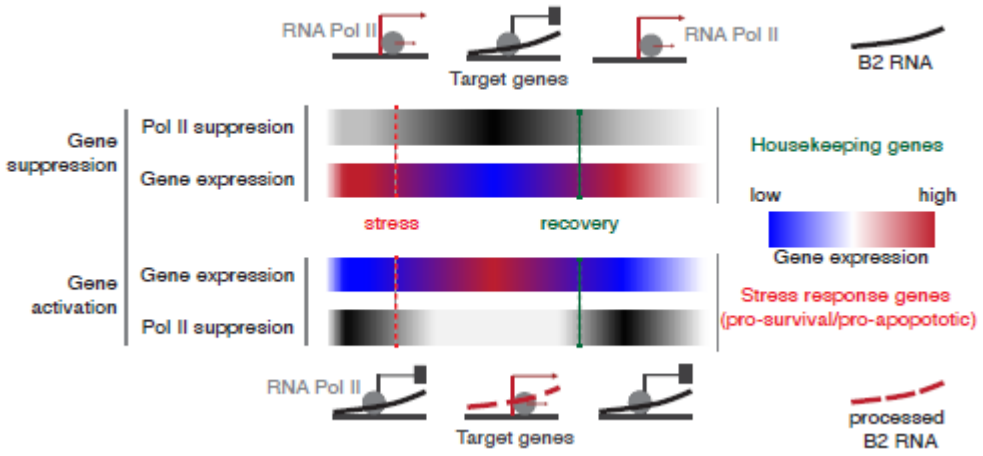

Figure S3.1.

Graphical representation of the mode of action of SINE RNAs and SINE RNA processing in mouse (B2 RNAs) with regard to transcriptome changes based on previous studies from the Kugel/Goodrich labs (Espinoza et al., 2007; Ponicsan et al., 2010, 2015; Yakovchuk et al., 2009) and our studies (Cheng et al., 2020; Hernandez et al., 2020; Zovoilis et al., 2016).

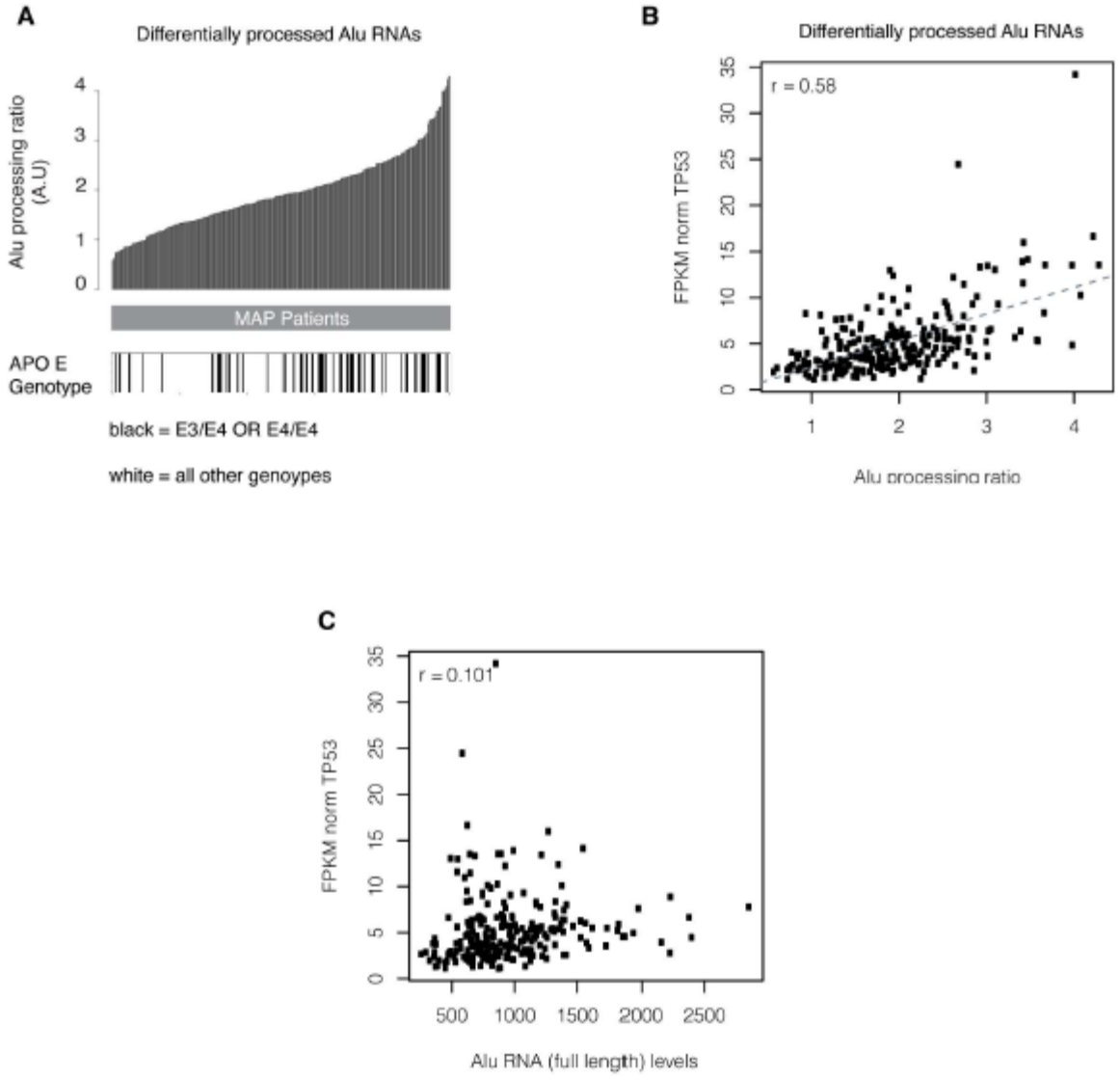

Figure S3.2. Relationship between APOE genotype and TP53 expression and Alu RNA processing ratio in MAP patients.

(A) Association between SINE Alu RNA ratio (upper panel) and APOE genotype (lower panel). Every column in both panels corresponds to the same MAP patient (n = 241). Patients are sorted from left to right in an ascending order with regard to Alu RNA processing ratio. Patients with at least one E4 allele that confers higher genetic risk to developing late onset AD are marked with black in the lower panel. The figure shows that as processing ratio climbs higher, it is more likely to identify an individual with this phenotype. Here it should be noted though that the connection between APOE and AD, despite APOE being one of the few reliable genetic markers shown to confer some degree of higher susceptibility to AD, is not a one to one absolute match (i.e. the vast majority of people with these genotypes will not develop AD). For this reason, we also do not expect the correlation between Alu RNA processing and this genotype to be a one to one absolute match, especially since Alu RNA processing is a continuous variable while ApoE

genotype is a discrete one. The reason why within the higher processing ratio, distribution of genotypes seems to be biphasic (with one density area in the middle of the range, and one towards the right end of the range) remains unknown and likely should be attributed to the large heterogeneity among AD patients and the multi-factorial nature of this disease.

(B) Scatterplot depicting the positive correlation between TP53 expression values and Alu RNA processing ratio in all MAP patients ($r = 0.58$, $p < 0.001$).

(C) Scatterplot depicting lack of correlation between TP53 mRNA expression values and full length Alu RNA levels in all MAP patients ($n = 241$).

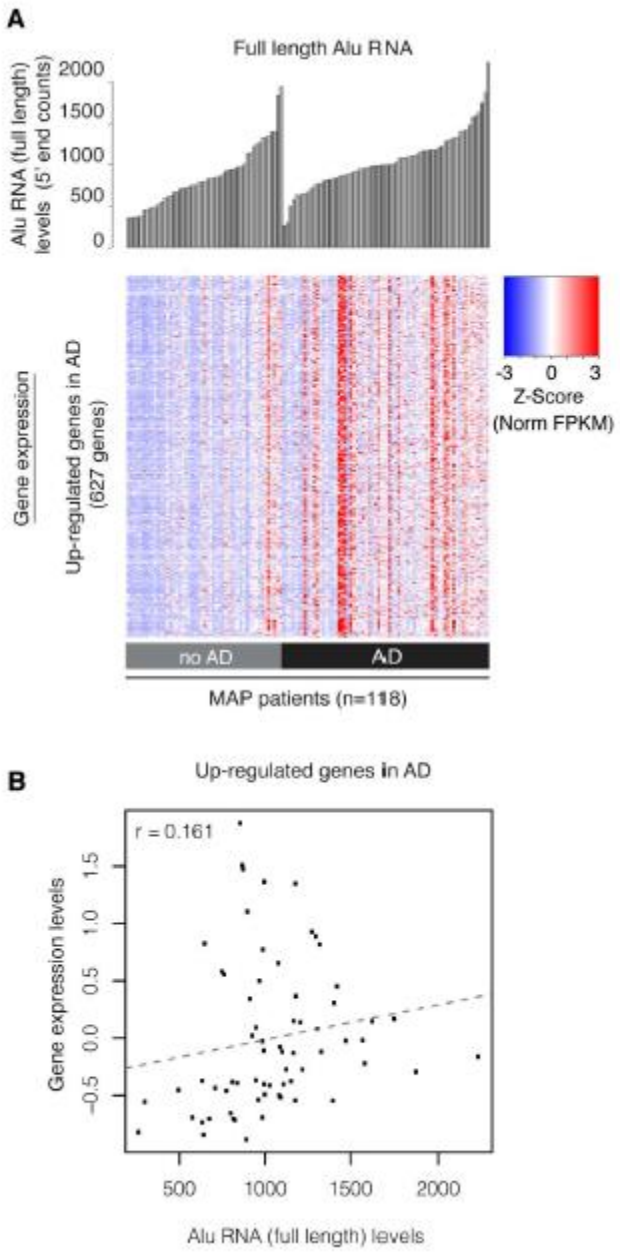

Figure S3.3. No correlation between up-regulated genes and full length Alu RNA levels.

(A) No association between full length Alu RNA levels (upper panel) and gene expression levels (lower panel) of genes up-regulated in AD (Table 3.1) is found in contrast to our observations with regard to Alu RNA processing ratio. Columns and rows as described in Figure 3.6 with every column in both panels corresponding to the same MAP patient sorted from left to right in an ascending order with regard to Alu RNA levels for either the no AD or AD group.

(B) Scatterplot depicting lack of correlation between average gene expression values of up-regulated genes in panel A and full length Alu RNA levels in AD patients (r=0.16).

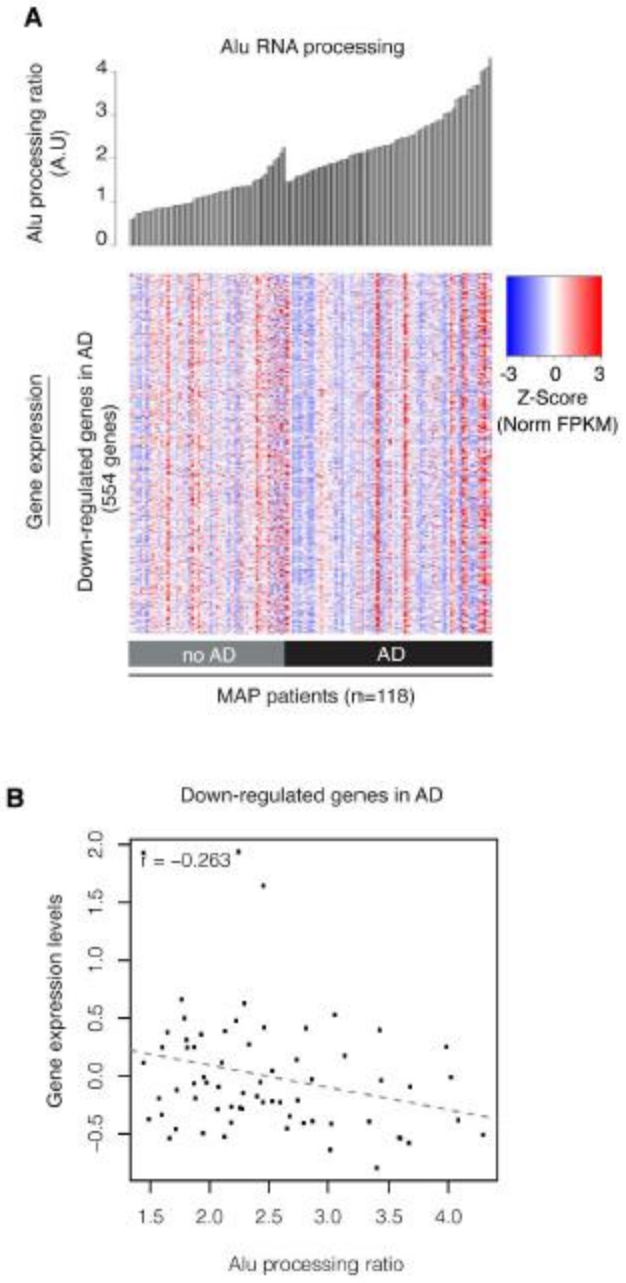

Figure S3.4. Weak correlation between down -regulated genes and Alu RNA processing ratio.

(A) Only a weak association between Alu RNA processing ratio (upper panel) and gene expression levels (lower panel) of genes down-regulated in AD (Table 3.2) is found in contrast to our observations with regard to full length Alu RNA levels. Columns and rows as described in Figure 3.6 with every column in both panels corresponding to the same MAP patient sorted from left to right in an ascending order with regard to Alu RNA processing ratio for either the no AD or AD group.

(B) Scatterplot depicting the weak negative correlation between average gene expression values of down-regulated genes in panel A and Alu RNA processing ratio in AD patients (r=-0.26).

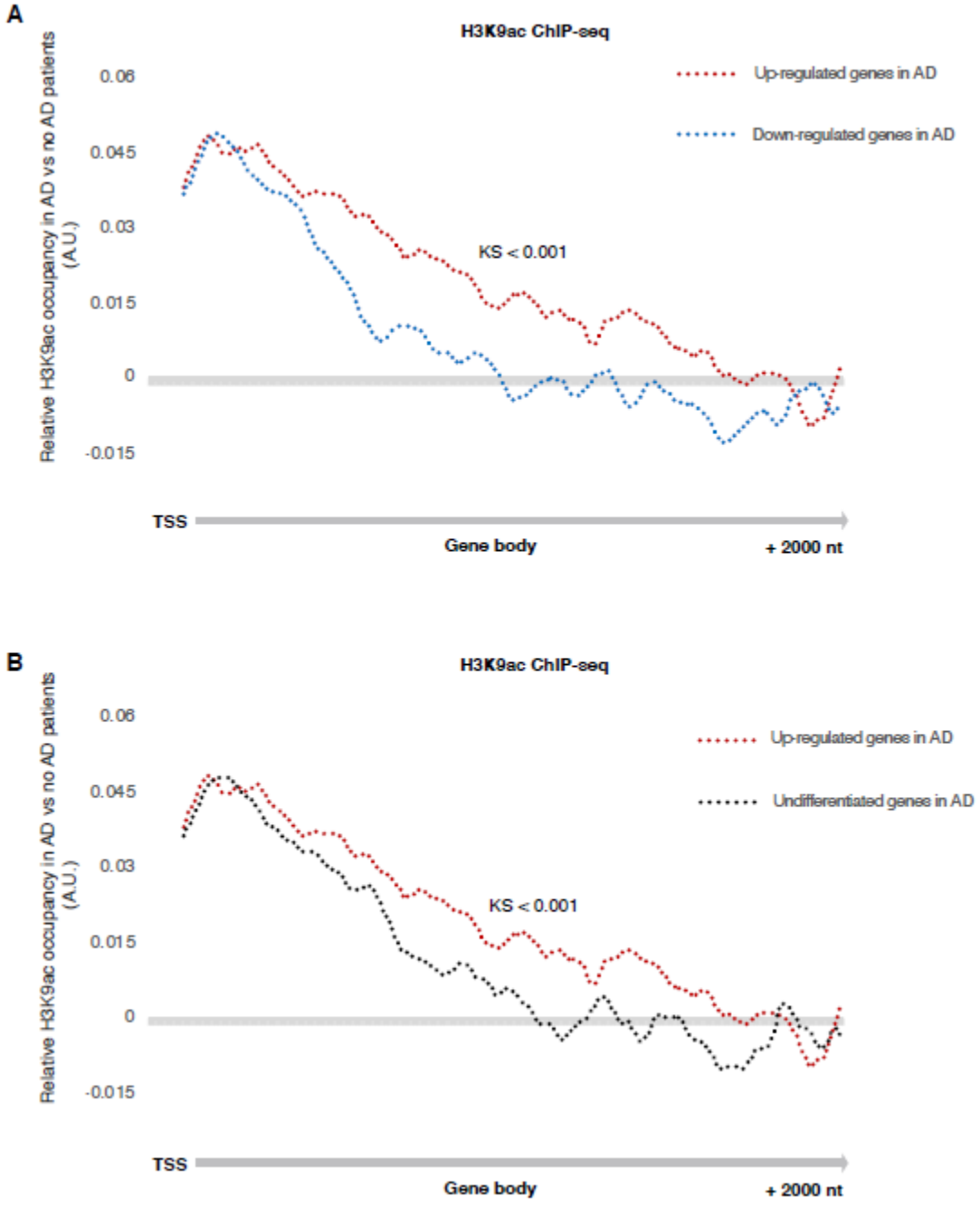

Figure S3.5. H3K9ac ChIP-seq for MAP patients.

(A) Comparison of H3K9ac occupancy downstream of Transcription Start Site (TSS) between AD and no AD patients for genes up-regulated and down-regulated in AD.

(B) Comparison of H3K9ac occupancy downstream of Transcription Start Site (TSS) between AD and no AD patients for genes up-regulated and a random set of non-differentiating genes

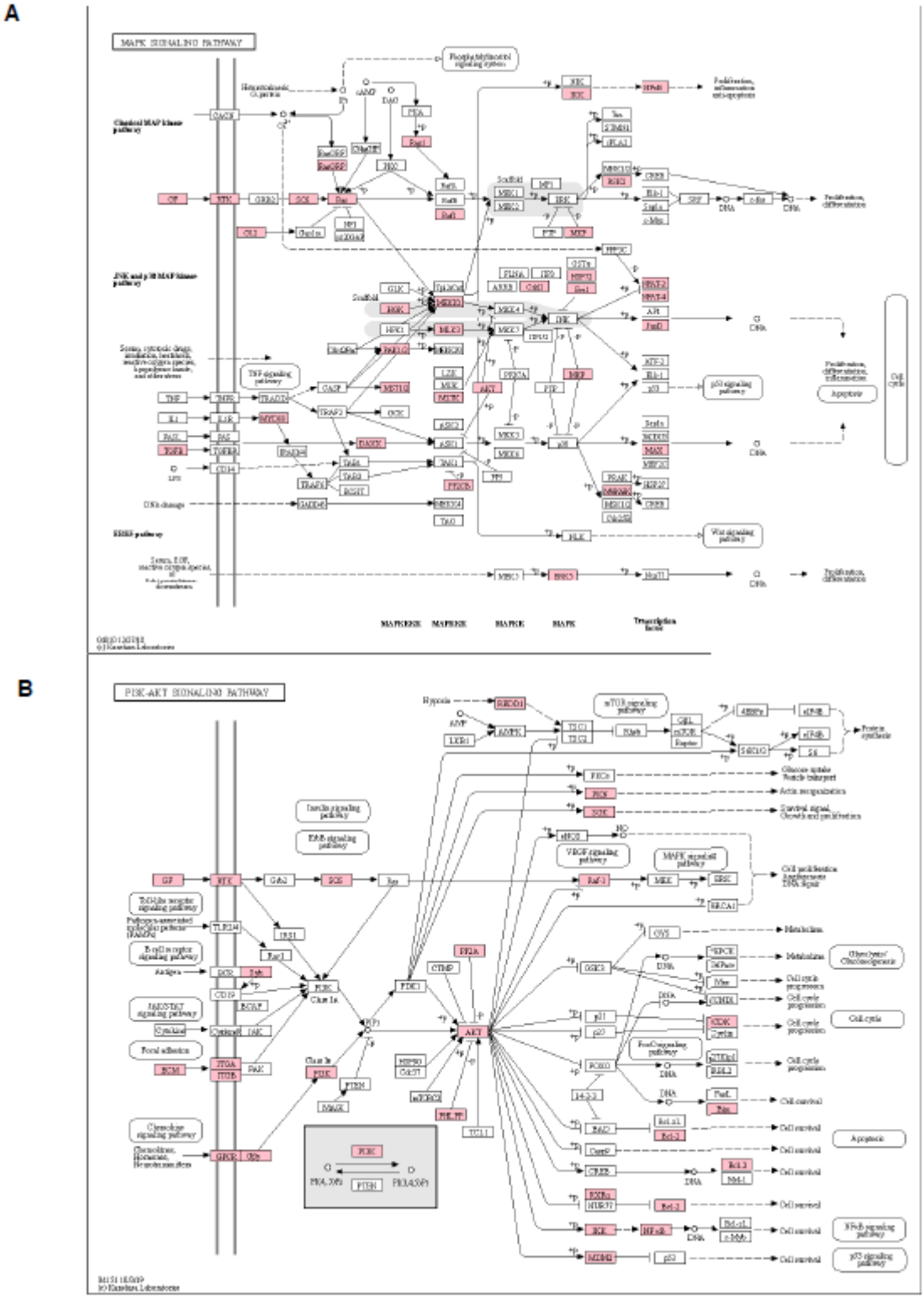

Figure S3.6. Pathways impaired in AD up-regulated genes that are strongly correlated with Alu RNA processing ratio. Pathways identified by KEGG pathway term enrichment analysis of AD

up-regulated genes the expression of which is strongly correlated with Alu RNA processing ratio ($r > 0.5$, p value < 0.05 Pearson correlation, Table 3.3). Selected pathways are among those with a padj < 0.05 in the KEGG enrichment term analysis by the DAVID platform (see methods). Pathways have been selected based on their association with functional terms such as cellular stress, cell survival, cell death and proliferation.

(A) MAPK signaling pathway. Multiple members (colored with pink) belong to the set of AD up-regulated genes correlated with Alu RNA processing ratio. This pathway is upstream of the TP53 signaling pathway and cell death and proliferation.

(B) PI3K-AKT pathway. This pathway intersects with various signaling pathways regulating TP53 signaling and cell cycle. Pink color as in A.

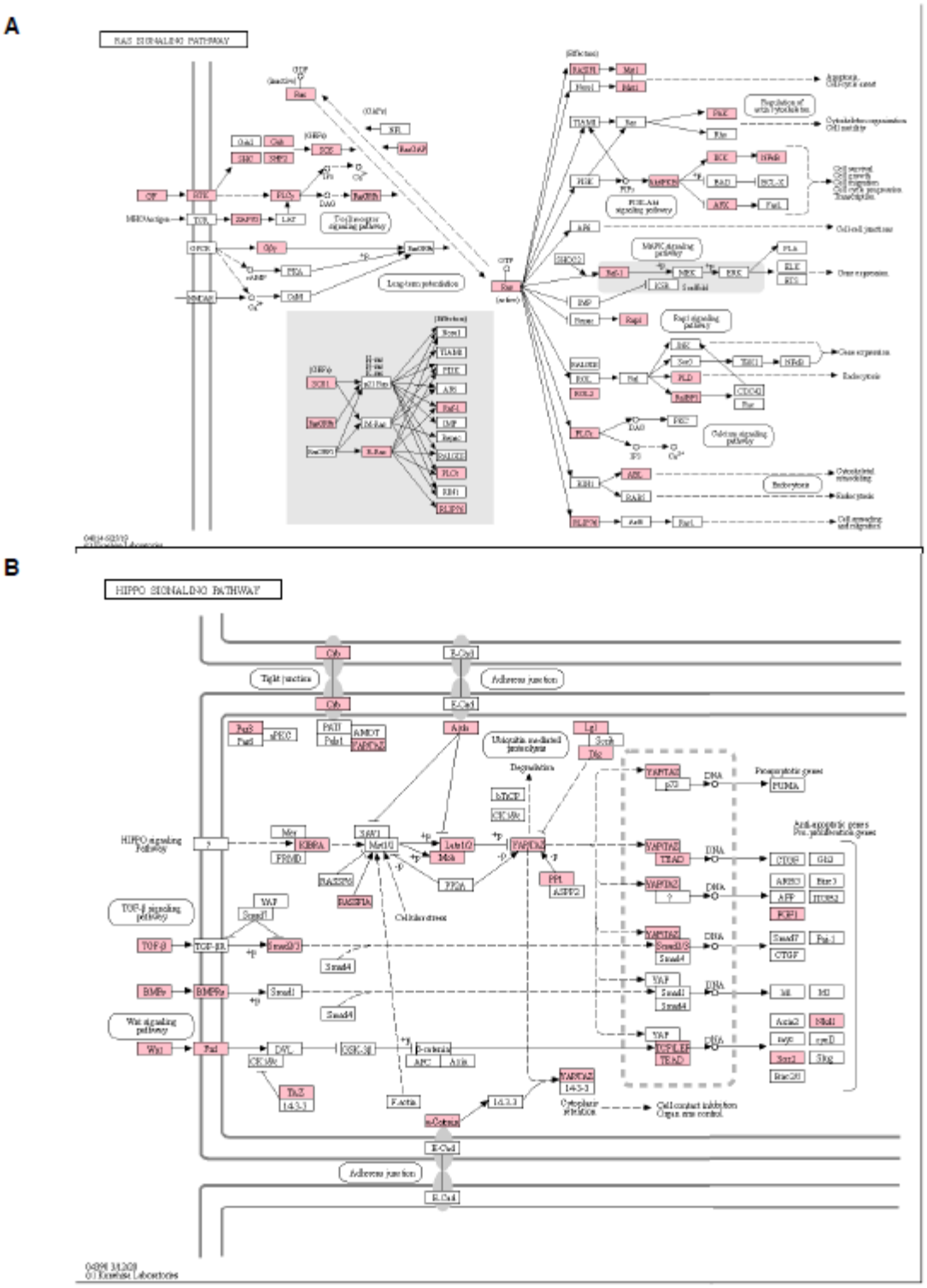

Figure S3.7. Additional pathways impaired in AD up-regulated genes that are strongly correlated with Alu RNA processing ratio.

(A) RAS signalling pathway. Multiple members (colored with pink) belong to the set of AD up-regulated genes correlated with Alu RNA processing ratio. This pathway is important for cell survival and also upstream TP53.

(B) HIPPO signalling pathway. This pathway intersects with various signaling pathways regulating cellular response to stress. Pink color as in A.

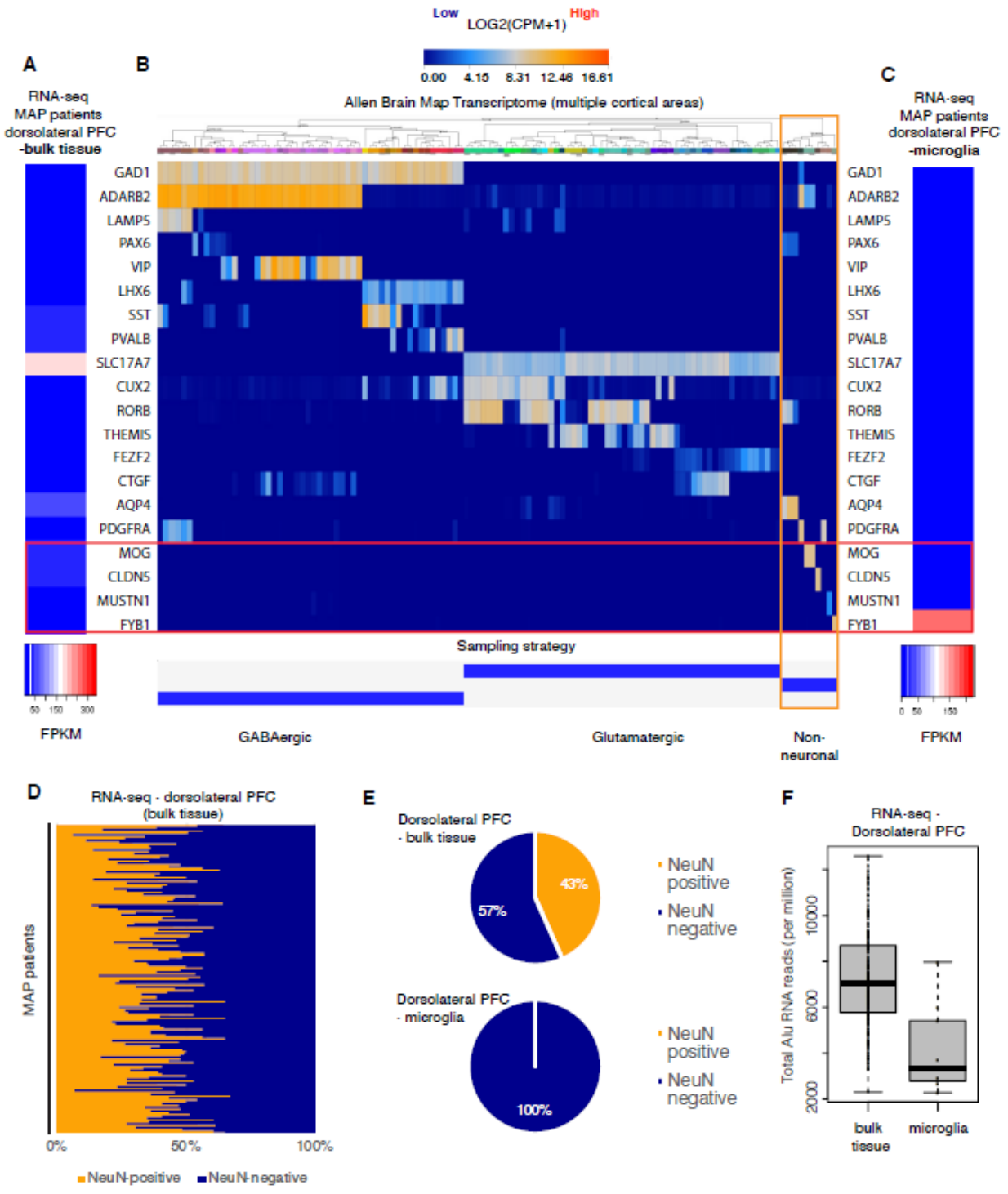

Figure S3.8. Expression of known hippocampal markers and cellular deconvolution in the MAP RNA-seq data.

(A-B-C) Expression levels comparison between RNA-seq data from MAP RNA-seq data used in our study (panel A), RNA-seq data from the Allen Brain Atlas (Panel B) and RNA-seq data generated from microglia cells within the ROSMAP study (Panel C). Comparison is done for the

standard panel genes of reference genes used by Allen Brain Atlas. Every column in panel B represents a different cell type in brain with cell types belonging to neuronal and non-neuronal cells depicted at the lower part of panel B labelled as GABAergic, Glutamatergic and Nonneuronal. Markers that are enriched in neuronal vs non-neuronal cells were extracted from: [https://celltypes.brain-map.org/rnaseq/human_ctx_smart-seq] based on (Hodge et al., 2019; Tasic et al., 2018).

(D-E) Cellular deconvolution of RNA-seq data from MAP patients (bulk tissue-dorsolateral prefrontal cortex) and microglia isolated cells within the ROSMAP study. D represents the percentage of neuronal (NeuN positive) vs non-neuronal (NeuN negative cells) per sequenced MAP sample used in our study. E represents the overall percentage of each of these categories in each RNA-seq data set.

(F) Alu RNA levels comparison between the MAP patients (bulk tissue-dorsolateral prefrontal cortex) and microglia isolated cells within the ROSMAP study.

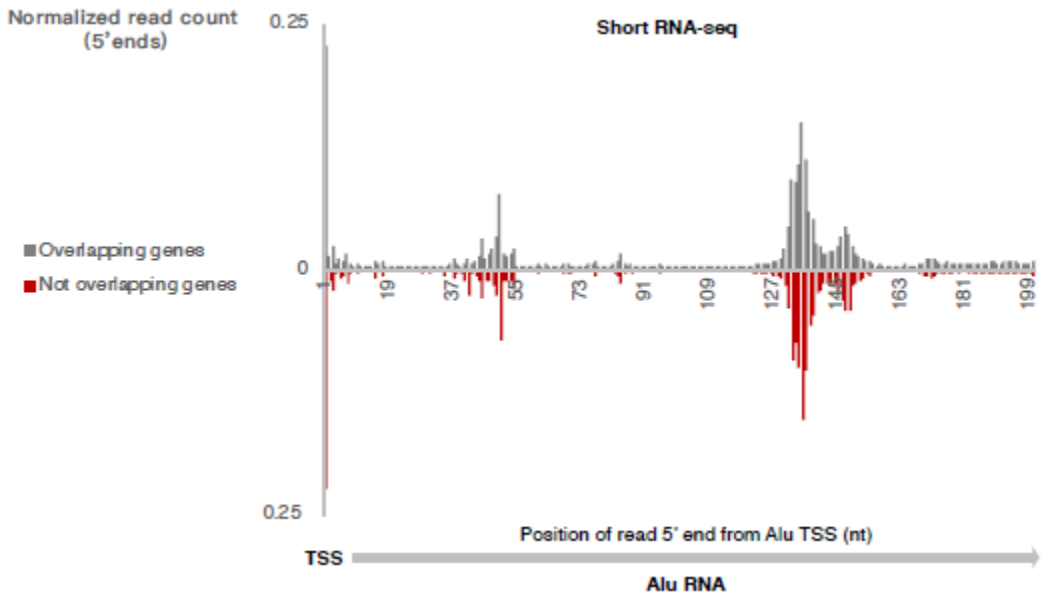

Figure S3.9.

Plotting of the position of the first base (5' end) of Alu RNA fragments in a CBB patient against Alus that fall within known Ensemble genes (primary within introns) (upper panel) and Alus outside genic areas (intergenic space) (lower panel). The x axis represents an Alu RNA metagene aligned at the TSS of the Alu elements and the y axis shows the 5' end count for Alu RNA fragments aligning to any position downstream of position +1.

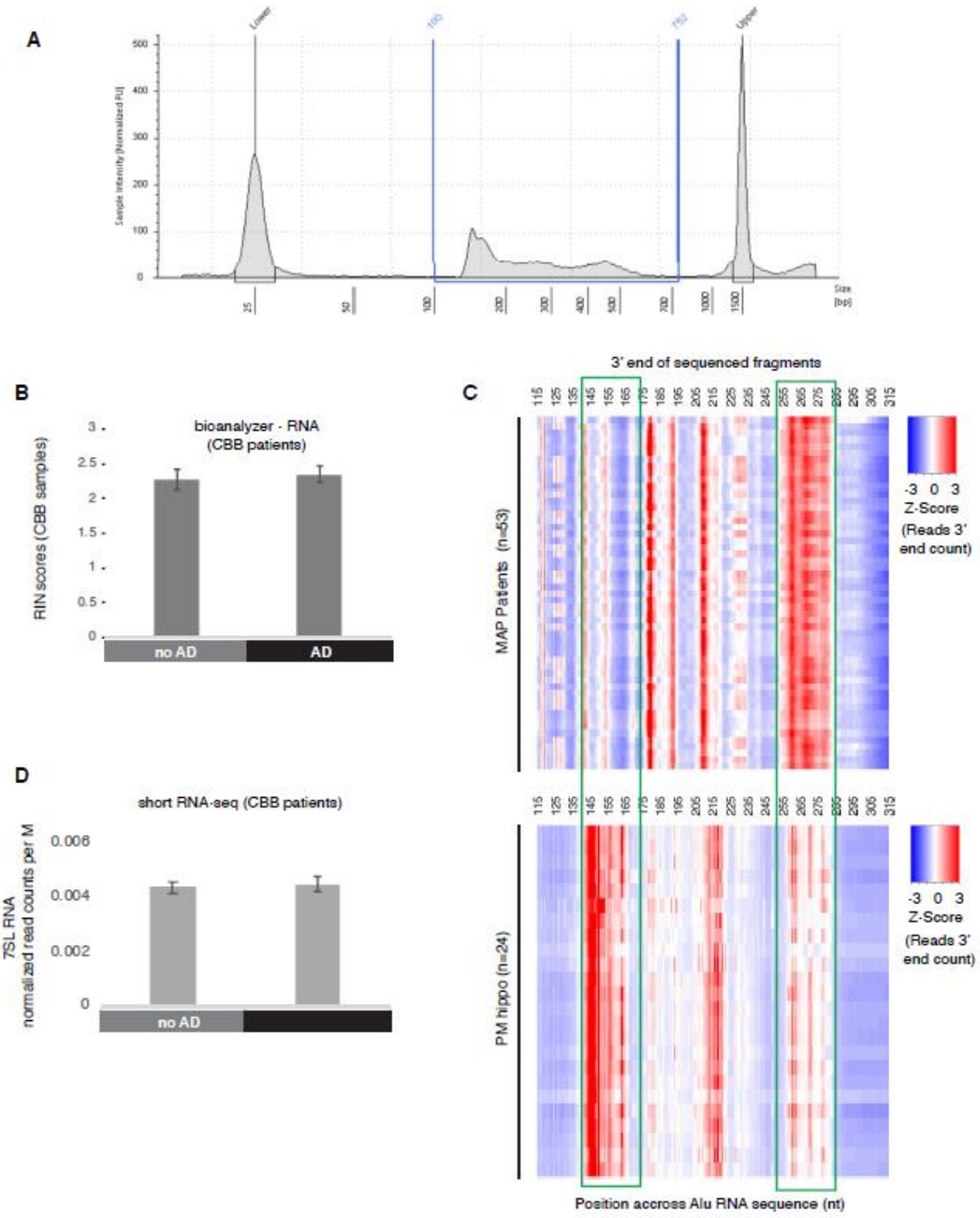

Figure S3.10.

(A) Agilent Bioanalyzer electropherogram of one of the short-RNA-seq libraries we produced from RNA from the CBB patients' hippocampi. It shows a fragment range of 150-650nt, that corresponds to initial RNA inserts of 30nt to approx. 530 nt (adapter is approx. 120nt).

(B) RIN scores of RNAs sequenced from CBB patients.

(C) Plotting of the position of the 3'end of Alu RNA fragments across the end of the consensus Alu metagene to depict potential 3' end positions of Alu RNAs in all post-mortem hippocampal tissues (PM hippo) from patients from the CBB (lower panel) and in MAP patients (upper panel). Each row in the heatmap depicts the distribution of counts of the 3'ends of reads mapped across the Alu metagene for each patient. The x-axis represents a metagene combining all unique Alu RNA sequences (ALUome) as in Figure 3.1. Heatmap density corresponds to normalized counts of the 3'end of the reads with red corresponding to higher density of these 3'ends at a specific position. Orange rectangles mark expected end positions for full length fragments (right) and fragments generated by the XR1 processing point (left).

(D) 7SL RNA levels based on short-RNA-seq in CBB patients used for the normalization of total Alu RNA base coverage in Figure 3.2.

Chapter 4: Conclusions and open questions

This thesis focuses on the role of two retrotransposon families, murine SINE B2 RNAs and human SINE Alu RNAs in response to amyloid beta neuro-toxicity, one of the major cause of Alzheimer's disease. Multiple bioinformatics tools and methods were applied to different RNA sequencing datasets in order to elucidate a possible connection between SINE RNAs and AD in both mouse models of AD and brain tissues from AD patients.

Our data reveals increased processing of SINE B2 RNAs as a novel type of transcriptome de-regulation underlying amyloid beta neuro-pathology. The B2 RNA processing ratio increases upon progression of amyloid beta pathology both in mouse hippocampus and hippocampal cell culture model, and B2-SRGs become hyper-activated. Moreover, Hsf1 is proved to be key for mediating B2 RNA processing in response to amyloid toxicity. B2-SRGs upregulation and B2 RNA increased processing were observed mainly during the active neurodegeneration phase of amyloid pathology and were not obvious in later stages, suggest that the initial active phase differs from the terminal stage regarding role of SINE B2 RNAs.

The findings in the AD mouse model were also confirmed in human patients. SINE Alu RNAs are also processed in human brains and our data reveals increased processing as a novel type of transcriptome de-regulation observed in AD patients. Alu RNAs processing is higher in the brain of AD patients compared to health individuals, and deregulates gene expressions, which indicates an association between SINE Alu RNA transcriptome and genome wide transcriptome changes in human brain.

Some of the most important discoveries are highlighted below. Firstly, this work provides a molecular mechanism underlying neural transcriptome deregulation during amyloid pathology in mouse involving SINE RNAs and a stress regulator called Hsf1, revealing a new function

independent of its well-known role as a transcriptional factor. It describes a novel Hsf1-SRG axis that is mediated by variable SINE B2 RNA processing and highlights that levels of fragmentation of SINE B2 RNA transcripts operate as a molecular switch during cellular response to stress. Secondly, it provides for the first time a connection between SINE RNA processing and a cellular pathological process. It is also the first described case of a self-cleaving ribozyme activity of an endogenous human RNA connected with a human disease. And lastly, it points for the first time to an additional molecular mechanism that could be underlying neural transcriptome deregulation in AD through SINE Alu RNAs.

These findings improve the evidences of SINE RNAs as something more than just transcriptional noise and with functional importance. Based on the data, to some degree the role of SINE RNA processing in mouse and human brain molecular pathology was revealed, with significant implications for amyloid beta pathology and Alzheimer's disease.

Further study should be performed about the mechanisms underlying molecular pathology of AD to reveal more specific functions of these SINE non-coding RNAs, and below are some open questions for guiding future directions of research in the field.

Firstly, the mouse models used in chapter two were exclusively based on amyloid beta cellular toxicity and pathology. However, our findings in human show a general connection with AD pathogenesis but not necessarily only with amyloid beta pathology. Given the predominant role that tau pathology also has in AD pathology, the role of SINE RNAs in AD lacks one of its most important hallmarks. Also, it is unknown whether tau mouse models depict a similar increased SINE RNA processing and hyper-activation of gene expression.

Secondly, the number of APP mice tested in chapter two did not draw any conclusions for potential differences between the two sexes regarding the timing and degree of SINE RNA

and transcriptome deregulation. According to evidence in the past on dramatic sex differences in the brain transcriptomes of individuals in multiple brain disorders, a connection of sex differences with differences in the SINE transcriptome is highly likely but still not clear.

Thirdly, the mechanistic experiments in chapter two on the causal connection between increased B2 RNA processing or decreased Hsf1 activity and hyperactivation of B2 RNA target genes was performed exclusively in hippocampal cell cultures. Confirmation of this causal connection in vivo has not been addressed yet.

Finally, other molecular factors that may affect SINE RNA instability in the case of AD besides Hsf1 remain unknown, which limits the potential therapeutic interventions that target increased SINE RNA processing in AD.

Appendix tables

Table 2.1: List of B2 RNA regulated SRGs (B2-SRGs). Data are compiled from Zovoilis et al, Cell 2016 and include those genes that are close to B2 CHART peaks (genome binding sites) before but not after the application of stress stimulus.

0610040F04Rik	1110002E22Rik	1110019D14Rik	1110032F04Rik
1500009C09Rik	1700001F09Rik	1700011L22Rik	1700013N06Rik
1700019A02Rik	1700024B05Rik	1700025F22Rik	1700025G04Rik
1700049E17Rik2	1700057H15Rik	1700060C16Rik	1700082M22Rik
1700113H08Rik	1700128F08Rik	2210408F21Rik	2210408I21Rik
2310002L09Rik	2310057J18Rik	2610035D17Rik	2610037D02Rik
2610203C22Rik	2610316D01Rik	2900079G21Rik	2900092C05Rik
4921539E11Rik	4930433N12Rik	4930440I19Rik	4930456L15Rik
4930467K11Rik	4930469K13Rik	4930471C06Rik	4930522L14Rik
4930524B15Rik	4930552P12Rik	4930554G24Rik	4930554H23Rik
4930558K02Rik	4931408C20Rik	4931428L18Rik	4932438A13Rik
4932441J04Rik	4933405D12Rik	5730522E02Rik	8030451A03Rik
9130019P16Rik	9130401M01Rik	9230106D20Rik	9330158H04Rik
9330182L06Rik	9530026P05Rik	9530036O11Rik	9930014A18Rik
A1cf	A230004M16Rik	A330008L17Rik	A430010J10Rik
A830018L16Rik	Abca12	Abca13	Abca16	Abca3	Abca4	Abca6
Abca7	Abca8b	Abcb1a	Abcb8	Abcc12	Abcc2	Abcc5	Abcc8	Abcd2
Abcg1	Abcg2	Abhd16a	Ablim2	Abtb1	AC188608.1	Ace3	Acnat2	Acss3
Acvrl1	Adad1	Adam26a	Adam34	Adamts12	Adamts20	Adamts3
Adamts6	Adamts9	Adamtsl1	Adarb1	Adarb2	Adcy8	Adcyap1
Adcyap1r1	Add3	Adk	Agbl1	Agbl3	Agbl4	Agmo	Agpat1	Agpat3	Ahi1	Ahr
AI838599	Aig1	Aim2	Ak5	Akap6	Akap9	Alb	Aldh1a7	Alg6	Alk
Alox5	Als2cr12	Alx1	Amy1	Angpt1	Ank1	Ank2	Ankrd22
Ankrd36	Anks1b	Ano10	Ano2	Ano4	Antxr2	Anxa13	Aoah	Aox1
Apaf1	Apba2	Aplf	Apoh	Apol10b	Apol11a	Arap2	Arfgef1	Arfip1
Arhgap18	Arhgap26	Arhgap27	Arhgap28	Arhgap29	Arhgap39
Arhgef10	Arhgef5	Arid1b	Arid2	Arid3a	Arid5b	Arl4a	Armc2	Arnt2	Arntl
Arsj	Arvcf	Asap1	Asb15	Asb3	Asb5	Ascc3	Astn2	Astx4a	Astx4d	Astx6	Asxl3
Asz1	Atad2b	Atg7	Atp10b	Atp11c	Atp13a5	Atp2b1	Atp2b2
Atp6v1b1	Atrnl1	Atxn1l	Atxn7l1	AW554918	AY512915	B3gat2
Baiap2l2	Bank1	Basp1	BB287469	Bbs7	BC005561	BC017158	Bcas3
Bckdha	Bcl11a	Bclaf1	Best3	Bicc1	Bicd1	Birc5	Blnk	Bmpr1b	Bnc1
Bnc2	Brd1	Brd2	Brd4	Brpf3	Bst2	Btbd11	Btbd9	Btrc	Bves
C030047K22Rik	C130026I21Rik	C130060K24Rik	C1qtnf3
C1qtnf7	C230029F24Rik	C6	C7	C8a	C9	Cabin1	Cacna1c
Cacna1e	Cacna1g	Cacna2d1	Cacna2d4	Cacng2	Cacng5
Cadps2	Calcr	Caln1	Camk2b	Capsl	Car10	Carf	Casd1	Casp12
Catsperb	Cbln1	Ccdc110	Ccdc129	Ccdc152	Ccdc34

Ccdc50 Ccdc60 Ccdc80 Ccdc86 Ccdc91 Cd1d1
Cd200r2 Cd36 Cd46 Cdc14a Cdc40 Cdcp1 Cdh10 Cdh11 Cdh12 Cdh13
Cdh18 Cdh20 Cdh23 Cdh4 Cdh6 Cdh8 Cdh9 Cdk14 Cdk17 Cdk5rap2 Cdk8
Cdyl2 Celsr1 Celsr2 Cenpo Cenpt Cenpw Cep290 Ces1g Cfhr3 Cftr Cgn
Chchd3 Chchd6 Chl1 Chn1 Chn2 Chrm2 Chst11 Chst9 Cilp2 Clcn7
Cldn22 Clec16a Clec1a Clec4a2 Clec4a4 Clec4b1 Clec4b2
Clec4d Clec4e Clec4n Clip4 Clnk Clvs2 Cmc1 CN725425 Cnksr3 Cnot2 Cnot6
Cnot6l Cntln Cntn1 Cntn3 Cntn4 Cntn5 Cntn6 Cntnap2 Cntnap3
Cntnap4 Cntnap5a Cntnap5b Cntnap5c Col11a1 Col14a1
Col19a1 Col22a1 Col23a1 Col24a1 Col28a1 Col2a1 Col6a1
Colec10 Cope Copg2 Cops5 Corin Cox7b2 Cpa1 Cpa5 Cpa6 Cpeb1
Cpeb3 Cpne8 Cpvl Cpxcr1 Crim1 Cript Crisp3 Crispld1 Crls1 Cry1
Csf2rb2 Csgalnact1 Csmd1 Csmd2 Csmd3 Csn1s1 Csnk2a2 Cthrc1 Ctif
Ctnna2 Ctnna3 Ctnnd2 Ctps2 Cttnbp2 Cxcl13 Cxcl15 Cyp2b10 Cyp2b9
Cyp2c29 Cyp2c37 Cyp2c38 Cyp2c39 Cyp2c40 Cyp2c55
Cyp2c66 Cyp2c67 Cyp2c68 Cyp2c69 Cyp2d12 Cyp2j11
Cyp2j12 Cyp2j13 Cyp2j5 Cyp2j6 Cyp2j8 Cyp4a10 Cyp4a12a
Cyp4a12b Cyp4a14 Cyp4a31 Cyp4a32 Cyp4f15 Cyp4f16
Cyp4f40 Cyth4 D5Ertd577e D6Ertd527e D830044D21Rik Dab1 Dab2
Dagla Dao Dapl1 Dbx2 Dcaf6 Dcaf7 Dclk1 Ddah2 Ddo Ddr1 Ddx24 Defa17
Defb38 Defb50 Deptor Dgkb Dgki Dhcr24 Dip2a Dkk2 Dlc1 Dlg1 Dlg2 Dlg4
Dlg5 Dlgap1 Dlgap2 Dlx6os1 Dmd Dnajc21 Dnajc6 Dner Dnm3 Dock2
Dock4 Dock8 Dok6 Dpp10 Dpp6 Dppa2 Dpyd Dpys Drosha Dtnb Dusp10
Dync1i1 Dynlrb2 Dysf E130114P18Rik E230016K23Rik
E330009J07Rik E330010L02Rik Ebag9 Ebf1 Ech1 Echdc1 Edem1 Eea1
Eepd1 Efcab6 Efna5 Efr3a Egfem1 Egflam Egfr Ehbp1 Ehbp1l1 Elac2
Elavl2 Elavl4 Eml6 Emx2 Enpp1 Enpp3 Enthd1 Epha5 Epm2a Epyc Erbb4 Erc1
Ergic1 Esr1 Esrra Etnk1 Etv3 Etv6 Evc Evc2 Exoc4 Exoc6 Exoc6b
Ext1 Eya1 Eya4 F13a1 Faf1 Fam110b Fam135b Fam13c
Fam155a Fam160b1 Fam162b Fam184a Fam19a1 Fam19a2
Fam19a4 Fam19a5 Fam49a Fam83a Fam83f Fam84b
Fam98a Fasn Fbln2 Fbxl17 Fbxl7 Fbxo18 Fbxo21 Fbxo32
Fbxo4 Fbxo5 Fer Fer1l5 Fer1l6 Fgd6 Fgf12 Fgf14 Fgfr2 Fggy Fhad1 Fhl3
Fig4 Flcn Flg Flrt2 Flt4 Fndc1 Fndc3b Fosb Foxd2 Foxd3 Foxi3
Foxn3 Foxo3 Foxp1 Foxp2 Foxp4 Fpr-rs4 Fpr3 Fras1 Frem1 Frk Frmd3
Frmd4a Frmd4b Fsd1l Fshr Fstl5 Fto Fuca2 Fzd6
G930045G22Rik Gabra2 Gabra4 Gabrb1 Gabrb3 Gabrg3 Galnt14 Galntl6 Gas2l1
Gbp5 Gc Gcn1l1 Ghr Gimap3 Glipr1 Glis3 Glp1r Glra3 Gm10033
Gm10212 Gm10283 Gm10327 Gm10339 Gm10373 Gm10384
Gm10406 Gm10570 Gm10649 Gm10696 Gm10715 Gm11217
Gm11228 Gm11240 Gm11261 Gm11376 Gm11751 Gm11757
Gm11758 Gm11762 Gm11823 Gm11867 Gm11884 Gm12023
Gm12068 Gm12132 Gm12296 Gm12474 Gm12478 Gm12519

Gm12532 Gm12600 Gm12602 Gm12637 Gm12648 Gm12649
Gm12666 Gm12668 Gm12695 Gm12708 Gm12724 Gm12811
Gm12841 Gm12886 Gm13272 Gm13327 Gm13849 Gm13974
Gm14061 Gm14271 Gm14643 Gm14697 Gm15104 Gm15155
Gm15404 Gm15494 Gm15581 Gm15631 Gm15668 Gm15723
Gm15825 Gm15834 Gm15939 Gm16029 Gm1604a Gm16070
Gm16156 Gm16268 Gm16365 Gm16430 Gm16513 Gm16537
Gm16630 Gm17033 Gm17067 Gm17412 Gm17473 Gm1993
Gm20388 Gm20429 Gm2128 Gm2244 Gm2464 Gm2694
Gm2800 Gm2824 Gm2832 Gm2895 Gm3072 Gm3149
Gm3164 Gm3222 Gm3264 Gm3404 Gm3558 Gm3629
Gm3636 Gm3676 Gm3739 Gm4219 Gm4301 Gm4788
Gm4876 Gm4952 Gm4981 Gm5045 Gm5105 Gm5127
Gm5150 Gm5420 Gm5559 Gm5570 Gm5622 Gm5796
Gm5852 Gm5860 Gm5934 Gm597 Gm6288 Gm6685
Gm6741 Gm7334 Gm765 Gm7714 Gm7732 Gm7792
Gm7822 Gm7954 Gm7995 Gm8082 Gm8369 Gm8374
Gm8882 Gm8897 Gm9008 Gm960 Gm9750 Gna14 Gnaq
Golga7 Golga7b Gp1ba Gpa33 Gpc5 Gpc6 Gpha2 Gphn Gpm6a Gpr108
Gpr132 Gpr158 Gprin3 Gpx3 Grb10 Grhl2 Gria4 Grid1 Grid2 Grik2
Grik3 Grin2a Grin2b Grina Grip1 Grm1 Grm3 Grm5 Grm7 Grm8 Grxcr1
Gsdmcl1 Gsta3 Gstcd Gstm5 Gulp1 H2-M2 H60b Habp2 Hace1 Hbs1l Hdac9
Hddc2 Heatr6 Heca Herc3 Hhat Hibadh Hipk2 Hirip3 Hivep2 Hivep3 Hk1 Hmcn1
Hmg20a Hmga2 Hnf4g Homer2 Hook1 Hpse2 Hrh1 Hs3st1 Hs3st2 Hs3st5
Hs6st3 Hsf2 Hsf2bp Htr7 Htt Hus1 Hyal4 Ica1 Ifit2 Ifna4 Ift27 Igf1
Igf2bp3 Ighv1-19 Ighv1-24 Ighv1-84 Ighv11-2 Ighv8-9
Igkv18-36 Igkv4-78 Igkv6-25 Igkv8-18 Igsf3 Ikbkap Il1rap
Il1rapl1 Il2rb Il31ra Immp1l Inpp4b Ints1 Ipo13 Iqcj Iqsec1 Iqsec3
Irak3 Irs1 Ispd Itgb4 Itgbl1 Itpr1 Itpr2 Jak2 Jakmip1 Jazf1 Jph1
Kank1 Kbtbd11 Kcnab1 Kcnb2 Kcnc1 Kcnc2 Kcnd2 Kcnh1 Kcnh3 Kcnh5
Kcnh6 Kcnh8 Kcnip1 Kcnip4 Kcnk10 Kcnk9 Kcnmb2 Kcnq3 Kcnq5 Kcnt2
Kctd8 Kdm4b Kdm4c Kdr Khdrbs2 Khdrbs3 Kif21a Kifap3 Klc2
Klf10 Klf15 Klk1b1 Klra9 Ksr2 L3mbtl3 L3mbtl4 Lama1 Lama2
Lama4 Larp6 Lbh Lclat1 Ldb2 Lemd3 Lgr5 Lhcgr Lifr Limch1 Lin28b
Lin7a Lingo2 Lipa Lipm Lipn Lipo1 Lmbrd1 Lmbrd2 Lmcd1 Lmo3
Lpp Lrba Lrfn2 Lrfn5 Lrp1 Lrp12 Lrp1b Lrpprc Lrrc42 Lrrc4c Lrrc61 Lrrc7
Lrriq1 Lrrk2 Lrrn1 Lrrtm4 Lsamp Ltbp1 Luzp2 Lyst Macf1 Macrod2 Magi1
Magi2 Mamdc2 Map2k2 Map3k4 Map3k5 Mapk10
Mapkap1 Mast4 Matk Matn2 Matn3 Mb Mcm5 Mcm9 Mcoln3 Mctp1
Mdfic Mdga1 Mdga2 Mecom Med12l Med13l Mef2a Megf9 Mei4
Meis1 Men1 Meox2 Met Mex3a Mfap5 Mgam Mgat4c Mgst1 Mical3 Mitf
Mkl1 Mkl2 Mllt3 Mllt6 Mmp16 Mmrn1 Mocs1 Morc1 Mpdz Mpp6
Mpped1 Mrap2 Mrpl13 Ms4a14 Ms4a4c Ms4a4d Ms4a7

Msl2 Msrb3 Mtap Mthfd1l Mthfd2l Mtss1 Muc16 Muc19 Muc20 Mug1
Mug2 Mup15 Mup16 Mup2 Myb Myh13 Myh2 Myo16 Myo18a Myo1d Myo3b
Myt1l Nalcn Nat2 Nav3 Nbea Nbeal1 Ncald Ncdn Ncf4 Ncoa7 Ncor2 Nde1
Ndrg1 Ndufs8 Nebl Negr1 Nell1 Nell2 Neto1 Neurl1a Neurl1b
Neurod6 Nf2 Nfe2 Nfia Nfib Nfic Nfya Nhlrc3 Nhsl1 Nipal2 Nkain2
Nkain3 Nkx2-5 Nlgn1 Nlrp4e Nlrp9c Nms Nos1 Nos2 Npas3 Npffr2 Npr3
Npy1r Nr2c1 Nrbp2 Nrg1 Nrxn1 Nrxn2 Nrxn3 Nsfl1c Nt5dc1 Nt5dc3 Ntf3 Ntm
Ntng1 Ntrk3 Nuak1 Nubpl Nudcd1 Nuf2 Numbl Nxph1 Obox3 Oc90 Oca2
Oit3 Olfm3 Olfml2b Olfr101 Olfr107 Olfr113 Olfr115
Olfr118 Olfr125 Olfr129 Olfr1294 Olfr1431 Olfr1491
Olfr1497 Olfr1500 Olfr308 Olfr339 Olfr38 Olfr398
Olfr403 Olfr448 Olfr460 Olfr76 Olfr810 Opcml Opn3 Opn5
Oprk1 Oprm1 Osbp2 Osbpl6 Osbpl9 Osmr Otogl Otud7a Oxct1 Oxr1 Pabpc1
Pabpc4l Pacrg Pacsin2 Pag1 Palld Palm2 Palmd Pam Papd4 Pappa
Pappa2 Pax2 Pcbp3 Pcdh15 Pcdh18 Pcdh7 Pcdh9 Pcdha11 Pclo
Pcmt1 Pcsk5 Pcx Pde10a Pde1a Pde1c Pde4b Pde5a Pde7b Pdzd2 Pdzrn3 Pdzrn4
Peg3 Pfkm Pgap1 Pgk1 Phc2 Phf14 Phf21b Phkb Phox2b Phyhipl
Pid1 Pigk Pik3ap1 Pik3c2g Pisd Pja2 Pkd1 Pkdcc Pkhd1 Pkib
Pla2g6 Plagl1 Plcb4 Plce1 Plch1 Plcl2 Plcxd3 Plcz1 Pld1 Pld5 Plec
Plekhg1 Plekhh2 Plscr3 Plxdc2 Plxna4 Plxnc1 Pofut2 Poli Polr3b Polrmt
Pon2 Postn Ppfia2 Ppfibp1 Ppm1h Ppm1k Ppp1r10 Ppp1r14c
Ppp1r3a Ppp1r9a Ppp4r4 Ppp6r3 Prdm1 Prdm5 Prep Prex2 Prh1
Prickle2 Prim2 Prima1 Prkag2 Prkar2b Prkce Prkd1 Prkg1 Prlr Prmt8
Prodh Prpf38b Prr5 Prune2 Psd3 Psg28 Psme4 Ptbp1 Ptk2 Ptn Ptpn3
Ptprcap Ptprd Ptprf Ptprk Ptprm Ptprq Ptprr Ptprs Ptprz1 Purg Pvt1
Qk Rab11fip4 Rab30 Rab31 Rabgap1l Rai1 Rai14 Ralyl Ranbp17
Rap1gds1 Rapgef5 Rasef Rassf3 Rassf8 Raver2 Rb1cc1 Rbfox1
Rbfox2 Rbfox3 Rbm14 Rbm20 Rcan2 Rdh16 Rdh19 Reg3g Rell1 Reln
Ret Rftn1 Rfx3 Rgma Rgs20 Rgs22 Rgs6 Rgs7 Rhag Rhbdd1
Rhobtb1 Rhoj Rhpn1 Rictor Rims1 Rims2 Rims3 Rmst Rnf144a Rnf152
Rnf220 Rnls Robo1 Robo2 Ror1 Rorb Rorc Ros1 Rp1 Rpn1 Rrp1
Rspo2 Rsrc1 Rtn1 Runx2 Safb2 Samd12 Samd3 Samsn1 Satb1 Scaf8
Sclt1 Scmh1 Sdk1 Sec22c Sema3c Sema3d Sema3e Sema5a
Sema6b Sema6d Serpina1f Serpina3i Serpinb3b Sesn1 Sfxn5
Sgcd Sgce Sgcz Sgip1 Sgk1 Sgms1 Sgsm3 Sh2d1b1 Sh3bp1 Sh3gl2
Sh3rf1 Shank3 Shisa6 Shisa9 Shpk Shq1 Sim1 Sirpb1a Six3os1
Skap2 Skint11 Skint5 Skint8 Skp2 Slamf6 Slc10a7 Slc13a4
Slc16a10 Slc16a7 Slc17a8 Slc18a1 Slc1a1 Slc1a3 Slc22a1
Slc22a22 Slc22a26 Slc22a27 Slc22a28 Slc22a29 Slc22a30
Slc24a2 Slc24a3 Slc25a13 Slc25a21 Slc25a26 Slc29a3
Slc2a12 Slc2a13 Slc2a9 Slc30a4 Slc35d1 Slc35f1
Slc35f3 Slc37a1 Slc38a1 Slc38a4 Slc44a5 Slc4a4 Slc4a8
Slc5a4a Slc6a1 Slc6a11 Slc6a12 Slc6a9 Slc8a1 Slc9a4 Slco1a5

Slco1b2	Slco1c1	Slco5a1	Smap1	Smarca2	Smarcad1					
Smchd1	Smg5	Smgc	Smndc1	Smoc1	Smoc2	Smr2	Smyd3	Snapc3	Snca	
Sncaip	Snd1	Snip1	Snora17	Snord95	Snrpn	Sntb1	Sntg1	Sntg2	Snx10	
Snx13	Snx25	Snx29	Sobp	Sorbs1	Sorbs2	Sorcs1	Sorcs2	Sorcs3	Sox2ot	Sox5	Spag16
Spag17	Spata16	Spata17	Spata22	Spata5	Spata6	Specc1l				
Speer2	Speer4e	Spef2	Spock3	Spon1	Srbd1	Srgap3	Srrm4	Srrt	St18	
St3gal3	St6galnac3	St7	St8sia1	Stambpl1	Stau2	Stk3	Stk31	Stk32b		
Stk38l	Ston2	Stx3	Stxbp4	Stxbp5	Stxbp6	Styk1	Sufu	Sulf1	Sult1b1	
Sult1c1	Sult2a4	Sult2a5	Sult2a6	Susd1	Svep1	Sybu	Syn2			
Syn3	Syne1	Synj2bp	Syt1	Syt10	Syt7	Taar6	Tab1	Tanc2	Tas2r106	
Tas2r107	Tatdn2	Tbc1d22a	Tbc1d5	Tbx15	Tbx19	Tbxas1	Tcf20	Tcl1b2		
Tcl1b5	Tcte1	Tcte2	Tdrd9	Tecrl	Tff2	Tg	Thada	Themis	Thsd7a	Thsd7b	
Tiam2	Tigd2	Tjp3	Tle1	Tle2	Tle4	Tll2	Tlr4	Tm9sf3	Tmc1	Tmcc1	
Tmcc3	Tmem117	Tmem132c	Tmem132d	Tmem135	Tmem178					
Tmem184b	Tmem2	Tmem200a	Tmem207	Tmem232	Tmem26					
Tmem71	Tmem9	Tmprss11a	Tmprss11d	Tmprss11f	Tmprss15					
Tmprss3	Tmtc2	Tmtc3	Tnc	Tnfsf14	Tnip3	Tnrc6b	Tns3	Tph2	Tpk1	
Tprg	Tpte	Traf3ip2	Trappc9	Trdn	Trerf1	Trhde	Trhr	Trim62	Trmt11	
Trmt12	Trmt2a	Trp63	Trpm1	Trpm3	Trpm6	Trps1	Tsga10	Tshz2	Tshz3	Tspan11	
Tspan12	Tspan9	Ttc23l	Ttc27	Ttc28	Tuba8	Txlnb	Txnrd3	Tyms	Ube3b	Ubr5	
Uchl5	Ugt1a10	Ugt2a3	Ugt3a1	Ugt3a2	Unc45b	Unc5c	Unc5d	Unc79	Ush2a		
Usp15	Usp19	Usp24	Ust	Utrn	Vac14	Vat1l	Vav3	Vcam1	Vdr	Veph1	Vezt
Vip	Vit	Vmn1r179	Vmn1r183	Vmn1r184	Vmn1r185	Vmn1r28					
Vmn1r3	Vmn1r31	Vmn1r42	Vmn1r43	Vmn1r79	Vmn2r-ps100						
Vmn2r-ps54	Vmn2r100	Vmn2r102	Vmn2r103	Vmn2r104	Vmn2r105						
Vmn2r106	Vmn2r108	Vmn2r109	Vmn2r110	Vmn2r13	Vmn2r18						
Vmn2r21	Vmn2r23	Vmn2r24	Vmn2r25	Vmn2r26	Vmn2r4						
Vmn2r48	Vmn2r58	Vmn2r60	Vmn2r61	Vmn2r62	Vmn2r63						
Vmn2r65	Vmn2r7	Vmn2r70	Vmn2r75	Vmn2r78	Vmn2r80						
Vmn2r82	Vmn2r87	Vmn2r91	Vmn2r92	Vmn2r93	Vmn2r95						
Vmn2r96	Vmn2r97	Vmn2r98	Vmn2r99	Vnn1	Vps13a						
Vps13b	Vsnl1	Vta1	Vti1a	Vwde	Wdpcp	Wdr25	Wdr27	Wdr63	Wisp1	Wnt2	
Wrn	Wscd2	Wwox	Xab2	Xdh	Xkr4	Xpnpep1	Xylt1	Yif1a	Ypel2	Zbbx	
Zbtb4	Zc3h3	Zc3h7a	Zdhhc14	Zdhhc17	Zdhhc6	Zeb1	Zfand3	Zfat			
Zfhx4	Zfp160	Zfp207	Zfp248	Zfp423	Zfp438	Zfp442	Zfp534	Zfp618	Zfp804b	Zfp81	
Zfp850	Zfp943	Zfp944	Zfp946	Zfp947	Zfp959	Zfp964	Zfpm2	Zhx2	Zkscan17	Zmat4	
Zmpste24	Zmym4	Zwint									

Table 2.2: List of B2 RNA regulated SRGs (B2-SRGs) (see Table 2.1) that are associated with learning based on Peleg et al, Science 2010.

1700025F22Rik Abcc5 Agpat1 Ahi1 Ak5 Apaf1 Apba2 Arhgap39 Arnt2 Arntl
Bmpr1b Btrc Cacna1g Cdh11 Cdh12 Cdh9 Cdk8 Cnksr3 Cntn1 Cntn6
Col6a1 Ctif Ctnnd2 Cttnbp2 Dab1 Dgkb Dlg1 Dlg5 Gabrb3 Gria4 Grm7
Heca Hipk2 Hivep2 Hs3st2 Inpp4b Kcnab1 Kcnc1 Kcnip4 Kcnt2 Kif21a Klc2
Ldb2 Lemd3 Lmbrd1 Lmo3 Lrp1b Lrrc42 Lrrc7 Map3k5 Mitf Mpdz
Myo18a Ncdn Ncoa7 Ntng1 Nuak1 Nxph1 Olfm3 Oxr1 Pacsin2 Pclo
Phkb Pisd Plekhg1 Ppp6r3 Ptprs Qk Rab11fip4 Rab31 Raver2 Rftn1
Rims2 Sesn1 Sh3gl2 Shank3 Slc35f1 Slc6a1 Slc8a1 Smap1 Smarcad1
Smchd1 Smoc2 Snrpn Spon1 St18 Sybu Tbc1d5 Thsd7b Tnc
Trim62 Ttc28 Ust Vav3 Vps13b Wrn Zdhhc17 Zfp248 Zfp423 Zfp959
Zhx2 Zmym4

Table 2.3: Up-regulated genes in hippocampi of APP 6m old mice compared to 6-month WT mice. Values were calculated using DESeq (see chapter 2 methods) on long-RNA-seq data. Only genes with an padj < 0.2 are depicted.

Gene Name	**baseMean**	**log2FoldChange**	**lfcSE**	**stat**	**pvalue**	**padj**
Htt	2401.16	0.329	0.109	3.008	0.003	0.153
Camk2a	20750.19	0.352	0.094	3.754	0.000	0.022
Arid1b	1219.19	0.354	0.097	3.639	0.000	0.031
Znfx1	424.85	0.360	0.121	2.976	0.003	0.163
Tub	1914.77	0.374	0.127	2.938	0.003	0.175
Rapgefl1	1201.87	0.385	0.110	3.495	0.000	0.046
Ddn	10750.02	0.385	0.121	3.175	0.001	0.106
Kcnq3	2922.62	0.388	0.128	3.043	0.002	0.142
Prr14l	1321.91	0.409	0.139	2.948	0.003	0.172
Tspoap1	1201.48	0.417	0.136	3.058	0.002	0.137
Ubash3b	370.93	0.423	0.147	2.874	0.004	0.199
Dscaml1	656.00	0.428	0.147	2.917	0.004	0.182
Adss	555.68	0.428	0.146	2.928	0.003	0.178
Adgrb2	2155.42	0.429	0.132	3.251	0.001	0.087
Ssh2	671.99	0.430	0.143	3.002	0.003	0.155
Slc7a14	2268.93	0.447	0.123	3.641	0.000	0.031
Klf9	1321.31	0.449	0.125	3.592	0.000	0.035
Ppip5k1	570.45	0.449	0.151	2.977	0.003	0.163
Prdm2	816.01	0.451	0.147	3.070	0.002	0.134
Neurod2	667.42	0.456	0.149	3.066	0.002	0.135
Prkag2	589.07	0.458	0.152	3.018	0.003	0.150
Adora1	640.70	0.466	0.138	3.377	0.001	0.064
Sowaha	1030.45	0.470	0.140	3.356	0.001	0.066
St3gal2	798.43	0.471	0.150	3.142	0.002	0.115

Kmt2c	1451.06	0.472	0.119	3.958	0.000	0.011
Zhx2	298.29	0.479	0.146	3.271	0.001	0.083
Galnt17	1015.30	0.482	0.160	3.016	0.003	0.151
Cbl	1372.06	0.487	0.169	2.884	0.004	0.194
Ddi2	648.13	0.492	0.170	2.884	0.004	0.194
Foxn3	667.06	0.493	0.170	2.903	0.004	0.187
Slc35f3	234.91	0.495	0.168	2.943	0.003	0.173
Mllt1	458.65	0.496	0.158	3.133	0.002	0.117
Chst2	1729.07	0.496	0.115	4.302	0.000	0.003
Smg1	2953.87	0.497	0.142	3.501	0.000	0.045
Peak1	541.24	0.497	0.157	3.160	0.002	0.110
Pdcd11	271.19	0.500	0.148	3.368	0.001	0.065
Jun	682.62	0.504	0.154	3.264	0.001	0.084
Sbk1	617.72	0.514	0.141	3.648	0.000	0.030
Tnr	2506.33	0.516	0.133	3.886	0.000	0.014
Srrm3	190.40	0.517	0.175	2.947	0.003	0.172
Foxo3	780.33	0.519	0.175	2.968	0.003	0.166
Adcy9	736.30	0.520	0.168	3.092	0.002	0.127
Plxna1	1492.48	0.522	0.106	4.924	0.000	0.000
Btbd9	949.04	0.524	0.178	2.948	0.003	0.172
Pcdh1	1113.41	0.526	0.168	3.130	0.002	0.118
Setd5	560.59	0.526	0.176	2.984	0.003	0.160
Pcdhga12	190.25	0.526	0.180	2.926	0.003	0.179
Picalm	261.78	0.530	0.180	2.944	0.003	0.173
Mfhas1	536.81	0.533	0.150	3.541	0.000	0.041
Adcy1	10834.31	0.535	0.113	4.739	0.000	0.001
Sash1	1348.12	0.535	0.143	3.734	0.000	0.023
Lrrc8a	481.83	0.536	0.170	3.158	0.002	0.111
Mbp	664.92	0.541	0.158	3.417	0.001	0.057
Gpt2	525.80	0.544	0.117	4.631	0.000	0.001
Kbtbd11	2031.49	0.545	0.127	4.300	0.000	0.003
Sptb	2518.72	0.546	0.148	3.682	0.000	0.028
Lingo3	209.25	0.548	0.191	2.875	0.004	0.198
Creb3l2	185.05	0.553	0.170	3.253	0.001	0.086
Mast3	1867.25	0.555	0.157	3.526	0.000	0.042
Gfod1	1353.44	0.558	0.164	3.395	0.001	0.061
Gpc4	347.77	0.559	0.167	3.355	0.001	0.066
Stox2	1998.84	0.561	0.174	3.226	0.001	0.093
Helz	1040.12	0.564	0.184	3.069	0.002	0.134
Klhl29	525.97	0.567	0.133	4.248	0.000	0.004
Plxna4	2841.62	0.569	0.130	4.380	0.000	0.002
Nrp1	660.07	0.573	0.195	2.944	0.003	0.173

Wnk1	280.61	0.573	0.187	3.063	0.002	0.135
Per2	309.08	0.578	0.171	3.372	0.001	0.064
Nr4a3	750.23	0.578	0.198	2.922	0.003	0.180
Plekhm1	234.12	0.580	0.189	3.076	0.002	0.132
Klhl3	708.17	0.583	0.199	2.928	0.003	0.178
Foxo1	545.26	0.586	0.165	3.543	0.000	0.041
Tmem28	246.29	0.587	0.192	3.063	0.002	0.135
Igf1r	977.38	0.587	0.166	3.529	0.000	0.042
Hip1	360.36	0.589	0.184	3.195	0.001	0.101
Kcnc1	958.28	0.593	0.190	3.127	0.002	0.118
Cacna1h	664.89	0.593	0.119	4.999	0.000	0.000
Ctif	717.53	0.593	0.169	3.513	0.000	0.044
Slit3	645.61	0.593	0.196	3.032	0.002	0.145
Hspa1b	118.33	0.593	0.191	3.105	0.002	0.124
Dagla	1010.45	0.594	0.131	4.534	0.000	0.001
Paqr8	1909.68	0.598	0.150	3.975	0.000	0.010
Slit1	870.97	0.604	0.179	3.383	0.001	0.063
Clstn2	838.89	0.604	0.198	3.054	0.002	0.138
Hipk2	1221.93	0.604	0.177	3.424	0.001	0.056
Tns3	832.45	0.606	0.147	4.110	0.000	0.006
Kdm6b	364.71	0.607	0.211	2.882	0.004	0.195
Foxk1	716.48	0.609	0.130	4.697	0.000	0.001
Eif4ebp2	660.18	0.610	0.205	2.968	0.003	0.166
Ankrd13a	237.32	0.610	0.181	3.380	0.001	0.063
Eif2s3x	1125.93	0.619	0.169	3.655	0.000	0.030
Zfhx2	757.75	0.627	0.127	4.949	0.000	0.000
Pkd1	1164.15	0.627	0.195	3.218	0.001	0.094
Arhgef17	1986.03	0.628	0.098	6.397	0.000	0.000
Otub2	201.32	0.641	0.217	2.955	0.003	0.170
Fbxl18	390.92	0.641	0.180	3.568	0.000	0.038
Kmt2d	2531.75	0.641	0.122	5.255	0.000	0.000
Dio2	855.09	0.644	0.200	3.226	0.001	0.093
Daam2	903.98	0.651	0.138	4.722	0.000	0.001
Gse1	862.77	0.651	0.123	5.309	0.000	0.000
Prox1	1278.75	0.665	0.219	3.040	0.002	0.143
Usp19	207.46	0.667	0.195	3.412	0.001	0.058
Rasgrf1	398.81	0.671	0.183	3.672	0.000	0.028
Tnrc18	1131.39	0.671	0.186	3.609	0.000	0.034
Klf13	2209.65	0.673	0.137	4.892	0.000	0.000
Samd4b	475.30	0.674	0.183	3.685	0.000	0.027
Slc39a14	265.16	0.677	0.183	3.700	0.000	0.026
Aff1	266.90	0.686	0.175	3.925	0.000	0.012

Tmub2	154.26	0.690	0.194	3.564	0.000	0.038
Bsn	6811.75	0.693	0.209	3.324	0.001	0.072
Itsn1	1065.44	0.700	0.226	3.100	0.002	0.125
Rere	837.50	0.715	0.202	3.538	0.000	0.041
Inhba	143.41	0.717	0.242	2.963	0.003	0.167
Hdac4	680.78	0.719	0.163	4.415	0.000	0.002
Gm26917	174416.94	0.720	0.190	3.789	0.000	0.019
Gm42829	64.23	0.720	0.248	2.903	0.004	0.187
Btaf1	1000.04	0.722	0.135	5.363	0.000	0.000
Znrf1	74.24	0.732	0.240	3.048	0.002	0.140
Soga1	524.02	0.739	0.208	3.558	0.000	0.039
Nptx1	3868.92	0.743	0.221	3.364	0.001	0.065
Doc2b	738.40	0.745	0.157	4.749	0.000	0.001
9230112E08Rik	67.42	0.745	0.258	2.887	0.004	0.194
Nrxn1	147.52	0.759	0.231	3.290	0.001	0.079
Gm45640	93.51	0.762	0.236	3.236	0.001	0.091
Pag1	321.28	0.766	0.183	4.182	0.000	0.005
Zswim6	194.09	0.770	0.266	2.896	0.004	0.190
Mdga1	541.01	0.776	0.185	4.196	0.000	0.005
Ap1ar	300.89	0.782	0.212	3.694	0.000	0.027
Cacna1i	751.83	0.796	0.181	4.398	0.000	0.002
Zbtb16	231.01	0.805	0.170	4.749	0.000	0.001
Irs2	999.69	0.819	0.242	3.379	0.001	0.063
9230112E08Rik	64.83	0.825	0.277	2.981	0.003	0.161
Nrp2	412.53	0.827	0.234	3.528	0.000	0.042
Tbc1d1	262.95	0.835	0.282	2.966	0.003	0.166
Trp53i11	273.50	0.837	0.271	3.086	0.002	0.129
Adar	897.52	0.853	0.288	2.965	0.003	0.167
Zbtb16	769.11	0.862	0.254	3.399	0.001	0.060
Klf15	92.70	0.888	0.276	3.218	0.001	0.094
Anks1b	559.27	0.914	0.191	4.777	0.000	0.000
Zbtb40	110.12	0.918	0.256	3.582	0.000	0.036
Bgn	84.33	0.921	0.309	2.985	0.003	0.160
Git1	676.32	0.927	0.312	2.967	0.003	0.166
Luzp1	484.57	0.928	0.212	4.374	0.000	0.002
Ide	830.64	0.930	0.207	4.496	0.000	0.001
Agap3	184.19	0.942	0.303	3.110	0.002	0.123
Focad	470.36	0.965	0.155	6.220	0.000	0.000
Gabra2	84.66	0.973	0.316	3.077	0.002	0.131
Cyhr1	108.78	0.974	0.240	4.053	0.000	0.008
Erc1	179.65	0.996	0.341	2.923	0.003	0.180
Fosl2	617.11	0.997	0.289	3.445	0.001	0.053

Mycl	164.85	1.017	0.349	2.914	0.004	0.183
Rapgef4	471.81	1.022	0.294	3.481	0.000	0.048
Taf1a	34.42	1.032	0.355	2.904	0.004	0.187
Arhgef12	45.59	1.036	0.318	3.259	0.001	0.085
Tspan18	158.59	1.039	0.233	4.458	0.000	0.002
Tnxb	133.22	1.061	0.207	5.138	0.000	0.000
Fbln2	36.64	1.067	0.348	3.061	0.002	0.136
Mat2b	44.79	1.077	0.348	3.098	0.002	0.126
Itpr1	48.14	1.078	0.363	2.968	0.003	0.166
R3hdm2	310.01	1.078	0.323	3.340	0.001	0.069
Epb41l1	160.79	1.109	0.344	3.219	0.001	0.094
C1ql2	328.57	1.113	0.270	4.126	0.000	0.006
Nfrkb	121.68	1.148	0.320	3.588	0.000	0.036
Spcs1	91.46	1.149	0.326	3.528	0.000	0.042
Cables1	101.51	1.160	0.261	4.437	0.000	0.002
Cdkal1	34.43	1.168	0.400	2.921	0.003	0.181
Gm37530	43.92	1.177	0.309	3.809	0.000	0.018
Mthfd2	40.98	1.179	0.383	3.079	0.002	0.131
Enox1	64.98	1.194	0.332	3.595	0.000	0.035
Lmo7	26.82	1.203	0.393	3.059	0.002	0.137
Auts2	109.25	1.207	0.356	3.386	0.001	0.062
Nrp1	97.79	1.214	0.303	4.007	0.000	0.009
Srp54a	41.41	1.237	0.346	3.572	0.000	0.037
Actn4	209.91	1.237	0.243	5.094	0.000	0.000
Nod1	24.82	1.246	0.413	3.020	0.003	0.150
Ube2d3	319.29	1.250	0.417	2.998	0.003	0.156
Nr2c1	72.26	1.293	0.391	3.308	0.001	0.076
Myef2	164.58	1.319	0.259	5.097	0.000	0.000
Gm21093	30.30	1.330	0.367	3.620	0.000	0.033
Iqsec1	357.54	1.343	0.394	3.405	0.001	0.059
Gm19439	55.65	1.343	0.431	3.115	0.002	0.121
Apba2	371.79	1.350	0.435	3.102	0.002	0.125
Zzef1	55.94	1.360	0.444	3.064	0.002	0.135
Gm3883	50.16	1.364	0.337	4.045	0.000	0.008
Mkks	118.79	1.374	0.412	3.339	0.001	0.069
Sh3bp5l	20.82	1.397	0.435	3.211	0.001	0.096
Baz2b	28.57	1.406	0.366	3.840	0.000	0.017
Chd5	453.83	1.412	0.433	3.259	0.001	0.085
Mxd4	404.64	1.412	0.189	7.490	0.000	0.000
Sfi1	43.81	1.412	0.486	2.905	0.004	0.187
Alkal2	18.89	1.423	0.465	3.057	0.002	0.137
Stx7	452.39	1.437	0.234	6.136	0.000	0.000

Armcx1	15.25	1.497	0.514	2.915	0.004	0.183
Ssrp1	42.10	1.500	0.352	4.258	0.000	0.004
Fastkd3	27.47	1.511	0.513	2.944	0.003	0.173
Cant1	106.93	1.522	0.505	3.013	0.003	0.152
Fam205a2	18.33	1.544	0.487	3.170	0.002	0.107
Kdm5c	379.95	1.552	0.496	3.132	0.002	0.117
Zfp316	74.95	1.554	0.538	2.890	0.004	0.192
Ogdh	21.55	1.580	0.490	3.225	0.001	0.093
Alkbh4	19.24	1.591	0.492	3.234	0.001	0.091
Ccnjl	34.85	1.593	0.353	4.510	0.000	0.001
Wdcp	63.33	1.601	0.285	5.610	0.000	0.000
Skiv2l	175.37	1.623	0.313	5.184	0.000	0.000
Nfat5	629.49	1.633	0.298	5.477	0.000	0.000
Zfp664	20.81	1.642	0.509	3.226	0.001	0.093
G530011O06Rik	35.32	1.646	0.430	3.829	0.000	0.017
Sema5a	81.63	1.660	0.578	2.873	0.004	0.199
Pex26	18.22	1.669	0.475	3.511	0.000	0.044
Myo5a	54.83	1.683	0.571	2.946	0.003	0.173
Ythdc1	46.12	1.685	0.421	4.001	0.000	0.009
Prpf38b	62.34	1.708	0.420	4.069	0.000	0.007
Tpm3	40.45	1.722	0.454	3.795	0.000	0.019
Gpr179	10.32	1.788	0.610	2.932	0.003	0.177
Hif3a	59.47	1.794	0.400	4.484	0.000	0.002
Spast	90.91	1.800	0.578	3.116	0.002	0.121
Cdc42bpa	28.23	1.877	0.631	2.975	0.003	0.164
Synj1	1402.52	1.909	0.376	5.072	0.000	0.000
6330418K02Rik	8.76	1.916	0.665	2.881	0.004	0.195
Wipi2	8.76	1.919	0.654	2.933	0.003	0.177
Ppme1	41.63	1.934	0.593	3.261	0.001	0.085
Prdm5	70.77	1.938	0.423	4.583	0.000	0.001
Mlph	19.16	1.943	0.631	3.078	0.002	0.131
Phc3	95.64	1.969	0.542	3.629	0.000	0.032
Ank2	4368.08	1.993	0.663	3.007	0.003	0.153
Clasp2	287.84	2.009	0.237	8.479	0.000	0.000
Rbm12b2	208.44	2.023	0.675	2.999	0.003	0.156
Proser1	9.15	2.032	0.679	2.993	0.003	0.157
C030029H02Rik	14.69	2.038	0.577	3.534	0.000	0.041
Pfkfb3	30.00	2.043	0.676	3.022	0.003	0.149
Srrm4	165.98	2.073	0.496	4.182	0.000	0.005
Trpm4	7.60	2.088	0.695	3.004	0.003	0.154
Cop1	11.70	2.134	0.585	3.644	0.000	0.031
Umad1	83.53	2.154	0.689	3.128	0.002	0.118

Sdccag3	22.23	2.155	0.551	3.913	0.000	0.013
Npr2	109.81	2.158	0.484	4.456	0.000	0.002
Edrf1	83.39	2.217	0.610	3.635	0.000	0.031
Enah	280.97	2.255	0.426	5.289	0.000	0.000
Gm16278	8.52	2.286	0.700	3.266	0.001	0.084
Bub1b	9.74	2.308	0.768	3.006	0.003	0.153
Ppp2r5c	71.09	2.323	0.791	2.938	0.003	0.175
Oplah	28.65	2.345	0.400	5.864	0.000	0.000
Dock9	554.46	2.348	0.712	3.299	0.001	0.077
Tmem267	48.66	2.412	0.734	3.287	0.001	0.079
Cdc42bpa	188.08	2.490	0.403	6.171	0.000	0.000
Klhl26	144.02	2.523	0.688	3.667	0.000	0.029
Cacnb3	71.86	2.524	0.840	3.006	0.003	0.153
Slco2b1	72.69	2.536	0.383	6.624	0.000	0.000
Rhobtb2	14.17	2.551	0.801	3.185	0.001	0.103
Acp2	108.56	2.555	0.734	3.479	0.001	0.048
Scamp3	21.66	2.579	0.713	3.615	0.000	0.033
Chka	21.46	2.587	0.631	4.097	0.000	0.007
Ptbp3	140.86	2.594	0.777	3.338	0.001	0.070
mt-Tr	91.68	2.642	0.330	8.007	0.000	0.000
Magi2	6.84	2.650	0.915	2.897	0.004	0.190
Lrrc14	15.74	2.662	0.724	3.674	0.000	0.028
Dmtn	30.71	2.678	0.835	3.209	0.001	0.097
Ccnh	120.44	2.686	0.875	3.069	0.002	0.134
Abr	18.72	2.688	0.539	4.989	0.000	0.000
Skil	396.47	2.717	0.664	4.092	0.000	0.007
Ankrd13c	133.88	2.777	0.549	5.058	0.000	0.000
Ssr4	11.16	2.800	0.767	3.649	0.000	0.030
Pa2g4	24.25	2.832	0.912	3.104	0.002	0.124
Gnao1	149.83	2.864	0.285	10.064	0.000	0.000
Pisd-ps1	18.86	2.891	0.934	3.094	0.002	0.127
Ercc6	41.01	2.895	0.945	3.064	0.002	0.135
Scube1	36.44	2.963	0.571	5.185	0.000	0.000
Sec24a	12.60	2.964	0.985	3.008	0.003	0.153
Pard3	25.16	2.998	0.954	3.142	0.002	0.115
Col4a3bp	277.30	3.015	0.833	3.618	0.000	0.033
Cttn	131.26	3.019	0.358	8.428	0.000	0.000
Mpzl2	11.11	3.032	0.990	3.061	0.002	0.136
Gfpt1	6.80	3.038	1.035	2.934	0.003	0.176
Ttll3	13.90	3.046	1.040	2.928	0.003	0.178
Atpaf1	11.68	3.054	0.981	3.112	0.002	0.122
Tbccd1	13.54	3.057	0.712	4.295	0.000	0.003

Slc36a1	335.68	3.098	0.475	6.518	0.000	0.000
Arhgef28	128.21	3.112	0.891	3.491	0.000	0.046
mt-Tg	61.40	3.117	0.365	8.543	0.000	0.000
Ppp4r1l-ps	12.09	3.120	1.086	2.874	0.004	0.199
Amd1	198.43	3.134	0.938	3.339	0.001	0.069
Supt20	24.18	3.142	1.026	3.064	0.002	0.135
Glrx2	11.28	3.160	0.889	3.557	0.000	0.039
Faim2	23.62	3.161	1.088	2.904	0.004	0.187
Rps19	40.37	3.171	0.900	3.524	0.000	0.042
Rnf220	57.80	3.197	0.651	4.913	0.000	0.000
Fam234b	329.89	3.201	0.253	12.652	0.000	0.000
Cnnm3	5.70	3.220	1.040	3.095	0.002	0.127
Glmp	5.64	3.226	1.115	2.893	0.004	0.191
Scyl2	17.36	3.235	1.098	2.947	0.003	0.172
Ago1	13.51	3.282	1.130	2.905	0.004	0.187
Gm21887	33.76	3.286	0.675	4.867	0.000	0.000
Ampd3	8.19	3.324	0.972	3.419	0.001	0.057
Qrich1	12.40	3.347	1.116	3.000	0.003	0.156
Camk2d	28.00	3.378	0.940	3.594	0.000	0.035
Ears2	10.86	3.469	0.842	4.120	0.000	0.006
Setd1b	6.64	3.479	1.062	3.277	0.001	0.082
Zfp128	11.53	3.482	1.033	3.370	0.001	0.064
Igsf8	6.34	3.491	1.187	2.942	0.003	0.173
Zdhhc18	6.41	3.508	1.216	2.886	0.004	0.194
Sin3a	100.81	3.531	0.847	4.167	0.000	0.005
Rab23	11.65	3.533	0.871	4.056	0.000	0.008
Shld1	16.20	3.562	0.690	5.161	0.000	0.000
Gm15446	80.59	3.599	0.425	8.467	0.000	0.000
Nfkb1	12.34	3.633	1.089	3.336	0.001	0.070
Ankrd6	4.91	3.640	1.240	2.936	0.003	0.175
Mid1	9.60	3.649	0.890	4.099	0.000	0.007
Cfap44	7.03	3.657	1.220	2.997	0.003	0.156
Traf4	19.98	3.675	0.729	5.045	0.000	0.000
Cd33	7.39	3.718	1.122	3.314	0.001	0.074
Ccnl1	10.20	3.719	0.874	4.258	0.000	0.004
Plce1	25.60	3.797	1.305	2.910	0.004	0.185
Snap91	5.28	3.808	1.232	3.092	0.002	0.127
Stx16	11.24	3.814	1.290	2.958	0.003	0.169
Adal	16.35	3.844	1.290	2.979	0.003	0.162
Cadm2	16.52	3.861	1.339	2.884	0.004	0.194
Cdk2ap1	20.00	3.918	1.298	3.020	0.003	0.150
Csmd2	37.68	3.919	0.901	4.350	0.000	0.003

Kif21b	183.66	3.922	0.620	6.330	0.000	0.000
Gm16867	5.68	3.937	1.352	2.911	0.004	0.184
Sec31a	8.99	3.951	1.370	2.885	0.004	0.194
Kdm3b	8.79	3.957	1.365	2.899	0.004	0.189
Atg16l1	23.69	3.958	1.177	3.362	0.001	0.065
Nktr	12.03	3.960	1.259	3.145	0.002	0.114
Rad9b	5.80	3.972	1.379	2.880	0.004	0.196
Eif1	117.13	3.998	0.461	8.665	0.000	0.000
9530077C05Rik	11.70	4.005	1.107	3.618	0.000	0.033
Hsph1	33.49	4.009	0.843	4.754	0.000	0.000
Myh14	84.86	4.025	1.153	3.493	0.000	0.046
Fn1	26.90	4.073	1.206	3.378	0.001	0.063
Ly6e	45.26	4.109	0.818	5.022	0.000	0.000
Gm5859	17.17	4.115	0.904	4.550	0.000	0.001
Sgms1	38.20	4.148	1.399	2.965	0.003	0.167
Golga4	17.07	4.151	0.976	4.254	0.000	0.004
Ylpm1	47.93	4.153	1.373	3.023	0.002	0.149
Lmo7	158.72	4.193	1.271	3.298	0.001	0.077
Sirt7	10.29	4.217	1.073	3.930	0.000	0.012
Pex12	31.43	4.219	0.639	6.604	0.000	0.000
Tia1	25.15	4.221	0.676	6.248	0.000	0.000
Rps13	7.05	4.221	1.165	3.625	0.000	0.032
Il1rap	20.00	4.233	1.410	3.003	0.003	0.155
Col11a2	19.80	4.247	1.412	3.009	0.003	0.153
Mical3	72.93	4.251	1.474	2.885	0.004	0.194
Rps23	19.44	4.260	1.173	3.632	0.000	0.032
Ldhb	11.19	4.262	1.292	3.299	0.001	0.077
Stard9	78.34	4.263	1.113	3.830	0.000	0.017
Myo9b	122.43	4.308	1.225	3.517	0.000	0.043
Nfasc	93.27	4.334	1.431	3.030	0.002	0.146
Gm5790	4.14	4.338	1.382	3.138	0.002	0.115
Tmem143	7.76	4.350	1.332	3.267	0.001	0.084
Tubgcp5	54.97	4.363	0.910	4.793	0.000	0.000
St5	4.25	4.387	1.363	3.220	0.001	0.094
Rufy3	603.52	4.391	0.714	6.147	0.000	0.000
Scmh1	105.26	4.393	1.105	3.976	0.000	0.010
Camk2d	59.92	4.412	1.342	3.287	0.001	0.079
Frmd4a	119.13	4.447	1.403	3.170	0.002	0.107
Tfdp2	4.49	4.450	1.428	3.115	0.002	0.121
Gdi2	84.91	4.476	0.572	7.823	0.000	0.000
Mapk12	4.53	4.484	1.375	3.260	0.001	0.085
Map4	244.04	4.505	1.231	3.660	0.000	0.029

Mapk3	17.43	4.513	1.441	3.132	0.002	0.117
Gria4	223.97	4.556	0.752	6.059	0.000	0.000
Dmtf1	19.06	4.561	1.205	3.785	0.000	0.020
4932438A13Rik	135.58	4.576	1.262	3.627	0.000	0.032
Cluh	249.76	4.578	1.193	3.838	0.000	0.017
Erbin	121.82	4.581	1.519	3.016	0.003	0.151
Kcnt2	55.44	4.587	1.414	3.244	0.001	0.088
Gm26760	2.47	4.621	1.593	2.900	0.004	0.188
Mrpl48	4.98	4.624	1.343	3.444	0.001	0.053
Inca1	5.04	4.637	1.384	3.349	0.001	0.067
Gm17751	2.51	4.638	1.537	3.017	0.003	0.150
Erlec1	18.57	4.645	1.571	2.956	0.003	0.170
A730020M07Rik	2.52	4.645	1.593	2.917	0.004	0.182
Kcnj9	19.12	4.656	0.978	4.761	0.000	0.000
Spg20	91.35	4.664	1.311	3.557	0.000	0.039
Ascc1	14.77	4.700	1.554	3.025	0.002	0.148
Pcyt1b	82.22	4.701	0.523	8.991	0.000	0.000
Palld	2.61	4.701	1.609	2.922	0.003	0.180
Gm16933	2.61	4.701	1.609	2.922	0.003	0.180
Armc9	2.64	4.713	1.580	2.982	0.003	0.161
Acmsd	2.64	4.715	1.558	3.026	0.002	0.148
L1cam	19.75	4.735	1.321	3.586	0.000	0.036
Pls3	41.48	4.753	1.541	3.086	0.002	0.129
Cenpt	2.78	4.790	1.525	3.142	0.002	0.115
Ppfibp1	2.80	4.797	1.520	3.157	0.002	0.111
Pomt1	2.82	4.805	1.547	3.107	0.002	0.124
Ctnnd1	2.83	4.810	1.595	3.015	0.003	0.151
Aasdh	29.04	4.821	1.392	3.464	0.001	0.050
Arhgef2	161.24	4.837	1.316	3.675	0.000	0.028
Col4a2	2.89	4.846	1.666	2.910	0.004	0.185
Surf4	2.93	4.866	1.479	3.290	0.001	0.079
Zfp408	2.93	4.866	1.590	3.061	0.002	0.136
Gm42715	467.15	4.870	0.738	6.596	0.000	0.000
Gm17081	2.97	4.883	1.561	3.127	0.002	0.118
Ctnnd1	2.98	4.885	1.606	3.041	0.002	0.143
Prkab1	2.99	4.892	1.695	2.886	0.004	0.194
Kcnj3	17.21	4.928	1.573	3.133	0.002	0.117
Tmem234	3.07	4.932	1.684	2.929	0.003	0.178
Tmc6	3.07	4.934	1.550	3.183	0.001	0.104
Tcerg1	26.71	4.934	1.513	3.262	0.001	0.085
Pram1	3.09	4.942	1.483	3.331	0.001	0.071
Il18bp	6.24	4.954	1.407	3.521	0.000	0.043

Srrt	3.12	4.954	1.600	3.097	0.002	0.126
Vps25	6.38	4.979	1.729	2.880	0.004	0.195
Plce1	46.30	4.987	1.624	3.071	0.002	0.134
Gab1	75.91	5.008	1.206	4.151	0.000	0.006
Tedc2	3.27	5.020	1.600	3.137	0.002	0.116
Nrf1	6.56	5.027	1.576	3.190	0.001	0.102
Cyth4	3.32	5.047	1.670	3.022	0.003	0.149
Taf2	3.33	5.051	1.633	3.094	0.002	0.127
Mme	37.84	5.052	1.326	3.810	0.000	0.018
Psme3	3.34	5.055	1.529	3.306	0.001	0.076
Zfp276	3.34	5.057	1.505	3.361	0.001	0.066
Fgd2	3.38	5.070	1.457	3.479	0.001	0.048
Eif1	108.95	5.075	0.676	7.503	0.000	0.000
4933416C03Rik	3.41	5.081	1.530	3.320	0.001	0.073
Tcirg1	6.95	5.114	1.454	3.518	0.000	0.043
Tjap1	35.86	5.115	1.176	4.349	0.000	0.003
Irf8	3.51	5.126	1.455	3.524	0.000	0.042
Rbm34	3.52	5.129	1.704	3.010	0.003	0.153
Xrcc3	3.56	5.144	1.614	3.187	0.001	0.103
Nrd1	278.27	5.158	1.282	4.024	0.000	0.009
Sybu	37.35	5.176	1.182	4.379	0.000	0.002
Tmem25	3.64	5.180	1.704	3.040	0.002	0.143
Ap2b1	3.66	5.188	1.442	3.597	0.000	0.035
Bcor	34.79	5.195	1.792	2.899	0.004	0.189
Gm13301	33.93	5.196	0.824	6.309	0.000	0.000
Wscd1	21.45	5.206	1.740	2.991	0.003	0.158
Abhd12	28.39	5.210	1.771	2.942	0.003	0.173
Mthfsd	13.43	5.212	1.255	4.153	0.000	0.006
Bud31	21.88	5.243	1.188	4.412	0.000	0.002
Npy5r	14.70	5.244	1.795	2.922	0.003	0.180
Mbtps2	3.83	5.252	1.446	3.633	0.000	0.032
Reep4	3.83	5.252	1.446	3.633	0.000	0.032
Sdc3	3.86	5.258	1.472	3.572	0.000	0.037
Card6	3.88	5.266	1.752	3.006	0.003	0.153
Prkab1	3.91	5.279	1.761	2.997	0.003	0.156
Pfkfb4	8.19	5.356	1.821	2.942	0.003	0.173
Scaper	37.95	5.358	1.645	3.258	0.001	0.085
Plscr1	4.14	5.361	1.579	3.396	0.001	0.061
Phldb1	55.44	5.377	1.105	4.866	0.000	0.000
Pts	15.82	5.383	1.307	4.117	0.000	0.006
Slc39a2	4.22	5.392	1.765	3.054	0.002	0.138
Pqlc1	15.26	5.395	1.695	3.182	0.001	0.104

Fam83d	4.24	5.400	1.557	3.468	0.001	0.049
Fam193a	4.26	5.405	1.403	3.851	0.000	0.016
Saal1	8.49	5.405	1.440	3.753	0.000	0.022
Pcbp4	8.46	5.407	1.624	3.330	0.001	0.071
Plekhb1	115.36	5.409	1.708	3.167	0.002	0.108
Mkrn1	92.27	5.413	1.390	3.895	0.000	0.014
Abl1	24.55	5.437	1.861	2.922	0.003	0.181
Adam8	4.39	5.447	1.869	2.915	0.004	0.183
Rab11a	4.39	5.449	1.409	3.867	0.000	0.015
Nrxn2	4.41	5.453	1.394	3.913	0.000	0.013
Sh3glb1	4.43	5.460	1.517	3.599	0.000	0.035
Psrc1	8.88	5.471	1.504	3.637	0.000	0.031
Tgfb1i1	4.47	5.472	1.767	3.096	0.002	0.126
Gm13302	4.48	5.474	1.537	3.561	0.000	0.038
Fosb	4.54	5.496	1.520	3.616	0.000	0.033
Rnf123	82.50	5.497	0.650	8.452	0.000	0.000
Gm13304	4.54	5.497	1.567	3.508	0.000	0.044
Gm10600	17.33	5.514	1.195	4.615	0.000	0.001
Gm12576	4.63	5.521	1.553	3.556	0.000	0.039
Adamts17	26.62	5.541	1.024	5.412	0.000	0.000
Gpatch2	16.34	5.568	1.908	2.918	0.004	0.182
Zfp219	4.98	5.628	1.761	3.197	0.001	0.100
Adgrl4	4.99	5.633	1.367	4.122	0.000	0.006
Trim27	46.66	5.635	1.185	4.756	0.000	0.000
Cops6	27.78	5.654	0.912	6.196	0.000	0.000
Pard3	44.08	5.668	1.105	5.131	0.000	0.000
Hsd17b7	5.12	5.670	1.374	4.127	0.000	0.006
Tcirg1	5.12	5.671	1.366	4.151	0.000	0.006
Fbxo18	5.13	5.673	1.378	4.116	0.000	0.006
Ulk1	92.45	5.678	1.729	3.285	0.001	0.080
Slc25a25	65.73	5.719	1.467	3.900	0.000	0.013
Pcsk6	97.91	5.723	1.600	3.576	0.000	0.037
Srrt	40.19	5.730	1.424	4.023	0.000	0.009
1810014B01Rik	5.45	5.759	1.388	4.148	0.000	0.006
Tars	5.52	5.780	1.458	3.963	0.000	0.011
Arhgef9	483.40	5.782	1.910	3.028	0.002	0.147
Kcnq2	1851.04	5.862	0.639	9.175	0.000	0.000
Hrh2	11.62	5.864	1.555	3.771	0.000	0.021
Enah	5.99	5.899	1.351	4.366	0.000	0.002
Ralbp1	132.77	5.910	1.450	4.076	0.000	0.007
Fbxo25	33.38	5.916	0.926	6.390	0.000	0.000
Cdc42bpa	228.65	5.918	1.187	4.985	0.000	0.000

Akt2	12.35	5.956	1.643	3.624	0.000	0.032
Pdlim5	6.32	5.974	1.369	4.362	0.000	0.002
Nfkb1	23.31	5.984	1.215	4.926	0.000	0.000
Acvr1	47.20	5.988	1.585	3.778	0.000	0.020
Memo1	12.90	6.020	1.796	3.352	0.001	0.067
Sdr39u1	13.72	6.113	1.692	3.613	0.000	0.033
Ly6c1	7.02	6.124	1.970	3.109	0.002	0.123
Klf15	7.18	6.159	1.347	4.572	0.000	0.001
Spag5	7.20	6.162	1.665	3.701	0.000	0.026
March11	7.20	6.162	1.494	4.126	0.000	0.006
Drd1	14.38	6.184	1.706	3.625	0.000	0.032
Alg9	7.39	6.198	1.345	4.607	0.000	0.001
Capn3	7.50	6.222	2.120	2.935	0.003	0.176
Smoc2	14.77	6.222	1.383	4.499	0.000	0.001
Tubgcp4	27.75	6.225	1.437	4.332	0.000	0.003
Opa1	7.89	6.295	1.368	4.603	0.000	0.001
Scaper	57.49	6.313	1.529	4.129	0.000	0.006
Lef1	8.08	6.330	2.082	3.040	0.002	0.143
Gm8995	8.36	6.376	1.848	3.450	0.001	0.052
Mpdz	8.37	6.379	1.303	4.897	0.000	0.000
Sipa1l3	31.65	6.404	1.273	5.032	0.000	0.000
Haus2	31.11	6.404	1.944	3.294	0.001	0.078
Eif5a	8.70	6.437	1.396	4.609	0.000	0.001
Kmt5b	147.18	6.438	1.774	3.630	0.000	0.032
Cpsf1	8.74	6.439	1.358	4.743	0.000	0.001
Zfp691	9.03	6.490	1.423	4.562	0.000	0.001
Dclk1	9.21	6.518	1.425	4.575	0.000	0.001
Cyth2	118.44	6.533	0.667	9.789	0.000	0.000
Abraxas1	18.37	6.536	2.015	3.244	0.001	0.088
Zfp651	18.64	6.558	2.032	3.228	0.001	0.092
Rbm18	9.50	6.562	1.442	4.552	0.000	0.001
Hltf	53.55	6.580	1.924	3.420	0.001	0.057
Phf21b	9.70	6.594	1.886	3.496	0.000	0.046
Zfp982	9.80	6.607	1.296	5.098	0.000	0.000
Cep250	9.97	6.632	1.314	5.046	0.000	0.000
Abcc10	10.21	6.668	1.306	5.104	0.000	0.000
Magi1	55.78	6.691	0.947	7.068	0.000	0.000
Nfkb1	10.42	6.694	1.418	4.722	0.000	0.001
Tmem241	10.48	6.702	1.353	4.953	0.000	0.000
Clmn	10.71	6.735	1.346	5.004	0.000	0.000
Sorbs2	39.18	6.783	1.887	3.595	0.000	0.035
Trit1	11.71	6.865	1.460	4.703	0.000	0.001

Tbc1d24	11.90	6.886	1.274	5.404	0.000	0.000
B3gnt9	11.92	6.891	1.587	4.342	0.000	0.003
Cdan1	12.05	6.906	1.624	4.252	0.000	0.004
Prdm10	23.83	6.918	2.047	3.379	0.001	0.063
Ciz1	12.23	6.926	1.370	5.057	0.000	0.000
Srek1	12.28	6.933	1.311	5.290	0.000	0.000
Fbrsl1	73.66	6.950	1.717	4.048	0.000	0.008
Dennd4b	12.45	6.951	2.240	3.104	0.002	0.124
Ddb2	12.61	6.973	1.374	5.074	0.000	0.000
Stx18	12.71	6.982	2.057	3.394	0.001	0.061
Pphln1	69.34	6.988	0.957	7.304	0.000	0.000
Wwp1	72.01	7.019	1.122	6.253	0.000	0.000
Zfhx3	194.51	7.045	1.585	4.445	0.000	0.002
Vash2	13.40	7.059	1.386	5.094	0.000	0.000
Uaca	13.56	7.076	1.603	4.415	0.000	0.002
Krba1	13.91	7.113	1.797	3.958	0.000	0.011
Lgals8	27.56	7.129	2.314	3.080	0.002	0.131
4932438A13Rik	79.07	7.163	1.896	3.777	0.000	0.020
Tmem106c	14.46	7.168	1.484	4.832	0.000	0.000
Hnrnpk	14.90	7.210	1.436	5.020	0.000	0.000
Frmd4b	84.63	7.259	0.918	7.907	0.000	0.000
Lysmd4	15.89	7.304	1.452	5.029	0.000	0.000
Mospd2	16.31	7.343	1.434	5.122	0.000	0.000
Galnt6	32.05	7.347	1.993	3.686	0.000	0.027
Gm15446	16.54	7.360	1.386	5.311	0.000	0.000
Slc25a35	16.64	7.372	1.273	5.792	0.000	0.000
Lysmd3	16.71	7.377	1.307	5.645	0.000	0.000
Strn4	16.82	7.387	1.663	4.441	0.000	0.002
Gm49527	16.89	7.393	1.330	5.558	0.000	0.000
Pi4ka	16.97	7.398	1.278	5.788	0.000	0.000
Zfp687	17.00	7.402	2.251	3.288	0.001	0.079
Bhlhb9	17.88	7.474	2.276	3.284	0.001	0.080
Epb41l3	17.91	7.476	1.274	5.867	0.000	0.000
Rrnad1	18.36	7.513	1.587	4.735	0.000	0.001
Thnsl1	18.53	7.525	1.578	4.769	0.000	0.000
Psd2	126.27	7.536	1.939	3.885	0.000	0.014
Flna	18.71	7.539	1.758	4.289	0.000	0.003
Cwc22	18.83	7.548	2.448	3.084	0.002	0.129
Wdr17	37.97	7.591	2.236	3.395	0.001	0.061
Fastk	19.46	7.597	1.304	5.828	0.000	0.000
Sgk1	253.15	7.670	1.701	4.509	0.000	0.001
Fam214b	20.84	7.695	1.274	6.040	0.000	0.000

C2cd3	22.42	7.801	1.312	5.945	0.000	0.000
Ccdc85a	44.05	7.807	2.575	3.032	0.002	0.146
Cxxc4	23.02	7.840	1.279	6.128	0.000	0.000
Papola	23.22	7.851	1.832	4.285	0.000	0.003
Ap2a1	23.26	7.853	2.152	3.649	0.000	0.030
Kctd10	23.32	7.858	1.240	6.335	0.000	0.000
Nat10	23.36	7.860	1.249	6.293	0.000	0.000
Porcn	23.54	7.872	1.416	5.559	0.000	0.000
Gh	23.78	7.886	2.279	3.461	0.001	0.050
Lig3	24.68	7.938	1.538	5.160	0.000	0.000
Sec24a	25.82	8.004	1.239	6.463	0.000	0.000
Pcdha11	26.39	8.036	1.940	4.143	0.000	0.006
Ccne2	27.21	8.079	1.531	5.276	0.000	0.000
Cnot4	27.55	8.097	1.320	6.135	0.000	0.000
Nagk	28.67	8.155	1.274	6.403	0.000	0.000
Csmd2	29.24	8.184	1.235	6.627	0.000	0.000
Xist	8355.03	8.191	0.351	23.339	0.000	0.000
Immt	274.19	8.206	0.840	9.766	0.000	0.000
Dnm2	31.64	8.297	1.242	6.682	0.000	0.000
Trmt6	33.26	8.371	1.256	6.662	0.000	0.000
Fnbp1	33.94	8.398	1.448	5.799	0.000	0.000
Pmm1	34.67	8.430	1.987	4.243	0.000	0.004
Grb10	128.78	8.440	2.730	3.092	0.002	0.127
Med12	73.54	8.548	2.644	3.233	0.001	0.091
Abcg2	38.46	8.579	1.246	6.883	0.000	0.000
Phldb1	40.08	8.639	1.238	6.981	0.000	0.000
Inpp4a	40.78	8.663	1.460	5.935	0.000	0.000
Adrm1	41.35	8.684	1.280	6.785	0.000	0.000
Xist	43.57	8.759	1.233	7.102	0.000	0.000
D430042O09Rik	44.84	8.800	2.266	3.884	0.000	0.014
Map3k12	49.74	8.950	1.241	7.212	0.000	0.000
Zc3h14	56.99	9.146	3.175	2.880	0.004	0.195
Smc6	65.37	9.344	3.228	2.895	0.004	0.190
Gpbp1	65.94	9.357	1.229	7.616	0.000	0.000
Kansl1l	67.05	9.381	3.201	2.930	0.003	0.178
Ssx2ip	68.91	9.421	3.200	2.944	0.003	0.173
Pisd	69.63	9.436	1.297	7.273	0.000	0.000
Cend1	254.99	9.453	2.424	3.900	0.000	0.013
Megf11	70.86	9.461	1.250	7.569	0.000	0.000
Oplah	73.67	9.517	1.237	7.695	0.000	0.000
Synpo2	75.01	9.543	1.685	5.665	0.000	0.000
Plek	75.32	9.549	3.243	2.944	0.003	0.173

Diaph1	282.04	9.617	1.103	8.718	0.000	0.000
Exosc10	84.55	9.716	3.212	3.025	0.002	0.148
Dzip1	87.92	9.772	3.317	2.946	0.003	0.173
Rab11fip3	308.52	9.777	2.113	4.626	0.000	0.001
Pogk	93.52	9.861	3.267	3.019	0.003	0.150
Rassf2	94.02	9.869	3.238	3.048	0.002	0.140
Tbc1d24	94.32	9.874	1.620	6.096	0.000	0.000
Dock9	96.17	9.901	3.240	3.056	0.002	0.138
Dnm2	96.69	9.909	1.283	7.721	0.000	0.000
Erbin	99.33	9.948	3.243	3.067	0.002	0.135
Zmym1	100.59	9.966	1.332	7.484	0.000	0.000
Ppp6r3	103.44	10.007	3.291	3.041	0.002	0.143
Tia1	110.82	10.106	3.264	3.096	0.002	0.126
Ptprs	111.95	10.121	3.260	3.105	0.002	0.124
Rab11b	112.39	10.126	2.321	4.363	0.000	0.002
Ipo4	113.47	10.140	3.268	3.103	0.002	0.124
Baz2a	121.92	10.244	3.278	3.125	0.002	0.119
Dsp	122.25	10.248	1.257	8.152	0.000	0.000
Kalrn	124.98	10.279	3.273	3.141	0.002	0.115
Pex5l	126.65	10.299	3.265	3.154	0.002	0.112
Pde10a	130.79	10.345	3.268	3.165	0.002	0.108
Phf8	134.60	10.387	1.220	8.514	0.000	0.000
Sept2	138.29	10.425	3.286	3.173	0.002	0.107
Kifc2	142.19	10.466	1.615	6.479	0.000	0.000
Fam219a	152.79	10.569	3.318	3.185	0.001	0.103
Setd1b	156.37	10.603	3.309	3.205	0.001	0.098
Cacna1b	160.00	10.636	3.305	3.218	0.001	0.094
Cacna1b	162.70	10.660	3.307	3.223	0.001	0.093
Myo9a	178.23	10.791	3.321	3.249	0.001	0.087
Stx16	197.18	10.937	3.323	3.292	0.001	0.079
4932438A13Rik	227.09	11.141	1.670	6.671	0.000	0.000
Fryl	245.50	11.253	3.351	3.358	0.001	0.066
Synj1	249.41	11.276	3.413	3.304	0.001	0.076
Atp13a3	274.96	11.417	1.216	9.389	0.000	0.000
Speg	275.99	11.422	3.376	3.383	0.001	0.063
Gad1	280.64	11.447	1.334	8.581	0.000	0.000
Ap2a1	379.03	11.880	3.430	3.464	0.001	0.050
Cacna2d1	521.22	12.340	3.453	3.573	0.000	0.037
Kcnab2	404.89	24.661	3.666	6.728	0.000	0.000

Table 2.4: List of B2 RNA regulated SRGs (B2-SRGs) (see Table 2.1) that are up-regulated in 6-month old APP mice compared to WT (see Table 2.3).

4932438A13Rik		Abcg2	Ank2	Anks1b		Apba2	Arid1b	Btbd9	Cacna2d1		Cenpt
Csmd2	Ctif	Cyth4	Dagla	Dclk1	Erc1	Fbln2	Fbxo18		Fosb	Foxn3	Foxo3
Frmd4a		Frmd4b		Gabra2	Grb10	Gria4	Hipk2	Htt	Il1rap	Iqsec1	Itpr1
Kbtbd11		Kcnc1	Kcnq3	Kcnt2	Klf15	Magi1	Magi2	Mdga1	Mical3	Mpdz	Nr2c1
Nrxn1	Nrxn2	Pag1	Palld	Pcdha11		Pde10a	Phf21b	Pisd	Pkd1	Plce1	Plxna4
Ppfibp1		Ppp6r3	Prdm5	Prkag2	Prpf38b		Ptprs	Rnf220		Scmh1	
Sema5a		Sgk1	Sgms1	Slc35f3		Smoc2	Sorbs2	Srrm4	Srrt	Sybu	Tns3
Usp19	Zhx2										

Table 2.5: List of B2 RNA regulated SRGs (B2-SRGs) (see Table 2.1) that are up-regulated in 6-month old APP mice (see Table 2.3) and are associated with learning based on Peleg et al, Science 2010.

Apba2	Ctif	Gria4	Hipk2	Kcnc1	Kcnt2	Mpdz	Pisd	Ppp6r3	Ptprs	Smoc2	Sybu	Zhx2

Table 2.6: Complete lists of enriched terms in B2 RNA regulated SRGs (B2-SRGs) that are up-regulated in 6-month old APP mice compared to WT (see Table 2.4) for Biological Process and Cellular Compartment. An EASE score cut-off of 0.05 has been applied.

GO Biological Process

Term	**Count**	**P-Value**	**Fisher Exact**
nervous system development	15	5.40E-03	2.40E-03
vocal learning	2	1.90E-02	1.40E-04
voluntary musculoskeletal movement	2	1.90E-02	1.40E-04
intracellular signal transduction	16	2.30E-02	1.20E-02
observational learning	2	2.40E-02	2.30E-04
auditory behavior	2	2.80E-02	3.40E-04
negative regulation of sequestering of calcium ion	3	3.20E-02	2.90E-03
release of sequestered calcium ion into cytosol	3	3.20E-02	2.90E-03
calcium ion import into cytosol	3	3.20E-02	2.90E-03
regulation of sequestering of calcium ion	3	4.30E-02	4.50E-03
sequestering of calcium ion	3	4.30E-02	4.50E-03
axon extension	3	4.50E-02	4.90E-03
synapse assembly	3	4.70E-02	5.30E-03
neurogenesis	10	4.90E-02	2.30E-02

GO Cellular Compartment

Term	Count	P-Value	Fisher Exact
ion channel complex	5	1.00E-02	1.70E-03
transmembrane transporter complex	5	1.40E-02	2.40E-03
cation channel complex	4	1.80E-02	2.30E-03
voltage-gated potassium channel complex	3	2.90E-02	2.50E-03

Table 2.7: Up-regulated genes in HT22 cells treated with amyloid beta and Scr LNA compared to cells treated with the control peptide and scr LNA. Values were calculated using DESeq (see chapter 2 methods) on long-RNA-seq data. Only genes with an padj < 0.2 are depicted.

Gene Name	baseMean	log2FoldChange	lfcSE	stat	pvalue	padj
Mbnl2	425.55	0.368	0.112	3.297	0.001	0.075
Lrch3	345.68	0.536	0.174	3.085	0.002	0.136
Bclaf1	117.96	0.540	0.162	3.327	0.001	0.069
Racgap1	142.86	0.660	0.214	3.089	0.002	0.135
Colgalt1	515.27	0.667	0.203	3.280	0.001	0.079
Cdc45	177.79	0.751	0.214	3.514	0.000	0.038
Cp	103.76	0.807	0.209	3.862	0.000	0.011
Nat10	103.82	0.831	0.261	3.182	0.001	0.105
Xab2	79.87	0.863	0.269	3.212	0.001	0.096
Nfatc3	39.62	0.905	0.307	2.948	0.003	0.189
Fars2	73.98	0.914	0.309	2.960	0.003	0.183
Pfkfb2	83.51	0.937	0.287	3.270	0.001	0.081
Acin1	41.03	0.941	0.316	2.982	0.003	0.174
Zfp398	68.85	0.963	0.302	3.193	0.001	0.101
Epb41l3	240.14	0.976	0.319	3.063	0.002	0.144
H6pd	296.81	1.008	0.247	4.084	0.000	0.005
Plekha5	106.30	1.022	0.262	3.897	0.000	0.010
Tsnax	34.58	1.032	0.341	3.028	0.002	0.157
Raf1	261.50	1.033	0.275	3.759	0.000	0.016
Ttf2	108.46	1.043	0.200	5.227	0.000	0.000
Csnk1e	17.88	1.065	0.362	2.939	0.003	0.193
Tcf4	31.38	1.078	0.332	3.248	0.001	0.086
Nprl2	28.71	1.078	0.316	3.418	0.001	0.052
Mesd	275.66	1.102	0.373	2.958	0.003	0.184
Grn	101.23	1.103	0.282	3.916	0.000	0.009
Mdn1	27.78	1.104	0.308	3.580	0.000	0.031
Nisch	151.34	1.115	0.290	3.842	0.000	0.012
Khnyn	43.41	1.121	0.342	3.277	0.001	0.079
Rspry1	200.37	1.123	0.326	3.450	0.001	0.046
Ganc	25.71	1.135	0.367	3.096	0.002	0.133

Trmt1l	13.91	1.162	0.396	2.930	0.003	0.196
Slc25a3	35.73	1.187	0.330	3.601	0.000	0.029
Srcap	30.75	1.224	0.355	3.449	0.001	0.046
Xrcc6	23.92	1.256	0.369	3.402	0.001	0.054
Prpf3	21.37	1.257	0.426	2.948	0.003	0.189
Wwp2	51.92	1.269	0.358	3.540	0.000	0.035
Ei24	254.24	1.374	0.440	3.126	0.002	0.122
Wdr61	76.46	1.383	0.372	3.715	0.000	0.019
Kif15	14.50	1.413	0.470	3.010	0.003	0.164
Hnrnpf	84.50	1.416	0.465	3.044	0.002	0.152
Adi1	12.44	1.417	0.458	3.094	0.002	0.133
Dnajc7	19.05	1.423	0.437	3.254	0.001	0.085
Sgms1	69.47	1.443	0.418	3.454	0.001	0.046
Sar1a	627.48	1.446	0.308	4.697	0.000	0.000
Matr3	178.82	1.488	0.454	3.280	0.001	0.079
Cyb5r3	59.53	1.520	0.276	5.516	0.000	0.000
Paxbp1	174.46	1.522	0.390	3.897	0.000	0.010
Capn15	17.29	1.535	0.509	3.013	0.003	0.163
Nat10	31.25	1.545	0.510	3.029	0.002	0.157
Glb1l	18.28	1.557	0.479	3.250	0.001	0.086
Ulk1	12.16	1.570	0.506	3.100	0.002	0.131
Eda2r	11.41	1.608	0.464	3.463	0.001	0.044
Papd5	25.51	1.612	0.502	3.209	0.001	0.097
Znrd1	25.09	1.618	0.539	3.002	0.003	0.166
2310022A10Rik	14.72	1.666	0.439	3.793	0.000	0.014
Ppp4r2	27.47	1.676	0.531	3.156	0.002	0.111
Obsl1	155.40	1.681	0.544	3.089	0.002	0.135
Dpy19l3	7.54	1.689	0.535	3.154	0.002	0.112
Dcakd	50.98	1.721	0.445	3.872	0.000	0.011
Osbpl5	12.68	1.733	0.592	2.927	0.003	0.198
Kptn	8.04	1.734	0.579	2.997	0.003	0.168
Sh3glb1	413.48	1.748	0.272	6.420	0.000	0.000
Coro1b	7.66	1.789	0.611	2.926	0.003	0.198
Cnpy3	13.52	1.798	0.439	4.099	0.000	0.004
Psma3	46.61	1.804	0.554	3.254	0.001	0.085
Mrpl2	14.65	1.834	0.588	3.118	0.002	0.124
Nme7	16.77	1.846	0.599	3.081	0.002	0.138
Scyl3	55.17	1.857	0.482	3.849	0.000	0.012
Gstcd	24.44	1.865	0.543	3.434	0.001	0.049
Serpinb6a	186.44	1.867	0.628	2.970	0.003	0.179
Xrcc6	46.20	1.891	0.416	4.548	0.000	0.001
Gcc2	18.02	1.908	0.526	3.628	0.000	0.026

Aes	97.12	1.967	0.656	3.000	0.003	0.167
4632433K11Rik	6.97	1.968	0.642	3.063	0.002	0.144
Gm46430	15.48	1.998	0.669	2.986	0.003	0.173
Sri	130.93	2.019	0.443	4.558	0.000	0.001
Plekhj1	21.04	2.031	0.618	3.285	0.001	0.078
Naa16	39.19	2.033	0.692	2.938	0.003	0.193
Zc3h14	130.22	2.042	0.379	5.393	0.000	0.000
Aak1	64.69	2.117	0.495	4.275	0.000	0.002
Apc	7.96	2.139	0.731	2.926	0.003	0.198
Ubqln1	227.49	2.143	0.546	3.926	0.000	0.009
Rb1cc1	29.86	2.184	0.551	3.964	0.000	0.008
Itm2b	70.90	2.223	0.596	3.730	0.000	0.018
Mapk1ip1l	41.56	2.262	0.751	3.013	0.003	0.163
Atp5a1	42.72	2.273	0.488	4.654	0.000	0.000
Rtel1	23.97	2.295	0.753	3.048	0.002	0.150
Nfe2l1	732.91	2.335	0.661	3.534	0.000	0.035
Wnk1	8.10	2.338	0.627	3.727	0.000	0.018
Pdcd5	6.97	2.396	0.673	3.558	0.000	0.033
Triobp	54.52	2.441	0.784	3.112	0.002	0.127
Csde1	1642.10	2.461	0.806	3.053	0.002	0.149
Zfp426	46.36	2.461	0.654	3.762	0.000	0.016
Mbd5	9.55	2.494	0.786	3.175	0.001	0.106
Dennd6b	15.87	2.535	0.850	2.982	0.003	0.174
Myl6	42.14	2.595	0.719	3.611	0.000	0.028
Dynlt1c	56.32	2.615	0.320	8.171	0.000	0.000
Rarg	269.50	2.670	0.908	2.940	0.003	0.192
Ephb2	63.37	2.727	0.708	3.854	0.000	0.011
Rai1	9.15	2.894	0.800	3.615	0.000	0.027
Clcn5	5.23	2.897	0.893	3.246	0.001	0.087
Yes1	70.66	2.954	0.738	4.005	0.000	0.006
Aifm2	7.42	3.056	0.881	3.467	0.001	0.044
P4ha2	10.51	3.142	0.900	3.491	0.000	0.041
Snord2	4.29	3.154	0.949	3.322	0.001	0.070
Evl	28.32	3.200	0.820	3.901	0.000	0.010
Klhl26	53.15	3.216	0.947	3.396	0.001	0.055
Arid4b	81.14	3.225	1.035	3.115	0.002	0.126
mt-Ts2	32.92	3.252	1.069	3.042	0.002	0.152
Mtx1	13.14	3.326	0.944	3.524	0.000	0.037
Polr1e	4.74	3.396	1.089	3.120	0.002	0.124
Pgap2	13.96	3.471	1.095	3.170	0.002	0.107
Dvl2	115.75	3.546	0.856	4.143	0.000	0.004
Fam214b	16.52	3.549	1.183	3.000	0.003	0.167

Ube3a	69.78	3.578	1.200	2.983	0.003	0.174
Sp100	5.71	3.639	1.109	3.282	0.001	0.078
Zfp809	12.93	3.651	1.096	3.331	0.001	0.068
Osgepl1	7.85	3.667	1.061	3.456	0.001	0.045
Cflar	15.02	3.679	1.250	2.945	0.003	0.190
4932438A13Rik	13.64	3.737	0.866	4.316	0.000	0.002
Apol8	50.84	3.739	1.104	3.388	0.001	0.057
Osbpl9	13.94	3.742	0.975	3.838	0.000	0.012
Aasdhppt	6.03	3.742	1.107	3.379	0.001	0.058
Stx6	15.57	3.786	0.967	3.916	0.000	0.009
Homer3	11.73	3.840	0.916	4.192	0.000	0.003
Pex2	20.66	3.913	1.179	3.319	0.001	0.071
Tut7	6.64	3.925	1.291	3.040	0.002	0.153
Acox3	8.69	4.008	0.885	4.530	0.000	0.001
Dcun1d4	7.00	4.015	1.061	3.784	0.000	0.015
Tfdp2	14.94	4.033	1.138	3.544	0.000	0.034
Cttnbp2nl	22.85	4.039	1.203	3.357	0.001	0.063
Zfp606	9.19	4.040	1.325	3.048	0.002	0.150
Ccnt1	128.75	4.071	0.836	4.869	0.000	0.000
Mcfd2	42.29	4.141	0.869	4.764	0.000	0.000
Nktr	2.28	4.160	1.304	3.190	0.001	0.102
Eci2	4.26	4.305	1.229	3.504	0.000	0.039
Trmt2a	20.82	4.329	0.947	4.573	0.000	0.001
Fkbp11	8.00	4.331	1.225	3.535	0.000	0.035
Abi1	181.45	4.343	1.117	3.889	0.000	0.010
Ccdc43	49.38	4.466	0.570	7.834	0.000	0.000
Btbd2	73.47	4.469	1.422	3.144	0.002	0.116
Rdx	50.50	4.490	1.340	3.351	0.001	0.064
Gm28036	8.27	4.491	1.202	3.737	0.000	0.018
Sorbs1	8.09	4.507	1.153	3.909	0.000	0.009
Lmod2	1.75	4.510	1.497	3.013	0.003	0.163
Lrrc51	1.82	4.557	1.513	3.011	0.003	0.164
Zfp235	5.42	4.645	1.167	3.981	0.000	0.007
Gm14411	1.90	4.661	1.469	3.172	0.002	0.107
Wasf1	22.28	4.664	1.540	3.029	0.002	0.157
Urgcp	5.63	4.679	1.109	4.217	0.000	0.003
Rwdd2a	8.51	4.703	0.953	4.936	0.000	0.000
Cdc26	14.71	4.726	1.128	4.188	0.000	0.003
Mfsd2b	2.02	4.735	1.597	2.965	0.003	0.182
Dpf2	79.93	4.743	0.764	6.210	0.000	0.000
Celf2	19.90	4.819	1.349	3.572	0.000	0.031
Cul4b	27.52	4.834	1.522	3.177	0.001	0.106

Kdm5a	15.79	4.835	1.638	2.953	0.003	0.186
Sema5a	25.57	4.838	1.416	3.416	0.001	0.052
Ints8	123.87	4.851	1.383	3.508	0.000	0.038
Men1	31.46	4.880	1.274	3.831	0.000	0.012
Phf8	90.36	4.997	1.177	4.244	0.000	0.002
Gripap1	30.64	5.064	1.378	3.674	0.000	0.022
Gm15787	2.66	5.175	1.382	3.744	0.000	0.017
Stx11	25.34	5.231	1.117	4.684	0.000	0.000
Kars	15.13	5.252	1.470	3.574	0.000	0.031
Apol9a	8.57	5.302	1.435	3.695	0.000	0.020
Maf1	37.39	5.308	1.503	3.530	0.000	0.036
Helz2	216.78	5.312	1.568	3.387	0.001	0.057
Atp5a1	514.03	5.360	0.420	12.752	0.000	0.000
Brd3	435.52	5.423	1.840	2.947	0.003	0.189
2310001H17Rik	5.36	5.481	1.527	3.591	0.000	0.030
Tbrg4	3.56	5.511	1.262	4.367	0.000	0.001
Mettl6	3.97	5.555	1.252	4.435	0.000	0.001
Odf2	9.34	5.589	1.688	3.310	0.001	0.072
Smad2	17.31	5.609	1.746	3.212	0.001	0.096
Ltbp4	24.59	5.658	1.786	3.168	0.002	0.108
Nkapd1	57.46	5.707	0.555	10.283	0.000	0.000
Krt80	18.59	5.715	1.278	4.472	0.000	0.001
Hmga1	7.33	5.775	1.204	4.796	0.000	0.000
Sgta	36.50	5.789	1.654	3.499	0.000	0.040
Klhl18	30.95	5.928	0.919	6.447	0.000	0.000
Dynlt1c	5.38	6.001	1.326	4.527	0.000	0.001
Trnau1ap	4.83	6.033	1.252	4.819	0.000	0.000
Nol8	25.08	6.063	2.008	3.020	0.003	0.160
Adarb1	28.61	6.088	1.723	3.532	0.000	0.036
Edem3	49.47	6.137	1.829	3.356	0.001	0.063
Jade3	31.36	6.161	2.019	3.051	0.002	0.150
Rubcn	23.50	6.234	1.708	3.650	0.000	0.024
Pag1	10.80	6.265	1.674	3.742	0.000	0.017
Ankrd13b	9.58	6.324	1.973	3.206	0.001	0.097
Asb7	15.90	6.373	1.991	3.201	0.001	0.099
Mfn2	40.07	6.395	1.823	3.508	0.000	0.038
Bvht	7.93	6.541	1.210	5.408	0.000	0.000
Arvcf	23.91	6.591	2.033	3.242	0.001	0.088
Hmga1	13.70	6.719	1.292	5.201	0.000	0.000
Mitf	13.88	6.862	2.005	3.423	0.001	0.051
Polrmt	21.58	6.910	1.943	3.556	0.000	0.033
Radil	16.17	6.915	1.305	5.299	0.000	0.000

Tnip2	22.07	6.919	2.193	3.155	0.002	0.112
Gstz1	10.21	7.089	1.217	5.826	0.000	0.000
Zfp422	20.43	7.296	2.479	2.943	0.003	0.191
Cd44	55.87	7.462	2.377	3.140	0.002	0.117
Rps6kb2	18.57	7.512	2.482	3.027	0.002	0.158
Anks1	44.38	7.574	2.272	3.334	0.001	0.068
Gramd1a	17.65	7.616	2.499	3.047	0.002	0.150
Vac14	34.10	7.623	2.472	3.084	0.002	0.136
Park7	26.73	7.775	2.594	2.997	0.003	0.168
Mia2	25.64	7.794	2.198	3.546	0.000	0.034
Dis3l2	18.73	7.837	2.534	3.093	0.002	0.133
Trim26	22.41	8.199	2.536	3.233	0.001	0.090
Psip1	24.32	8.332	2.843	2.930	0.003	0.196
Lig3	33.02	8.612	2.852	3.019	0.003	0.160
Rfx5	34.37	8.628	2.487	3.470	0.001	0.044
Naa50	62.70	9.453	2.627	3.598	0.000	0.029
Pcdh1	56.01	9.571	1.100	8.698	0.000	0.000
Pcnx	100.59	9.923	2.708	3.664	0.000	0.023
Ptbp1	239.58	10.184	3.422	2.976	0.003	0.176
Adam9	268.04	10.263	3.422	2.999	0.003	0.167
Flna	418.06	10.279	3.422	3.004	0.003	0.166
Lig3	101.95	10.298	2.724	3.781	0.000	0.015
Jmjd1c	400.51	10.421	3.422	3.046	0.002	0.151
Smc6	284.88	11.798	1.049	11.251	0.000	0.000
Herc2	588.56	11.838	3.422	3.460	0.001	0.045
Oxr1	317.93	12.015	3.052	3.936	0.000	0.008
Dab2	26.44	18.534	3.620	5.120	0.000	0.000
Ptprs	30.27	18.631	3.620	5.147	0.000	0.000
Map4k4	36.04	18.756	3.620	5.181	0.000	0.000
Lmf2	39.42	18.821	3.620	5.199	0.000	0.000
Map4k4	45.18	18.919	3.620	5.226	0.000	0.000
Acox1	51.13	19.008	3.620	5.251	0.000	0.000
Abr	54.42	19.053	3.620	5.263	0.000	0.000
Zfx	68.78	19.221	3.620	5.310	0.000	0.000
Mta1	71.62	19.250	3.620	5.318	0.000	0.000
Tmem184b	77.97	19.311	3.620	5.334	0.000	0.000
Fosb	113.85	19.583	3.620	5.410	0.000	0.000
Fosb	132.44	19.691	3.620	5.440	0.000	0.000
Flnc	150.10	19.781	3.620	5.464	0.000	0.000
Sept2	175.06	19.890	3.620	5.494	0.000	0.000
Chd4	184.49	19.929	3.620	5.505	0.000	0.000
Abcd3	26.99	21.968	3.535	6.215	0.000	0.000

Gm28036	27.13	21.972	3.535	6.216	0.000	0.000
Cep290	21.88	22.124	3.535	6.259	0.000	0.000
Rtn3	48.24	22.209	3.534	6.284	0.000	0.000
Plk4	34.29	22.652	3.534	6.409	0.000	0.000
Mtch2	35.78	22.764	3.534	6.441	0.000	0.000
Ewsr1	41.05	22.957	3.534	6.495	0.000	0.000
Cul7	41.21	22.959	3.534	6.496	0.000	0.000
Exosc10	46.32	23.062	3.534	6.525	0.000	0.000
Itsn1	46.80	23.135	3.534	6.546	0.000	0.000
U2surp	91.20	23.349	3.563	6.554	0.000	0.000
Wdfy1	76.61	23.534	3.500	6.723	0.000	0.000
Hp1bp3	113.77	24.084	3.500	6.881	0.000	0.000
Rpl41	111.65	24.234	3.534	6.857	0.000	0.000
Asxl1	107.49	24.679	3.534	6.983	0.000	0.000

Table 2.8: List of genes that are up-regulated in HT22 cells treated with amyloid beta (see Table 2.7) and in 6-month old APP mice (see Table 2.3).

4932438A13Rik Abr Epb41l3 Exosc10 Fam214b Flna Fosb Itsn1 Klhl26 Lig3 Nat10 Nktr Pag1 Pcdh1 Phf8 Ptprs Sema5a Sept2 Sgms1 Sh3glb1 Smc6 Tfdp2 Ulk1 Wnk1 Zc3h14

Table 2.9: List of B2 RNA regulated SRGs (B2-SRGs) (see Table 2.1) that are up-regulated in HT22 cells treated with amyloid beta and Scr LNA compared to cells treated with the control peptide and scr LNA (see Table 2.7).

4932438A13Rik Adarb1 Arvcf Bclaf1 Cep290 Dab2 Fosb Gstcd Men1 Mitf Osbpl9 Oxr1 Pag1 Polrmt Ptbp1 Ptprs Rai1 Rb1cc1 Sema5a Sgms1 Sorbs1 Tmem184b Trmt2a Vac14 Xab2

Table 2.10: Complete lists of enriched terms in B2 RNA regulated SRGs (B2-SRGs) that are up-regulated in HT22 cells treated with amyloid beta (see Table 2.9) for Biological Process and Cellular Compartment.

GO Biological Process

Term	**Count**	**P-Value**	**Fisher Exact**
regulation of apoptotic process	6	1.40E-02	3.60E-03
regulation of programmed cell death	6	1.50E-02	3.80E-03
negative regulation of RNA metabolic process	5	2.80E-02	6.90E-03

positive regulation of transforming growth factor beta receptor signaling pathway	2	3.00E-02	4.50E-04
positive regulation of cellular response to transforming growth factor beta stimulus	2	3.00E-02	4.50E-04
positive regulation of DNA-templated transcription, initiation	2	3.10E-02	4.90E-04
RNA metabolic process	10	3.30E-02	1.60E-02
cell surface receptor signaling pathway	7	3.30E-02	1.20E-02
positive regulation of transcription, DNA-templated	5	4.00E-02	1.10E-02
negative regulation of nucleobase-containing compound metabolic process	5	4.00E-02	1.10E-02
regulation of DNA-templated transcription, initiation	2	4.00E-02	8.40E-04
positive regulation of RNA biosynthetic process	5	4.10E-02	1.10E-02
positive regulation of RNA metabolic process	5	4.60E-02	1.30E-02

GO Cellular Compartment

Term	**Count**	**P-Value**	**Fisher Exact**
transferase complex, transferring phosphorus-containing groups	4	2.80E-03	2.10E-04
nucleus	13	3.60E-02	2.20E-02

Table 2.11: Correlation coefficients and p-values for genes of Figure 2.15E. Includes genes for which there was read coverage across all sample and the correlation p value was less than 0.05.

	r	**p-value**
Eea1	0.805898426	4.49E-08
Vmn1r28	0.77155313	3.75E-07
Lrp1	0.768150647	4.54E-07
Hhat	0.763814555	5.76E-07
Ints1	0.742754809	1.71E-06
Rhoj	0.741644276	1.81E-06
Atad2b	0.732228722	2.84E-06
Gcn1l1	0.731022511	3.01E-06
Lrrk2	0.725883989	3.81E-06
Mast4	0.725563474	3.87E-06
Exoc4	0.724584335	4.04E-06
Gstcd	0.72239414	4.46E-06
Evc2	0.721594287	4.63E-06
Myo18a	0.716895416	5.70E-06
Cabin1	0.715325799	6.11E-06

Zdhhc6	0.714168297	6.43E-06
Vac14	0.712455093	6.92E-06
Zfp959	0.708286988	8.28E-06
Prkd1	0.705705908	9.23E-06
Sufu	0.701867952	1.08E-05
Macf1	0.700929776	1.13E-05
Stx3	0.699857129	1.18E-05
Pacsin2	0.696922122	1.33E-05
Thada	0.695311077	1.42E-05
Brd4	0.694684997	1.45E-05
Myo1d	0.694371856	1.47E-05
Dlg5	0.691027694	1.68E-05
Asb3	0.690784097	1.70E-05
Ror1	0.689439904	1.79E-05
Mocs1	0.689198584	1.81E-05
Pofut2	0.689115586	1.81E-05
Slc16a10	0.688842016	1.83E-05
Matn2	0.68596525	2.05E-05
Thsd7a	0.685278436	2.10E-05
Ttc28	0.685079818	2.12E-05
Arid3a	0.683537642	2.25E-05
Rbm14	0.683264184	2.27E-05
Fam160b1	0.68287177	2.31E-05
Gm6685	0.682729822	2.32E-05
Mapkap1	0.681781903	2.41E-05
Etv6	0.681483773	2.44E-05
Ext1	0.680280324	2.55E-05
Scaf8	0.680162926	2.56E-05
Dtnb	0.680124541	2.56E-05
Clcn7	0.680037908	2.57E-05
Ikbkap	0.678935881	2.68E-05
Med13l	0.677605965	2.82E-05
Snd1	0.677066082	2.88E-05
Tmem2	0.676691461	2.92E-05
Dhcr24	0.676658211	2.92E-05
Sh3bp1	0.676505929	2.94E-05
Fasn	0.675739183	3.03E-05
Papd4	0.675437448	3.06E-05
Faf1	0.674951814	3.12E-05
Specc1l	0.674620844	3.15E-05

Slc35d1	0.674524119	3.17E-05
Nf2	0.673938319	3.24E-05
Csnk2a2	0.673360012	3.31E-05
Ubr5	0.673212351	3.32E-05
Dusp10	0.673024121	3.35E-05
Frk	0.671017266	3.60E-05
Polr3b	0.670592141	3.66E-05
Rai14	0.670450149	3.68E-05
Usp24	0.670311636	3.70E-05
Zfp207	0.670021472	3.74E-05
Cnksr3	0.669767733	3.77E-05
Ascc3	0.667687402	4.07E-05
Gpc6	0.667011432	4.17E-05
Atxn1l	0.666430456	4.26E-05
Nfya	0.666101116	4.31E-05
Mcm5	0.664704918	4.53E-05
Etv3	0.66391344	4.66E-05
Slc25a13	0.663516664	4.73E-05
Foxp4	0.661276354	5.12E-05
Tyms	0.660687977	5.23E-05
Oxct1	0.659870497	5.38E-05
Apaf1	0.656300451	6.10E-05
Flcn	0.655844303	6.19E-05
Edem1	0.655135661	6.35E-05
Igf2bp3	0.654997583	6.38E-05
Map3k4	0.65494698	6.39E-05
Trerf1	0.65455492	6.48E-05
Tspan9	0.653077354	6.81E-05
Slc38a4	0.653067645	6.82E-05
Snapc3	0.652999638	6.83E-05
Fer1l6	0.652519063	6.95E-05
Adk	0.652358696	6.98E-05
Smg5	0.651859263	7.11E-05
Lpp	0.650399649	7.47E-05
AW554918	0.65017625	7.52E-05
Xdh	0.64840956	7.99E-05
Akap9	0.648308994	8.02E-05
Ncor2	0.647625726	8.20E-05
Lrpprc	0.646880656	8.41E-05
Antxr2	0.646381845	8.55E-05

Zmpste24	0.646321584	8.57E-05
Aplf	0.646261152	8.59E-05
Zc3h7a	0.646055193	8.65E-05
Vdr	0.645261302	8.88E-05
Dcaf7	0.645063211	8.94E-05
Tspan11	0.645013376	8.95E-05
Tmtc3	0.643471687	9.43E-05
Xpnpep1	0.643436949	9.44E-05
Arhgap18	0.643028968	9.57E-05
Snx25	0.6429117	9.60E-05
Cnot6	0.642267852	9.81E-05
Ccdc80	0.641347836	0.00010112
Drosha	0.641131797	0.000101842
Msrb3	0.640923754	0.000102542
Ift27	0.640646971	0.000103479
Rab31	0.640511946	0.000103939
Hus1	0.639593892	0.000107117
Fbxo4	0.63949797	0.000107454
Mdfic	0.639282755	0.000108213
Gas2l1	0.639204754	0.00010849
Rictor	0.639188575	0.000108547
Ccdc50	0.638423425	0.000111293
Tm9sf3	0.638289331	0.000111781
Rpn1	0.637977101	0.000112924
Snord95	0.636820519	0.000117249
Cdk8	0.636556133	0.000118258
Cdk5rap2	0.635848019	0.000120999
Casp12	0.63569375	0.000121604
Pcdh18	0.634798945	0.000125164
Prim2	0.634261467	0.000127347
Kdm4c	0.634073111	0.00012812
Smchd1	0.633924275	0.000128734
Utrn	0.632871419	0.000133151
Zfp160	0.632464767	0.000134893
Map2k2	0.632266481	0.00013575
Ipo13	0.632165029	0.00013619
Plekhh2	0.631960653	0.000137081
Gm9008	0.631655178	0.000138422
Tnc	0.631217988	0.000140361
Tbx15	0.631133875	0.000140737

Zmym4	0.630149962	0.000145201
Heatr6	0.629685903	0.00014735
Ptbp1	0.629132096	0.000149952
Svep1	0.62908938	0.000150154
Fndc3b	0.628855595	0.000151266
Zc3h3	0.628300869	0.000153934
Bclaf1	0.627978101	0.000155505
Men1	0.625869122	0.000166128
Nfic	0.625753645	0.000166728
Bicc1	0.625059786	0.000170373
2610037D02Rik	0.625026738	0.000170548
Plec	0.624823619	0.00017163
Brd1	0.624599715	0.000172829
Fig4	0.623965297	0.000176267
Psme4	0.623850162	0.000176898
Asap1	0.623782968	0.000177266
Evc	0.622938315	0.000181962
Rhbdd1	0.622761788	0.000182957
Pdzrn3	0.621546	0.000189944
Slc30a4	0.62150998	0.000190154
Prr5	0.621301385	0.000191378
Itgbl1	0.621126171	0.000192411
Arhgap28	0.621020282	0.000193038
Nhlrc3	0.61891024	0.000205911
Rassf8	0.618779593	0.000206732
Fam98a	0.618743643	0.000206959
Tcf20	0.618686822	0.000207317
Ctps2	0.61851892	0.00020838
Deptor	0.618484345	0.000208599
Nfib	0.618458311	0.000208765
Osbpl9	0.617568313	0.000214489
Rgma	0.617419018	0.000215463
Olfr460	0.616850255	0.000219208
Tle1	0.616633759	0.000220649
Nuf2	0.616512937	0.000221457
Arid2	0.616090879	0.000224299
Ppp1r10	0.615907218	0.000225546
Met	0.615855501	0.000225899
Foxp1	0.61584422	0.000225975
Ghr	0.615430207	0.000228814

Pvt1	0.615078093	0.000231253
Polrmt	0.615049261	0.000231453
Fbxo5	0.614924364	0.000232325
Lclat1	0.614470023	0.000235519
Zkscan17	0.614209323	0.000237369
Efna5	0.614099537	0.000238152
Col6a1	0.613732273	0.000240788
Skp2	0.613720248	0.000240875
Pkdcc	0.613629568	0.00024153
Arfip1	0.613606029	0.0002417
Pla2g6	0.612872643	0.00024706
Arhgap29	0.612754121	0.000247936
Tbc1d22a	0.612158066	0.000252383
Ifit2	0.611966269	0.000253829
Cdc40	0.610727699	0.000263346
Pabpc1	0.609422817	0.000273713
Atp11c	0.609046127	0.000276772
Tab1	0.608357309	0.000282444
Ebf1	0.608120465	0.000284419
Runx2	0.607866924	0.000286545
Mkl1	0.606854378	0.000295181
Abca7	0.60671201	0.000296413
Nde1	0.606276053	0.000300215
Vps13b	0.606161526	0.000301221
Adamts12	0.606156227	0.000301268
Glis3	0.606152371	0.000301302
Birc5	0.605886212	0.000303652
Tlr4	0.605860478	0.00030388
St3gal3	0.605816812	0.000304267
Ano10	0.605190866	0.000309868
Immp1l	0.604929665	0.000312233
Stk3	0.604780763	0.000313587
Pcbp3	0.604007478	0.000320708
Lipa	0.603331122	0.000327052
Ddah2	0.603014567	0.00033006
Brpf3	0.601330563	0.000346474
Zfat	0.600513673	0.000354693
Elac2	0.600131596	0.000358597
Mllt3	0.600038843	0.00035955
Slc29a3	0.599905489	0.000360924

Pon2	0.59989247	0.000361059
2610316D01Rik	0.599606711	0.000364021
Ptprk	0.599549951	0.000364612
Bnc2	0.598449293	0.000376239
Nsfl1c	0.597916242	0.000381987
Zfp442	0.597707367	0.00038426
Spata6	0.597329456	0.000388404
Tiam2	0.597314774	0.000388565
Glipr1	0.597110259	0.000390825
Slc6a9	0.596678851	0.00039563
Mthfd2l	0.596406087	0.000398694
Ptprf	0.595950226	0.000403863
Abhd16a	0.595680962	0.000406944
Dysf	0.595613015	0.000407725
Brd2	0.595547076	0.000408484
Prkar2b	0.59518681	0.000412652
Chchd3	0.595167467	0.000412877
Dlg1	0.593971966	0.000426987
Cyp2j6	0.593027995	0.000438427
Mgst1	0.591907215	0.000452361
Srbd1	0.591707532	0.000454884
Smoc1	0.591387066	0.000458959
Prep	0.590587679	0.000469265
Ehbp1	0.59034246	0.000472468
Vta1	0.589403318	0.000484911
Phc2	0.589029346	0.000489945
Mrpl13	0.588935517	0.000491216
Hbs1l	0.587954979	0.000504667
Nudcd1	0.587923216	0.000505108
Lrp12	0.586634855	0.00052329
Tatdn2	0.586388553	0.000526831
Safb2	0.586127411	0.000530608
Smarcad1	0.585703106	0.000536796
Lrrc42	0.585583402	0.000538553
Ube3b	0.585057177	0.000546339
Echdc1	0.584863922	0.000549222
Cnot2	0.583221121	0.000574285
Cyp4f16	0.582099878	0.000591963
Dock8	0.581779988	0.000597094
Mex3a	0.580667271	0.000615248

Rell1	0.579564363	0.000633719
Skap2	0.579224089	0.000639515
Slc10a7	0.579152469	0.000640741
Hddc2	0.577715541	0.000665779
Tmem184b	0.577222881	0.000674559
Ptk2	0.576890021	0.000680549
Yif1a	0.576078224	0.000695353
Tmcc1	0.575861408	0.000699355
Trmt2a	0.57550783	0.000705924
Ergic1	0.575036976	0.000714757
Plscr3	0.575033161	0.000714829
Mcm9	0.574691548	0.000721298
Pld1	0.573482432	0.000744611
Fer	0.572369335	0.000766655
Mtap	0.571423853	0.000785828
Msl2	0.569265276	0.000831186
Txnrd3	0.56742562	0.00087164
Zfand3	0.5660923	0.00090203
Arid5b	0.565927756	0.000905844
Wrn	0.565798137	0.000908858
Gm17067	0.564836534	0.000931497
Hsf2	0.564149604	0.000947971
Sgsm3	0.562690584	0.00098381
Snip1	0.558797848	0.001085301
Tle2	0.556415046	0.001151847
Jak2	0.55600795	0.001163566
Cdc14a	0.555457479	0.001179579
Ddr1	0.555217963	0.001186606
Tnrc6b	0.554632123	0.001203948
Gm16156	0.554262571	0.001215001
Nt5dc1	0.553739192	0.001230807
Gm12666	0.553434581	0.001240088
Tigd2	0.552345864	0.001273763
Cdyl2	0.552302383	0.001275125
Pam	0.551812306	0.001290557
Stambpl1	0.551103012	0.00131318
Osmr	0.551050019	0.001314884
Xab2	0.549461173	0.001366881
Lrba	0.549365253	0.001370077
Tbc1d5	0.549216251	0.001375054

Ndrg1	0.549089423	0.001379303
Egfr	0.549054267	0.001380483
L3mbtl3	0.547052961	0.001449114
Zfp248	0.546664038	0.001462791
Apoh	0.546074289	0.001483746
Arfgef1	0.545062733	0.001520298
Ehbp1l1	0.545013515	0.001522096
Gpr108	0.544588016	0.00153772
Cnot6l	0.543863037	0.001564663
Cenpo	0.543706454	0.001570536
Ccdc86	0.542980302	0.001598023
Gulp1	0.541606119	0.001651189
Eya1	0.541149115	0.001669209
Vcam1	0.540646955	0.001689205
Epm2a	-0.540082722	0.001711923
BC017158	0.539831577	0.001722119
Dip2a	0.538935551	0.001758931
Aim2	0.538770603	0.001765782
Pde5a	0.538058923	0.001795607
Usp15	0.53587339	0.001889952
Trmt11	0.53530096	0.001915364
Slc38a1	0.535015657	0.00192814
Rsrc1	0.534384075	0.001956686
Sox5	-0.534119908	0.001968734
Lmcd1	-0.534088995	0.001970148
Zfp947	0.532915604	0.00202448
Nat2	0.531482432	0.002092602
Npr3	0.530426691	0.002144048
BC005561	0.530193487	0.002155559
Gm16268	0.530171274	0.002156658
Rai1	0.529248304	0.002202763
Mecom	0.528891267	0.002220826
Med12l	-0.528274206	0.002252347
Meis1	0.527392842	0.002298042
Nkain2	-0.527177706	0.002309317
Snrpn	-0.526322071	0.002354636
Smyd3	0.525408943	0.002403848
Mctp1	-0.525041983	0.002423875
Zfp946	0.524888274	0.002432306
Cdh11	-0.524402183	0.002459137

Nrg1	0.523925374	0.002485704
Abcd2	-0.52375141	0.002495459
Aig1	-0.523622893	0.002502687
Irs1	0.523436695	0.00251319
Kcnab1	-0.52327111	0.002522563
Pcdh15	-0.523233688	0.002524686
Cdh13	-0.522045844	0.002592864
Kcnb2	-0.521644318	0.002616268
Dab2	0.521557176	0.002621372
Gsta3	-0.521214353	0.002641532
Alg6	0.521213813	0.002641564
Vsnl1	-0.521122605	0.002646951
Ccdc34	0.520728719	0.002670321
Dgki	-0.520450883	0.002686913
Cops5	0.518877858	0.002782543
Akap6	-0.518697505	0.002793693
Col11a1	-0.518676781	0.002794976
Wisp1	0.518587914	0.002800487
Cntn3	-0.517697869	0.002856196
Lrp1b	-0.517608885	0.002861818
Nlgn1	-0.517563693	0.002864677
Mapk10	-0.516873902	0.002908621
Palmd	-0.516835387	0.002911092
Cntnap2	-0.516574866	0.002927851
Tsga10	-0.516540572	0.002930064
Ispd	-0.516519232	0.002931441
Fam135b	-0.515902694	0.002971479
Nalcn	-0.515805983	0.002977802
Heca	0.51540317	0.003004263
Abca8b	-0.5153458	0.003008048
Khdrbs2	-0.515287248	0.003011916
Pigk	0.515221138	0.003016287
Rtn1	-0.515113004	0.00302345
Homer2	-0.514618333	0.003056404
Fgf14	-0.513908099	0.003104259
Slc35f1	-0.513541661	0.003129201
Unc5c	-0.513320325	0.003144351
Elavl2	-0.513309377	0.003145102
Myt1l	-0.513117811	0.003158267
Nrxn3	-0.512642314	0.003191152

Hook1	-0.51256757	0.003196348
Pdzrn4	-0.51246435	0.003203535
Gstm5	-0.512460729	0.003203787
Grip1	-0.512269261	0.003217158
Matk	-0.512071676	0.003231005
Sorcs3	-0.511813186	0.003249199
Dner	-0.511794502	0.003250518
Stau2	-0.511298243	0.003285707
Agmo	-0.511288048	0.003286433
Phyhipl	-0.510921614	0.003312632
Camk2b	-0.510674282	0.003330417
Rab11fip4	-0.510469865	0.003345178
Ppm1k	-0.510420667	0.003348739
Cpne8	-0.51028978	0.003358229
Plxnc1	-0.509891996	0.003387212
Limch1	-0.509708156	0.00340068
Kcnh3	-0.509577288	0.003410295
Raver2	-0.508763994	0.003470575
Fam19a2	-0.508752703	0.003471419
Stxbp4	0.508642044	0.003479693
Enpp3	0.508622877	0.003481128
Grm8	-0.508316428	0.003504138
Srgap3	-0.508126692	0.003518451
Osbp2	-0.507897923	0.003535774
Amy1	-0.507818626	0.003541796
Opcml	-0.507768119	0.003545637
Golga7b	-0.507693809	0.003551293
Adamtsl1	-0.507430257	0.003571417
Sgip1	-0.507311514	0.003580517
Arap2	-0.507308913	0.003580716
Hdac9	-0.507291856	0.003582025
Atg7	0.507214817	0.003587941
Mtss1	-0.506921563	0.003610538
H60b	0.506863908	0.003614995
Trpm3	-0.506738106	0.003624737
Cry1	0.506725896	0.003625684
Gprin3	-0.506720658	0.00362609
Ldb2	-0.506657256	0.00363101
Traf3ip2	0.506522276	0.003641503
Mrap2	-0.505837681	0.003695126

Zdhhc14	-0.505636327	0.003711026
Grik2	-0.505497629	0.003722013
Osbpl6	-0.505419513	0.003728213
Dnajc6	-0.505346148	0.003734044
Dnm3	-0.505101167	0.003753572
Cacng2	-0.504915408	0.003768438
Zfpm2	-0.504647198	0.003789992
Ica1	-0.503948923	0.003846604
Gabrb1	-0.503817283	0.003857358
Arnt2	-0.503614812	0.003873948
Crim1	0.503015434	0.003923421
9330182L06Rik	-0.502807127	0.003940741
Angpt1	-0.502599447	0.003958075
Pdzd2	-0.502440871	0.003971354
Slc2a13	-0.502305148	0.00398275
Ksr2	-0.502257802	0.003986732
Rhpn1	-0.501923127	0.004014978
Ppp1r9a	-0.501824767	0.004023312
Lbh	0.501506017	0.004050421
Atp2b2	-0.501220075	0.004074873
Sema6b	-0.501115429	0.004083854
Kcnh1	-0.500919507	0.004100713
Slc24a3	-0.500911785	0.004101379
Sfxn5	-0.499745192	0.004203022
Ncald	-0.499660753	0.004210463
Sorcs2	-0.499578395	0.00421773
Gm3739	0.497437449	0.004410476
Igsf3	-0.497333117	0.004420059
Dlgap2	-0.49708397	0.004443015
Kcnk10	-0.496318454	0.00451419
9130401M01Rik	0.495522505	0.004589229
Mthfd1l	0.495321711	0.004608327
Arhgap26	-0.495262623	0.00461396
Lifr	-0.494760837	0.004662034
Grid1	-0.494320519	0.004704573
Syn2	-0.494154351	0.004720712
Dab1	-0.494067149	0.004729201
Herc3	-0.493831864	0.00475217
Abcb1a	-0.493751266	0.00476006
Ech1	0.493118366	0.004822408

Psd3	-0.49289579	0.0048445
Ppp1r14c	-0.492763089	0.004857713
Tmem132d	-0.49271259	0.004862749
Prickle2	-0.49241517	0.004892501
Dlgap1	-0.492396998	0.004894323
Jazf1	-0.492214402	0.004912672
Dlg2	-0.491606579	0.004974175
Spata5	0.491323945	0.005002997
Kcnip4	-0.491264144	0.005009113
Celsr2	-0.491104144	0.00502551
Bank1	-0.491083182	0.005027662
Nubpl	0.490698065	0.005067331
Oxr1	0.489934762	0.005146748
Rab30	-0.489825474	0.005158206
Ptprcap	0.489597409	0.005182186
Adamts6	0.489439044	0.005198893
Cntln	0.48924397	0.005219536
Lemd3	0.48823871	0.005327031
Kank1	-0.488191937	0.005332078
Adarb2	-0.487915632	0.005361978
Celsr1	-0.487462306	0.005411344
Reln	-0.487188127	0.005441389
4930522L14Rik	0.486914127	0.005471557
Abcc8	-0.48690091	0.005473016
Hivep2	-0.486609666	0.005505247
Nav3	-0.486604434	0.005505827
Ppm1h	-0.486393864	0.005529233
Fhl3	0.486101017	0.005561925
Dnajc21	0.485420599	0.005638522
Ptprm	-0.483512234	0.005858178
Efr3a	0.483220256	0.00589242
Stxbp6	-0.482985743	0.005920047
Cdh4	-0.482586013	0.005967392
Cntnap4	-0.482414545	0.0059878
Ncdn	-0.482344562	0.005996146
Sntb1	-0.481779313	0.006063923
Spon1	-0.481770627	0.00606497
Exoc6	-0.48155212	0.006091349
Sema3d	-0.48131413	0.006120191
Mfap5	0.481250293	0.006127947

Tcte2	0.481025725	0.006155299
Nhsl1	-0.48059194	0.006208427
Rbfox2	0.480234838	0.006252456
Adcy8	-0.479956263	0.006286988
9530026P05Rik	-0.479511794	0.00634242
Fuca2	0.479461892	0.006348669
Sox2ot	-0.479393487	0.006357245
Rmst	-0.479131242	0.006390211
Ahr	0.478009406	0.006532883
Pja2	-0.477910664	0.00654557
Ank1	-0.477715553	0.0065707
Alk	-0.477595677	0.00658618
Kcnmb2	-0.477212688	0.006635847
Slc13a4	-0.476825848	0.006686336
Zfp944	0.476295439	0.006756094
Smndc1	0.474927583	0.006938855
Wscd2	-0.474851342	0.006949164
Snora17	0.474684368	0.006971788
Neurl1a	-0.474531086	0.006992611
Slc1a3	-0.474272348	0.007027881
Macrod2	-0.474148515	0.007044814
Cep290	0.473314741	0.007159733
Fras1	-0.472852772	0.00722409
Casd1	0.472733017	0.007240853
Hibadh	0.472470128	0.007277767
Phkb	0.47225871	0.00730757
Susd1	-0.470859824	0.007507388
Rhobtb1	0.470110983	0.007616246
Cacna1g	-0.470034846	0.007627388
Txlnb	-0.469554997	0.007697932
Pde4b	-0.468080777	0.007918134
Prodh	-0.467990811	0.007931743
Itgb4	0.467310466	0.008035302
Kifap3	-0.467286946	0.008038903
Col2a1	-0.467110558	0.008065948
Gm6741	0.466494103	0.008161076
Rcan2	-0.466362506	0.008181506
Mpp6	0.465142818	0.008372928
Ak5	-0.464789895	0.008429019
Ntf3	-0.464388904	0.008493135

Cntn6	-0.46338548	0.008655389
Slc2a12	-0.462928387	0.008730166
Zfp618	-0.46213142	0.008861851
Abca4	-0.461996567	0.008884298
Arhgap27	-0.461653255	0.008941662
Nuak1	0.460952966	0.009059645
Plch1	-0.460570241	0.00912468
Prkce	-0.460228724	0.009183045
Ttc27	0.45934225	0.009336017
Ahi1	-0.457799084	0.009607443
Purg	-0.457245825	0.009706364
Armc2	-0.456423428	0.009854992
Flrt2	-0.455316216	0.010058121
Gm15834	0.453361787	0.010425297
Atp13a5	0.452448316	0.010600743
Gm4876	0.452402071	0.010609691
8030451A03Rik	0.452067094	0.010674694
Kdm4b	0.451953523	0.010696809
Dlg4	-0.4510618	0.01087179
Rabgap1l	-0.450906559	0.010902498
Cript	0.450500376	0.010983188
Ptn	0.450280495	0.011027078
Chrm2	-0.450015426	0.011080184
Eya4	-0.447973489	0.011496533
Btbd11	-0.447431324	0.011609262
Sorbs1	-0.446340845	0.011838812
Nos1	-0.446021801	0.011906688
Pfkm	-0.4459692	0.01191791
Slc44a5	-0.445265365	0.012068925
Cpeb3	-0.443797564	0.012389026
Adamts20	-0.442111899	0.012765391
Cdh6	-0.43933499	0.013406274
Hmga2	0.438760561	0.013542152
Bbs7	0.438229293	0.013668843
Dock4	-0.43734706	0.013881418
Inpp4b	-0.436951503	0.013977621
Rassf3	0.436713903	0.014035675
Cenpw	0.436571943	0.014070457
Atp2b1	-0.436051469	0.014198596
Zbtb4	-0.435318939	0.014380592

Syne1	-0.435308964	0.014383083
Asxl3	-0.434683411	0.014540062
Carf	-0.433169595	0.01492587
Ano2	-0.432447718	0.015112831
Zfp850	-0.431008535	0.015491399
Fzd6	0.43039198	0.015655979
Eepd1	-0.430373629	0.0156609
St7	0.430045204	0.015749185
Cdk17	-0.429066163	0.016014824
Fam13c	-0.428827744	0.016080075
Rbm20	-0.428049199	0.016294691
Pgk1	0.427342625	0.016491525
Qk	-0.427025897	0.016580397
Lmbrd2	0.425945322	0.016886602
Myb	-0.424637431	0.017263493
Gp1ba	0.424398731	0.017333026
Btrc	-0.420980376	0.018354572
Nbea	-0.419776573	0.018725989
Cacna1c	-0.418208685	0.01921905
Ltbp1	0.417095108	0.019575727
Lmbrd1	-0.416622316	0.019728808
Col23a1	-0.416592586	0.019738467
Fbxl17	0.41524458	0.020180546
Arntl	0.414512197	0.02042414
Golga7	0.414195691	0.02053016
Trps1	0.414148379	0.020546047
Zwint	-0.412317398	0.021168721
Rfx3	-0.410942852	0.021646331
Mkl2	-0.41088671	0.021666026
Syn3	-0.409697827	0.022086567
Wdr25	0.408773914	0.022418003
Rorc	-0.406814472	0.023134471
Hace1	0.406696533	0.023178189
Cdh23	-0.405008345	0.02381145
Tmem232	-0.404860193	0.023867696
Zfp438	-0.403329363	0.024455282
C1qtnf3	-0.401070633	0.025343892
Rrp1	0.400729582	0.025480335
Apol10b	0.400527937	0.025561289
Snx10	-0.399228285	0.026088128

Slco1a5	-0.398531496	0.026374223
Wwox	0.397608478	0.026757153
Veph1	0.39704338	0.026993828
Shq1	0.396183472	0.027357257
Gm10033	0.395596516	0.027607614
Prex2	-0.394578061	0.028046458
Peg3	-0.393958364	0.028316255
Tjp3	-0.391444017	0.02943273
Tmem132c	-0.390808808	0.02972039
Smarca2	-0.389996572	0.030091548
Crls1	0.388971978	0.030565114
Chchd6	-0.388036568	0.031002736
Pcmt1	0.386333034	0.031812791
Gpx3	-0.384421824	0.032741962
Gm10327	-0.383722793	0.033087255
Arhgef10	0.382217396	0.033840884
Spata17	-0.38183727	0.034033363
Tpk1	0.381637977	0.034134629
Sclt1	0.381050755	0.034434433
Nfe2	0.380596956	0.034667574
Abcc5	0.378372052	0.035829166
Gm9750	-0.377744769	0.03616228
Chst11	0.37323337	0.038632326
1110002E22Rik	-0.373126574	0.038692402
Zfp81	0.373062466	0.038728501
Hirip3	0.372747859	0.038906047
Ccdc91	-0.372195524	0.039219335
Arl4a	-0.3720757	0.039287568
Csgalnact1	0.370651042	0.040106155
Fbxo32	-0.368476194	0.041382152
Nt5dc3	-0.366811463	0.042380688
1700025G04Rik	-0.366440669	0.042605704
Gphn	-0.364125925	0.044032112
Abca12	-0.362187018	0.045256074
Dlc1	-0.362041452	0.04534905
Gnaq	-0.362011181	0.045368404
Ntng1	-0.361458568	0.045722876
Cd46	-0.360414884	0.046398368
Tmcc3	-0.359711352	0.04685818
Baiap2l2	-0.359049328	0.04729417

Foxd2	0.358827108	0.04744124
Adarb1	-0.358685039	0.047535454
Atxn7l1	0.358365744	0.047747743
Best3	-0.356026089	0.049326414

Table 2.12: List of non B2 RNA regulated genes (random set) used throughout the study.

Gm13293 Cfap45 Nek8 Gm24273 Gm44616 Tmem53 Gm4767
Gm24306 Gm37777 9330159M07Rik Zfp114 Gm25926 Gm49396
Gm18368 Gm38257 Gm4824 Gm6612 9430031K09Rik
Snord73a Vgll3 AC129214.1 Gm47488 Gm38192 Art3 Gm21972
Osr1 Gm9575 Gm48655 Gm37686 Dnah7b Gm37848
Gm23570 Abhd11os Mir5129 Gm10800 Rpl7a-ps7 Sfmbt2
Gm29163 Gm17096 Gm22446 Fermt3 Gm37689 Tmem204 Rbbp8
Rapgef4os1 Gm22510 Gm23676 Gm14425 Nat8f5 4930512B01Rik
Gm22887 Arhgap20os Gm42984 Kbtbd6 Mir599
4930532I03Rik Gm26347 Mir335 Nat8f3 4732416N19Rik Kcnrg
Gm44899 Gm43504 Gm43654 Ppp1r13l Alkbh2 Gm37367
4921511C10Rik Gm23940 Exosc6 Gm48542 Gm24878 Gm36963
Gm29155 Gm6781 Gm48726 Gm16894 Gm36638 Gm43875
Gm45094 Atp6ap1l A330040F15Rik Gm7979 Gm44895
Dynlt1f Gm25146 B230110C06Rik Gm42851 Ccdc173
Gm22105 Ebpl C130073E24Rik Gm43844 Zfp568 Gm6296
Zfp335os Gm13226 Gm6013 Nadsyn1 Spidr Gm47765 Col9a2
Gm23575 Havcr2 Gm43330 Gm43658 Gm24876 2900072N19Rik
Gm31282 Gm9917 Gm7049 Gm7908 Gm28424 Gm44746
Gm44093 Gm6169 Gm31172 Nek10 Gm21814 1700001K19Rik
Gm43519 Gm41041 Irgm2 Parp9 Gm7701 Gm37578 Relb
Gm7985 Gm9719 Mir343 Tuft1 Gm24451 Card9
4931403G20Rik Ly6g6e 4921531C22Rik Gm38228
D630036H23Rik Zgrf1 Gm15265 Gm26011 Gm43113 Gm8337
Gm17194 Gm48743 Gm43162 Gm48181 Bdh2 Gm11750 Itih2
Gm44234 Gm43696 P2rx6 Snord100 Ovgp1 Gpr150 Zfp879 Thbs1
Gm37677 Klk6 Hist1h2an Gpr4 Gm38048 Clic3 Rapgef4os2
Gm43084 Impa2 Il6ra BC025920 Zfp229 Gm37879 Gm28229
Gm43133 Gm25294 Gm13709 Gm45804 A930035D04Rik Cand2
Gm48006 Mir708 Gm48593 Gm43260 Gm7665 Gm10645
Gm27415 Tfcp2l1 Zscan30 Gm20548 Gm9812 Gm44664
Gm3544 Gm10540 Gm42763 Syde2 1810010H24Rik Gm42549
Gm38147 Ccdc62 Gm5850 Serpinb1b Trmo Gm3510
Gm43457 Gm27313 Bmp4 A730056A06Rik Gm16297 AC122487.1
Gm27588 Lsr 1700101I11Rik Cmklr1 Tmem173 Rnf135
AI429214 Gm8899 2810403D21Rik Vstm4 Gm25364 Gm26499

Gm11417 Gm24610 Runx2os2 Gm38910 D930015M05Rik
Gm37725 Gm37470 Gm43808 Gm6054 A330049N07Rik
Gm11944 Gm16006 Gm15535 Gm43379 Gm25578 Gm49397
Gm20387 Gm36527 Gm10863 1700018L02Rik Gm15719
2900005J15Rik Gm25600 Gm45709 Prc1 Espn Gm15726 Dnah5
Gm44836 Gm46367 Gm24620 Gm3160 Gm23310 Gm18791
D330050G23Rik Gm42462 Gm42509 Gm26674 6030443J06Rik
Snord35b A530083M17Rik Gm37018 Prokr2 AF357399
2510046G10Rik Gm18422 Meig1 Snora41 4930500M09Rik
Gm6654 Hkdc1 Gm14285 Gm29626 9330188P03Rik Gm48291
Atp2a31700029J07Rik Gm20633 Gm25761 Gm5511 AC129203.3
Gm5093 Gm18212 Smco4 Gm29156 Gm25128 Gm9780
E530001F21Rik Gm37397 Gm25813 Gm38036 1600002K03Rik
Stox1 Gm24143 Gm19187 Gm5415 Gm13328 Myadml2
Gm37633 1110025M09Rik Gm17102 Gm43061 Gm42659
Gm26049 Gm37246 Gm42578 Gm37653 Gm44453 Tfpi
Gm22454 Gm16254 2610035F20Rik AW822252 9130023H24Rik
Gm23094 Angpt2 Glipr2 Gm17655 A230083G16Rik Gm43826
2700099C18Rik Crh Cmtm7 Ccdc160 Grem1 Gbp3
4933431G14Rik Zmiz1os1 Gm45767 Gm2735 Ifih1 Gm22973
Gm37553 Fam228a Mir6951 Gm43145 Gm22391 Gm6109
Gm41115 Sp9 Gm15285 Gm42576 Gm42611 Gm47026
F830112A20Rik Gm5535 Spata1 Gm12216 Gm42693 Fcgr1
Gm48452 Hist1h2ac Gm14372 Il4ra Gm26683 4930415C11Rik
Fbxo47 Gm23200 Gm47797 Timeless Gm24411 Nipal4
Gm42739 Mir6915 Gm12362 1700020D05Rik Xylb Gm37621
Hspg2 Gm44503 Gm29808 Snord50b Mtag2 Gm22897
4930539E08Rik Terc Gm16279 Slc22a6 Gsdmd AC087898.4
4930517G19Rik Zfp853 Degs2 Megf6 Gm42588 Gm15868 AC121560.1
Higd1b Cfap206 Gm49283 Mboat1 Gm26901 Gm24794
Foxc1 Gm24091 D430013B06Rik C130083M11Rik Cideb
1700013F07Rik Gm26711 AC131339.2 Gm47664 1300014J16Rik
Gm9884 9330161L09Rik 9930017N22Rik Gm8930 Gm49525
Lpar4 Gm43665 Gm45769 Gm13961 Gm47370 Pitpnm2os2 Zfp808
Gm26736 Gm10778 4933433G19Rik Gm6588 Gm8034
Gm2178 Gm16353 Gm10059 Pcdhb21 Mir3100 Gm43012
Gm17112 Dnph1 Gm44607 Gm38043 Gm30934 6330549D23Rik
2700033N17Rik A430106G13Rik Gm35405 Kcnu1 Gm14794
Gm47132 - Gm11405 Gm22558 4930596I21Rik Gm5630
Gpr18 Mcub Gm45635 Kank4 Gm26983 4930404I05Rik Gm7645
Gm15583 4831440E17Rik Gm12926 Mir6402 Gm15956
Gm9670 Dnah2 4930525G20Rik 9630009A06Rik Gm43331
Gm25301 Gm26814 Gm4707 Sertad3 Fank1 Itga1

1700040D17Rik Gm43071 Gm47246 A930003O13Rik Dnah6
Gm13767 Gm22579 6430710M23Rik Gm13171 Gm23209 Rcsd1
Depdc7 Mir6906 Gm25363 Nat1 Gm45084 Nhs Gm17377
Mir103-2 1700047K16Rik Gm22073 Gm45846 Gm13830
Gm6212 Gm42864 Mir3080 - Gm37918 Gm24776
D430036J16Rik C730002L08Rik Dnali1 Gm13525 1700007J10Rik
Snord66 Nr6a1os Gm23356 Gm44668 4933440N22Rik
Gm42595 Hmgb1-ps6 Gm37953 Gm38365 Gm48091 Gm14774
Gm45479 Tnnc1 Gm26767 Mir350 Prg4 Cpeb1os1 Cnn2
Gm3200 Gm44220 Gm12404 Zbtb8b Gm12774 Npl
2810442N19Rik Gm37769 Plscr2 Gm49437 Gm43437 Fign Plac9b
Gm24786 Muc3a Gm5822 Rpp40 Hyal1 Gins3 Gm6123 Pifo
Mir7027 Ifi203 Klc3 Plcg2 Gm43787 Gm24732 Gm15328 Derl3
Tbc1d2 A230103J11Rik Zfp202 Gpr25 Lcp2 Gm27711 Gm26334
Gm47870 Gm24530 9430021M05Rik Gm20149 Gm43000
4633401B06Rik Gm15398 Isg15 Gm47827 1600029O15Rik Tex52
Gm38562 Gna15 F8 Gm36638 Gm47504 Dnase1l2 Gm45508
Gm24457 Gm25710 Gm17045 Rgl3 Polq Gm37069 Gm5851
Gm15702 Gm37138 Gm24923 Hmgb1-ps4 Gm48701 Gm23344
Gm14769 Emid1 Gm16200 Gm13556 Mir5623 Gm9806
Gm47580 Gbp2 Gm9989 Gm47286 Rps6-ps1 Gm47726
Gm37159 Gm13604 Gm7380 Gm17193 Ttc21a Gm22320
Gm12470 Gm43560 Gm28530 3222401L13Rik Gm11870
Gm15743 Hist1h2aj Gm37979 4931414P19Rik Shroom1
Mir6374 Ehhadh Gm49085 Gm17753 Evi2 Mir7663
Gm48357 Gm23736 Mir6907 Angptl1 Gm24379
1700096K18Rik Gm7192 Gal3st4 Chn1os1 Gm26037 n-
R5s201 Gm40466 Rpl34-ps2 Gm44008 Gm9947 Gm25406
Gm44011 Zfp647 Gm37143 Gm25120 Gm15379 Gm10484
Gm43259 Gm5446 Nrg4 Gm43566 2210412B16Rik
A430027C01Rik Mypopos 4930545L23Rik Gm45131 Gm37978
Fibin Gm44249 Gm15046 Nudt15 Gm26798 Gm26618
5430434F05Rik Gm37292 Gm12272 Gm25017 Gm26265
Gm6994 Scn7a AC091463.1 Gm45088 Trim65 Clec3b Gm48194
Gm27582 Gm23851 Zfp607a Gm23039 Gm12359 Lenep
Gm9723 Gm44550 Ccna2 Gm26762 Gm5086 Fam78a
Gm22720 Pi4k2b Gm42615 Gm22613 Tha1 Krt12 Fam241a
Gm45493 Gm15414 Spsb4 Gm48129 Trpv6 Mir874 Gm23370
Psmb8 Gm24171 Gm42568 Zfp36 Gm28048 Gm44721 Gm48838
Gm6397 Ttc39aos1 Gm25905 Gm27843 Gm9064 Gm43059
Gm48381 Mir1933 Gm45345 Tmc4 Gm42748 Pkmyt1
Slc35f2 Tcf19 Gm15651 A430018G15Rik Gm37248 Gad1-ps
Gm22042 Gm42969 Loxl1 Gm42727 Gm47572 Gm43178

Gm16243 Gm23202 1810059H22Rik Gm22449 Gm7808 Zfp217
Gm22121 Gm16364 Gm9752 Gm3325 Cited4 Gm43508 Polr2k-
ps Gm9905 Gm48872 Cldn34c1 Gm16310 Gm22085 Gm2164
Dsc3 Gm37297 Tes AC116468.1 Apobec4 Gm14212 Gm45645
Gm45165 Gm8318 Gm10723 Gm43256 - Gm5191 Nme4
Gm36992 4931413K12Rik Dsn1 Gm27942 Gm16183 Gm9974
Apobec1 Gm18077 Gm26931 Gm42937 Gm42986 Gm22136
Prrg4 Mir369 Gm24918 Gm26854 Gm37738 Gm38057
Tmem266 Gm47284 Pcdha2 Ube4bos1 Gm43807 Gm49309
Gm14376 C2 Gm25517 2410004P03Rik Gm38359 Mir29a
Gm23999 Rec8 Gm20692 Gm48175 Gm44769 Gm15609
Gm43692 Gm15443 Gm27206 Gm27252 Cyp4f17 Phf2os1
Mir132 Gm12227 Gm10642 Gm45428 Gm26285 AI506816
Gm29083 5430402O13Rik Gm13392 Mir6769b Gm24016
Gm11628 Gm13617 Gm46234 Gm45615 Gm37090 Gm17092
Creb3l1 Rnf207 Fyb2 Gm12808 Gm3081 Gm26233
Gm45869 Gm26413 Gm19967 Fbln5 Gm17022 Ldha-ps2
Gm38300 Gm11199 Gm43483 Gm13090 Gem Gm24866
Gm44643 Gm26594 Gngt2 Gm37651 Gm10766 4930413G21Rik
Gm6533 Gm22255 Zfp78 Gm15853 Nusap1 Slco4c1
Gm45151 Ovol2 B230377A18Rik Frem2 Gm29325 3110070M22Rik
Gm46436 Cfb Gm22549 Gm16210 Gm23691 Panct2 Gm45630
Gm24328 Gm37934 Gm13380 Mrto4-ps2 4930563E22Rik
Gm48146 1500002C15Rik Chmp4c Gm44144 Gm20537
Slc26a11 8430432A02Rik Gm17823 Gm38158 3110082J24Rik
Gm3511 Tmem238 Gm26859 Gm19337 Gm17205 Gm3693
1700063D05Rik Itga9 Gm26621 Gm26789 CT030161.1 Bora
Gm45041 Bambi Gm38253 9830144P21Rik Gm21680 Stac
Gm47218 Gm14387 Gm24272 3110009E18Rik Gm15860
Gm15381 Gm8666 Gm12039 Mir338 Gm26890 Zfp764n-
R5s171 Gm38097 Gm37551 E230020A03Rik Nes Gm37132 Sfxn2
Gm12229 Tmem210 Gm18755 Gm26070 Hebp2 Gm25694
Gm43216 Gm27931 Gm26732 Gm48382 Gm7589 Gm15879
Pgf Gm44022 Gm22948 Gm48552 Gm14335 Gm42930
Gm38169 Gm22506 Neu3 Gm15994 Gm44981 Gm37860 Ifitm1
Gm19280 Gm3355 Gm24399 Flt3l Gm17893 Gm44040
Gm27301 Gm20475 2900078I11Rik Gm25474 Gm14382 Uba7
Gpsm3 4933407L21Rik Gm43112 3110062G12Rik Gm42878
Gm13642 AA914427 Gm32983 Gm32014 Gm23286 Gm23419
Gm14472 Trim30a Gm10382 Zic3 Gm45838 Has3
4930408O17Rik Gm47134 Gm32391 Asb18 A230107N01Rik
Gm47644 Gm2412 Hvcn1 Gm23126 Gm11245 Naaladl2 Cnmd
Nthl1 Gm38340 Gm44439 C2cd4d Gm30873 1700085D07Rik

Gm22300 2310043M15Rik Gm25190 4930587E11Rik Gm38259
Lppos Gm37052 Gm24671 Gm16740 Gm22063 Gm15601
Gm9003 Gm25871 Gm43201 Nrtn Wdr66 Gm47882 Gm4651
Gm12737 Adam12 Rasgef1c Pola2 Gm49545 Gm47234
Gm21009 Gm16539 Gm23483 Gm14411 BC037039 Gm26097
Gm25720 Gm45477 Gm25998 Gm14093 Gm43172 Gm11926
Tceanc Gm25965 2900035J10Rik Gm19371 n-R5s15 Gm12788
Gm26721 Gm37466 Map3k8 Gm2065 Gm18329 Gm17056
Sypl2 4930579K19Rik Gm14966 Gm32647 Sox18 Gm38166
Gm6665 Gm21844 Gm42651 A530046M15Rik Gm37776 Dtnbos
Gm4432 Gm37962 4931440F15Rik Ankef1 Gm15991 Emp3
Gm7054 Prkag2os1 Gm37788 Gm45623 Gm12538 Gm48147
Gm45733 Gm18988 Gm13361 Gm5452 Gm23143 Gm17825
Gm37949 Cfap43 Tdrd5 Ctsk Yy2 Gm4593 Gm22971 Rbx1-ps
Gm47583 AC164314.2 Airn Gm46448 Gm15029 Gm11096 Mir98
Gm15696 Lnx2 Gm7278 1700110C19Rik Gng8 Gm26123
A730063M14Rik Cish Gm43707 D130020L05Rik Gm20045
Mir6902 Cmya5 Gm15688 Fam198b Gm16093 Gm13572
Gm9104 Accs Hic2 Gm12568 Gm7160 Akna Gm6611 Rps19-
ps2 Gm9891 A730011C13Rik Gm37023 Cfap161 Gm44897
Gm43817 Gm37509 Gm15775 Six3 9130019O22Rik
6430571L13Rik Gm43480 2810402E24Rik Hdc Dynlt1a
AC170998.1 Abhd15 Gm10075 Gm20713 Gm16892 AC151275.1
Gm45209 Gm48512 Mirlet7a-1 Aox3 Gm34727 Tacr3 Mir124a-2
Lca5l Pex11g Gm14052 Gm42483 AC165953.1 Sycp2 Gm48855
F420014N23Rik D630030B08Rik Gm37183 H2-M10.2 Gm16179
Gm37212 Xkr8 Gm38285 Akirin1-ps Gm13880 Gm15744 Prph
Gm47536 Tmem114 5930403N24Rik Gm45053 Zap70 Tlr13 Gja6
Polg2 Gm37452 Gm38200 Lrrc71 Gm25447 Bcl2a1b Zfp429 Catip
Gm26628 Gm42507 4833421G17Rik Gm28307 4930465K09Rik
Cstad Tdg-ps Gm37309 Gm44103 Stk36 Zwilch 9930024M15Rik
Gm6963 Gm22396 Gm18940 Pip5kl1 6820408C15Rik Pou5f2
Gm44075 Gm47700 Rtkn2 2310058D17Rik Mir185 Cela1 Sdsl
4930455C13Rik 9430065F17Rik Tifab Glb1l2 Gm18338 Gm16214
Gm8990 Mir6932 Pemt Gm37745 Mfap4 A930037H05Rik Pus7l
Gm22952 Lyl1 Gm25225 Gm20732 4921511I17Rik Gm26020
Gm7467 Atcayos Syk Gm7613 Spint1 Snord11 Tmie
Gm14970 Gm37566 Tnfrsf1b Gm47911 Gm22540
A830052D11Rik Gm38115 Gm15806 Gm47121 Gm48349
Gm44891 Gm27017 Gm37980 Gm13562 Pim1 Gm15751
Gm24650 Cenps AC126254.1 Gm38297 Tgif1 Mir3106 Gm37655
Gm10657 Gm44437 Gm38059 Tacc3 Gm12322 Gm44848 Aoc2
Gm24561 Gm38014 Gm37137 2310030G06Rik Mir6920

Hist1h2ah Gm49376 Gm22583 Gm13038 Lbhd2 Gm43466
Gm37115 Gm47597 Gm38134 Gm25559 Gm25235 Wdr46-ps
Adamts8 Gm45137 Thap6 Gpx7 Gm24771 Gm17875 Gm17191
Tap1 Gm7842 Gm44089 Gm16334 1700024B18Rik Gm22661
Gm25178 Gm46231 Gm37321 Gm45841 Spats1 Gm35339
1810012K08Rik Akr1c18 Oaz3 Gm45453 Gm29783 Gm27326
Mir6997 Mir8112 Gm9157 Wnt10a Cdkn2c Ehd2
Gm47303 4930577N17Rik Tespa1 Fes Gm37195 Slc30a2
Gm47086 Gm20445 Rab32 Gm24647 Dnajb3 Gm8960 Ell3
Plekhf1 Gm3527 4930428E07Rik Kctd14 Gm6473 Gm42492
Gm45464 Gm37792 D330041H03Rik Gm43237 Gm13140
Gm23862 Gm14174 Gm43011 Rpl22-ps1 Gm16240 Gm42782
Mageb16-ps2 Olfr1564 4921513H07Rik Gm37105 Gm45797
Gm37255 Gm49201 Gm43967 Gm29257 Gm37720 Gm20186
AC078895.1 Gm10644 Esd-ps Gm17171 Gm14393 1700126G02Rik
Cchcr1 Gm44280 Gm44982 Gm49003 Gm14200 Gm13586
5930409G06Rik Slc25a45 Cd86 Gm23656 Snord8 Gm13342
Gm8850 Gm43029 Tubb4b-ps2 Mir1251 Snord35a Gm17160
Gm22840 C920006O11Rik 1700016K19Rik Gm25455 Htr2b
Gm27285 Gm24959 Gm45309 Gm15952 Angptl3 Gm37649
Kcnk6 Gm25544 A530058O07Rik Gm25209 Gm22020 Gm43841
Pcdha1 Wfdc1 9930004E17Rik Gm8546 Plxna4os1 Gm23184
Gm45867 Gm18782 Gm11659

Table 3.1: Up-regulated genes in the cortices of AD patients of the MAP study (Figure 3.6B). Values were calculated using DESeq (see chapter 3 methods) on RNA-seq data. Genes correspond to a padj < 0.05 and log2 fold change > 0.5.

Gene Name	**baseMean**	**log2FoldChange**	**lfcSE**	**stat**	**padj**
AC005670.2	4.58	3.323	1.007	3.300	0.011
AC008764.1	2.10	2.762	0.774	3.569	0.006
AL662899.1	2.40	2.421	0.619	3.909	0.003
AC239799.1	4.37	2.144	0.776	2.763	0.034
OR7A5	26.45	2.017	0.288	7.008	0.000
AL450313.1	3.59	2.008	0.548	3.663	0.005
AC008403.2	2.34	1.831	0.695	2.634	0.044
AC010323.1	4.43	1.760	0.608	2.896	0.026
AC243964.2	26.17	1.602	0.293	5.457	0.000
LINC02204	2.14	1.558	0.360	4.326	0.001
AL021707.5	9.82	1.548	0.386	4.011	0.002
AC008737.3	2.02	1.544	0.340	4.544	0.000

LINC02397	6.26	1.509	0.272	5.544	0.000
LINC01108	4.31	1.501	0.473	3.174	0.015
AC091167.2	31.06	1.397	0.536	2.606	0.047
SIX2	3.03	1.394	0.378	3.687	0.005
VNN1	1.86	1.352	0.465	2.910	0.025
CXCR2	6.27	1.342	0.335	4.000	0.002
GAPDHP45	3.29	1.312	0.219	5.990	0.000
OR7C1	16.48	1.308	0.233	5.604	0.000
AC073508.2	2.57	1.264	0.412	3.067	0.018
SGO1-AS1	1.74	1.242	0.473	2.627	0.045
CXCR1	3.64	1.187	0.420	2.824	0.030
RPL12P37	2.95	1.174	0.288	4.076	0.002
TEX48	2.42	1.172	0.328	3.576	0.006
S100A4	67.52	1.169	0.198	5.895	0.000
LINC02393	4.22	1.169	0.282	4.141	0.001
AC007906.2	3.03	1.149	0.429	2.680	0.041
AC002428.2	3.57	1.147	0.387	2.967	0.023
LINC02172	18.67	1.124	0.195	5.759	0.000
AC112504.1	21.70	1.122	0.179	6.250	0.000
RASEF	9.71	1.107	0.210	5.260	0.000
AC011510.1	2.21	1.088	0.352	3.092	0.017
SERPINA5	11.04	1.074	0.392	2.736	0.036
SLC4A11	148.57	1.072	0.135	7.957	0.000
RNA5SP255	3.05	1.065	0.226	4.710	0.000
AC005041.3	4.08	1.051	0.270	3.897	0.003
LBX2	5.74	1.024	0.248	4.132	0.001
AC023538.1	11.09	1.021	0.205	4.986	0.000
AC133540.1	4.23	1.011	0.263	3.841	0.003
WISP1	11.86	1.010	0.198	5.092	0.000
LINC01338	17.98	1.007	0.215	4.683	0.000
SALRNA2	1.67	0.991	0.279	3.552	0.006
RN7SL377P	1.75	0.991	0.319	3.105	0.017
WDR64	5.68	0.987	0.340	2.904	0.026
CDC42BPG	4.87	0.983	0.286	3.440	0.008
MTRNR2L1	151.29	0.976	0.354	2.756	0.035
MT1H	67.33	0.975	0.237	4.119	0.002
AC026398.1	16.64	0.975	0.336	2.899	0.026
RIPOR3	247.88	0.974	0.149	6.539	0.000
LINC01736	56.76	0.954	0.182	5.236	0.000
MTND5P11	157.00	0.952	0.241	3.958	0.002

NANOS2	6.43	0.952	0.265	3.594	0.006
SLC12A3	6.23	0.949	0.259	3.663	0.005
AC136603.1	1.78	0.941	0.265	3.547	0.006
RN7SL622P	4.54	0.925	0.216	4.292	0.001
AC091180.5	11.60	0.921	0.174	5.288	0.000
LCN6	16.38	0.916	0.250	3.664	0.005
AC011120.1	3.36	0.907	0.289	3.142	0.016
TSLP	3.76	0.897	0.276	3.247	0.012
AC007406.1	4.10	0.897	0.266	3.372	0.009
AC137590.2	1.57	0.895	0.310	2.890	0.027
LINC01134	9.86	0.894	0.184	4.862	0.000
AC012507.4	2.84	0.891	0.333	2.675	0.041
ANGPT2	360.27	0.888	0.205	4.335	0.001
SH2D3A	10.74	0.887	0.207	4.289	0.001
GABRR2	3.64	0.886	0.339	2.612	0.046
GAREM2	1085.38	0.883	0.137	6.435	0.000
RN7SL744P	4.56	0.875	0.275	3.185	0.014
LINC00930	31.12	0.874	0.216	4.054	0.002
ESPNL	7.39	0.873	0.240	3.644	0.005
SNORD17	18.22	0.870	0.228	3.823	0.003
AC121247.2	3.38	0.866	0.249	3.473	0.008
TCF4-AS1	1.58	0.865	0.294	2.942	0.024
MT1JP	14.40	0.864	0.246	3.513	0.007
AC009063.2	72.18	0.857	0.165	5.177	0.000
UBTFL6	2.67	0.847	0.241	3.509	0.007
DNAAF3	6.91	0.847	0.249	3.398	0.009
APLN	594.56	0.846	0.126	6.720	0.000
DNAH11	23.07	0.839	0.291	2.884	0.027
DDX11L9	5.42	0.838	0.239	3.505	0.007
OR2B11	1.97	0.835	0.246	3.393	0.009
MTND2P8	2.43	0.835	0.265	3.148	0.015
MTND6P4	137.56	0.833	0.245	3.394	0.009
AL159163.1	3.89	0.832	0.261	3.192	0.014
MT1F	1490.92	0.831	0.176	4.715	0.000
GIPR	69.81	0.830	0.201	4.120	0.002
OLIG2	468.87	0.829	0.205	4.038	0.002
AL355974.3	11.78	0.828	0.231	3.584	0.006
AC092119.1	12.73	0.824	0.181	4.554	0.000
MTDHP4	4.75	0.823	0.312	2.636	0.044
AC068768.1	55.19	0.822	0.181	4.549	0.000

IRS3P	34.24	0.817	0.168	4.851	0.000
AC026401.2	3.84	0.817	0.233	3.505	0.007
AC105429.2	2.14	0.813	0.278	2.923	0.025
TUBB1	14.44	0.812	0.286	2.839	0.029
AC119674.2	4.45	0.807	0.225	3.583	0.006
ZBTB38	218.68	0.807	0.203	3.978	0.002
AL353653.1	2.59	0.806	0.264	3.057	0.019
ETV4	51.90	0.805	0.190	4.231	0.001
OR7E26P	7.28	0.805	0.165	4.890	0.000
NWD1	662.49	0.802	0.136	5.903	0.000
UBE2F-SCLY	3.58	0.802	0.259	3.098	0.017
RAX2	8.18	0.801	0.263	3.047	0.019
AP000302.1	7.65	0.799	0.172	4.645	0.000
HSD11B2	124.61	0.798	0.174	4.573	0.000
AC026726.1	2.52	0.796	0.236	3.369	0.009
P2RY8	4.56	0.791	0.251	3.151	0.015
A2ML1	149.27	0.790	0.123	6.437	0.000
AC016687.1	3.28	0.785	0.221	3.549	0.006
AC025755.1	3.38	0.784	0.246	3.188	0.014
TRIP10	435.71	0.783	0.131	5.974	0.000
AC005086.2	5.28	0.782	0.259	3.023	0.020
AL080273.1	7.21	0.777	0.185	4.194	0.001
LCN10	69.59	0.771	0.203	3.795	0.003
AC092447.7	31.07	0.771	0.297	2.598	0.048
SLC6A12	983.78	0.768	0.131	5.878	0.000
AC027130.1	65.37	0.768	0.140	5.478	0.000
OR7E14P	18.06	0.768	0.122	6.310	0.000
MYOT	75.63	0.767	0.129	5.959	0.000
ABCC2	7.41	0.765	0.249	3.079	0.018
SLC5A11	274.67	0.762	0.156	4.900	0.000
A2ML1-AS1	4.82	0.762	0.273	2.786	0.033
AL512274.1	4.12	0.757	0.171	4.436	0.001
HMGB1P49	13.64	0.757	0.207	3.660	0.005
SGO1	7.64	0.755	0.198	3.808	0.003
RF00017	3.89	0.750	0.240	3.125	0.016
SAMD4A	454.03	0.749	0.181	4.129	0.001
IRX3	5.59	0.749	0.279	2.681	0.040
DDIT4	2172.15	0.748	0.138	5.425	0.000
SLC25A48	240.98	0.746	0.122	6.102	0.000
RF00017	1.73	0.745	0.270	2.764	0.034

AF279873.3	17.56	0.744	0.190	3.918	0.003
ISYNA1	722.31	0.743	0.098	7.542	0.000
AC008121.1	9.44	0.742	0.196	3.781	0.004
TFAP2C	28.70	0.738	0.154	4.789	0.000
AC005479.2	2.40	0.738	0.201	3.661	0.005
GAPT	6.42	0.737	0.174	4.245	0.001
AC092756.1	2.55	0.735	0.229	3.217	0.013
-	44.54	0.735	0.165	4.466	0.001
PIEZO2	200.20	0.735	0.136	5.408	0.000
AL355490.2	13.70	0.734	0.173	4.253	0.001
MTCO1P2	18.52	0.734	0.203	3.621	0.005
MIR663AHG	8.55	0.733	0.200	3.660	0.005
ELOBP4	4.84	0.732	0.223	3.288	0.011
L1TD1	3.27	0.730	0.266	2.750	0.035
CLDN7	7.98	0.728	0.184	3.959	0.002
AQP6	41.29	0.727	0.146	4.985	0.000
FNDC11	7.13	0.725	0.168	4.308	0.001
AC009063.1	2.84	0.725	0.235	3.079	0.018
AC006064.5	13.27	0.724	0.157	4.596	0.000
AC016245.1	30.28	0.723	0.179	4.039	0.002
AP001858.2	1.84	0.722	0.273	2.642	0.044
AC105206.1	4.52	0.722	0.224	3.221	0.013
AC091230.1	20.62	0.717	0.261	2.749	0.035
RF00092	2.01	0.716	0.237	3.022	0.020
AC009716.1	3.59	0.716	0.276	2.594	0.048
GLI1	80.99	0.716	0.149	4.796	0.000
RN7SL231P	1.90	0.715	0.233	3.066	0.018
OR2L6P	1.84	0.715	0.240	2.973	0.022
RF00019	1.54	0.713	0.263	2.714	0.038
ANLN	1061.27	0.710	0.126	5.613	0.000
GHRHR	6.34	0.710	0.171	4.139	0.001
MT1G	1603.08	0.707	0.164	4.303	0.001
CHRNG	9.16	0.706	0.216	3.271	0.012
OLAH	12.62	0.706	0.183	3.848	0.003
GBP4	286.10	0.705	0.213	3.306	0.011
AC005702.2	7.49	0.705	0.194	3.628	0.005
MTRNR2L6	3.46	0.704	0.229	3.072	0.018
FOXD1	46.75	0.703	0.154	4.562	0.000
MTCO1P40	171.42	0.703	0.165	4.253	0.001
RN7SL693P	2.81	0.701	0.248	2.829	0.030

HIST1H2AD	2.08	0.700	0.241	2.903	0.026
TFAP2A	7.56	0.700	0.224	3.130	0.016
UPB1	17.58	0.700	0.152	4.602	0.000
RLIMP1	6.89	0.696	0.267	2.608	0.047
AC109441.1	5.06	0.696	0.222	3.129	0.016
C11orf94	5.41	0.695	0.159	4.385	0.001
AC073111.4	32.82	0.695	0.266	2.613	0.046
PHYHD1	489.55	0.695	0.147	4.717	0.000
AC106028.1	2.22	0.692	0.251	2.752	0.035
HIST1H3E	13.57	0.692	0.224	3.090	0.017
SLCO4A1	1173.31	0.691	0.164	4.218	0.001
CPM	543.22	0.690	0.122	5.659	0.000
AC233992.1	3.79	0.688	0.242	2.843	0.029
AC087645.3	1.97	0.688	0.243	2.829	0.030
MTRNR2L8	292.77	0.688	0.185	3.712	0.004
FAM167B	48.83	0.687	0.202	3.401	0.009
LINC00689	63.27	0.687	0.204	3.371	0.009
AL137781.1	5.92	0.686	0.238	2.876	0.027
HIF3A	2311.62	0.685	0.159	4.312	0.001
DDIT4L	166.98	0.682	0.148	4.599	0.000
ARHGEF5	23.17	0.682	0.161	4.245	0.001
AC091180.2	22.66	0.682	0.134	5.085	0.000
CRYAA2	3.85	0.681	0.238	2.862	0.028
CCDC102A	65.06	0.681	0.136	4.996	0.000
SMTN	909.87	0.681	0.127	5.360	0.000
PRELP	1096.50	0.679	0.105	6.500	0.000
AP003117.1	10.32	0.677	0.206	3.295	0.011
BLID	2.29	0.677	0.215	3.143	0.016
PGPEP1	1122.08	0.677	0.237	2.856	0.028
F2RL3	19.86	0.677	0.239	2.825	0.030
LINC01094	179.91	0.675	0.164	4.125	0.001
AC103810.6	5.64	0.675	0.191	3.532	0.007
MT-ND5	434372.12	0.675	0.157	4.310	0.001
AL590093.1	32.22	0.674	0.162	4.167	0.001
AC092332.1	2.60	0.673	0.250	2.696	0.039
RF00017	7.95	0.673	0.180	3.734	0.004
ELOCP28	4.35	0.673	0.249	2.705	0.039
TDRD12	11.91	0.672	0.197	3.410	0.009
AL031587.2	4.73	0.671	0.241	2.786	0.033
AC114296.1	11.11	0.671	0.171	3.923	0.003

FZD9	199.81	0.670	0.112	5.984	0.000
PIRT	37.80	0.670	0.207	3.230	0.013
AL133215.3	3.48	0.670	0.183	3.668	0.005
STX8P1	3.19	0.669	0.225	2.970	0.022
LINC01354	80.01	0.668	0.138	4.844	0.000
RNU6-758P	2.95	0.668	0.219	3.049	0.019
MTRNR2L9	2.16	0.667	0.215	3.104	0.017
KCNJ16	204.94	0.666	0.206	3.227	0.013
COL27A1	406.24	0.664	0.117	5.692	0.000
LINC00484	4.30	0.664	0.228	2.908	0.026
RNY3P16	7.50	0.663	0.163	4.065	0.002
AL031731.1	258.91	0.663	0.099	6.679	0.000
CCDC36	33.48	0.663	0.148	4.484	0.001
NEAT1	8739.82	0.662	0.203	3.264	0.012
LENEP	2.29	0.661	0.213	3.110	0.017
C22orf34	36.28	0.661	0.175	3.783	0.004
CXCR4	111.08	0.660	0.172	3.849	0.003
RN7SKP180	3.47	0.660	0.185	3.571	0.006
AL513283.1	9.70	0.660	0.198	3.331	0.010
VHLL	4.42	0.660	0.247	2.673	0.041
RF02104	10.32	0.660	0.215	3.061	0.018
AC011632.1	2.66	0.659	0.239	2.758	0.035
HLA-J	5.09	0.659	0.240	2.742	0.036
RF00017	5.00	0.658	0.225	2.931	0.024
AC010619.2	4.97	0.658	0.179	3.673	0.005
LINC00310	9.96	0.656	0.184	3.562	0.006
GJA4	194.77	0.655	0.161	4.057	0.002
RN7SL378P	3.24	0.654	0.253	2.586	0.049
HIGD1B	262.57	0.654	0.142	4.609	0.000
MT-ATP6	207166.66	0.653	0.160	4.069	0.002
AC020917.3	12.09	0.652	0.177	3.694	0.004
AC121247.1	21.22	0.652	0.179	3.652	0.005
NCF1C	24.81	0.652	0.211	3.089	0.017
MT-TA	13327.44	0.650	0.204	3.191	0.014
SYTL4	310.86	0.649	0.169	3.843	0.003
NMUR2	23.59	0.649	0.172	3.767	0.004
AC092810.2	2.08	0.648	0.226	2.873	0.028
AL513479.1	3.25	0.648	0.236	2.749	0.035
AC104574.2	5.71	0.646	0.233	2.772	0.034
MT-TK	3270.71	0.646	0.183	3.530	0.007

PACRG-AS3	62.65	0.645	0.129	5.013	0.000
RPL23AP12	12.65	0.645	0.192	3.350	0.010
AL035425.1	6.51	0.644	0.192	3.357	0.010
AC097382.2	8.61	0.644	0.202	3.193	0.014
AL590096.1	10.96	0.644	0.144	4.487	0.001
AL137784.3	6.88	0.644	0.171	3.762	0.004
AC010469.1	45.27	0.643	0.185	3.477	0.007
HPR	172.97	0.642	0.209	3.069	0.018
HSPA2	2006.51	0.642	0.190	3.385	0.009
AL353708.3	12.99	0.642	0.178	3.603	0.006
AC058791.1	737.16	0.641	0.173	3.702	0.004
AC002401.3	3.45	0.640	0.170	3.762	0.004
AC084754.1	1.63	0.640	0.248	2.578	0.050
RF00432	3.49	0.639	0.238	2.690	0.040
AP001350.2	17.55	0.638	0.107	5.971	0.000
GLRA1	9.68	0.638	0.191	3.331	0.010
NCMAP	6.67	0.637	0.175	3.653	0.005
AC138866.2	17.39	0.637	0.183	3.485	0.007
LINC02080	41.54	0.637	0.155	4.099	0.002
HP	31.37	0.637	0.171	3.716	0.004
MT-TN	9520.58	0.635	0.205	3.103	0.017
ADCYAP1R1	974.12	0.635	0.231	2.750	0.035
TNS3	3081.62	0.635	0.127	5.000	0.000
CHST6	442.74	0.634	0.148	4.276	0.001
MT1L	138.16	0.633	0.180	3.509	0.007
AC083822.1	3.06	0.630	0.178	3.549	0.006
MTCO1P27	5.53	0.630	0.157	4.002	0.002
AZGP1	296.27	0.630	0.165	3.818	0.003
SLC6A9	484.15	0.629	0.086	7.356	0.000
AC010424.1	14.20	0.629	0.165	3.811	0.003
AC002044.3	9.61	0.629	0.186	3.376	0.009
MMP19	7.30	0.628	0.197	3.189	0.014
VCAN	538.53	0.627	0.148	4.233	0.001
AC015908.3	11.53	0.627	0.148	4.244	0.001
HSPE1P16	2.76	0.625	0.192	3.260	0.012
AC002044.2	16.98	0.625	0.176	3.540	0.006
ALOX15B	47.41	0.624	0.165	3.782	0.004
RF00017	2.53	0.624	0.234	2.669	0.041
AKNAD1	5.61	0.624	0.220	2.831	0.030
ZBTB20	1524.45	0.624	0.215	2.906	0.026

HERC2P3	2578.18	0.622	0.153	4.074	0.002
RNU6-1138P	1.96	0.622	0.236	2.637	0.044
MTATP6P27	11.62	0.622	0.191	3.262	0.012
AC007683.2	2.21	0.621	0.216	2.883	0.027
AC009108.3	27.20	0.621	0.139	4.480	0.001
AC091144.2	2.70	0.621	0.205	3.029	0.020
AL049840.4	249.01	0.621	0.108	5.772	0.000
NUP210L	25.90	0.621	0.198	3.140	0.016
AC087392.1	10.25	0.619	0.207	2.991	0.021
AC136632.2	8.37	0.619	0.184	3.372	0.009
TBX6	63.02	0.619	0.131	4.721	0.000
AC019278.1	2.86	0.617	0.232	2.663	0.042
AL449403.2	36.63	0.616	0.163	3.782	0.004
NAV2-AS5	2.75	0.615	0.215	2.867	0.028
CTNNA3	265.82	0.613	0.152	4.036	0.002
PPP1R3G	188.31	0.613	0.112	5.487	0.000
NME8	4.14	0.613	0.187	3.275	0.012
RNU6-1085P	3.00	0.612	0.213	2.869	0.028
JPH2	18.71	0.612	0.186	3.284	0.011
AC104389.4	10.27	0.611	0.154	3.976	0.002
FP325332.1	10.14	0.611	0.145	4.208	0.001
CD180	17.76	0.611	0.187	3.260	0.012
AC011483.3	3.70	0.610	0.214	2.855	0.028
AC013472.1	30.82	0.610	0.166	3.664	0.005
PERM1	11.37	0.609	0.190	3.198	0.014
AC012447.1	2.56	0.609	0.201	3.030	0.020
AL356258.1	37.82	0.609	0.135	4.506	0.001
GZMM	17.96	0.608	0.182	3.335	0.010
AC104564.1	5.58	0.608	0.157	3.873	0.003
MAFF	526.75	0.607	0.171	3.559	0.006
AC005220.1	8.86	0.607	0.173	3.516	0.007
AC245123.1	8.65	0.606	0.233	2.602	0.047
AP001527.1	2.59	0.606	0.230	2.630	0.045
TSPAN11	178.18	0.606	0.195	3.109	0.017
AL031056.2	6.92	0.606	0.232	2.605	0.047
TEAD2	123.99	0.605	0.138	4.375	0.001
CLCA4	83.90	0.604	0.154	3.919	0.003
AL513497.1	13.70	0.604	0.139	4.355	0.001
AC012486.1	5.97	0.604	0.203	2.967	0.023
ITPKB	7003.25	0.603	0.117	5.175	0.000

AC012173.1	2.68	0.603	0.213	2.832	0.030
CYTL1	17.14	0.602	0.195	3.094	0.017
LINC02123	8.17	0.601	0.220	2.734	0.036
AC004223.3	4.83	0.601	0.152	3.954	0.002
AC004852.3	4.60	0.601	0.193	3.113	0.017
AC112777.1	26.38	0.601	0.137	4.379	0.001
RF00019	2.81	0.600	0.202	2.973	0.022
CNTF	11.02	0.600	0.121	4.975	0.000
G0S2	81.91	0.600	0.193	3.103	0.017
HIPK2	12047.44	0.599	0.138	4.348	0.001
AL136115.1	7.80	0.599	0.216	2.769	0.034
FOXD2	9.22	0.598	0.155	3.862	0.003
AC016831.3	3.10	0.598	0.201	2.969	0.022
AL033519.1	3.79	0.597	0.212	2.812	0.031
AC013244.2	3.19	0.596	0.167	3.577	0.006
KANK2	760.12	0.595	0.116	5.124	0.000
AC004223.1	6.13	0.595	0.182	3.275	0.012
AC007950.2	3.26	0.594	0.181	3.278	0.012
HPSE2	345.63	0.594	0.141	4.200	0.001
AC008745.1	4.11	0.594	0.220	2.703	0.039
AC009509.4	24.35	0.593	0.142	4.185	0.001
RNU1-59P	1.98	0.593	0.211	2.805	0.032
KCNMB3	40.63	0.593	0.159	3.720	0.004
CSRP1	6179.43	0.591	0.163	3.619	0.005
IL17RB	475.00	0.591	0.121	4.897	0.000
PTH1R	788.03	0.591	0.123	4.788	0.000
AC025430.1	15.73	0.590	0.154	3.833	0.003
RF00019	20.98	0.590	0.182	3.234	0.013
RPL30P14	4.21	0.589	0.188	3.136	0.016
COL5A3	4038.64	0.589	0.102	5.793	0.000
AC007423.1	3.48	0.588	0.216	2.721	0.037
TCF15	35.22	0.587	0.125	4.715	0.000
AC004491.1	16.94	0.585	0.167	3.508	0.007
CYP1A1	11.47	0.585	0.184	3.176	0.014
FOXO4	1688.51	0.585	0.103	5.700	0.000
AL137784.1	6.11	0.585	0.179	3.263	0.012
AL512383.1	14.25	0.584	0.176	3.328	0.010
LINC00513	58.59	0.584	0.144	4.051	0.002
MIR5690	3.20	0.582	0.207	2.816	0.031
TGFB3	587.15	0.582	0.132	4.411	0.001

CARHSP1	942.69	0.581	0.097	5.996	0.000
AC004678.2	20.85	0.581	0.143	4.052	0.002
SELENOP	1164.63	0.581	0.124	4.665	0.000
RF00019	15.58	0.580	0.198	2.935	0.024
KIF19	431.64	0.579	0.173	3.351	0.010
SIGLEC1	27.94	0.579	0.183	3.158	0.015
TRIM56	1127.01	0.578	0.132	4.368	0.001
LINC00499	59.23	0.578	0.171	3.385	0.009
AL390066.1	10.29	0.578	0.168	3.441	0.008
ARRDC2	1055.80	0.578	0.103	5.584	0.000
RNA5SP212	4.91	0.578	0.156	3.710	0.004
DLL4	311.56	0.578	0.131	4.395	0.001
AL031708.1	16.83	0.578	0.150	3.846	0.003
VGLL3	10.88	0.576	0.140	4.131	0.001
AC097359.1	10.51	0.576	0.150	3.830	0.003
ANPEP	88.92	0.575	0.149	3.852	0.003
AC130448.1	20.43	0.574	0.178	3.219	0.013
MT-ND6	148037.55	0.574	0.159	3.607	0.006
KIF1C	6425.82	0.574	0.116	4.936	0.000
UHRF1	63.95	0.573	0.126	4.563	0.000
AC006387.1	55.01	0.573	0.175	3.271	0.012
AC244034.3	9.49	0.573	0.166	3.450	0.008
BIRC5	8.80	0.573	0.160	3.577	0.006
AC093535.2	712.53	0.572	0.188	3.040	0.019
MT-TL2	5685.68	0.570	0.150	3.796	0.003
AC093535.1	35.76	0.570	0.148	3.843	0.003
RF00019	5.98	0.570	0.185	3.079	0.018
LBX2-AS1	17.84	0.570	0.161	3.537	0.006
AC092068.2	16.56	0.570	0.164	3.471	0.008
PTAFR	142.67	0.568	0.139	4.076	0.002
MT-TE	8777.83	0.567	0.155	3.665	0.005
ASCL1	766.56	0.566	0.121	4.690	0.000
ZNF621	478.15	0.566	0.122	4.656	0.000
RNU6ATAC39P	14.67	0.566	0.204	2.768	0.034
TNFAIP8	24.22	0.566	0.151	3.746	0.004
MIR5196	2.42	0.565	0.202	2.798	0.032
AC079117.1	3.41	0.565	0.203	2.784	0.033
MT-ND4L	217969.01	0.564	0.159	3.552	0.006
TMEM150B	9.80	0.563	0.160	3.514	0.007
NFE2	9.89	0.563	0.206	2.738	0.036

BX470102.1	6.80	0.562	0.149	3.776	0.004
AC131009.2	64.53	0.562	0.207	2.720	0.037
BTNL8	4.62	0.562	0.207	2.707	0.038
CDA	69.05	0.561	0.165	3.405	0.009
AC004918.1	17.13	0.561	0.173	3.237	0.013
AL023803.2	3.72	0.561	0.174	3.229	0.013
AP000280.1	11.78	0.561	0.209	2.677	0.041
AC016831.4	74.47	0.561	0.201	2.793	0.032
ANKRD40	3175.89	0.561	0.093	6.022	0.000
SPN	54.61	0.560	0.199	2.817	0.031
AL359183.1	30.37	0.560	0.140	4.011	0.002
MAP4K4	4289.57	0.560	0.115	4.857	0.000
AL022329.2	12.02	0.559	0.189	2.955	0.023
FAM107B	909.64	0.559	0.118	4.736	0.000
AL645940.1	12.64	0.559	0.197	2.843	0.029
AL161793.1	10.67	0.559	0.157	3.568	0.006
ITIH5	829.61	0.559	0.134	4.163	0.001
TPTEP1	91.62	0.559	0.156	3.577	0.006
AL158827.1	2.44	0.558	0.201	2.774	0.034
AC005414.1	14.35	0.558	0.126	4.426	0.001
TNFRSF10D	120.32	0.558	0.170	3.288	0.011
AC008434.1	6.53	0.558	0.156	3.581	0.006
GPER1	391.75	0.556	0.119	4.672	0.000
DIO1	4.78	0.556	0.204	2.725	0.037
KRT19	20.98	0.555	0.168	3.315	0.011
GPR82	6.71	0.555	0.169	3.291	0.011
AC026474.1	6.71	0.555	0.186	2.987	0.022
MIR657	4.46	0.554	0.155	3.585	0.006
MTATP8P2	13.90	0.554	0.190	2.912	0.025
AC106028.4	14.10	0.554	0.112	4.957	0.000
ARHGEF35	4.82	0.554	0.192	2.890	0.027
MRGPRF	72.39	0.553	0.129	4.275	0.001
MTCO1P12	326976.95	0.553	0.146	3.794	0.003
SH2D6	29.94	0.552	0.162	3.408	0.009
AC018557.2	23.57	0.552	0.184	3.007	0.021
LINC00926	39.77	0.552	0.109	5.086	0.000
TNFRSF10C	8.42	0.552	0.189	2.926	0.025
AL049840.3	13.03	0.551	0.178	3.094	0.017
PGF	117.63	0.551	0.144	3.825	0.003
AL031651.2	17.97	0.551	0.134	4.124	0.001

SLC38A2	1653.72	0.551	0.098	5.623	0.000
GRIK1-AS1	16.86	0.551	0.125	4.396	0.001
AF279873.4	2.54	0.551	0.213	2.588	0.049
PRR26	303.58	0.551	0.143	3.857	0.003
GGTA2P	17.89	0.550	0.162	3.401	0.009
RN7SL382P	4.40	0.550	0.171	3.223	0.013
OAS1	81.92	0.550	0.184	2.995	0.021
AC080128.2	24.60	0.549	0.163	3.362	0.010
AC104417.2	50.90	0.548	0.142	3.859	0.003
FHL5	31.47	0.547	0.182	3.010	0.021
SLC25A30-AS1	6.98	0.547	0.165	3.308	0.011
RF01225	3.12	0.547	0.187	2.929	0.024
AC104662.1	3.12	0.547	0.195	2.808	0.031
FSTL3	266.64	0.547	0.208	2.625	0.045
MTRNR2L3	7.12	0.546	0.163	3.359	0.010
AC103855.4	2.51	0.546	0.189	2.890	0.027
LILRA2	21.66	0.546	0.178	3.066	0.018
AL137784.2	22.29	0.546	0.173	3.162	0.015
MIR2052HG	2.61	0.546	0.206	2.647	0.043
MAGI1-AS1	3.54	0.545	0.185	2.955	0.023
RN7SL846P	3.53	0.545	0.180	3.033	0.020
RPL30P7	4.62	0.545	0.171	3.186	0.014
AF107885.1	17.30	0.544	0.188	2.892	0.026
ATP6V0E1P1	2.99	0.544	0.202	2.698	0.039
AC090673.1	6.51	0.544	0.184	2.950	0.023
EZR	3455.58	0.543	0.101	5.357	0.000
ADAM33	492.78	0.543	0.100	5.438	0.000
RF00017	41.44	0.543	0.176	3.089	0.017
CTAGE4	2.77	0.543	0.211	2.575	0.050
HSD17B1	324.78	0.542	0.150	3.619	0.005
LRRC63	9.57	0.542	0.172	3.153	0.015
C4orf19	91.61	0.542	0.123	4.390	0.001
CLMN	986.57	0.542	0.116	4.685	0.000
AC016027.2	99.26	0.542	0.180	3.015	0.020
NPIPP1	330.71	0.541	0.201	2.685	0.040
LPIN3	112.76	0.541	0.146	3.694	0.004
MAPKAPK2	849.95	0.540	0.107	5.034	0.000
AC046158.4	11.04	0.540	0.164	3.294	0.011
VENTX	24.57	0.540	0.164	3.293	0.011
RN7SL689P	8.97	0.539	0.162	3.326	0.010

-	28.05	0.539	0.128	4.212	0.001
AC103810.5	44.00	0.538	0.192	2.807	0.031
AC099513.1	5.34	0.538	0.165	3.269	0.012
AC099684.2	28.18	0.538	0.134	4.019	0.002
QDPR	4474.40	0.538	0.092	5.822	0.000
AC026979.1	7.45	0.538	0.161	3.331	0.010
LINC01561	64.97	0.537	0.137	3.911	0.003
SLC51B	9.78	0.537	0.176	3.053	0.019
PRKX	544.83	0.537	0.118	4.559	0.000
AC019227.1	18.18	0.537	0.159	3.367	0.010
MT-TM	24033.19	0.536	0.187	2.871	0.028
AL031600.2	3.06	0.535	0.176	3.039	0.019
AC005072.1	26.59	0.535	0.144	3.719	0.004
AC007546.2	13.64	0.535	0.148	3.608	0.006
RUNX3	52.49	0.535	0.152	3.519	0.007
SLCO4A1-AS1	29.14	0.535	0.168	3.178	0.014
ITGA6-AS1	6.97	0.534	0.179	2.984	0.022
HNRNPA3P14	6.96	0.533	0.166	3.210	0.013
AC245297.2	29.68	0.533	0.147	3.630	0.005
TRDN	35.56	0.533	0.144	3.704	0.004
MT-TL1	38946.42	0.533	0.188	2.830	0.030
NFKBIA	1252.62	0.533	0.107	4.970	0.000
AC022001.1	4.48	0.532	0.149	3.563	0.006
AL589739.1	11.29	0.532	0.121	4.390	0.001
ACSM1	7.34	0.531	0.149	3.566	0.006
MTSS1L	11883.51	0.531	0.107	4.978	0.000
AC139792.1	25.44	0.531	0.198	2.676	0.041
RNU6-1004P	3.41	0.530	0.180	2.947	0.024
AC099518.2	6.19	0.530	0.140	3.787	0.004
EMX2	1372.31	0.529	0.118	4.473	0.001
ANXA9	104.96	0.529	0.118	4.475	0.001
IL15	13.54	0.528	0.127	4.148	0.001
UBE2R2-AS1	9.79	0.528	0.144	3.653	0.005
MT-TR	5820.90	0.528	0.204	2.584	0.049
TNS1	2167.09	0.527	0.109	4.820	0.000
PPFIBP2	261.61	0.527	0.095	5.529	0.000
NACC2	3965.31	0.527	0.118	4.458	0.001
NCF1	36.49	0.527	0.183	2.883	0.027
AL355312.5	103.49	0.526	0.180	2.923	0.025
DOCK1	1425.29	0.526	0.104	5.070	0.000

AC131009.4	153.93	0.525	0.130	4.045	0.002
AC007193.2	42.71	0.525	0.149	3.527	0.007
SH3PXD2A-AS1	5.19	0.525	0.172	3.047	0.019
AC016705.1	158.47	0.525	0.144	3.658	0.005
MPRIP-AS1	20.53	0.525	0.193	2.713	0.038
AC068254.2	7.81	0.524	0.176	2.983	0.022
TLR7	35.46	0.524	0.148	3.547	0.006
AC006441.1	10.16	0.524	0.183	2.861	0.028
LRRC32	443.37	0.524	0.186	2.817	0.031
FOXD2-AS1	14.34	0.524	0.168	3.111	0.017
SYDE1	229.95	0.523	0.117	4.489	0.001
ARHGEF19	41.87	0.523	0.133	3.929	0.002
RF00017	5.84	0.523	0.152	3.445	0.008
AL157712.2	9.06	0.523	0.182	2.866	0.028
PRRG4	28.65	0.522	0.178	2.941	0.024
AJUBA	47.28	0.522	0.132	3.949	0.002
RN7SL596P	13.14	0.522	0.199	2.626	0.045
MIR8485	3.75	0.521	0.189	2.753	0.035
AC011239.2	13.73	0.521	0.163	3.188	0.014
CHKB-CPT1B	162.78	0.521	0.181	2.874	0.027
MT-CO1	1625669.33	0.521	0.145	3.592	0.006
ARHGEF34P	18.12	0.520	0.127	4.088	0.002
MT-TS2	2626.23	0.520	0.147	3.526	0.007
AL365209.1	121.03	0.520	0.160	3.248	0.012
MTND6P25	7.85	0.519	0.182	2.853	0.029
COL1A2	212.38	0.519	0.154	3.360	0.010
AC079600.3	6.55	0.519	0.165	3.137	0.016
AC092032.1	5.28	0.519	0.172	3.008	0.021
MT1M	1249.66	0.518	0.149	3.480	0.007
TRARG1	31.27	0.517	0.161	3.213	0.013
AC005324.5	10.49	0.517	0.191	2.697	0.039
RF00026	2.86	0.516	0.198	2.605	0.047
GJC1	370.66	0.516	0.103	5.016	0.000
AC106028.2	3.71	0.516	0.171	3.008	0.021
AC145207.7	2.62	0.515	0.191	2.693	0.040
AL583810.2	21.12	0.515	0.122	4.208	0.001
DOCK5	860.26	0.515	0.107	4.806	0.000
SLC25A18	3146.88	0.514	0.104	4.938	0.000
HIST1H2BJ	5.49	0.514	0.191	2.693	0.040
ERBIN	1087.81	0.513	0.127	4.036	0.002

AC011933.2	15.93	0.513	0.133	3.862	0.003
AC012183.1	6.04	0.513	0.166	3.085	0.018
BTBD9-AS1	42.61	0.513	0.180	2.846	0.029
FOXJ1	159.27	0.513	0.189	2.706	0.039
AC105150.1	5.20	0.513	0.159	3.232	0.013
C7orf61	83.77	0.512	0.180	2.840	0.029
LINC00862	11.00	0.512	0.129	3.961	0.002
AC096677.1	49.72	0.512	0.100	5.098	0.000
BEST2	5.63	0.511	0.195	2.621	0.046
RNU5E-8P	19.05	0.511	0.143	3.558	0.006
AC004223.2	4.58	0.511	0.168	3.044	0.019
ZNF664	1765.94	0.510	0.166	3.070	0.018
AC022146.2	32.58	0.509	0.141	3.602	0.006
AL355974.2	41.80	0.509	0.179	2.848	0.029
AC090589.1	3.67	0.509	0.172	2.959	0.023
RN7SL587P	8.31	0.509	0.173	2.944	0.024
ASNSP6	8.18	0.509	0.140	3.633	0.005
KBTBD11-OT1	10.69	0.508	0.135	3.769	0.004
ASH2LP3	6.90	0.508	0.191	2.659	0.042
AL158071.2	12.96	0.508	0.142	3.581	0.006
SLCO1A2	1031.14	0.508	0.169	3.003	0.021
ZCCHC24	4089.66	0.508	0.124	4.098	0.002
MCM7	814.06	0.508	0.095	5.323	0.000
CA3-AS1	17.58	0.507	0.130	3.908	0.003
MIR210HG	57.52	0.507	0.172	2.946	0.024
AC010973.2	24.53	0.506	0.177	2.867	0.028
TRG-AS1	13.15	0.506	0.168	3.008	0.021
AC104463.2	6.64	0.506	0.196	2.585	0.049
MS4A14	41.60	0.506	0.177	2.855	0.028
SMIM3	285.82	0.506	0.118	4.302	0.001
AC091133.5	3.87	0.505	0.178	2.837	0.030
SPACA6	460.87	0.505	0.085	5.959	0.000
EDA2R	31.20	0.505	0.144	3.513	0.007
AC133528.1	20.88	0.505	0.175	2.880	0.027
OR2A20P	29.42	0.505	0.123	4.109	0.002
INPPL1	1386.34	0.504	0.094	5.388	0.000
AC004672.2	3.52	0.504	0.184	2.745	0.036
S1PR1	632.66	0.504	0.161	3.128	0.016
SIGLEC8	88.37	0.504	0.151	3.333	0.010
RC3H1-IT1	5.87	0.504	0.193	2.610	0.047

MIR1237	2.21	0.503	0.195	2.582	0.049
AP000852.1	3.90	0.503	0.180	2.802	0.032
TPTE2P2	3.40	0.503	0.162	3.111	0.017
FLJ46906	166.93	0.503	0.111	4.519	0.000
AL355073.2	3.33	0.503	0.180	2.799	0.032
AC127496.1	20.08	0.503	0.180	2.795	0.032
IP6K3	72.86	0.503	0.144	3.481	0.007
PLIN4	547.01	0.502	0.130	3.869	0.003
SELPLG	194.89	0.502	0.123	4.088	0.002
AC016745.2	26.53	0.502	0.166	3.015	0.020
GBP3	75.36	0.501	0.184	2.728	0.037
MTND1P23	25904.83	0.501	0.146	3.445	0.008
C5orf64-AS1	12.95	0.501	0.179	2.792	0.032
IFNA13	3.19	0.501	0.184	2.719	0.037
AC130364.2	4.74	0.500	0.192	2.603	0.047

Table 3.2: Down-regulated genes in the cortices of AD patients of the MAP study (Figure 3.6C). Values were calculated using DESeq (see methods) on RNA-seq data. Genes correspond to a padj < 0.05 and log2 fold change < -0.5.

Gene Name	**baseMean**	**log2FoldChange**	**lfcSE**	**stat**	**padj**
TMEM189-UBE2V1	40.22656	-8.907	1.919	-4.641	0.000
NPAS4	32.71	-2.847	0.467	-6.098	0.000
EEF1DP5	2.63	-2.573	0.983	-2.618	0.046
MATR3	736.20	-2.518	0.522	-4.820	0.000
PCDHGB4	60.16	-2.147	0.767	-2.798	0.032
XIRP1	1.97	-1.876	0.579	-3.241	0.013
NA	3.38	-1.760	0.595	-2.957	0.023
C6orf222	2.32	-1.584	0.416	-3.810	0.003
MUC5AC	6.68	-1.573	0.481	-3.267	0.012
C1orf94	5.85	-1.566	0.373	-4.192	0.001
KHDC3L	3.62	-1.491	0.335	-4.443	0.001
AL662899.2	56.56	-1.478	0.514	-2.875	0.027
ASTL	2.59	-1.469	0.481	-3.052	0.019
SELE	24.20	-1.456	0.418	-3.479	0.007
FUT3	4.39	-1.398	0.321	-4.348	0.001
AP001107.5	10.61	-1.383	0.354	-3.908	0.003
PCDHGA7	108.93	-1.382	0.304	-4.543	0.000
LINC02594	2.12	-1.362	0.399	-3.415	0.009
LINC01605	7.51	-1.342	0.335	-4.008	0.002
MROH5	1.67	-1.314	0.504	-2.606	0.047
AL662884.1	3.73	-1.306	0.411	-3.180	0.014

DLX4	7.28	-1.302	0.237	-5.495	0.000
AC021127.1	1.52	-1.279	0.406	-3.155	0.015
ERVH-1	1.59	-1.279	0.458	-2.791	0.032
WNT1	12.34	-1.279	0.335	-3.814	0.003
AC073610.3	20.83	-1.273	0.306	-4.165	0.001
AC046130.2	2.76	-1.257	0.431	-2.919	0.025
LPA	1.93	-1.245	0.444	-2.804	0.032
IL1B	24.70	-1.204	0.343	-3.514	0.007
LINC00269	1.97	-1.193	0.463	-2.576	0.050
LINC01257	3.23	-1.185	0.419	-2.828	0.030
FOSB	167.45	-1.173	0.276	-4.256	0.001
FREM3	46.37	-1.163	0.260	-4.473	0.001
PCDHGB3	49.51	-1.162	0.341	-3.413	0.009
AC104407.1	2.99	-1.144	0.394	-2.900	0.026
C6orf141	7.04	-1.134	0.304	-3.726	0.004
AC005077.4	27.28	-1.126	0.193	-5.827	0.000
AC091182.2	2.38	-1.119	0.398	-2.810	0.031
SLC46A2	5.00	-1.112	0.330	-3.367	0.010
AC027801.1	2.20	-1.112	0.404	-2.755	0.035
LINC00398	5.95	-1.108	0.318	-3.482	0.007
AC117402.1	4.07	-1.097	0.261	-4.199	0.001
IL13RA2	4.35	-1.092	0.384	-2.841	0.029
CLEC4F	3.09	-1.088	0.338	-3.216	0.013
SLN	13.72	-1.086	0.276	-3.940	0.002
FGFBP2	5.46	-1.085	0.366	-2.968	0.023
CRH	56.96	-1.084	0.269	-4.037	0.002
LINC02023	2.18	-1.078	0.405	-2.661	0.042
VWA8-AS1	2.07	-1.072	0.329	-3.255	0.012
ALG1L13P	2.06	-1.051	0.334	-3.143	0.016
DSG3	2.42	-1.044	0.372	-2.803	0.032
GLP2R	54.92	-1.041	0.186	-5.586	0.000
AC233702.4	3.39	-1.037	0.302	-3.435	0.008
FRMPD2B	62.98	-1.011	0.240	-4.204	0.001
MYOZ2	6.74	-1.006	0.205	-4.910	0.000
NSG2	786.41	-1.002	0.267	-3.745	0.004
NBEAP3	2.91	-0.998	0.349	-2.857	0.028
PCDHA7	25.46	-0.995	0.260	-3.826	0.003
AP003393.1	50.33	-0.979	0.157	-6.239	0.000
C7orf57	1.89	-0.974	0.374	-2.609	0.047
AC011379.2	20.38	-0.964	0.290	-3.321	0.011
SST	281.97	-0.962	0.230	-4.190	0.001
GTF2IP7	4.55	-0.959	0.316	-3.032	0.020
GFRA4	2.38	-0.959	0.369	-2.601	0.047

EGR4	172.97	-0.958	0.212	-4.524	0.000
CFAP97D1	3.13	-0.945	0.249	-3.794	0.003
PCDHGA4	129.59	-0.945	0.249	-3.793	0.003
AC005077.2	2.43	-0.944	0.245	-3.855	0.003
SOWAHB	94.58	-0.943	0.243	-3.886	0.003
AC020629.1	3.25	-0.942	0.205	-4.608	0.000
AC026748.1	5.06	-0.929	0.197	-4.721	0.000
MISP	6.41	-0.924	0.200	-4.620	0.000
CGB7	2.57	-0.918	0.327	-2.810	0.031
VGF	1481.76	-0.917	0.256	-3.581	0.006
RFX8	15.11	-0.912	0.220	-4.142	0.001
EGR2	34.99	-0.912	0.277	-3.291	0.011
PCAT7	7.32	-0.909	0.262	-3.470	0.008
AC243829.1	24.80	-0.900	0.210	-4.275	0.001
CNR1	428.07	-0.889	0.311	-2.857	0.028
EGR1	1003.50	-0.886	0.235	-3.765	0.004
AC016576.1	8.16	-0.886	0.252	-3.516	0.007
PRAP1	7.84	-0.865	0.272	-3.180	0.014
C4orf36	5.91	-0.862	0.306	-2.819	0.031
KRT80	3.16	-0.858	0.304	-2.824	0.030
KLHL14	10.27	-0.856	0.271	-3.161	0.015
AC079154.1	3.04	-0.854	0.296	-2.889	0.027
FBN3	16.69	-0.854	0.209	-4.091	0.002
LINC02288	5.27	-0.854	0.267	-3.197	0.014
AC015819.3	14.76	-0.851	0.184	-4.629	0.000
ZNF382	128.87	-0.851	0.220	-3.872	0.003
FAM228A	20.85	-0.850	0.297	-2.862	0.028
AC211476.3	6.89	-0.849	0.222	-3.825	0.003
AC125603.4	7.71	-0.843	0.169	-4.981	0.000
AL449403.1	10.08	-0.843	0.261	-3.234	0.013
AC121757.1	3.62	-0.842	0.307	-2.747	0.036
AC007249.2	9.46	-0.841	0.191	-4.395	0.001
-	5.88	-0.835	0.220	-3.792	0.003
NECTIN3-AS1	5.26	-0.834	0.243	-3.435	0.008
AL024507.2	30.26	-0.832	0.153	-5.448	0.000
DUSP2	199.02	-0.832	0.174	-4.776	0.000
AC023055.1	13.63	-0.832	0.265	-3.140	0.016
AC078925.2	2.65	-0.830	0.296	-2.799	0.032
AL583722.3	5.99	-0.827	0.240	-3.438	0.008
LINC01007	159.52	-0.824	0.197	-4.188	0.001
LINC02273	3.34	-0.824	0.280	-2.947	0.024
CCL3L1	46.36	-0.823	0.229	-3.590	0.006
GDA	487.01	-0.822	0.238	-3.460	0.008

LINC02458	27.51	-0.820	0.178	-4.601	0.000
CHRM4	59.11	-0.818	0.222	-3.679	0.005
LINC01476	20.20	-0.816	0.216	-3.779	0.004
DUSP4	172.42	-0.812	0.188	-4.330	0.001
AC009185.1	1.86	-0.812	0.298	-2.723	0.037
AL021068.1	6.45	-0.811	0.207	-3.923	0.003
AC236972.4	2.21	-0.810	0.270	-3.001	0.021
AL137782.1	52.22	-0.809	0.247	-3.277	0.012
LINC00898	14.35	-0.808	0.207	-3.901	0.003
AL136531.2	75.88	-0.804	0.298	-2.696	0.039
LINC01494	4.27	-0.800	0.234	-3.418	0.009
AKAP5	248.81	-0.793	0.280	-2.835	0.030
AC073314.1	2.43	-0.793	0.215	-3.684	0.005
ARRDC3-AS1	2.15	-0.792	0.287	-2.761	0.034
SERTM1	135.68	-0.792	0.205	-3.860	0.003
PCSK1	582.66	-0.791	0.200	-3.945	0.002
BDNF	98.59	-0.790	0.186	-4.236	0.001
HRG	1.55	-0.786	0.277	-2.836	0.030
RF02160	6.65	-0.785	0.224	-3.510	0.007
AC099654.2	5.96	-0.785	0.268	-2.934	0.024
AC128687.1	4.39	-0.785	0.216	-3.626	0.005
PPEF1	46.54	-0.784	0.187	-4.191	0.001
PCDHGC5	792.61	-0.784	0.253	-3.100	0.017
AC097460.1	2.98	-0.782	0.262	-2.989	0.022
SCG2	1584.12	-0.781	0.172	-4.536	0.000
ARC	724.83	-0.779	0.209	-3.719	0.004
NR2C2	325.58	-0.777	0.198	-3.916	0.003
AL359195.2	2.30	-0.776	0.253	-3.066	0.018
LINC01376	4.99	-0.773	0.264	-2.934	0.024
ALG1L	13.87	-0.773	0.224	-3.451	0.008
EWSAT1	8.79	-0.773	0.181	-4.277	0.001
AL390778.2	5.25	-0.771	0.287	-2.692	0.040
OR1L3	1.60	-0.771	0.286	-2.699	0.039
ARID3C	10.81	-0.767	0.238	-3.227	0.013
AF131216.3	39.57	-0.765	0.139	-5.501	0.000
AC140847.2	4.07	-0.764	0.208	-3.667	0.005
AGBL1	24.46	-0.763	0.166	-4.600	0.000
ADRB3	4.40	-0.760	0.217	-3.501	0.007
OR10A2	49.84	-0.760	0.176	-4.318	0.001
MYLK3	32.78	-0.760	0.143	-5.313	0.000
LINC01219	5.48	-0.758	0.291	-2.601	0.047
PAK1	2257.15	-0.757	0.224	-3.381	0.009
GABRA6	7.40	-0.757	0.207	-3.663	0.005

ARL4D	276.15	-0.756	0.167	-4.541	0.000
CCL4L2	13.67	-0.756	0.235	-3.218	0.013
RXFP4	2.18	-0.755	0.279	-2.703	0.039
THBS1	135.55	-0.755	0.160	-4.711	0.000
AL035696.4	46.63	-0.754	0.267	-2.825	0.030
KRT8P7	2.09	-0.753	0.217	-3.473	0.008
PCDH8	590.72	-0.752	0.218	-3.450	0.008
HTR2C	25.19	-0.752	0.216	-3.478	0.007
CH25H	54.77	-0.751	0.196	-3.831	0.003
PP12613	34.33	-0.751	0.220	-3.417	0.009
ATF3	145.18	-0.749	0.239	-3.137	0.016
CHGB	2168.75	-0.747	0.187	-4.001	0.002
ICAM5	1127.21	-0.746	0.142	-5.233	0.000
AP001057.1	2.07	-0.743	0.274	-2.715	0.038
RHCE	18.95	-0.743	0.158	-4.697	0.000
C11orf97	11.62	-0.741	0.269	-2.751	0.035
-	45.18	-0.736	0.191	-3.850	0.003
CLUL1	26.29	-0.736	0.233	-3.158	0.015
SCAMP5	1556.73	-0.733	0.240	-3.054	0.019
ADAMTSL1	20.99	-0.730	0.160	-4.554	0.000
OR11H7	2.21	-0.729	0.274	-2.660	0.042
FRMPD2	148.40	-0.729	0.161	-4.533	0.000
SSTR4	6.41	-0.725	0.250	-2.904	0.026
RNU6-1123P	1.70	-0.724	0.219	-3.301	0.011
FUT5	2.47	-0.724	0.256	-2.831	0.030
HTR3B	32.62	-0.722	0.203	-3.551	0.006
ZCCHC12	291.43	-0.720	0.177	-4.070	0.002
AP004833.2	4.06	-0.720	0.210	-3.426	0.008
CYP24A1	6.75	-0.719	0.246	-2.925	0.025
C1QL3	208.93	-0.719	0.202	-3.559	0.006
LINC01132	3.70	-0.718	0.275	-2.606	0.047
TAC1	102.70	-0.716	0.192	-3.734	0.004
PTGS2	79.55	-0.716	0.204	-3.511	0.007
HTR6	27.80	-0.715	0.192	-3.723	0.004
AL121987.2	15.11	-0.715	0.175	-4.077	0.002
STK24-AS1	4.01	-0.715	0.173	-4.122	0.002
CCT6B	33.50	-0.713	0.200	-3.571	0.006
MIR628	5.20	-0.713	0.209	-3.407	0.009
PCDHGA5	112.75	-0.713	0.243	-2.940	0.024
AC092159.2	10.41	-0.713	0.216	-3.293	0.011
NSFP1	266.52	-0.712	0.242	-2.948	0.024
AC092720.1	10.32	-0.708	0.195	-3.632	0.005
AC068870.2	9.13	-0.707	0.155	-4.570	0.000

KRT5	38.64	-0.706	0.257	-2.746	0.036
FEM1AP2	4.31	-0.706	0.243	-2.910	0.025
AC103952.1	5.48	-0.704	0.202	-3.484	0.007
ANXA8	5.32	-0.703	0.212	-3.317	0.011
UROC1	5.38	-0.703	0.190	-3.701	0.004
C9orf106	20.37	-0.700	0.168	-4.158	0.001
AC100797.4	21.65	-0.699	0.148	-4.723	0.000
BRAFP1	2.56	-0.697	0.258	-2.702	0.039
AC008738.1	2.91	-0.696	0.251	-2.772	0.034
AL132822.1	2.68	-0.694	0.255	-2.719	0.037
IL1RAPL2	7.45	-0.693	0.243	-2.846	0.029
LINC00501	2.45	-0.691	0.235	-2.941	0.024
AC005865.2	59.85	-0.691	0.129	-5.358	0.000
HMGCR	394.98	-0.688	0.201	-3.418	0.009
TYRP1	18.36	-0.688	0.226	-3.044	0.019
LINC00602	4.54	-0.686	0.234	-2.934	0.024
CSNKA2IP	3.87	-0.684	0.181	-3.775	0.004
YWHAZP5	35.85	-0.683	0.176	-3.885	0.003
PHBP9	13.58	-0.683	0.166	-4.100	0.002
AC011995.2	12.60	-0.683	0.192	-3.560	0.006
AC007424.1	6.82	-0.682	0.217	-3.150	0.015
AP001880.1	2.14	-0.678	0.214	-3.163	0.015
AL627402.1	74.09	-0.678	0.174	-3.891	0.003
DYDC2	14.72	-0.678	0.183	-3.712	0.004
GPR3	97.76	-0.677	0.175	-3.865	0.003
AC008780.1	7.73	-0.677	0.213	-3.173	0.015
SLC32A1	269.46	-0.677	0.208	-3.263	0.012
CALML3	9.64	-0.676	0.167	-4.055	0.002
AC105345.1	116.67	-0.674	0.132	-5.121	0.000
OR10AC1	3.10	-0.673	0.202	-3.323	0.011
AC004408.1	3.76	-0.672	0.204	-3.288	0.011
KCNH4	149.05	-0.672	0.154	-4.376	0.001
CRY2	1497.44	-0.671	0.193	-3.480	0.007
HSPB3	70.18	-0.670	0.161	-4.174	0.001
AC010266.2	18.52	-0.670	0.146	-4.582	0.000
PRSS16	50.60	-0.670	0.170	-3.931	0.002
WDR17	228.33	-0.669	0.183	-3.652	0.005
ASS1P1	5.88	-0.668	0.170	-3.939	0.002
MPO	38.35	-0.668	0.140	-4.763	0.000
KRBOX1	15.16	-0.667	0.169	-3.936	0.002
AC105046.1	9.98	-0.665	0.164	-4.065	0.002
AMDHD2	475.91	-0.664	0.167	-3.984	0.002
LINC01310	24.59	-0.663	0.158	-4.200	0.001

CBLN4	323.00	-0.663	0.183	-3.634	0.005
AC015819.1	2.22	-0.662	0.202	-3.270	0.012
RTN3P1	516.69	-0.659	0.196	-3.366	0.010
AC034228.2	2.23	-0.659	0.191	-3.458	0.008
AP003170.1	5.41	-0.658	0.188	-3.505	0.007
AL049779.3	1.71	-0.658	0.226	-2.906	0.026
AC245164.1	5.19	-0.657	0.214	-3.066	0.018
AC107081.1	1.78	-0.657	0.219	-2.997	0.021
SVOP	1424.45	-0.657	0.164	-3.993	0.002
RHO	10.13	-0.656	0.217	-3.026	0.020
WNT8A	9.69	-0.656	0.157	-4.182	0.001
CCDC188	46.12	-0.655	0.161	-4.079	0.002
PCYOX1L	388.45	-0.654	0.120	-5.440	0.000
CYR61	389.80	-0.653	0.203	-3.219	0.013
AP003680.1	13.86	-0.653	0.201	-3.244	0.012
AC005921.4	5.82	-0.652	0.212	-3.078	0.018
ABCC11	18.04	-0.651	0.207	-3.151	0.015
ALOX12B	38.65	-0.650	0.163	-3.989	0.002
PRMT8	458.36	-0.648	0.137	-4.728	0.000
SMPD4P1	9.47	-0.648	0.233	-2.786	0.033
STYK1	95.17	-0.647	0.178	-3.629	0.005
FSTL4	302.31	-0.647	0.167	-3.876	0.003
AC116021.1	3.32	-0.645	0.221	-2.924	0.025
KCNAB2	3490.39	-0.645	0.245	-2.626	0.045
AC092645.1	19.17	-0.644	0.222	-2.900	0.026
RPH3A	2712.07	-0.643	0.198	-3.257	0.012
KREMEN2	86.29	-0.642	0.105	-6.127	0.000
C2orf48	5.58	-0.641	0.216	-2.966	0.023
MCHR2	86.56	-0.641	0.145	-4.411	0.001
LINC02225	4.62	-0.640	0.209	-3.061	0.018
PNMA6B	245.08	-0.638	0.161	-3.961	0.002
BEST4	36.00	-0.638	0.148	-4.322	0.001
NBAT1	4.45	-0.638	0.201	-3.171	0.015
AL929472.1	1.68	-0.637	0.228	-2.795	0.032
ZNF763	31.59	-0.637	0.228	-2.796	0.032
ANKRD31	6.21	-0.636	0.188	-3.386	0.009
AC020934.1	2.36	-0.636	0.189	-3.356	0.010
AC087203.3	38.30	-0.635	0.143	-4.452	0.001
DUX4L27	6.62	-0.635	0.218	-2.911	0.025
AL132709.1	11.50	-0.635	0.214	-2.966	0.023
AC211476.4	4.88	-0.634	0.176	-3.607	0.006
OR8S1	1.73	-0.634	0.238	-2.659	0.042
AL137028.2	2.26	-0.632	0.213	-2.968	0.023

MAS1	128.47	-0.631	0.166	-3.795	0.003
LINC02254	4.25	-0.631	0.223	-2.836	0.030
SP7	5.60	-0.631	0.172	-3.668	0.005
GGNBP1	5.54	-0.630	0.198	-3.182	0.014
ZBTB45P2	117.78	-0.630	0.161	-3.920	0.003
GAD2	604.17	-0.627	0.195	-3.225	0.013
AL021918.4	5.84	-0.626	0.196	-3.189	0.014
FAM163A	41.74	-0.626	0.185	-3.393	0.009
AC122710.2	11.44	-0.626	0.193	-3.246	0.012
KRT17P1	85.47	-0.625	0.184	-3.393	0.009
LINC00664	8.19	-0.624	0.202	-3.085	0.018
ADCYAP1	193.10	-0.623	0.197	-3.170	0.015
AL360270.3	13.52	-0.623	0.215	-2.891	0.026
LINC01303	3.04	-0.618	0.238	-2.598	0.048
TGM3	4.09	-0.617	0.234	-2.637	0.044
LINC01844	7.49	-0.617	0.196	-3.140	0.016
AL049836.1	9.49	-0.615	0.150	-4.093	0.002
SEC13P1	5.10	-0.615	0.175	-3.515	0.007
AL135905.1	5.63	-0.614	0.199	-3.092	0.017
DHRS2	6.62	-0.614	0.165	-3.724	0.004
CITED2	471.78	-0.613	0.153	-3.996	0.002
POM121L2	1.91	-0.613	0.220	-2.790	0.033
STARD5	26.14	-0.612	0.159	-3.843	0.003
RPLP0P2	29.83	-0.612	0.184	-3.328	0.010
LINC01168	55.79	-0.611	0.135	-4.536	0.000
PNOC	36.05	-0.611	0.193	-3.166	0.015
TNFSF18	8.56	-0.611	0.184	-3.321	0.011
AC116456.1	8.72	-0.610	0.198	-3.082	0.018
RARRES2P1	7.14	-0.610	0.185	-3.296	0.011
TUBB3	4346.40	-0.608	0.159	-3.824	0.003
SDSL	160.16	-0.608	0.100	-6.075	0.000
CFAP161	4.42	-0.608	0.175	-3.473	0.008
OSTN	18.04	-0.607	0.212	-2.858	0.028
IL1RL2	33.26	-0.606	0.130	-4.680	0.000
SNORD115-20	2.58	-0.606	0.188	-3.220	0.013
STBD1	135.22	-0.606	0.180	-3.363	0.010
C2orf73	9.84	-0.606	0.192	-3.158	0.015
AL445437.1	4.17	-0.605	0.161	-3.760	0.004
RASGRF1	1109.12	-0.605	0.198	-3.050	0.019
CDH9	122.90	-0.605	0.152	-3.986	0.002
AL162574.1	6.04	-0.604	0.214	-2.817	0.031
KLHL30-AS1	8.60	-0.604	0.133	-4.538	0.000
BX255923.2	168.28	-0.604	0.156	-3.879	0.003

FAM90A25P	8.52	-0.604	0.167	-3.604	0.006
DNAH8	4.83	-0.603	0.195	-3.097	0.017
LINC01511	27.80	-0.603	0.171	-3.536	0.006
AC024909.2	90.63	-0.603	0.207	-2.914	0.025
TUBA8	434.20	-0.603	0.186	-3.248	0.012
GALNTL6	75.90	-0.602	0.115	-5.244	0.000
AC116407.1	14.30	-0.602	0.156	-3.848	0.003
YWHAZP3	273.46	-0.601	0.171	-3.519	0.007
AL023581.2	3.68	-0.601	0.192	-3.129	0.016
CACNA1G-AS1	11.86	-0.601	0.148	-4.068	0.002
LINC02009	32.75	-0.601	0.150	-3.999	0.002
STAT4	362.77	-0.601	0.154	-3.902	0.003
OLFM3	355.90	-0.601	0.177	-3.392	0.009
SEPT7P9	5.54	-0.600	0.220	-2.730	0.037
RBM3	784.45	-0.600	0.134	-4.476	0.001
LNCOC1	54.35	-0.599	0.217	-2.763	0.034
NPBWR2	8.65	-0.598	0.221	-2.708	0.038
AC027045.3	13.49	-0.598	0.202	-2.960	0.023
AL583827.1	20.04	-0.598	0.176	-3.387	0.009
CRYM	1502.66	-0.596	0.177	-3.366	0.010
GPR151	7.64	-0.596	0.167	-3.567	0.006
PTGER1	21.25	-0.594	0.195	-3.050	0.019
AC068538.1	7.04	-0.594	0.172	-3.441	0.008
RIIAD1	44.17	-0.593	0.143	-4.138	0.001
PAK6	568.41	-0.593	0.171	-3.465	0.008
USP32P1	617.46	-0.593	0.180	-3.292	0.011
FGF13	804.73	-0.593	0.139	-4.248	0.001
AL513217.1	10.83	-0.592	0.206	-2.876	0.027
PENK	35.66	-0.591	0.224	-2.635	0.044
CCKBR	452.42	-0.591	0.130	-4.537	0.000
NODAL	5.33	-0.590	0.197	-2.992	0.021
AC126755.1	717.50	-0.589	0.148	-3.989	0.002
FAM90A11P	7.84	-0.589	0.211	-2.798	0.032
FAM86B3P	51.48	-0.589	0.162	-3.641	0.005
AL359852.1	3.17	-0.588	0.190	-3.102	0.017
AC010624.4	3.85	-0.588	0.160	-3.663	0.005
DUXAP8	54.32	-0.587	0.155	-3.793	0.003
EFNB3	749.73	-0.586	0.137	-4.282	0.001
GABRG2	1236.92	-0.585	0.180	-3.242	0.013
AC011477.6	2.47	-0.584	0.221	-2.646	0.043
C3orf80	262.19	-0.584	0.155	-3.776	0.004
AL390955.2	5.24	-0.582	0.192	-3.035	0.020
TMC3	6.26	-0.581	0.168	-3.453	0.008

AC018358.1	130.30	-0.581	0.167	-3.483	0.007
MAL2	605.42	-0.581	0.192	-3.023	0.020
HPX	13.39	-0.580	0.157	-3.697	0.004
NMNAT2	2341.00	-0.580	0.154	-3.775	0.004
COL26A1	344.72	-0.580	0.155	-3.737	0.004
AC034268.1	2.31	-0.579	0.200	-2.892	0.026
TMEM200A	32.97	-0.576	0.176	-3.278	0.012
TUBB2BP1	575.12	-0.576	0.106	-5.419	0.000
SFTPA2	13.25	-0.575	0.161	-3.564	0.006
WASF1	2455.05	-0.575	0.165	-3.476	0.007
SCTR	9.44	-0.575	0.223	-2.581	0.049
LINC00507	175.55	-0.575	0.176	-3.260	0.012
AF106564.1	277.51	-0.574	0.152	-3.772	0.004
MDK	231.50	-0.574	0.119	-4.807	0.000
LY86-AS1	141.79	-0.574	0.156	-3.679	0.005
PARM1	1102.79	-0.573	0.168	-3.414	0.009
ELFN2	54.41	-0.573	0.142	-4.028	0.002
PNMA5	264.67	-0.572	0.128	-4.485	0.001
CFAP61	15.26	-0.572	0.156	-3.674	0.005
AP000894.2	55.06	-0.571	0.150	-3.818	0.003
AL139398.1	6.89	-0.571	0.204	-2.798	0.032
DSG2	4.71	-0.570	0.201	-2.830	0.030
LINC02552	29.03	-0.569	0.150	-3.788	0.004
IQGAP3	42.65	-0.567	0.112	-5.068	0.000
AL049775.1	41.19	-0.567	0.157	-3.611	0.005
AC012508.2	16.20	-0.567	0.159	-3.566	0.006
HOOK1	98.59	-0.567	0.178	-3.181	0.014
AL160412.1	7.47	-0.567	0.220	-2.580	0.049
ZBBX	108.96	-0.566	0.111	-5.103	0.000
CALML3-AS1	9.77	-0.566	0.159	-3.550	0.006
ADTRP	31.74	-0.565	0.171	-3.313	0.011
HTR5A	256.08	-0.565	0.179	-3.162	0.015
SNORD94	5.18	-0.565	0.148	-3.808	0.003
EPHA10	325.17	-0.564	0.165	-3.425	0.008
AC062029.1	16.34	-0.564	0.125	-4.513	0.000
SLC30A3	1220.19	-0.563	0.138	-4.093	0.002
AC021491.2	6.44	-0.563	0.212	-2.652	0.043
LINC02055	15.58	-0.563	0.183	-3.070	0.018
ADRA1D	73.01	-0.562	0.151	-3.711	0.004
AC106782.1	34.58	-0.561	0.181	-3.097	0.017
DUSP5	245.64	-0.561	0.164	-3.427	0.008
TAC4	2.92	-0.561	0.216	-2.591	0.048
TARBP1	827.67	-0.560	0.143	-3.931	0.002

AL136964.1	27.42	-0.560	0.123	-4.545	0.000
NT5DC3	892.71	-0.560	0.181	-3.101	0.017
ALDOAP2	123.89	-0.559	0.180	-3.116	0.016
AC114947.2	59.80	-0.559	0.130	-4.310	0.001
AL121899.1	7.98	-0.559	0.176	-3.181	0.014
BFSP1	53.23	-0.559	0.128	-4.369	0.001
CHRM2	32.17	-0.558	0.178	-3.130	0.016
NECAP1P1	4.19	-0.558	0.214	-2.609	0.047
ABRA	7.38	-0.557	0.215	-2.592	0.048
AC091305.1	7.83	-0.557	0.196	-2.846	0.029
SLC6A17	3727.43	-0.557	0.136	-4.090	0.002
FBXL21	3.60	-0.556	0.210	-2.644	0.044
FLJ31104	12.07	-0.556	0.194	-2.869	0.028
AL357673.1	6.63	-0.556	0.141	-3.937	0.002
ANKRD30BP1	8.44	-0.555	0.180	-3.085	0.018
DCLK1	2106.54	-0.555	0.203	-2.726	0.037
AC148477.1	74.56	-0.554	0.147	-3.772	0.004
AMMECR1LP1	4.24	-0.554	0.166	-3.344	0.010
PRKCG	2132.13	-0.553	0.131	-4.223	0.001
RORB-AS1	28.34	-0.551	0.151	-3.658	0.005
AC044849.1	111.91	-0.551	0.155	-3.553	0.006
RAB3A	2661.97	-0.551	0.193	-2.858	0.028
DES	27.04	-0.551	0.204	-2.704	0.039
PLK4	15.71	-0.551	0.154	-3.580	0.006
CLDN16	8.31	-0.551	0.174	-3.175	0.015
RPL18AP2	2.68	-0.550	0.173	-3.183	0.014
SPDEF	37.30	-0.549	0.131	-4.176	0.001
AC008780.2	85.14	-0.548	0.127	-4.310	0.001
RHOV	80.44	-0.548	0.130	-4.226	0.001
MARCH10	11.82	-0.547	0.161	-3.403	0.009
HSPA8P1	100.18	-0.546	0.151	-3.610	0.006
AC091874.1	14.28	-0.546	0.159	-3.442	0.008
ZNF702P	46.80	-0.545	0.149	-3.666	0.005
KIRREL2	16.12	-0.545	0.114	-4.796	0.000
RAB27B	270.32	-0.545	0.163	-3.352	0.010
EFCAB1	36.01	-0.545	0.189	-2.878	0.027
AL359258.3	15.98	-0.545	0.165	-3.294	0.011
OPN3	246.69	-0.545	0.196	-2.774	0.034
NAP1L5	1946.37	-0.544	0.148	-3.669	0.005
LGMNP1	10.97	-0.543	0.146	-3.735	0.004
AL450992.2	21.14	-0.543	0.209	-2.600	0.048
TESMIN	12.72	-0.542	0.180	-3.006	0.021
AC068787.1	4.38	-0.542	0.175	-3.108	0.017

C8orf34-AS1	7.58	-0.541	0.173	-3.129	0.016
HTR1A	42.61	-0.541	0.195	-2.776	0.033
FAM225B	42.02	-0.541	0.170	-3.183	0.014
ROS1	74.63	-0.540	0.210	-2.576	0.050
CHRNB2	811.90	-0.540	0.147	-3.670	0.005
PRSS12	55.37	-0.539	0.149	-3.624	0.005
AL390955.1	4.26	-0.539	0.154	-3.495	0.007
VWA7	227.87	-0.539	0.167	-3.229	0.013
AC013553.1	3.55	-0.539	0.161	-3.341	0.010
TAC3	123.03	-0.538	0.148	-3.627	0.005
TUBB2A	7799.74	-0.538	0.104	-5.171	0.000
NPHS1	9.85	-0.537	0.186	-2.885	0.027
DCLK3	36.23	-0.537	0.151	-3.560	0.006
ZBTB45P1	100.98	-0.536	0.145	-3.702	0.004
AC023421.1	2.93	-0.535	0.166	-3.232	0.013
DIRAS2	1779.85	-0.535	0.162	-3.298	0.011
PRAG1	382.82	-0.535	0.134	-3.998	0.002
CFAP57	61.39	-0.534	0.194	-2.755	0.035
ATP6V1E1P1	81.26	-0.534	0.141	-3.794	0.003
BX323046.1	2.59	-0.534	0.182	-2.939	0.024
AL139246.1	6.94	-0.534	0.176	-3.034	0.020
SPHKAP	203.98	-0.534	0.151	-3.542	0.006
MAP2K1P1	63.50	-0.533	0.172	-3.099	0.017
SH2D5	909.78	-0.533	0.136	-3.913	0.003
C5orf34	24.41	-0.533	0.127	-4.202	0.001
AC012645.3	26.55	-0.532	0.136	-3.915	0.003
LINC02347	15.52	-0.532	0.205	-2.592	0.048
PTH2R	86.91	-0.532	0.140	-3.807	0.003
RTN1	7937.40	-0.532	0.159	-3.338	0.010
NRXN3	771.45	-0.532	0.164	-3.243	0.012
INHBA-AS1	31.38	-0.531	0.122	-4.339	0.001
RGS7BP	233.49	-0.530	0.186	-2.855	0.028
MYCBPAP	46.82	-0.530	0.110	-4.836	0.000
CYP26B1	287.05	-0.529	0.142	-3.721	0.004
HNRNPA1P46	8.25	-0.528	0.138	-3.825	0.003
GPR88	92.08	-0.527	0.140	-3.762	0.004
CLSTN3	4168.68	-0.526	0.142	-3.712	0.004
AC090164.2	4.89	-0.526	0.166	-3.173	0.015
ZNF441	183.46	-0.526	0.089	-5.888	0.000
RGS4	3652.01	-0.525	0.150	-3.506	0.007
AC133637.1	3.66	-0.524	0.188	-2.796	0.032
ARMCX5	96.03	-0.524	0.114	-4.602	0.000
CALB2	229.68	-0.524	0.186	-2.822	0.031

NCALD	2394.66	-0.524	0.143	-3.651	0.005
SMIM17	55.97	-0.523	0.174	-3.000	0.021
AC037441.1	28.50	-0.523	0.189	-2.766	0.034
MCM4	465.58	-0.522	0.112	-4.664	0.000
CORT	126.07	-0.522	0.122	-4.270	0.001
DUSP8P3	8.37	-0.522	0.129	-4.048	0.002
GLIS2-AS1	7.87	-0.521	0.126	-4.128	0.001
CDH22	965.15	-0.521	0.138	-3.762	0.004
GOLT1A	23.95	-0.521	0.171	-3.038	0.019
PLPPR4	562.74	-0.521	0.154	-3.376	0.009
AP003108.5	20.41	-0.521	0.160	-3.250	0.012
AC106795.3	2.32	-0.521	0.189	-2.748	0.035
KLHL10	6.49	-0.521	0.176	-2.964	0.023
UBE2NP1	16.84	-0.520	0.141	-3.695	0.004
PACERR	8.90	-0.520	0.190	-2.739	0.036
CRYZL2P-SEC16B	117.88	-0.520	0.200	-2.593	0.048
MSLNL	24.06	-0.519	0.187	-2.782	0.033
LRRC53	12.92	-0.518	0.172	-3.014	0.020
-	36.73	-0.518	0.150	-3.443	0.008
SNAP25	26952.11	-0.518	0.158	-3.276	0.012
GLT1D1	432.78	-0.516	0.156	-3.311	0.011
IQCH	15.52	-0.516	0.122	-4.222	0.001
LAMP5	708.43	-0.515	0.155	-3.316	0.011
GPR89P	3.33	-0.515	0.180	-2.855	0.028
AC024601.1	15.92	-0.514	0.169	-3.045	0.019
CNTNAP3P2	19.53	-0.514	0.173	-2.980	0.022
SYPL1P2	7.53	-0.514	0.153	-3.361	0.010
CDNF	13.03	-0.513	0.176	-2.913	0.025
AC135279.2	89.09	-0.513	0.150	-3.430	0.008
AC000403.1	37.26	-0.513	0.154	-3.323	0.011
AL365255.1	5.13	-0.513	0.190	-2.703	0.039
SLC27A2	38.98	-0.513	0.158	-3.239	0.013
GASAL1	8.87	-0.512	0.164	-3.126	0.016
ATP2B3	1061.60	-0.512	0.146	-3.499	0.007
AMPH	1575.32	-0.511	0.158	-3.238	0.013
AL157902.2	3.00	-0.511	0.182	-2.809	0.031
SYCE1	325.79	-0.510	0.125	-4.075	0.002
YWHAZP2	82.83	-0.509	0.152	-3.346	0.010
AC087203.1	6.06	-0.509	0.189	-2.693	0.040
SCN3B	2000.94	-0.508	0.166	-3.061	0.018
REM2	35.07	-0.508	0.131	-3.894	0.003
C11orf87	796.35	-0.508	0.146	-3.474	0.008
LINC00643	121.32	-0.507	0.165	-3.071	0.018

TASP1	95.13	-0.507	0.103	-4.936	0.000
NRG3	293.00	-0.506	0.144	-3.527	0.007
PPM1E	310.22	-0.506	0.152	-3.322	0.011
KRTAP5-10	4.33	-0.506	0.186	-2.724	0.037
NAT16	38.06	-0.506	0.152	-3.318	0.011
LIN28B-AS1	9.23	-0.506	0.150	-3.376	0.009
ADPGK-AS1	26.50	-0.506	0.120	-4.219	0.001
MIR6841	3.92	-0.506	0.167	-3.032	0.020
EID2B	298.87	-0.505	0.087	-5.813	0.000
FREM1	37.79	-0.504	0.155	-3.249	0.012
TDO2	26.38	-0.503	0.179	-2.804	0.032
AC005722.2	13.14	-0.503	0.131	-3.841	0.003
GFRA2	606.24	-0.503	0.161	-3.131	0.016
FAM66A	28.56	-0.503	0.167	-3.014	0.020
KCNK1	637.10	-0.501	0.141	-3.557	0.006
MDH1B	48.75	-0.500	0.130	-3.837	0.003
ORC6	89.02	-0.500	0.122	-4.093	0.002

Table 3.3: Enriched terms in AD up-regulated genes the expression of which is strongly associated ($r > 0.5$, pvalue < 0.05) with Alu RNA processing ratio (gene list). Terms are depicted for KEGG pathways and Gene Ontology Biological Process.

gene list

Gene Name	**correlation**	**pvalue**
MCM7	0.892820369	3.36E-24
MTND2P28	0.887639108	1.43E-23
BAZ1A	0.887340603	1.55E-23
MT-CYB	0.886047348	2.21E-23
MT-ND5	0.885676978	2.44E-23
MT-RNR2	0.884609589	3.24E-23
LPAR1	0.884566455	3.28E-23
AC023389.1	0.884040069	3.77E-23
HIPK2	0.883412632	4.44E-23
DYNC1LI2	0.880707878	8.96E-23
MT-ND6	0.880627722	9.15E-23
KIF5B	0.880272357	1.00E-22
MT-ND1	0.880195806	1.02E-22
ANXA9	0.879987401	1.08E-22
AC026401.3	0.87759973	1.97E-22
KIF1C	0.877300133	2.12E-22
MT-ND4	0.876966349	2.30E-22

MTND1P23	0.875069134	3.67E-22
MT-CO2	0.87462386	4.09E-22
MT-ND2	0.873360532	5.55E-22
MTATP6P1	0.873016985	6.03E-22
AL353743.1	0.872940826	6.14E-22
PKP4	0.872378853	7.02E-22
HIGD1B	0.871949549	7.78E-22
FOXO4	0.870824124	1.01E-21
SMARCC1	0.868547678	1.72E-21
MT-ND3	0.868278865	1.84E-21
FGF1	0.867275539	2.31E-21
PAIP2B	0.867014625	2.45E-21
MT-TP	0.865796411	3.23E-21
MT-ND4L	0.865757943	3.26E-21
FBXW4	0.865155475	3.74E-21
TGFB3	0.864993582	3.87E-21
AC007406.3	0.863872478	4.98E-21
MT-RNR1	0.863035573	5.99E-21
MT-CO3	0.862202328	7.20E-21
SLTM	0.862179355	7.23E-21
CASC3	0.861906023	7.68E-21
MT-TE	0.861674034	8.08E-21
MT-CO1	0.861562542	8.28E-21
NEK7	0.861224052	8.92E-21
C22orf46	0.860756557	9.87E-21
PTP4A2	0.860656493	1.01E-20
MT-TL2	0.860138744	1.13E-20
CPM	0.860088611	1.14E-20
PTH1R	0.860042624	1.15E-20
TNS1	0.858911979	1.47E-20
EBF1	0.857798907	1.86E-20
MTCO1P12	0.857641778	1.92E-20
DENND2A	0.85649664	2.45E-20
ANKRD40	0.85577213	2.85E-20
UPF2	0.855463106	3.04E-20
SLC6A12	0.854857998	3.45E-20
MAP4K4	0.854819668	3.48E-20
ANKRD36B	0.85407751	4.06E-20
LARP7	0.853995046	4.13E-20
CENPB	0.853052441	5.01E-20

SHTN1	0.852979282	5.08E-20
MT-TL1	0.85270365	5.38E-20
MT-TR	0.852078735	6.11E-20
FLT3LG	0.851410597	6.99E-20
AC107375.1	0.851012719	7.58E-20
SASH1	0.850937801	7.69E-20
RAP1A	0.850599432	8.24E-20
PTP4A2P1	0.850301732	8.74E-20
TAF3	0.849467468	1.03E-19
PRR26	0.849163627	1.10E-19
CRTAP	0.848614572	1.22E-19
AC245297.3	0.848289136	1.31E-19
MT-TK	0.848236159	1.32E-19
AC131212.2	0.848123447	1.35E-19
HSPB2	0.847651704	1.48E-19
FCHSD2	0.846862825	1.73E-19
GGTA2P	0.846856923	1.73E-19
AP001350.2	0.846567414	1.83E-19
LRRFIP1P1	0.846138176	1.99E-19
AL365209.1	0.846073472	2.02E-19
AC034102.1	0.84579291	2.13E-19
PINLYP	0.845759314	2.14E-19
ROCK1	0.845464591	2.27E-19
MT-TM	0.844994178	2.49E-19
ZFHX3	0.844977487	2.49E-19
HIP1	0.844923174	2.52E-19
KTN1	0.844553641	2.71E-19
PPP1R14BP3	0.843966292	3.03E-19
BTBD9-AS1	0.843754892	3.16E-19
KANK2	0.843569335	3.27E-19
CHD1	0.843376803	3.39E-19
AC096677.1	0.84321108	3.50E-19
CHD9	0.842847383	3.75E-19
GPR108	0.842809264	3.78E-19
CARHSP1	0.84258463	3.94E-19
GDF11	0.842455387	4.04E-19
ARAP1	0.842174983	4.26E-19
GLTP	0.841968713	4.43E-19
CSPP1	0.841431418	4.91E-19
AC026356.2	0.841405338	4.93E-19

MITF	0.841137518	5.19E-19
MYO1C	0.840813781	5.51E-19
HNRNPH3	0.840065587	6.34E-19
AC097381.3	0.83989911	6.54E-19
BCL7C	0.839829524	6.62E-19
ZBTB47	0.839780446	6.69E-19
TRAK2	0.839729148	6.75E-19
GCK	0.83960652	6.91E-19
TP53INP1	0.839585273	6.93E-19
NT5DC2	0.839497959	7.05E-19
HBP1	0.838663416	8.23E-19
HMG20B	0.838484315	8.50E-19
DAAM2	0.838397371	8.64E-19
RASSF1	0.837992413	9.31E-19
HOOK2	0.837969986	9.35E-19
DNAJC1	0.837287071	1.06E-18
CALD1	0.837140642	1.09E-18
CMTM3	0.836389755	1.25E-18
ANP32B	0.836373734	1.25E-18
FBXL19-AS1	0.836015721	1.34E-18
AL121753.2	0.835673337	1.42E-18
STON1	0.835394211	1.50E-18
AC009779.2	0.835135331	1.57E-18
ADIPOR2	0.834804795	1.66E-18
DEK	0.834541914	1.74E-18
PPFIBP2	0.833850867	1.97E-18
RUNX3	0.833674863	2.04E-18
AL049840.4	0.833405163	2.14E-18
RN7SL589P	0.832761833	2.40E-18
ARRDC2	0.832644787	2.45E-18
WDR20	0.832511817	2.51E-18
CMTM6	0.832374372	2.57E-18
NIFK-AS1	0.832250771	2.63E-18
ADAM33	0.831963948	2.76E-18
SNRNP48	0.831653292	2.92E-18
TGFB1	0.831347542	3.08E-18
CDK11B	0.831166775	3.18E-18
FOXC2	0.830730653	3.43E-18
ITPRID2	0.830461701	3.60E-18
PGF	0.830262452	3.73E-18

CEP112	0.830152304	3.80E-18
KLHL5	0.829967545	3.92E-18
LINC00511	0.829824805	4.02E-18
AC022146.2	0.829675822	4.13E-18
RN7SL744P	0.829094294	4.57E-18
TCF7L1	0.829049201	4.60E-18
MAPKAPK2	0.829041316	4.61E-18
GALM	0.828921707	4.71E-18
UPF3AP3	0.828783262	4.82E-18
ZEB2	0.828526205	5.04E-18
TNS2	0.828294372	5.24E-18
ANAPC16	0.82805884	5.46E-18
RASSF2	0.827827886	5.68E-18
AL590093.1	0.827522	5.99E-18
AC008895.1	0.8270242	6.52E-18
CREBBP	0.826245898	7.45E-18
N4BP2L2-IT2	0.825917113	7.88E-18
MECOM	0.825900218	7.90E-18
RBM17	0.825893153	7.91E-18
MT-ATP8	0.825678723	8.21E-18
CRK	0.825530007	8.42E-18
KRCC1	0.8253944	8.61E-18
UBXN7	0.825365568	8.66E-18
PPIC	0.825232678	8.85E-18
ARL5A	0.825175417	8.94E-18
VASH1	0.825156991	8.97E-18
TRIM56	0.824703354	9.68E-18
RP9	0.824674884	9.73E-18
MTF1	0.824613902	9.83E-18
ZNF768	0.824161174	1.06E-17
AC004951.1	0.824114913	1.07E-17
MINDY1	0.823973966	1.09E-17
PDGFRB	0.823626931	1.16E-17
POGK	0.823546367	1.18E-17
CAVIN1	0.823433155	1.20E-17
SMIM3	0.823406227	1.20E-17
RPS19P3	0.823342466	1.22E-17
TBC1D2B	0.823128775	1.26E-17
ITGB1	0.822905102	1.31E-17
AC145285.3	0.822737278	1.35E-17

SNORD17	0.822661406	1.36E-17
AATF	0.822558786	1.39E-17
STK38	0.822453036	1.41E-17
CEP104	0.822237587	1.46E-17
SOX6	0.821855747	1.56E-17
KIF13A	0.821812506	1.57E-17
RF00017	0.821676431	1.61E-17
AL136295.6	0.821588194	1.63E-17
GKAP1	0.821382404	1.69E-17
CCDC69	0.821317159	1.70E-17
ASCC1	0.821171877	1.75E-17
HMBOX1	0.820941045	1.81E-17
CSK	0.820624678	1.91E-17
WNK1	0.820549334	1.93E-17
BCAM	0.820491453	1.95E-17
ISYNA1	0.820386233	1.99E-17
ZNF609	0.820309332	2.01E-17
MITD1	0.820289422	2.02E-17
AC006547.1	0.820153438	2.06E-17
AC058791.1	0.820007179	2.11E-17
MPRIP-AS1	0.819979374	2.12E-17
FOXF2	0.819972874	2.13E-17
AL445363.3	0.819913801	2.15E-17
AC026979.4	0.819715253	2.22E-17
SAMD1	0.819372085	2.35E-17
MAFK	0.819305438	2.37E-17
AC122718.1	0.819063614	2.47E-17
ANXA2R	0.819056795	2.47E-17
AC087284.1	0.818893461	2.54E-17
SGPL1	0.81883555	2.56E-17
SREK1	0.818786046	2.58E-17
NIPBL	0.818764874	2.59E-17
AC016245.1	0.818758428	2.59E-17
HS1BP3	0.818679174	2.63E-17
SOCS4	0.818487464	2.71E-17
YES1	0.818443888	2.73E-17
CLDN15	0.818391246	2.75E-17
UPF3A	0.818365735	2.76E-17
MSRB3	0.818298215	2.79E-17
PSG8-AS1	0.818013387	2.92E-17

YBX1P1	0.817865553	3.00E-17
FXYD5	0.817730663	3.06E-17
NES	0.817671476	3.09E-17
GNA12	0.817592648	3.13E-17
TBX6	0.817127442	3.37E-17
CPNE2	0.817103025	3.39E-17
AC090198.1	0.816644514	3.65E-17
PCBP1-AS1	0.816480633	3.74E-17
PHF10	0.816443195	3.77E-17
TCF4	0.816379175	3.81E-17
SNAP23	0.816260475	3.88E-17
LINC00320	0.816154242	3.95E-17
CREBRF	0.816062417	4.00E-17
ATXN1L	0.815969775	4.06E-17
MAP3K11	0.815686995	4.25E-17
EEF1D	0.815647981	4.28E-17
RAB3IL1	0.815630034	4.29E-17
RFC1	0.815367587	4.47E-17
AL928654.4	0.815069211	4.69E-17
DOCK6	0.815050049	4.70E-17
RILPL2	0.814735331	4.95E-17
RP9P	0.814511456	5.12E-17
AC122129.1	0.814357224	5.25E-17
RHOG	0.814136266	5.44E-17
CHST6	0.814000002	5.56E-17
C2orf68	0.813925069	5.62E-17
SLC12A7	0.813867699	5.67E-17
ERBIN	0.813722501	5.81E-17
HSP90AB4P	0.813513433	6.00E-17
MAN2B1	0.813511638	6.00E-17
YBX1P2	0.813419572	6.09E-17
MCPH1-AS1	0.813304256	6.20E-17
ESAM	0.813267092	6.24E-17
AL357078.1	0.813264137	6.24E-17
ZSWIM7	0.813087016	6.42E-17
ZNF621	0.812657042	6.86E-17
FAM129B	0.812586389	6.94E-17
TMEM120A	0.8124435	7.10E-17
JADE3	0.812398525	7.15E-17
MICALL1	0.812329262	7.23E-17

PRELP	0.812271665	7.29E-17
PGPEP1	0.81195162	7.67E-17
LYAR	0.81182611	7.82E-17
AL358154.1	0.811712253	7.96E-17
MTATP8P2	0.811196495	8.62E-17
AL356258.1	0.811088066	8.77E-17
TMEM219	0.810872203	9.07E-17
ZNF618	0.810756344	9.23E-17
SLC16A4	0.810250365	9.98E-17
RF00019	0.810180856	1.01E-16
AC027279.1	0.810180305	1.01E-16
BRD7	0.810159902	1.01E-16
COBL	0.809971364	1.04E-16
GJC1	0.809902338	1.05E-16
REST	0.809591687	1.11E-16
AL355338.1	0.809566971	1.11E-16
CYSTM1	0.809535146	1.11E-16
ABL1	0.809331252	1.15E-16
EFCAB2	0.809225246	1.17E-16
SYS1	0.809086554	1.19E-16
MAK	0.808857935	1.24E-16
SLC35E3	0.808827329	1.24E-16
FAM107B	0.808808476	1.25E-16
KCTD11	0.808554084	1.30E-16
HEY2	0.80844727	1.32E-16
ZNF845	0.808158502	1.38E-16
DOCK1	0.807955948	1.42E-16
EPB41L2	0.807570206	1.51E-16
AL136164.3	0.80747098	1.53E-16
STX2	0.807064722	1.63E-16
GAB2	0.807030026	1.63E-16
VSTM4	0.806837119	1.68E-16
PREX1	0.806733257	1.71E-16
WDR59	0.806588228	1.75E-16
BAZ1B	0.806433418	1.79E-16
AC022149.1	0.806001038	1.91E-16
RRAS	0.805792414	1.97E-16
AEN	0.805676591	2.00E-16
AC130448.1	0.805555524	2.04E-16
THOC2	0.805325555	2.11E-16

AL357055.3	0.805304267	2.12E-16
SNX6	0.805262567	2.13E-16
SNX33	0.805096827	2.19E-16
TMEM216	0.805093699	2.19E-16
GIMAP5	0.804998547	2.22E-16
ITIH5	0.804993122	2.22E-16
MAP3K20	0.804970887	2.23E-16
CTBP2	0.804746251	2.31E-16
AL031587.5	0.804585067	2.36E-16
PCOLCE	0.804560741	2.37E-16
GPSM2	0.804356387	2.44E-16
AC099778.1	0.804165704	2.51E-16
DFFA	0.804154882	2.52E-16
MXD4	0.804055897	2.56E-16
PIP4K2A	0.803830277	2.64E-16
ASCL1	0.803743465	2.68E-16
SCUBE3	0.803644448	2.72E-16
AUP1	0.803443808	2.80E-16
PHF21A	0.803268535	2.87E-16
CARD6	0.803209535	2.90E-16
NFIA	0.803208619	2.90E-16
PRKX	0.803190107	2.91E-16
MID1IP1	0.803090925	2.95E-16
AC006449.6	0.802799536	3.08E-16
ALOX12-AS1	0.802657876	3.14E-16
ECE1	0.802330782	3.30E-16
AC005034.3	0.802224665	3.35E-16
ARHGAP22	0.801952295	3.49E-16
VAT1	0.801830174	3.55E-16
MTSS1L	0.801821214	3.56E-16
AC018557.2	0.801616761	3.67E-16
ARHGEF37	0.801512213	3.72E-16
MT-TF	0.801462792	3.75E-16
AC011477.1	0.801364051	3.81E-16
SLC43A3	0.801357968	3.81E-16
CYB561A3	0.801163268	3.92E-16
POLR2H	0.801120305	3.94E-16
ZFP91	0.800843022	4.11E-16
SERPINB6	0.800801492	4.13E-16
RIPOR3	0.800794578	4.14E-16

FOXD1	0.800700665	4.19E-16
KCNMA1-AS1	0.800685915	4.20E-16
CERS4	0.800682758	4.20E-16
AC005332.6	0.800653065	4.22E-16
ASLP1	0.800518094	4.31E-16
SWAP70	0.800508897	4.31E-16
ORAI1	0.800481951	4.33E-16
WWC3	0.800349119	4.41E-16
ARHGAP29	0.80025218	4.48E-16
GPS2	0.800251327	4.48E-16
XKR8	0.800219185	4.50E-16
MYO10	0.800141562	4.55E-16
ENTPD3-AS1	0.800109408	4.57E-16
POLDIP3	0.800032644	4.62E-16
ZBTB12	0.799932421	4.69E-16
EGFL8	0.799890106	4.72E-16
UIMC1	0.799743471	4.82E-16
ANXA5	0.799636244	4.90E-16
PERP	0.799634347	4.90E-16
TRIM41	0.799515717	4.98E-16
AC023509.3	0.799514402	4.98E-16
KRI1	0.799347102	5.11E-16
NFIB	0.799255494	5.18E-16
ERGIC1	0.799251146	5.18E-16
CHMP4A	0.799239881	5.19E-16
TINAGL1	0.799222664	5.20E-16
PECAM1	0.799119534	5.28E-16
FAM107A	0.799072499	5.31E-16
SIPA1	0.798893644	5.45E-16
COLGALT1	0.79882952	5.51E-16
DOCK5	0.798579782	5.71E-16
AC105942.1	0.798532456	5.75E-16
ZNF24	0.798430925	5.83E-16
ADCY10P1	0.798421011	5.84E-16
SPACA6	0.798384166	5.87E-16
TJP1	0.798358938	5.89E-16
GAREM2	0.798342625	5.91E-16
AC032044.1	0.798263225	5.97E-16
TSSK4	0.798261996	5.98E-16
SYNGR2	0.798255739	5.98E-16

SIM2	0.798141094	6.08E-16
DENND5A	0.798122487	6.10E-16
UNC5B	0.797958058	6.24E-16
KAT6B	0.797938103	6.26E-16
TRIP4	0.797897033	6.30E-16
DOK1	0.797518322	6.65E-16
AC100788.2	0.79749095	6.68E-16
MTATP8P1	0.797442817	6.72E-16
AC006387.1	0.797248158	6.91E-16
RFTN2	0.797118462	7.04E-16
TBC1D14	0.796973241	7.19E-16
ZNF32	0.796936683	7.23E-16
UNC119B	0.796692151	7.49E-16
AC005089.1	0.796654782	7.53E-16
CDK18	0.796582141	7.60E-16
AC243654.3	0.796576779	7.61E-16
AC120114.3	0.796418345	7.78E-16
ERMN	0.79636049	7.85E-16
GNA11	0.796107618	8.14E-16
ITGA5	0.796090719	8.16E-16
CCP110	0.795983202	8.28E-16
TEAD2	0.795958092	8.31E-16
UCK1	0.795916453	8.36E-16
PALD1	0.795866884	8.42E-16
AC022150.4	0.795665283	8.67E-16
VEGFB	0.79557968	8.77E-16
ZNF765	0.795491886	8.88E-16
HMGN5	0.795392288	9.01E-16
TNIP1	0.795319398	9.10E-16
ACTL6A	0.795224593	9.23E-16
SYNM	0.795200844	9.26E-16
FAM151A	0.795159601	9.31E-16
OLIG1	0.79508551	9.41E-16
RALBP1	0.795024786	9.49E-16
LINC01560	0.794912515	9.64E-16
PANTR1	0.794863639	9.71E-16
MT-TT	0.794847027	9.73E-16
DLC1	0.794771144	9.84E-16
PRPF38B	0.79474384	9.88E-16
TMEM204	0.794705664	9.93E-16

ARHGAP17	0.794587221	1.01E-15
NDRG1	0.794581302	1.01E-15
GIMAP2	0.794505433	1.02E-15
GNG7	0.794410632	1.04E-15
AL035413.2	0.794155001	1.07E-15
RHBDL2	0.794095545	1.08E-15
AC005828.4	0.79405506	1.09E-15
MOB3B	0.793697233	1.14E-15
RRP8	0.793425317	1.19E-15
HOMER3	0.793257494	1.22E-15
UBTD2	0.793171022	1.23E-15
YBX1P10	0.793131197	1.24E-15
SIRT1	0.793038003	1.26E-15
AL157396.1	0.792988345	1.26E-15
FOXP1-IT1	0.792772834	1.30E-15
AIMP1P1	0.792732417	1.31E-15
USP54	0.792578352	1.34E-15
CARD8-AS1	0.792551346	1.34E-15
HDAC1	0.792439683	1.37E-15
CHD7	0.792284758	1.40E-15
CHD4	0.792276196	1.40E-15
EHMT1	0.792209169	1.41E-15
KNOP1	0.792163043	1.42E-15
AC116667.1	0.792037368	1.44E-15
ZDHHC20-IT1	0.792036422	1.44E-15
KAT2B	0.791949141	1.46E-15
SPAG9	0.79184883	1.48E-15
AC016716.2	0.791704729	1.51E-15
MALAT1	0.791672123	1.52E-15
ATP11C	0.791618905	1.53E-15
RBM6	0.791583142	1.54E-15
PTPN21	0.791475225	1.56E-15
AC004000.1	0.791469632	1.56E-15
MAPRE1	0.7913908	1.58E-15
ZKSCAN2-DT	0.791291464	1.60E-15
AC141586.4	0.791201772	1.62E-15
NFATC3	0.79098511	1.67E-15
CHDH	0.790801594	1.71E-15
PSKH1	0.790611337	1.76E-15
AC016722.2	0.790509372	1.79E-15

AC006042.3	0.790501877	1.79E-15
RDX	0.790166568	1.87E-15
AP000769.1	0.79012077	1.88E-15
SHROOM4	0.790116005	1.88E-15
RASSF8	0.789937631	1.93E-15
AC093909.6	0.789798298	1.97E-15
CALCOCO2	0.789382002	2.09E-15
HNRNPA3P10	0.789372586	2.09E-15
AC016027.2	0.789296318	2.11E-15
CTDSP2	0.789181648	2.14E-15
Z69666.1	0.789155779	2.15E-15
AC131009.4	0.789128653	2.16E-15
RASGRP3	0.789127028	2.16E-15
AC005332.5	0.788933235	2.22E-15
MOB3A	0.788780473	2.26E-15
NFATC2	0.788716943	2.28E-15
RABGAP1L-IT1	0.788564236	2.33E-15
Z97989.1	0.788493449	2.36E-15
ZHX1	0.788486044	2.36E-15
N4BP2	0.788027404	2.51E-15
CGNL1	0.788014868	2.51E-15
HSBP1L1	0.78796704	2.53E-15
GOLGA4	0.787947783	2.54E-15
LAMB2	0.787793853	2.59E-15
MYOT	0.787760476	2.60E-15
EBF4	0.787680707	2.63E-15
AL512306.2	0.787670822	2.63E-15
RHOJ	0.787635692	2.65E-15
EDA2R	0.787501095	2.70E-15
ZCCHC24	0.787432215	2.72E-15
ZSWIM9	0.7873143	2.77E-15
GPER1	0.787304833	2.77E-15
MT-ATP6	0.787130412	2.84E-15
AL355490.2	0.78702583	2.88E-15
TOR4A	0.787003784	2.88E-15
MRPS5	0.786976325	2.90E-15
CEP350	0.786792541	2.97E-15
COG8	0.786753333	2.98E-15
FYCO1	0.786660846	3.02E-15
AC023024.1	0.786629351	3.03E-15

DLG5	0.786580378	3.05E-15
TRIP10	0.786540908	3.07E-15
AC093278.2	0.786531899	3.08E-15
GAB1	0.786341046	3.16E-15
ABHD15	0.786192642	3.22E-15
Z97634.1	0.786121451	3.25E-15
BOK	0.786054577	3.28E-15
PAK2	0.785870377	3.36E-15
SGK1	0.78570094	3.44E-15
PLEKHB1	0.785618383	3.48E-15
SLC44A1	0.785589881	3.49E-15
AC083964.1	0.78545221	3.56E-15
EFNB1	0.785348737	3.61E-15
ZBTB34	0.785339332	3.61E-15
DISC1	0.785193951	3.68E-15
BACH1	0.785032121	3.76E-15
PURA	0.784894235	3.83E-15
ANLN	0.784839108	3.86E-15
AC092279.2	0.784795472	3.89E-15
AC005776.1	0.784787353	3.89E-15
ZNF322	0.784616611	3.98E-15
DAP	0.784576857	4.00E-15
LINC01094	0.78451667	4.03E-15
UBE2R2-AS1	0.78445212	4.07E-15
USP24	0.784446009	4.07E-15
AL136164.4	0.78442303	4.08E-15
CXXC1	0.784353777	4.12E-15
LINC01232	0.784208165	4.20E-15
CTDNEP1	0.784086628	4.27E-15
AC010319.4	0.784038577	4.30E-15
VPS54	0.783985124	4.33E-15
AC024267.3	0.78397684	4.33E-15
ELK3	0.783928944	4.36E-15
SMC1A	0.783903534	4.38E-15
GSN	0.783823232	4.42E-15
AC016705.1	0.783668437	4.52E-15
AIF1L	0.783665538	4.52E-15
TBL1X	0.783624779	4.54E-15
BTBD7	0.783550547	4.59E-15
SRARP	0.783441771	4.65E-15

EDC3	0.783355174	4.71E-15
AP000350.2	0.783177662	4.82E-15
AVEN	0.783141923	4.84E-15
PLXNB1	0.782854909	5.03E-15
AC007390.2	0.782694257	5.14E-15
LHPP	0.782662878	5.16E-15
ECI1	0.782551941	5.24E-15
DSTNP2	0.782525868	5.26E-15
MTUS1	0.782500632	5.27E-15
CNKSR3	0.782424585	5.33E-15
NKX6-1	0.782392087	5.35E-15
MGAT1	0.782391208	5.35E-15
CLK1	0.782261834	5.44E-15
MGLL	0.78220274	5.49E-15
TMEM273	0.782083647	5.57E-15
ROM1	0.781959361	5.67E-15
RBL1	0.781775264	5.80E-15
PROB1	0.781703002	5.86E-15
DBI	0.781662717	5.89E-15
P2RY14	0.781650304	5.90E-15
AC127459.1	0.781609504	5.93E-15
GYPC	0.781582869	5.95E-15
IL27RA	0.781532909	5.99E-15
AC006330.1	0.781399704	6.10E-15
METAP2	0.781371653	6.12E-15
FCGRT	0.781073885	6.37E-15
VAMP3	0.781039817	6.40E-15
CDKN2C	0.780884969	6.53E-15
GTF2IP4	0.780537628	6.83E-15
EMP2	0.780533134	6.83E-15
AC127070.4	0.780499911	6.86E-15
CERS2	0.780193059	7.15E-15
CPQ	0.780129414	7.21E-15
NOTCH3	0.780103544	7.23E-15
FZD9	0.780020816	7.31E-15
C12orf65	0.780005451	7.32E-15
SCAMP2	0.780003197	7.33E-15
CDK11A	0.77992186	7.40E-15
RGL2	0.779777438	7.54E-15
DAXX	0.779726893	7.59E-15

ATOH8	0.779638074	7.68E-15
TMCC3	0.779489106	7.83E-15
RHBDF1	0.779435302	7.89E-15
EMX2	0.779379588	7.95E-15
RUFY1	0.77936908	7.96E-15
BBX	0.779367438	7.96E-15
AC009509.4	0.779362994	7.96E-15
DNMT1	0.779356702	7.97E-15
WAPL	0.779351852	7.98E-15
AC019227.1	0.779142623	8.20E-15
SP1	0.779004491	8.34E-15
MAVS	0.778943588	8.41E-15
NR2F2-AS1	0.778777611	8.59E-15
ZNF704	0.778654406	8.73E-15
PIGM	0.778602899	8.79E-15
ASAP1-IT2	0.778557089	8.84E-15
SIGIRR	0.778459629	8.96E-15
QKI	0.778455455	8.96E-15
RENBP	0.778444131	8.97E-15
AC069281.2	0.778443925	8.97E-15
AC007683.1	0.778443362	8.97E-15
8-Mar	0.778208442	9.25E-15
PPP4R3A	0.777914227	9.61E-15
PHLPP1	0.777837269	9.71E-15
EVA1B	0.777783863	9.77E-15
ZNF565	0.777765617	9.80E-15
KIAA1147	0.777749619	9.82E-15
SYNJ2	0.777742666	9.83E-15
AC016027.3	0.777677706	9.91E-15
MTMR10	0.777385727	1.03E-14
RBM38	0.777280772	1.04E-14
OTUD7B	0.777167395	1.06E-14
AL731532.2	0.777076	1.07E-14
TMX1	0.777035591	1.08E-14
PRKCH	0.776773378	1.11E-14
TNS3	0.776686389	1.13E-14
CDK19	0.776638264	1.13E-14
AZGP1	0.776627633	1.13E-14
ITGB5	0.776583808	1.14E-14
RXRA	0.776488404	1.15E-14

CDK2AP1	0.776483779	1.16E-14
EMP3	0.776402946	1.17E-14
LRRC58	0.776215751	1.20E-14
RAPGEF3	0.776190863	1.20E-14
BRD3	0.776146186	1.21E-14
AL136380.1	0.775993344	1.23E-14
PTPN11	0.775927931	1.24E-14
RIN3	0.775911898	1.24E-14
EDA	0.775842505	1.25E-14
ADAM10	0.77580262	1.26E-14
SMO	0.775781556	1.26E-14
LHFPL2	0.775670734	1.28E-14
SH3BP4	0.775639306	1.29E-14
SOS 2	0.775565956	1.30E-14
AC139792.1	0.775343624	1.34E-14
PHF2	0.775218956	1.36E-14
URI1	0.775206758	1.36E-14
RAB29	0.775129535	1.37E-14
RPS6KA1	0.774942737	1.41E-14
MAX	0.774849716	1.42E-14
DLGAP1-AS1	0.774758749	1.44E-14
HDGF	0.774587591	1.47E-14
POLD1	0.774556574	1.48E-14
PIAS4	0.774538457	1.48E-14
BMP1	0.774523107	1.48E-14
ILK	0.774470558	1.49E-14
RNF24	0.774372486	1.51E-14
GPSM3	0.774266275	1.53E-14
SKA2	0.774232437	1.54E-14
NOTCH4	0.77421516	1.54E-14
MOB3C	0.774156952	1.55E-14
AC105052.4	0.774122306	1.56E-14
NBPF10	0.774100235	1.57E-14
ZNF528-AS1	0.774051606	1.58E-14
OLMALINC	0.774018054	1.58E-14
MORC4	0.773907259	1.60E-14
SERTAD3	0.773886266	1.61E-14
AC013472.1	0.773631469	1.66E-14
IRF2BP2	0.77352833	1.68E-14
EFCAB14	0.773448151	1.70E-14

POU3F3	0.773444767	1.70E-14
SEPHS1	0.773396499	1.71E-14
MYO1E	0.773307415	1.73E-14
RPL17P50	0.773016196	1.80E-14
TTC23	0.772868869	1.83E-14
AL158068.2	0.772847347	1.83E-14
PARD3B	0.772738507	1.86E-14
AC005776.2	0.772719718	1.86E-14
YBX1	0.772625847	1.89E-14
ZNF438	0.772427518	1.93E-14
PHF19	0.772406164	1.94E-14
CSAG1	0.772397183	1.94E-14
TFAP2A	0.772373849	1.95E-14
TGIF2	0.772360152	1.95E-14
FAM89A	0.772323813	1.96E-14
MVB12B	0.77225863	1.98E-14
ZSWIM1	0.772045977	2.03E-14
Z95331.1	0.771998116	2.04E-14
ZNF664	0.77190028	2.07E-14
MFNG	0.771859765	2.08E-14
DIP2B	0.771826343	2.09E-14
SYDE1	0.771760183	2.10E-14
PLXDC2	0.771682797	2.12E-14
ZHX2	0.771677351	2.13E-14
AC010335.3	0.771667363	2.13E-14
SMOX	0.771616975	2.14E-14
MDM2	0.771590203	2.15E-14
HNRNPCP1	0.771480187	2.18E-14
FOXD2-AS1	0.771474661	2.18E-14
ARHGEF40	0.771311364	2.22E-14
KCNK6	0.77130131	2.23E-14
SWSAP1	0.77121614	2.25E-14
DDB2	0.771163353	2.27E-14
ARHGAP31	0.771105131	2.28E-14
TGFB1I1	0.771045647	2.30E-14
RNPEPL1	0.77095641	2.33E-14
ST5	0.770935306	2.33E-14
AC004491.1	0.770795866	2.37E-14
PRKD2	0.7706549	2.41E-14
LINC00997	0.770630265	2.42E-14

TXLNA	0.7706005	2.43E-14
SELENON	0.770583076	2.44E-14
AC132192.2	0.770556927	2.44E-14
FTSJ3	0.770481176	2.47E-14
SHROOM1	0.770397994	2.49E-14
AC009120.1	0.770379903	2.50E-14
NPC1	0.770285319	2.53E-14
AC005086.2	0.770219372	2.55E-14
G3BP1	0.770167781	2.57E-14
SLC4A2	0.770160086	2.57E-14
HEATR5A	0.770145067	2.57E-14
APPL2	0.769990871	2.62E-14
DDAH2	0.769941285	2.64E-14
SOX12	0.769837913	2.67E-14
SALL1	0.769600451	2.75E-14
PARP4	0.769590234	2.76E-14
LEF1	0.769570685	2.76E-14
AF131215.6	0.769556115	2.77E-14
SNRNP35	0.76946392	2.80E-14
ARL6IP6	0.769415748	2.82E-14
ERC2-IT1	0.769407998	2.82E-14
MYBPC1	0.769394426	2.82E-14
PLPP2	0.769127358	2.92E-14
RORA	0.769010558	2.96E-14
FAM53B	0.768826944	3.03E-14
VASP	0.76879347	3.04E-14
AC026979.1	0.768759095	3.05E-14
SPOUT1	0.768673171	3.09E-14
GIMAP4	0.768661703	3.09E-14
GUCD1	0.768438399	3.18E-14
ITPKB	0.768319798	3.22E-14
MLLT6	0.768310809	3.23E-14
ERBB3	0.768147081	3.29E-14
ZNF740	0.767928785	3.38E-14
ABTB2	0.767912771	3.39E-14
SLC38A11	0.767859744	3.41E-14
NBPF25P	0.767709301	3.48E-14
PELI2	0.76768803	3.49E-14
GIMAP6	0.767634401	3.51E-14
TCEA3	0.767588162	3.53E-14

PPM1N	0.767529163	3.55E-14
MED13	0.767424866	3.60E-14
FZD2	0.767394678	3.61E-14
B4GALT2	0.767383863	3.62E-14
AL359183.1	0.767379101	3.62E-14
RIN2	0.767377029	3.62E-14
SOX13	0.76713296	3.73E-14
UFD1	0.766405337	4.08E-14
MOB1A	0.766304004	4.13E-14
KHNYN	0.766213833	4.17E-14
MPST	0.766173245	4.19E-14
PTMAP2	0.7661552	4.20E-14
AC093726.2	0.765977155	4.30E-14
RAI14	0.765975478	4.30E-14
UBAC1	0.765830729	4.37E-14
AC092068.3	0.765807037	4.39E-14
FEM1A	0.765787915	4.40E-14
MT-TA	0.765698179	4.44E-14
ZBTB40	0.765686224	4.45E-14
CAB39L	0.765525357	4.54E-14
PLPP1	0.765517406	4.54E-14
CSPG4	0.765458753	4.58E-14
MGA	0.765382974	4.62E-14
AC010618.3	0.765367935	4.63E-14
AC093535.1	0.765183775	4.73E-14
NR1H3	0.765112536	4.77E-14
PPP1R18	0.765100172	4.78E-14
IRS3P	0.765013757	4.83E-14
VEZF1	0.76494886	4.87E-14
SYNCRIP	0.764790481	4.96E-14
IRF2	0.764677657	5.03E-14
BNIP2	0.764658158	5.04E-14
ZCCHC8	0.764515109	5.13E-14
MCRIP2	0.764265954	5.29E-14
FAM111A	0.764185515	5.34E-14
TNRC6C-AS1	0.76405329	5.42E-14
NR2F1	0.763950197	5.49E-14
LOXL3	0.763940927	5.50E-14
SAFB2	0.763842237	5.56E-14
NFYA	0.763839851	5.56E-14

FANCE	0.763742004	5.63E-14
SLCO3A1	0.763570658	5.75E-14
MTCO1P40	0.763498157	5.80E-14
FGFR1	0.763467574	5.82E-14
LIX1L	0.76344992	5.83E-14
PPP4R2	0.763416651	5.86E-14
PARVA	0.763414137	5.86E-14
DST	0.763403106	5.86E-14
RNF135	0.763378219	5.88E-14
RN7SL689P	0.763356542	5.90E-14
SUFU	0.763267007	5.96E-14
FAM118B	0.763231203	5.99E-14
AC020917.3	0.763228295	5.99E-14
AC245297.2	0.763072435	6.10E-14
PLEKHM2	0.763069259	6.10E-14
AC084036.1	0.762964397	6.18E-14
MEX3C	0.762927086	6.21E-14
SOX10	0.762882837	6.24E-14
NPRL3	0.762863562	6.26E-14
SLC9A3R2	0.76283972	6.28E-14
GAS2L1	0.762828743	6.28E-14
DDX39A	0.762817622	6.29E-14
TSPO	0.762776525	6.32E-14
LATS2	0.762648879	6.42E-14
MAML1	0.762645139	6.42E-14
TAF4	0.762618795	6.44E-14
NKD1	0.762528857	6.51E-14
ZMYND8	0.762493296	6.54E-14
IKBKB	0.762473794	6.56E-14
NEBL	0.762325124	6.67E-14
CCDC97	0.762204068	6.77E-14
COL6A2	0.762169069	6.80E-14
USP40	0.762085769	6.87E-14
PIEZO1	0.762017841	6.92E-14
AL662907.2	0.761870783	7.05E-14
BCL2	0.761870192	7.05E-14
FAM84B	0.761807261	7.10E-14
GRAP	0.761759541	7.14E-14
NFKB1	0.761743264	7.15E-14
COPZ2	0.761660436	7.22E-14

BRI3	0.761589231	7.29E-14
MKLN1-AS	0.761545938	7.32E-14
-	0.761449316	7.41E-14
AC010335.2	0.761357075	7.49E-14
TP53TG1	0.761293689	7.55E-14
INTS13	0.761279537	7.56E-14
AC006441.1	0.761269852	7.57E-14
FGD6	0.761207845	7.62E-14
AL157829.1	0.761186054	7.64E-14
CHST9	0.761048616	7.77E-14
CDK6	0.761013653	7.80E-14
AC103810.5	0.760872095	7.93E-14
LRP5	0.760775704	8.03E-14
TNFRSF10D	0.76063388	8.16E-14
ZNF853	0.76061922	8.18E-14
NCKAP5L	0.760497115	8.30E-14
AC009118.3	0.760433242	8.36E-14
RARG	0.760428384	8.36E-14
IQGAP1	0.760295928	8.50E-14
AC131571.1	0.760081644	8.71E-14
INPPL1	0.760059042	8.74E-14
GNG12	0.760012805	8.79E-14
C3orf62	0.759952854	8.85E-14
NKX2-2	0.759885259	8.92E-14
CD151	0.75985938	8.95E-14
PAWR	0.759766306	9.04E-14
PLCE1	0.759753342	9.06E-14
LINC01561	0.759638776	9.18E-14
NFKBIB	0.759566965	9.26E-14
CNNM3	0.75936588	9.48E-14
NFIC	0.759334086	9.52E-14
ZNF439	0.759312966	9.54E-14
SLC16A1-AS1	0.759227196	9.64E-14
EFNA4	0.759165825	9.71E-14
SLC35E1	0.759131133	9.75E-14
FBXO17	0.759020363	9.88E-14
NRG2	0.758991178	9.91E-14
MYO9B	0.758778363	1.02E-13
TRIM21	0.758735677	1.02E-13
AL135960.1	0.758579974	1.04E-13

CAVIN4	0.758574566	1.04E-13
AL590705.3	0.758512922	1.05E-13
AF127577.4	0.758335626	1.07E-13
OLFML1	0.758324103	1.07E-13
AC134407.2	0.758006264	1.11E-13
NPIPB6	0.757859317	1.13E-13
PCED1A	0.757774908	1.14E-13
ATG4C	0.757680612	1.16E-13
CHST14	0.757674162	1.16E-13
AC073349.2	0.757668372	1.16E-13
USF2	0.757609823	1.17E-13
SGMS1	0.757583431	1.17E-13
ALAD	0.757511951	1.18E-13
ARID3A	0.757459416	1.19E-13
SETD2	0.757458393	1.19E-13
AC006001.3	0.757397361	1.19E-13
AC092117.2	0.757363398	1.20E-13
PPP1R14BP2	0.757332988	1.20E-13
PLCB3	0.757301596	1.21E-13
SMTN	0.757191642	1.22E-13
WWC1	0.757122697	1.23E-13
AL512383.1	0.756980292	1.25E-13
ARHGAP10	0.756786861	1.28E-13
KANK1	0.756760972	1.29E-13
HMGXB4	0.756653839	1.30E-13
POU3F2	0.756623988	1.31E-13
WDFY2	0.756619505	1.31E-13
SEC22C	0.756586602	1.31E-13
AC244669.1	0.756526969	1.32E-13
MTCO3P12	0.756430331	1.34E-13
PKN1	0.756416238	1.34E-13
ZNF611	0.756363269	1.35E-13
BGN	0.756339229	1.35E-13
RAB41	0.756298511	1.36E-13
CDA	0.756217641	1.37E-13
FLT4	0.756142035	1.38E-13
TK2	0.756125965	1.38E-13
MUTYH	0.756108701	1.39E-13
SLC25A53	0.756000408	1.41E-13
ZFP36L1	0.755931151	1.42E-13

AL031658.1	0.755929034	1.42E-13
TMCO3	0.755903157	1.42E-13
SOX2	0.755871636	1.43E-13
F10	0.755827292	1.43E-13
DLG1	0.755768906	1.44E-13
LRRC32	0.755758472	1.45E-13
CHRAC1	0.755755857	1.45E-13
AC015813.6	0.755651848	1.46E-13
PRX	0.755632982	1.47E-13
CCDC159	0.755396369	1.51E-13
FKBP10	0.755368328	1.51E-13
ZSCAN16-AS1	0.755328402	1.52E-13
AC104333.3	0.755226905	1.54E-13
NFAM1	0.755141945	1.55E-13
LCAT	0.75502718	1.57E-13
AIFM3	0.754937905	1.59E-13
ZIC2	0.754916862	1.59E-13
RAB3IP	0.754738873	1.63E-13
MIR3609	0.754734286	1.63E-13
KIF13B	0.754693353	1.63E-13
ZNF577	0.754664916	1.64E-13
AC015909.3	0.754539357	1.66E-13
AC245884.9	0.754497255	1.67E-13
TLN1	0.754476921	1.68E-13
IRAK3	0.754461609	1.68E-13
ITPRIPL2	0.754386866	1.69E-13
SLC52A3	0.754073137	1.76E-13
EZR	0.75406157	1.76E-13
MT-TN	0.753966693	1.78E-13
MAPKAP1	0.753902108	1.79E-13
SP100	0.753835677	1.80E-13
DMPK	0.753577614	1.86E-13
EHD2	0.753461506	1.88E-13
YIPF4	0.753418098	1.89E-13
ASXL2	0.753379021	1.90E-13
FGR	0.753374653	1.90E-13
RPS20P33	0.753353591	1.91E-13
PLIN3	0.753306264	1.92E-13
SPTSSA	0.753210215	1.94E-13
TNFRSF10B	0.753116408	1.96E-13

C15orf39	0.75311331	1.96E-13
HTR1DP1	0.753113146	1.96E-13
TRAF7	0.753023329	1.98E-13
MAP3K1	0.752992035	1.99E-13
RF00019	0.752897419	2.01E-13
AC093535.2	0.752886758	2.01E-13
ELF1	0.752734922	2.05E-13
GIGYF2	0.752590911	2.08E-13
TAPT1	0.752540476	2.09E-13
PHETA1	0.752433575	2.12E-13
HNRNPM	0.752388077	2.13E-13
TADA3	0.752333197	2.14E-13
SOX8	0.752281046	2.15E-13
ARHGEF26	0.752154199	2.19E-13
HSD17B1	0.752129274	2.19E-13
PKN3	0.752054955	2.21E-13
DUSP16	0.752037046	2.22E-13
ARMCX7P	0.751804318	2.27E-13
AC002044.2	0.75180288	2.28E-13
NINJ1	0.751750879	2.29E-13
NTN1	0.75166997	2.31E-13
LINC01137	0.751577946	2.33E-13
ACBD5	0.751559347	2.34E-13
HIST1H2AC	0.75145229	2.37E-13
AL109976.1	0.751443163	2.37E-13
TES	0.751379948	2.39E-13
DLL1	0.751346543	2.40E-13
DNM2	0.751299193	2.41E-13
DPP9	0.751185936	2.44E-13
NTAN1	0.751133562	2.45E-13
PLEKHA4	0.750847434	2.54E-13
NDUFAF8	0.750672529	2.59E-13
H2AFV	0.750657912	2.59E-13
ZNF143	0.750605011	2.61E-13
AC011466.4	0.75047723	2.64E-13
FAM124A	0.750436885	2.66E-13
AC136632.2	0.750229613	2.72E-13
PARP10	0.750226424	2.72E-13
ZIC5	0.750051728	2.77E-13
RRNAD1	0.750006561	2.79E-13

AC112722.1	0.749633922	2.91E-13
SGCB	0.749579302	2.93E-13
DTYMK	0.749569176	2.93E-13
CCDC85C	0.74951865	2.95E-13
BISPR	0.749443552	2.97E-13
TMEM150A	0.749364626	3.00E-13
AC139495.1	0.749342918	3.00E-13
MAPKAPK3	0.749280628	3.03E-13
AC005072.1	0.749146071	3.07E-13
TRIP11	0.749066402	3.10E-13
ZNF300	0.749064246	3.10E-13
EFHD1	0.749054797	3.10E-13
ARHGEF10	0.749013984	3.12E-13
ZBTB42	0.748834269	3.18E-13
PLEKHO2	0.748747399	3.21E-13
RBM4B	0.748673252	3.24E-13
NADK	0.748604185	3.26E-13
PPP1R13L	0.748360142	3.35E-13
CHRNB1	0.748347538	3.36E-13
MED13L	0.748327705	3.37E-13
KLF3	0.748288547	3.38E-13
KDSR	0.74824959	3.40E-13
CTNNA3	0.748054178	3.47E-13
PDE9A	0.748018341	3.48E-13
TOB2	0.747979396	3.50E-13
IBA57	0.747914657	3.53E-13
RND2	0.747884202	3.54E-13
KCNJ2	0.747870696	3.54E-13
PDE4DIP	0.747833314	3.56E-13
SIX5	0.747806158	3.57E-13
KLF15	0.747794748	3.57E-13
TMEM9B	0.747779167	3.58E-13
FUT11	0.747744193	3.59E-13
SCARNA7	0.74757684	3.66E-13
NR2F2	0.747575441	3.66E-13
AC093028.1	0.747574873	3.66E-13
UBTD1	0.747260445	3.79E-13
PIGP	0.747159392	3.83E-13
SHKBP1	0.747155683	3.84E-13
AQP5	0.747144708	3.84E-13

RPL9P29	0.747064501	3.88E-13
STAG1	0.746845518	3.97E-13
AJUBA	0.7465551	4.10E-13
INSR	0.746416993	4.16E-13
MVB12A	0.74632079	4.21E-13
PADI2	0.746147521	4.29E-13
TMC6	0.746007375	4.36E-13
WDR76	0.745983442	4.37E-13
CLK3	0.745946559	4.39E-13
PPM1B	0.745929631	4.40E-13
AC025580.3	0.745853075	4.43E-13
HIBCH	0.745823258	4.45E-13
CMC4	0.74581261	4.45E-13
WTIP	0.745715714	4.50E-13
TFEB	0.745688629	4.51E-13
LTBR	0.745686666	4.51E-13
ZNF430	0.745640131	4.54E-13
GSDMD	0.745590546	4.56E-13
SALL3	0.745585974	4.57E-13
CCDC102A	0.745511733	4.60E-13
CRB2	0.74530955	4.71E-13
CASKIN2	0.745238869	4.74E-13
AC005324.5	0.745176883	4.78E-13
CDC42EP4	0.745136944	4.80E-13
LINC00513	0.745032812	4.85E-13
PDE11A	0.74500308	4.87E-13
WDR81	0.745000469	4.87E-13
UHRF1	0.744885002	4.93E-13
NADSYN1	0.744776424	4.99E-13
RPSAP36	0.744748244	5.01E-13
OLAH	0.744694538	5.04E-13
KEAP1	0.744638737	5.07E-13
IPO8	0.74461221	5.08E-13
KRT8P12	0.74454077	5.12E-13
NMUR2	0.74436769	5.22E-13
SLC19A3	0.744352765	5.23E-13
TPD52L1	0.744289991	5.27E-13
LYPD1	0.744239894	5.29E-13
PDZD2	0.744170075	5.33E-13
ZDHHC24	0.744026838	5.42E-13

IRAK1	0.743869462	5.51E-13
SLC15A3	0.743844107	5.53E-13
AP000962.1	0.743811344	5.55E-13
AC007608.4	0.743725321	5.60E-13
SLC39A11	0.743651569	5.65E-13
PARD3	0.743603928	5.68E-13
SPG21	0.743549683	5.71E-13
OR2A20P	0.743448557	5.77E-13
FAM222A	0.743300551	5.87E-13
MSL2	0.743028743	6.04E-13
GIMAP8	0.742968853	6.08E-13
C8orf58	0.742939618	6.10E-13
MMP2	0.742909759	6.12E-13
CCNI2	0.742832827	6.17E-13
AC126118.1	0.742787517	6.21E-13
WWTR1	0.742742199	6.24E-13
C1QTNF3	0.742560717	6.36E-13
VGLL3	0.742462472	6.43E-13
LINC01089	0.742415836	6.46E-13
TCIRG1	0.742399225	6.47E-13
MTCO1P2	0.742378445	6.49E-13
HCAR1	0.742280772	6.56E-13
AL592158.1	0.742246289	6.58E-13
RN7SL596P	0.742201498	6.61E-13
CASC10	0.74216393	6.64E-13
LINC01896	0.742074614	6.71E-13
ANPEP	0.742052246	6.72E-13
AC016745.2	0.741858442	6.87E-13
SMG5	0.741746073	6.95E-13
NXN	0.741728174	6.96E-13
FBXL7	0.741714103	6.97E-13
PAN2	0.741634673	7.03E-13
HCP5	0.741592817	7.07E-13
AL049840.2	0.74155389	7.10E-13
FGD5-AS1	0.7414851	7.15E-13
RBM4	0.741405967	7.21E-13
EFEMP2	0.741304983	7.29E-13
FLT1	0.741243579	7.34E-13
RIMKLB	0.741162807	7.40E-13
ANO6	0.741129425	7.43E-13

PPP1CC	0.741042628	7.50E-13
TBX18	0.741016931	7.52E-13
GJA4	0.740998574	7.54E-13
NUTM2G	0.740915288	7.60E-13
CDR2L	0.740781732	7.71E-13
FBL	0.740749427	7.74E-13
PACSIN3	0.740650629	7.82E-13
LINC02024	0.740543817	7.91E-13
PPP1R14B	0.74047879	7.97E-13
SIX1	0.740435953	8.01E-13
8-Sep	0.740234136	8.18E-13
AP001542.1	0.740202283	8.21E-13
KIF26A	0.7401538	8.25E-13
RPL7P18	0.740144421	8.26E-13
AC115102.1	0.740101617	8.30E-13
CCDC17	0.740025277	8.37E-13
NOTCH1	0.739986094	8.40E-13
AL162390.1	0.739983333	8.41E-13
TBC1D12	0.739943922	8.44E-13
MAP7	0.73987096	8.51E-13
IGDCC3	0.739867093	8.51E-13
HERC2P9	0.739721073	8.65E-13
UNC93B1	0.739694424	8.67E-13
TPM2	0.739682444	8.68E-13
ZNF271P	0.739672719	8.69E-13
CLIP2	0.739611882	8.75E-13
MTCO2P12	0.739609709	8.75E-13
AC020978.6	0.739529558	8.83E-13
PRRG2	0.739456275	8.90E-13
TMEM19	0.73944231	8.91E-13
PHETA2	0.739425639	8.93E-13
SPTLC2	0.739308866	9.04E-13
RPL21P135	0.739283336	9.06E-13
C1QTNF5	0.739276663	9.07E-13
AC002310.1	0.739104903	9.24E-13
ADAMTSL3	0.738828918	9.52E-13
RFNG	0.738824086	9.52E-13
ZBTB5	0.738807619	9.54E-13
FRMD4B	0.738709367	9.64E-13
PLCG1	0.738678761	9.67E-13

ZNF532	0.738650524	9.70E-13
AC015908.3	0.738614124	9.74E-13
AL590096.1	0.73850231	9.85E-13
SAP25	0.738454421	9.90E-13
CLIP1	0.738452911	9.91E-13
MAML2	0.738166762	1.02E-12
FGD5	0.738040389	1.04E-12
TAX1BP3	0.737997681	1.04E-12
FABP7P1	0.73781922	1.06E-12
PYROXD2	0.737818416	1.06E-12
FANCC	0.737717166	1.07E-12
AC106760.2	0.737493762	1.10E-12
AC079322.1	0.737438875	1.10E-12
EVI2B	0.737295189	1.12E-12
MFSD13B	0.737133983	1.14E-12
AC025430.1	0.737106677	1.14E-12
C5orf64-AS1	0.736994982	1.16E-12
SELENOP	0.736893251	1.17E-12
SLC6A8	0.73683863	1.18E-12
RELA	0.736808129	1.18E-12
SORBS3	0.736804368	1.18E-12
SLC25A18	0.736657124	1.20E-12
UNG	0.736536739	1.21E-12
KIAA1958	0.736435192	1.23E-12
CXorf36	0.736425012	1.23E-12
HIC1	0.736099641	1.27E-12
AC012645.4	0.735808348	1.31E-12
AL451165.2	0.735800273	1.31E-12
ZBTB7B	0.735527935	1.35E-12
STK4	0.735412512	1.37E-12
DHFR	0.735396998	1.37E-12
TMEM136	0.735316931	1.38E-12
LZIC	0.73530307	1.38E-12
AC008537.4	0.73527187	1.39E-12
AC011815.2	0.735255574	1.39E-12
SMG9	0.735247606	1.39E-12
AC130324.1	0.735147443	1.41E-12
ZBTB16	0.735079159	1.42E-12
RNF220	0.735055677	1.42E-12
AL161793.1	0.735035893	1.42E-12

MSI1	0.735003361	1.43E-12
CAHM	0.734806483	1.46E-12
TBXA2R	0.734753458	1.47E-12
WEE1	0.734748941	1.47E-12
TMEM139	0.734681665	1.48E-12
RHOXF2	0.73465747	1.48E-12
ZNF850	0.734335178	1.53E-12
AL137009.1	0.734330386	1.53E-12
MYD88	0.734208357	1.55E-12
DCAF7	0.734171326	1.56E-12
RFX1	0.734050914	1.58E-12
MT-TS2	0.733966939	1.59E-12
EGLN1	0.733958776	1.59E-12
AC006971.1	0.733838387	1.61E-12
IVNS1ABP	0.73375804	1.63E-12
INPP5D	0.733750663	1.63E-12
WHRN	0.733722354	1.63E-12
MMP14	0.733675571	1.64E-12
NFATC4	0.733618718	1.65E-12
FNBP1	0.733561088	1.66E-12
NSL1	0.733353366	1.70E-12
PTMAP5	0.733279225	1.71E-12
PPP1R3C	0.733186426	1.73E-12
SPATA5	0.733165146	1.73E-12
PACRG-AS3	0.733102033	1.74E-12
FP671120.4	0.732863005	1.79E-12
RARRES2	0.732822355	1.79E-12
C14orf93	0.732819078	1.79E-12
AHNAK	0.732800166	1.80E-12
SPEN	0.732767147	1.80E-12
AC109441.1	0.732711607	1.82E-12
PNPT1	0.732626366	1.83E-12
AL160006.1	0.732563835	1.84E-12
MFGE8	0.732427285	1.87E-12
AL591135.1	0.732426127	1.87E-12
NBPF1	0.732340918	1.89E-12
GLUL	0.732330327	1.89E-12
OR7E14P	0.732156485	1.92E-12
ELOVL1	0.732156264	1.92E-12
APOBEC3C	0.732147088	1.92E-12

S1PR5	0.73214446	1.93E-12
KAT6A	0.732042749	1.95E-12
OTULIN	0.73201325	1.95E-12
PLIN4	0.732011335	1.95E-12
TMEM104	0.731893897	1.98E-12
SAMD4A	0.731830638	1.99E-12
ATP11A-AS1	0.731825578	1.99E-12
CD22	0.731792661	2.00E-12
CERS1	0.731775873	2.00E-12
POLA1	0.73175328	2.01E-12
SCRIB	0.731734377	2.01E-12
AL356481.1	0.731687416	2.02E-12
ADGRG1	0.731656937	2.03E-12
RAB9A	0.731654701	2.03E-12
PAK4	0.731622903	2.03E-12
COL9A2	0.731552491	2.05E-12
AC005414.1	0.731497315	2.06E-12
PLXND1	0.731387006	2.08E-12
SMARCD2	0.731316512	2.10E-12
TMEM129	0.731210375	2.12E-12
ZNF493	0.731118985	2.14E-12
AC000068.1	0.731064486	2.15E-12
CBFB	0.731019415	2.16E-12
ZC3H12C	0.73101677	2.16E-12
AC137932.1	0.730837213	2.20E-12
TNIP2	0.730708489	2.23E-12
CYP2J2	0.730661618	2.24E-12
ZIC3	0.73065154	2.25E-12
AC106820.4	0.730641472	2.25E-12
WDR5B	0.730606714	2.26E-12
AC103810.6	0.730571678	2.27E-12
CA3-AS1	0.730511176	2.28E-12
MIR5196	0.73032765	2.32E-12
KIF5C	0.730294821	2.33E-12
ARHGAP11A	0.730068613	2.39E-12
ZNF395	0.729949579	2.42E-12
TMEM100	0.729907142	2.43E-12
FMNL2	0.729865985	2.44E-12
TAL1	0.72981724	2.45E-12
ZNF511	0.729747807	2.47E-12

BVES	0.729731477	2.47E-12
PLCD3	0.729276364	2.59E-12
AP000350.7	0.729253493	2.59E-12
TRIOBP	0.728916211	2.69E-12
AC004678.2	0.728841118	2.71E-12
TLE1	0.728691322	2.75E-12
ZNF37A	0.728610643	2.77E-12
LBX2-AS1	0.728166986	2.90E-12
AC080013.6	0.728166761	2.90E-12
BCAT2	0.728159374	2.90E-12
EYA2	0.728118425	2.91E-12
AC022400.2	0.728027854	2.94E-12
SIRT2	0.727945549	2.97E-12
AC009065.8	0.727812126	3.01E-12
FYN	0.727803086	3.01E-12
TEX261	0.727741794	3.03E-12
CDCA4P4	0.727734596	3.03E-12
CBX5	0.727711069	3.04E-12
GNA13	0.727570256	3.08E-12
PPP2R3B	0.727378201	3.14E-12
LDLRAD3	0.727339397	3.15E-12
NME4	0.726963685	3.28E-12
PCSK6	0.726943723	3.28E-12
TSPAN12	0.726863032	3.31E-12
AC008147.3	0.726837869	3.32E-12
SESN3	0.726794263	3.33E-12
AP003419.3	0.726785593	3.34E-12
SLC25A20	0.72660314	3.40E-12
AL445248.1	0.726518418	3.43E-12
SLCO1A2	0.726516917	3.43E-12
ZBTB1	0.726462344	3.45E-12
AL157871.5	0.726351818	3.49E-12
GCNT2	0.726263586	3.52E-12
PXDC1	0.726249868	3.52E-12
NFKBIA	0.726223098	3.53E-12
LINC00632	0.726144526	3.56E-12
DDIT4L	0.725972332	3.62E-12
DDX23	0.725956106	3.63E-12
LAMP2	0.725932138	3.64E-12
UGT8	0.725923909	3.64E-12

FHL5	0.725895076	3.65E-12
ARHGEF6	0.725723282	3.72E-12
PRKG1	0.725720923	3.72E-12
LINC00685	0.7256418	3.75E-12
FOXN2	0.725570887	3.77E-12
N4BP1	0.725567959	3.77E-12
AC097468.3	0.725314427	3.87E-12
ITGA8	0.725268105	3.89E-12
IGF2	0.725262086	3.89E-12
CLDND1	0.725003615	4.00E-12
B3GALT5-AS1	0.724899968	4.04E-12
SPOPL	0.724872303	4.05E-12
TIGD5	0.72483127	4.07E-12
KCNN3	0.724616487	4.15E-12
COL27A1	0.724551684	4.18E-12
RF00019	0.724488859	4.21E-12
TOP1MT	0.72448696	4.21E-12
SS18	0.724315038	4.28E-12
ARHGAP21	0.724101891	4.37E-12
RBMS2P1	0.723988892	4.42E-12
PAXIP1	0.723936137	4.45E-12
AC010326.4	0.723893186	4.47E-12
TBX15	0.723827889	4.50E-12
UBALD2	0.723726899	4.54E-12
DPF2	0.723587219	4.61E-12
CBSL	0.72355297	4.62E-12
AL049872.1	0.723535443	4.63E-12
NFATC1	0.72341707	4.69E-12
AP001107.1	0.723353211	4.72E-12
POLR3H	0.723225431	4.78E-12
POMT2	0.723199766	4.79E-12
MTND5P16	0.723140479	4.82E-12
AC244034.3	0.723094513	4.84E-12
AC104564.1	0.722956623	4.91E-12
-	0.722903	4.93E-12
HSPA12B	0.72281234	4.98E-12
CFHR1	0.722764804	5.00E-12
HNRNPH1P1	0.722529023	5.12E-12
MIF4GD	0.722463667	5.15E-12
ITGA10	0.72241058	5.18E-12

MMS22L	0.722313792	5.23E-12
MZF1-AS1	0.722298869	5.24E-12
SFXN5	0.722217577	5.28E-12
FIZ1	0.722094219	5.35E-12
CLMN	0.7220058	5.39E-12
AC017006.2	0.721784507	5.51E-12
TJAP1	0.721776424	5.52E-12
MIRLET7BHG	0.721772404	5.52E-12
RNF216	0.721689579	5.56E-12
STAG2	0.721652398	5.59E-12
SLC45A3	0.721636645	5.59E-12
AC133552.1	0.721601071	5.61E-12
SLC6A9	0.721441704	5.70E-12
GSPT1	0.721235339	5.82E-12
ARHGEF19	0.721187704	5.85E-12
PCA3	0.7210683	5.92E-12
HERC2P3	0.721029094	5.94E-12
NKX6-2	0.720994819	5.96E-12
FOXD2	0.720961248	5.98E-12
GJA9	0.720835093	6.06E-12
IKBIP	0.720683406	6.15E-12
NRN1L	0.720380388	6.33E-12
LSS	0.720334067	6.36E-12
ABCD1	0.720224052	6.43E-12
CHST3	0.720134996	6.49E-12
TCF15	0.720014934	6.57E-12
AC092068.2	0.719993779	6.58E-12
AC105101.1	0.719971232	6.59E-12
DHCR7	0.719940183	6.61E-12
LINC-PINT	0.719606202	6.84E-12
RBPMS2	0.719544156	6.88E-12
CTDSP1	0.719413806	6.97E-12
CC2D1B	0.719412913	6.97E-12
AC231981.1	0.71933375	7.02E-12
GLTPP1	0.719260314	7.07E-12
ENTR1	0.719244609	7.08E-12
TIMMDC1	0.719158792	7.14E-12
HYI	0.719099305	7.18E-12
SFT2D2	0.718999174	7.26E-12
USP47	0.718913698	7.32E-12

STARD7	0.718885283	7.34E-12
SLC39A1	0.718878639	7.34E-12
PARP1	0.718853531	7.36E-12
COL1A2	0.718774573	7.42E-12
AC022613.3	0.718757403	7.43E-12
CACNA1C-AS4	0.718678431	7.49E-12
PYGM	0.718674341	7.49E-12
ST3GAL2	0.71852911	7.60E-12
TCF3	0.718260851	7.80E-12
AL022329.2	0.718217	7.83E-12
TMEM170A	0.718205577	7.84E-12
PPP1R1A	0.718038364	7.97E-12
USP21	0.718019684	7.99E-12
RNU6-1004P	0.718004775	8.00E-12
RXRG	0.717973496	8.02E-12
AL607028.1	0.717962813	8.03E-12
ZNF500	0.717896463	8.08E-12
AC135050.3	0.71775909	8.19E-12
AC091181.1	0.717600108	8.32E-12
FBLN1	0.717570133	8.34E-12
USE1	0.717473988	8.42E-12
AC015689.2	0.717342357	8.53E-12
HYAL1	0.717218771	8.63E-12
CAPS	0.717169807	8.68E-12
ADGRA3	0.717108794	8.73E-12
TIE1	0.717061987	8.77E-12
CAPN15	0.717053486	8.77E-12
AC089999.2	0.717024556	8.80E-12
CNOT6	0.716993508	8.83E-12
NEDD4	0.71692445	8.88E-12
TPTEP2	0.716899317	8.91E-12
CNTF	0.71688905	8.92E-12
HEXIM1	0.716780175	9.01E-12
AC138894.1	0.716763544	9.02E-12
RN7SL262P	0.716753874	9.03E-12
NWD1	0.716632097	9.14E-12
OR2A9P	0.716496409	9.26E-12
SLC26A6	0.716395458	9.35E-12
HMGB1P49	0.716254455	9.48E-12
ZSCAN29	0.716204065	9.53E-12

AC005183.1	0.716081791	9.64E-12
BDH2	0.715936077	9.78E-12
STX10	0.715751438	9.95E-12
RNU5E-8P	0.715704238	1.00E-11
RNU6-758P	0.715593182	1.01E-11
TMEM140	0.715529285	1.02E-11
AC022558.1	0.715483472	1.02E-11
CYTH1	0.715412581	1.03E-11
THOC6	0.715405723	1.03E-11
LINC00674	0.715374346	1.03E-11
AC004852.3	0.715356415	1.03E-11
AC091769.2	0.715063426	1.06E-11
OXSR1	0.715062617	1.06E-11
AL136366.1	0.715048733	1.07E-11
PACS2	0.715048371	1.07E-11
ZNF582	0.71480142	1.09E-11
RN7SL130P	0.714776057	1.09E-11
AC138866.2	0.714642313	1.11E-11
RF00019	0.714525217	1.12E-11
AL022322.2	0.714497701	1.12E-11
AK4	0.714218506	1.15E-11
GAS6-AS1	0.71417782	1.16E-11
MACF1	0.713989205	1.18E-11
PXN	0.713937521	1.19E-11
PIGV	0.713898486	1.19E-11
CABP4	0.713798737	1.20E-11
TPRA1	0.713640223	1.22E-11
GATA2	0.713588311	1.23E-11
AC008759.2	0.713462313	1.24E-11
AC020907.1	0.713427062	1.25E-11
CENPO	0.713406036	1.25E-11
JPH2	0.71336578	1.25E-11
IFIT2	0.713221503	1.27E-11
LRP4	0.713073181	1.29E-11
AL731571.1	0.713006695	1.30E-11
AC020915.2	0.713005681	1.30E-11
AL158206.1	0.712820921	1.32E-11
PLOD2	0.712796143	1.32E-11
AC009063.2	0.712786183	1.32E-11
CA2	0.712606607	1.35E-11

AC092279.1	0.712561708	1.35E-11
AKT1	0.712343631	1.38E-11
AC105206.1	0.712222387	1.40E-11
PLEKHF1	0.712159175	1.41E-11
TRIM62	0.712021046	1.42E-11
AF107885.1	0.711726192	1.46E-11
ZNF385A	0.711701346	1.47E-11
SRGAP2-AS1	0.711678475	1.47E-11
AC011468.1	0.71167339	1.47E-11
RAMP1	0.711584972	1.48E-11
AC002310.6	0.711561172	1.49E-11
CBS	0.711513541	1.49E-11
PEX2	0.71122697	1.54E-11
SMCR5	0.711156089	1.55E-11
ZNF394	0.71097518	1.57E-11
MAP7D3	0.710973508	1.57E-11
P2RY13	0.710920371	1.58E-11
AC007066.2	0.710792089	1.60E-11
PLD1	0.710662233	1.62E-11
HPSE2	0.710396092	1.66E-11
C20orf96	0.710380264	1.66E-11
PSPH	0.710280978	1.68E-11
PDE1C	0.709923497	1.74E-11
PTGDR2	0.709900634	1.74E-11
KLF2	0.709518307	1.80E-11
AC010969.2	0.709459433	1.81E-11
JUP	0.709456886	1.82E-11
AC005220.1	0.7092475	1.85E-11
AC018904.1	0.709232678	1.85E-11
LINC00926	0.709139887	1.87E-11
RTKN	0.708997743	1.90E-11
RILP	0.70899165	1.90E-11
TBX3	0.708964688	1.90E-11
TPTEP1	0.70884972	1.92E-11
ALOX12	0.708802867	1.93E-11
AC114296.1	0.708638829	1.96E-11
SLC25A30	0.708556902	1.98E-11
AP000711.1	0.708399872	2.00E-11
CUEDC1	0.708331557	2.02E-11
NR2E1	0.708050441	2.07E-11

AC020558.3	0.708026318	2.08E-11
AP001469.3	0.707901992	2.10E-11
NYNRIN	0.707658349	2.15E-11
INTS12	0.707652154	2.15E-11
SPATA13	0.707639467	2.15E-11
HIP1R	0.707591696	2.16E-11
GPM6B	0.707569317	2.17E-11
AC019270.1	0.70751271	2.18E-11
BCAN	0.707454878	2.19E-11
APOBR	0.707422063	2.20E-11
TNRC6B	0.707352075	2.21E-11
KMT5A	0.707279614	2.23E-11
PHGDH	0.707250774	2.23E-11
SCD	0.707245649	2.23E-11
AP002433.2	0.706941734	2.30E-11
MYO1F	0.706871161	2.31E-11
LINC01772	0.706673074	2.36E-11
PAXX	0.706543051	2.38E-11
LCOR	0.706430205	2.41E-11
C1orf229	0.706428453	2.41E-11
AL662795.2	0.706116403	2.48E-11
SNTA1	0.706102584	2.48E-11
SMOC1	0.706101294	2.48E-11
AGFG2	0.705622276	2.60E-11
CENPBD1	0.705366546	2.66E-11
RPL37P2	0.705332988	2.67E-11
APBB2	0.705176244	2.71E-11
RN7SL587P	0.705115269	2.72E-11
AL513534.1	0.704803501	2.80E-11
LIPH	0.704794591	2.80E-11
AC005225.4	0.704687565	2.83E-11
BDH2P1	0.704598242	2.86E-11
CHPT1	0.704534851	2.87E-11
ERMAP	0.704472498	2.89E-11
FES	0.704304143	2.93E-11
GGT1	0.70418091	2.97E-11
FKBP5	0.704173917	2.97E-11
FNDC3B	0.704142684	2.98E-11
AC055811.3	0.703989764	3.02E-11
SLC7A2	0.703754965	3.09E-11

VCAN	0.703705184	3.10E-11
SLC22A13	0.703693172	3.10E-11
MED11	0.703561275	3.14E-11
TGFB2-OT1	0.703538742	3.15E-11
LZTS2	0.703387851	3.19E-11
AC007537.1	0.703350183	3.20E-11
GPAM	0.703015463	3.30E-11
BTBD10P2	0.702997094	3.31E-11
Z97832.2	0.702986676	3.31E-11
PTAFR	0.702897114	3.34E-11
NCKAP5	0.702804288	3.37E-11
RNU6ATAC39P	0.702782008	3.37E-11
B4GALNT4	0.702553886	3.45E-11
AL136115.1	0.70252896	3.45E-11
AC008738.4	0.702367995	3.50E-11
IL17RC	0.702286279	3.53E-11
NINL	0.702048292	3.61E-11
DLL4	0.702011906	3.62E-11
AL034417.4	0.701788741	3.70E-11
HEXDC	0.701652601	3.74E-11
ZNF451-AS1	0.701541857	3.78E-11
AC104836.1	0.701414031	3.82E-11
AL449403.2	0.701404089	3.83E-11
AL445309.1	0.701195818	3.90E-11
GIT1	0.701001452	3.97E-11
AC108449.2	0.700978932	3.98E-11
RAF1	0.700883609	4.01E-11
BMP7	0.700776757	4.05E-11
AP004609.3	0.700775259	4.05E-11
AC092368.3	0.700615255	4.11E-11
AL731563.3	0.700540342	4.14E-11
REP15	0.700458738	4.17E-11
AC007546.2	0.700389709	4.20E-11
AC005696.1	0.700379078	4.20E-11
SMG1P7	0.700349376	4.21E-11
CTD-2201I18.1	0.699821873	4.42E-11
WNT6	0.699704465	4.47E-11
ZNF423	0.699664532	4.48E-11
AC013244.2	0.699624784	4.50E-11
COL5A3	0.699568369	4.52E-11

WNK4	0.699565474	4.52E-11
FLJ46906	0.699542752	4.53E-11
SLC25A48	0.69911054	4.71E-11
TFAP2C	0.699022286	4.75E-11
AC025755.1	0.698831008	4.83E-11
AC068860.1	0.698801015	4.84E-11
C19orf54	0.69859027	4.94E-11
SGF29	0.698558289	4.95E-11
RPEP4	0.698407076	5.02E-11
ZFP41	0.698328659	5.06E-11
ZNF552	0.698136651	5.14E-11
LOXL1	0.69799767	5.21E-11
AC055822.1	0.697909259	5.25E-11
ZNF814	0.697851412	5.28E-11
PPM1D	0.697644792	5.38E-11
STOX1	0.697631857	5.38E-11
AL158212.5	0.697537469	5.43E-11
TLE4	0.697363059	5.51E-11
GNRH1	0.697359634	5.51E-11
ZNF891	0.697077305	5.66E-11
ZBTB20	0.696884185	5.75E-11
AL121989.1	0.696878234	5.76E-11
TMEM255B	0.696758689	5.82E-11
AC127502.2	0.69651929	5.95E-11
P2RY8	0.696411122	6.00E-11
PBXIP1	0.696339649	6.04E-11
CTF1	0.696310394	6.06E-11
ELOCP28	0.696236575	6.10E-11
TIMELESS	0.696217111	6.11E-11
RFX2	0.696171051	6.13E-11
LINC02172	0.695988169	6.23E-11
AC092168.2	0.695949571	6.26E-11
ZNF592	0.695883625	6.29E-11
NACC2	0.695816032	6.33E-11
DCXR	0.695815282	6.33E-11
CLASRP	0.695695708	6.40E-11
CARD10	0.695684165	6.40E-11
SYNE2	0.69545455	6.54E-11
AC103853.2	0.695427394	6.55E-11
MS4A14	0.695401772	6.57E-11

C4orf19	0.695352211	6.60E-11
ST18	0.695323747	6.61E-11
HNRNPF	0.695269157	6.65E-11
GIPC3	0.69508621	6.75E-11
AC100793.4	0.695059659	6.77E-11
AL080273.1	0.694794248	6.93E-11
KIF5A	0.694688126	7.00E-11
ZHX3	0.69463365	7.03E-11
AP003733.4	0.694447319	7.15E-11
FAAP20	0.694338508	7.22E-11
QDPR	0.694307256	7.24E-11
WSCD1	0.694194079	7.31E-11
ST6GALNAC3	0.693865625	7.53E-11
CIZ1	0.69382317	7.55E-11
AC007036.3	0.69352475	7.76E-11
NR0B1	0.693371706	7.86E-11
AC106028.2	0.693248126	7.95E-11
MXI1	0.693239945	7.95E-11
WISP1	0.693193039	7.99E-11
AC007193.2	0.693036136	8.10E-11
THADA	0.692915609	8.18E-11
NPIPB9	0.692856175	8.23E-11
MT1E	0.692745564	8.31E-11
AC011595.1	0.692615196	8.40E-11
NBPF14	0.692492653	8.49E-11
HSD17B7	0.692490389	8.49E-11
SLC35G5	0.692444621	8.53E-11
AC046158.3	0.692423547	8.54E-11
AL355974.2	0.692418615	8.55E-11
SMAD2	0.69237078	8.58E-11
ZSCAN32	0.69236674	8.59E-11
PATL1	0.692334412	8.61E-11
FRYL	0.69205876	8.82E-11
CLN3	0.692018837	8.85E-11
AC048341.2	0.691625059	9.16E-11
KCTD18	0.691616967	9.17E-11
AL138799.2	0.691541261	9.23E-11
GRIK1-AS1	0.69144478	9.31E-11
HIF3A	0.691368597	9.37E-11
HIPK1	0.691341131	9.39E-11

AC091231.1	0.690724465	9.91E-11
TGIF1	0.690624359	1.00E-10
THAP8	0.690548629	1.01E-10
CTCF	0.690297409	1.03E-10
SOGA1	0.690240801	1.03E-10
ENO3	0.690020978	1.05E-10
PPFIA1	0.689889141	1.07E-10
GPRC5B	0.689790896	1.08E-10
VANGL2	0.689592122	1.09E-10
CDKN1C	0.68951466	1.10E-10
SLC12A4	0.689481645	1.10E-10
CRYBG3	0.689425138	1.11E-10
AC004771.1	0.689396782	1.11E-10
LINC00638	0.689377918	1.11E-10
ZNRF3-IT1	0.689292392	1.12E-10
MYORG	0.689213368	1.13E-10
IGF1R	0.689135835	1.14E-10
PPP3CB-AS1	0.688948755	1.16E-10
CDH19	0.688855002	1.17E-10
AL035681.1	0.688676251	1.18E-10
HERC2P2	0.68863054	1.19E-10
MTA1	0.688556805	1.20E-10
PPP1R3G	0.688549725	1.20E-10
CCDC160	0.688530707	1.20E-10
PSAT1	0.688444466	1.21E-10
AC017083.1	0.688428496	1.21E-10
PPP1R16A	0.688315278	1.22E-10
RGCC	0.68788327	1.27E-10
BX255925.3	0.687631392	1.30E-10
ANXA3	0.687391862	1.32E-10
FA2H	0.68732572	1.33E-10
PRICKLE3	0.686619332	1.41E-10
WIZ	0.686607634	1.42E-10
LINC01354	0.686506327	1.43E-10
LHX2	0.686489964	1.43E-10
DIO3	0.686416357	1.44E-10
ADAMTSL5	0.686394567	1.44E-10
ALDH4A1	0.686335273	1.45E-10
ZBTB14	0.686271245	1.46E-10
SEMA3F	0.686116815	1.48E-10

CSF1	0.686044815	1.49E-10
CATSPERG	0.685943965	1.50E-10
AC008985.1	0.68570233	1.53E-10
SALL2	0.685547257	1.55E-10
AC002550.2	0.685531734	1.55E-10
LINC01567	0.685502097	1.56E-10
NPIPB8	0.685348796	1.58E-10
ZFAND4	0.685224519	1.59E-10
MGARP	0.684851632	1.64E-10
RANBP3L	0.684714	1.66E-10
AC004836.1	0.684439576	1.70E-10
AC106028.3	0.684396694	1.71E-10
AL031432.5	0.684381572	1.71E-10
TTYH2	0.684309811	1.72E-10
AC106869.1	0.684295613	1.72E-10
ITGA11	0.684133328	1.75E-10
LLGL1	0.683948049	1.78E-10
ZNF787	0.683942008	1.78E-10
UPB1	0.683928994	1.78E-10
CTXND1	0.683860885	1.79E-10
ITPRIP	0.683693102	1.82E-10
HP1BP3	0.683187064	1.89E-10
AL139220.2	0.682874896	1.95E-10
AKAP3	0.682810976	1.96E-10
ST6GALNAC4P1	0.682807064	1.96E-10
ID3	0.682775852	1.96E-10
AL031587.3	0.682696014	1.98E-10
AC211486.5	0.682556046	2.00E-10
AC104417.2	0.682494067	2.01E-10
AC048380.2	0.682395531	2.03E-10
MAPK7	0.68238354	2.03E-10
AQP6	0.682206986	2.06E-10
AL022323.5	0.682012846	2.09E-10
AC090907.2	0.68170142	2.15E-10
AP000254.1	0.68164657	2.16E-10
MLANA	0.681433657	2.20E-10
AP002761.4	0.681420128	2.20E-10
AC006064.5	0.681170097	2.25E-10
BCL9L	0.681160815	2.25E-10
AC009145.4	0.681104312	2.26E-10

WDR34	0.680460461	2.38E-10
AC010285.2	0.680418881	2.39E-10
HDAC10	0.680320928	2.41E-10
RN7SL404P	0.679961289	2.49E-10
MAGI1-AS1	0.679701315	2.54E-10
AL390066.1	0.679663769	2.55E-10
RF00017	0.679514081	2.58E-10
FAM171A1	0.679503717	2.58E-10
ARL17A	0.679357224	2.61E-10
THSD1	0.679122762	2.67E-10
LLGL2	0.679083407	2.67E-10
AC023538.1	0.678698441	2.76E-10
NPIPB4	0.678654662	2.77E-10
GRTP1	0.678594791	2.79E-10
EBLN2	0.67828172	2.86E-10
TP53I3	0.678264408	2.86E-10
AC012073.1	0.678122934	2.90E-10
3-Mar	0.677945191	2.94E-10
AL513165.1	0.677052835	3.17E-10
AC079600.3	0.676933025	3.20E-10
ADORA3	0.676831011	3.22E-10
TCEANC	0.676763793	3.24E-10
ZNF571	0.676534343	3.30E-10
PABPC1L	0.676411144	3.34E-10
NPIPB11	0.676310685	3.36E-10
LIME1	0.676275136	3.37E-10
VAC14-AS1	0.676036002	3.44E-10
TLCD2	0.676033998	3.44E-10
ARGFXP2	0.675990036	3.45E-10
AC007406.1	0.675895801	3.48E-10
AC097359.1	0.675654008	3.55E-10
LINC01176	0.675560547	3.58E-10
SLC25A39	0.675497398	3.60E-10
CEP89	0.675467682	3.61E-10
NSMF	0.675415831	3.62E-10
MEX3D	0.675310438	3.65E-10
PSTPIP1	0.675280332	3.66E-10
AC124312.2	0.674887388	3.78E-10
PNISR	0.674761261	3.82E-10
MAFF	0.674560954	3.88E-10

AC027130.1	0.674266168	3.98E-10
SLCO4A1	0.674041998	4.05E-10
SLC41A1	0.673980883	4.07E-10
HHIPL1	0.673964787	4.08E-10
ALDH1L1-AS2	0.67396116	4.08E-10
AC026401.2	0.673833531	4.12E-10
AC007790.1	0.673687772	4.17E-10
AF067845.5	0.673587368	4.21E-10
MAP4K5	0.673572172	4.21E-10
FP325332.1	0.673386427	4.28E-10
CD37	0.673322625	4.30E-10
PRKD3	0.673231012	4.33E-10
IDI2-AS1	0.673222173	4.33E-10
ARAP2	0.673203274	4.34E-10
AC092032.1	0.673187686	4.35E-10
AL132780.5	0.673090067	4.38E-10
MTHFD2L	0.673053093	4.39E-10
NEXN	0.672882789	4.45E-10
AC016042.1	0.672854031	4.47E-10
HEPH	0.672761596	4.50E-10
KCNJ10	0.672740377	4.51E-10
SRRT	0.672420428	4.63E-10
ENOX2	0.672357116	4.65E-10
NUP188	0.672229804	4.70E-10
SNX27	0.672052025	4.77E-10
ZNF506	0.671984562	4.79E-10
TSEN54	0.671964499	4.80E-10
AC010175.1	0.671923247	4.82E-10
TJP2	0.671807848	4.86E-10
AC011483.3	0.671711708	4.90E-10
HNRNPCP7	0.671404744	5.02E-10
AP003117.1	0.671358322	5.04E-10
SPTBN5	0.671341691	5.05E-10
AC074043.1	0.670908656	5.23E-10
AL035461.2	0.670759695	5.29E-10
AC091180.5	0.670739845	5.30E-10
FURIN	0.670694032	5.32E-10
AL589740.1	0.670519262	5.39E-10
AC069209.1	0.670480938	5.41E-10
CARD8	0.670069647	5.59E-10

PPIAP51	0.669877154	5.68E-10
AC121247.1	0.669536753	5.84E-10
PLOD3	0.669282535	5.96E-10
KPTN	0.669097783	6.05E-10
METTL25	0.668924967	6.13E-10
ABHD17B	0.668560113	6.31E-10
FGFBP3	0.668548093	6.32E-10
AL031708.1	0.668497935	6.34E-10
AC134407.1	0.668440381	6.37E-10
CPSF2	0.668389385	6.40E-10
NPIPB3	0.667991349	6.61E-10
AC106028.4	0.667935972	6.64E-10
MTFP1	0.667755255	6.73E-10
OTOS	0.667678959	6.77E-10
AL713852.1	0.667661434	6.78E-10
AC010469.1	0.667626808	6.80E-10
DDR1	0.667247322	7.01E-10
FAM181B	0.667166618	7.06E-10
CTNS	0.666795512	7.27E-10
ZNF652	0.666640504	7.36E-10
CEMIP2	0.666639174	7.36E-10
AC024610.2	0.666589225	7.39E-10
AL139353.2	0.666191638	7.62E-10
AC079117.1	0.665854243	7.83E-10
RN7SL270P	0.665730168	7.91E-10
FITM1	0.665647224	7.96E-10
10-Sep	0.665640867	7.96E-10
NCLP1	0.665513141	8.04E-10
MRGPRF	0.665450585	8.08E-10
MED12	0.665368694	8.14E-10
KBTBD11-OT1	0.66497842	8.39E-10
ZBED3	0.664470886	8.73E-10
BMPR1A	0.664210239	8.91E-10
EPHB4	0.664209367	8.92E-10
SPN	0.664122863	8.98E-10
NBPF19	0.664108066	8.99E-10
AC127024.6	0.664103486	8.99E-10
RNY3P16	0.6640342	9.04E-10
APOD	0.663742983	9.25E-10
ZNF219	0.663148811	0.000000001

AC092338.2	0.663043911	0.000000001
TCF4-AS1	0.662974594	0.000000001
A2ML1-AS1	0.662805584	0.000000001
LRRC1	0.662668258	0.000000001
AL357140.5	0.662346675	0.000000001
AP003084.1	0.662311654	0.000000001
ATF1	0.662290498	0.000000001
PSD4	0.66201173	1.06E-09
SOX21	0.661960242	1.06E-09
AL031587.2	0.661838388	1.07E-09
SH2D3A	0.661384716	1.11E-09
NPIPB12	0.661356628	1.11E-09
SLC38A2	0.661249121	1.12E-09
NCOA5	0.661155569	1.13E-09
AC016747.3	0.661139499	1.13E-09
LGALS9	0.661037072	1.14E-09
AC018362.1	0.660852239	1.16E-09
ZNF252P	0.660698499	1.17E-09
PHYHD1	0.660466413	1.19E-09
GAS1	0.660211311	1.22E-09
SOX21-AS1	0.660188867	1.22E-09
CYP51A1P3	0.66018392	1.22E-09
UBE2J2	0.659795044	1.26E-09
ANKRD13D	0.659764395	1.26E-09
AL662907.1	0.659650349	1.27E-09
RPL5P18	0.659590109	1.28E-09
C17orf82	0.659581315	1.28E-09
AC133435.1	0.659535934	1.28E-09
AL049776.1	0.659474517	1.29E-09
LINC00862	0.659111382	1.33E-09
FBXL4	0.659036716	1.33E-09
AL022344.2	0.658955061	1.34E-09
TUSC7	0.658875172	1.35E-09
EEF2K	0.658836621	1.35E-09
TMEM189	0.658723947	1.37E-09
SCAMP4	0.658684745	1.37E-09
AC015883.1	0.658598135	1.38E-09
MT-TH	0.658570095	1.38E-09
AC146944.2	0.658561181	1.38E-09
LYG1	0.658246962	1.42E-09

MTATP6P26	0.658213505	1.42E-09
ZNF69	0.657972939	1.45E-09
CSRP1	0.65747837	1.50E-09
RF00019	0.657474744	1.50E-09
RPL14	0.657131943	1.54E-09
CSNK1G2	0.656883402	1.57E-09
MT2P1	0.656834497	1.58E-09
AMER2	0.656695544	1.60E-09
IFT140	0.656678188	1.60E-09
BLM	0.656606152	1.61E-09
LTBP3	0.656527496	1.62E-09
FAM19A5	0.656521072	1.62E-09
ZNF513	0.656412278	1.63E-09
AL008721.2	0.656286601	1.65E-09
RPA4	0.656063386	1.68E-09
DPYD	0.656032084	1.68E-09
CA5BP1	0.655913521	1.70E-09
DDIT4	0.655815099	1.71E-09
DTX1	0.655742816	1.72E-09
LRRC8A	0.655730933	1.72E-09
GRM6	0.655451834	1.76E-09
ZFP82	0.655161276	1.79E-09
AC131097.2	0.654922526	1.83E-09
ARHGEF10L	0.654728921	1.85E-09
SLFN11	0.654256161	1.92E-09
RABEP2	0.654198389	1.93E-09
AC012404.2	0.653861165	0.000000002
AL355974.3	0.653781152	0.000000002
LRRC3	0.653693986	0.000000002
ELOBP4	0.653680659	0.000000002
PLIN5	0.653622784	0.000000002
AC004158.1	0.653609412	0.000000002
RN7SL846P	0.653568183	0.000000002
RGS9BP	0.652992694	2.12E-09
ATP10D	0.652735894	2.16E-09
LRCH4	0.652672863	2.17E-09
BTN3A2	0.652383864	2.21E-09
TANC1	0.652329155	2.22E-09
PROX1	0.651984031	2.28E-09
AL603839.3	0.651966028	2.29E-09

NBEAL2	0.6518955	2.30E-09
ZBTB7A	0.651775544	2.32E-09
FBRSL1	0.651657213	2.34E-09
AL353653.1	0.651334672	2.40E-09
OLIG2	0.651309804	2.40E-09
ZNF444	0.65120143	2.42E-09
AC007262.2	0.651135017	2.43E-09
ANGPT2	0.650959451	2.46E-09
PTMAP1	0.650943457	2.47E-09
AC004223.1	0.650860982	2.48E-09
MSX1	0.650850448	2.48E-09
LEAP2	0.650561542	2.54E-09
LINC00598	0.65047182	2.56E-09
ELN	0.650337137	2.58E-09
ARHGEF34P	0.650276975	2.59E-09
LY6G5C	0.650269921	2.59E-09
AL356275.1	0.650234892	2.60E-09
AL035071.1	0.649919697	2.66E-09
AL031432.3	0.649860677	2.68E-09
AL513283.1	0.649767163	2.69E-09
WWOX	0.649529135	2.74E-09
CARD14	0.649416784	2.77E-09
AC004877.2	0.649215261	2.81E-09
AL008582.1	0.648692324	2.92E-09
OR2A4	0.648518699	0.000000003
AC105429.2	0.648222277	0.000000003
AC083822.1	0.648079026	3.05E-09
IL17RB	0.648035018	3.06E-09
HSPB9	0.647948452	3.08E-09
AC009093.2	0.647609452	3.16E-09
TMEM119	0.647575116	3.17E-09
AC012486.1	0.64731701	3.23E-09
HNRNPA3P14	0.647151063	3.27E-09
AP002807.1	0.6469013	3.33E-09
SYTL4	0.646607913	3.40E-09
MIR4451	0.64643221	3.45E-09
GTF2IRD2	0.646315234	3.48E-09
CHRNG	0.646218576	3.50E-09
S100A6	0.64612045	3.53E-09
CAPN2	0.646039449	3.55E-09

TARDBP	0.645913503	3.58E-09
HLA-DPB1	0.645891784	3.59E-09
BPTF	0.645709144	3.64E-09
AC091563.1	0.645563683	3.68E-09
AC005546.1	0.645484298	3.70E-09
TCP11L2	0.645303433	3.75E-09
AC012183.1	0.645013784	3.83E-09
ADRA2C	0.644969833	3.84E-09
SLC18B1	0.644963226	3.84E-09
AL031666.2	0.644919552	3.85E-09
SLC5A11	0.64485809	3.87E-09
PLP1	0.644741546	3.90E-09
PTCH1	0.644455651	0.000000004
A2ML1	0.644402042	0.000000004
ARAP1-AS2	0.644117765	4.09E-09
PDCL3P6	0.644096604	4.09E-09
HEATR4	0.644083862	4.10E-09
SHC4	0.643963578	4.13E-09
AC005480.1	0.643828679	4.17E-09
AFF1	0.643774477	4.19E-09
TMC8	0.643643796	4.23E-09
FGFRL1	0.643531701	4.27E-09
DNAJC21	0.643458467	4.29E-09
ZNHIT6	0.643452835	4.29E-09
SLC19A1	0.643394771	4.31E-09
RORA-AS1	0.643283352	4.34E-09
OLFM2	0.64308024	4.41E-09
PRR34-AS1	0.6430557	4.42E-09
UCKL1	0.642807877	4.50E-09
AC002470.2	0.642685958	4.54E-09
AC010332.1	0.642421225	4.62E-09
AL353804.1	0.642262834	4.68E-09
SLC51B	0.642169087	4.71E-09
AC008764.6	0.641969826	4.78E-09
PIDD1	0.641600926	4.91E-09
PLTP	0.641587539	4.91E-09
AC136624.2	0.641512115	4.94E-09
AL008727.1	0.641371689	0.000000005
SYK	0.641038951	5.11E-09
ZNF605	0.640931625	5.15E-09

OR7C1	0.640914508	5.16E-09
RNU6-33P	0.640735806	5.22E-09
AC008121.1	0.640541012	5.30E-09
AC005277.2	0.640401217	5.35E-09
CD84	0.640279333	5.40E-09
ZNF234	0.640012085	5.50E-09
AC097637.2	0.639705956	5.63E-09
AC112777.1	0.639501285	5.71E-09
AL023284.4	0.639381182	5.76E-09
PRKD1	0.639288331	5.80E-09
AL031731.1	0.639012993	5.91E-09
AC099518.2	0.638937407	5.94E-09
ARID3B	0.63879606	0.000000006
AC018638.6	0.638637488	6.07E-09
DIO2	0.638259244	6.24E-09
MEMO1	0.638104317	6.31E-09
C21orf62	0.6377825	6.46E-09
CDH12P2	0.637701147	6.49E-09
MT1JP	0.637660577	6.51E-09
KRT19	0.637586787	6.55E-09
APLN	0.637214709	6.72E-09
TRIM5	0.637193805	6.73E-09
CXCR2	0.637193536	6.73E-09
HIST1H2BD	0.637191448	6.73E-09
GOLPH3	0.63702527	6.81E-09
TMEM63A	0.636965072	6.84E-09
FRAT2	0.636261927	7.19E-09
FOXO6	0.636225146	7.21E-09
LINC00484	0.63611707	7.27E-09
HES6	0.63552447	7.58E-09
AC015910.1	0.635052706	7.84E-09
NHSL1	0.634876942	7.93E-09
RF02271	0.634809902	0.000000008
PNRC1	0.634703026	0.000000008
ID4	0.634538307	8.13E-09
AP000462.3	0.634370929	8.22E-09
KCNJ16	0.634182739	8.33E-09
ACSS1	0.63401504	8.43E-09
AL391069.3	0.633814123	8.55E-09
MDGA1	0.633733632	8.60E-09

GTF2IRD2B	0.633538552	8.72E-09
AC025682.1	0.633527361	8.73E-09
NFE2	0.633405705	8.80E-09
AC091057.1	0.633223475	8.91E-09
DSE	0.633148881	0.000000009
C22orf34	0.6324161	9.43E-09
RHOQP2	0.632206629	9.57E-09
HAGHL	0.631963842	9.74E-09
RNU6-1085P	0.631899417	9.78E-09
TREX1	0.631509902	0.00000001
LPIN3	0.631055062	1.04E-08
AC068254.2	0.631000127	1.04E-08
AC024610.1	0.630886103	1.05E-08
IP6K3	0.630879747	1.05E-08
SLC4A11	0.630848662	1.05E-08
LRR1	0.630830746	1.05E-08
MIR648	0.630704936	1.06E-08
TMUB1	0.630625768	1.07E-08
ARHGEF5	0.630348612	1.09E-08
AC009102.3	0.630304452	1.09E-08
GLI3	0.630179507	0.000000011
OR7E26P	0.629764268	1.13E-08
AC106800.2	0.629351073	1.17E-08
AC018647.1	0.629122111	1.19E-08
AGPAT4-IT1	0.628745803	1.22E-08
PIEZO2	0.628673456	1.22E-08
AC002044.3	0.628481545	1.24E-08
RPS27P15	0.628303478	1.26E-08
ZNF467	0.628056015	1.28E-08
AC004918.1	0.628043195	1.28E-08
SLC7A7	0.627669586	1.31E-08
MT2A	0.627614606	1.32E-08
SLC8A1-AS1	0.62751194	1.33E-08
KRT18P5	0.627429774	1.33E-08
GRAMD1C	0.627219006	1.35E-08
MTATP6P27	0.627088369	1.36E-08
FOXF1	0.627085009	1.37E-08
MBD3	0.627039423	1.37E-08
GJA1	0.627023787	1.37E-08
ZNF580	0.626839532	1.39E-08

PARVG	0.626760331	0.000000014
AC073254.1	0.626386087	1.43E-08
BPTFP1	0.626163154	1.45E-08
MIR663AHG	0.625851178	1.49E-08
CLCA4	0.625747096	0.000000015
WFS1	0.625491302	1.52E-08
AC007191.1	0.625405496	1.53E-08
CLEC18A	0.625226874	1.55E-08
AC119674.2	0.6247757	0.000000016
AC112504.1	0.624333317	1.65E-08
AL138781.2	0.624328099	1.65E-08
FLCN	0.623788702	1.71E-08
RHOQP1	0.623677426	1.72E-08
NPIPA7	0.623512533	1.74E-08
CPT1B	0.623460789	1.75E-08
FZD8	0.623414291	1.75E-08
TSPAN11	0.623085049	1.79E-08
RN7SKP80	0.623051985	0.000000018
AC136628.3	0.622799309	1.83E-08
PSD2	0.622613823	1.85E-08
AL592148.3	0.622601744	1.85E-08
MT1P3	0.622596961	1.85E-08
AC063926.3	0.622439938	1.87E-08
TF	0.622376087	1.88E-08
GPT	0.622307339	1.89E-08
KCNQ1	0.62199015	1.93E-08
NT5CP1	0.621976163	1.93E-08
IKZF2	0.62192509	1.94E-08
SGCZ	0.621781674	1.96E-08
RNA5SP255	0.621463929	0.00000002
ERCC8	0.621101265	2.05E-08
AL354836.1	0.621054626	2.06E-08
LIPE	0.621028016	2.06E-08
MIR4534	0.620761272	0.000000021
AC105285.1	0.620702618	2.11E-08
AC006538.3	0.620431003	2.14E-08
AC018653.4	0.620362856	2.15E-08
ADA	0.620219871	2.17E-08
ZNF488	0.620207892	2.18E-08
CREBL2	0.619968455	2.21E-08

HNRNPA3P2	0.619875061	2.23E-08
AC098679.2	0.619575462	2.27E-08
AC007639.1	0.619000983	2.36E-08
ABO	0.618023899	2.52E-08
AC007598.3	0.61800135	2.52E-08
AC100832.1	0.617734377	2.57E-08
TMEM45B	0.61737967	2.63E-08
PRRG4	0.617210596	2.66E-08
AC012511.1	0.617179339	2.66E-08
TCAP	0.617031424	2.69E-08
LDHAL6A	0.617010009	2.69E-08
METTL4	0.617007621	2.69E-08
AL031651.2	0.616710706	2.75E-08
LINC00299	0.616553349	2.78E-08
TJP3	0.615918245	2.89E-08
AL137784.2	0.61575416	2.93E-08
RF00017	0.615635971	2.95E-08
NUP210L	0.615566308	2.96E-08
RASL12	0.615220359	3.03E-08
AC010435.1	0.615167516	3.04E-08
SETD1A	0.615117807	3.05E-08
LRP2	0.615041669	3.07E-08
AC069528.2	0.614909893	3.09E-08
NCAPD2	0.61480912	3.11E-08
AC092332.1	0.61455183	3.17E-08
GAS2L3	0.614396674	0.000000032
AL133367.1	0.614221043	3.24E-08
NAGLU	0.614026758	3.28E-08
AC140134.2	0.613967793	3.29E-08
RPL23AP12	0.613936025	0.000000033
SLC6A16	0.613650291	3.36E-08
IRAK2	0.613489948	0.000000034
AC110749.1	0.613413712	3.41E-08
AC107294.3	0.613215097	3.46E-08
FBXO2	0.613207764	3.46E-08
AL137784.1	0.612922916	3.52E-08
AL133520.1	0.61289836	3.53E-08
C17orf67	0.612816051	3.55E-08
COL8A2	0.612766594	3.56E-08
HARBI1	0.612396303	3.65E-08

GALNT6	0.612325938	3.66E-08
LINC01301	0.61227986	3.68E-08
MYBL1	0.61217626	0.000000037
DVL1	0.612031508	3.74E-08
ATP6V0E1P1	0.611830332	3.78E-08
AC009690.2	0.611337566	3.91E-08
AL035456.1	0.61129791	3.92E-08
S1PR1	0.611239658	3.93E-08
AF279873.4	0.611216544	3.94E-08
BNC2	0.610884611	4.02E-08
RN7SL378P	0.610197344	4.21E-08
PHF8	0.610066808	4.24E-08
FABP7	0.609944159	4.28E-08
RRN3P3	0.609856568	0.000000043
AC009078.3	0.609769226	4.33E-08
SLC39A12	0.609574939	4.38E-08
FZD7	0.609475666	4.41E-08
HPN	0.609457087	4.41E-08
AC127024.5	0.609360135	4.44E-08
TMEM80	0.608950033	4.56E-08
FAM131C	0.608452193	4.71E-08
DPF3	0.607968281	4.86E-08
AC093495.1	0.607903893	4.88E-08
AC007216.3	0.607810303	4.91E-08
TMCC2	0.607482311	5.01E-08
AC090602.1	0.607260327	5.08E-08
TNPO1P1	0.607055939	5.15E-08
FOXJ1	0.606868361	5.21E-08
CXCR4	0.606809177	5.23E-08
WASH3P	0.60669362	5.27E-08
AL354696.2	0.606379358	5.38E-08
AC138207.3	0.606202274	5.44E-08
UBTFL6	0.605473486	0.000000057
PURG	0.605342568	5.75E-08
AC026474.1	0.605168075	5.81E-08
AC005293.1	0.605142952	5.82E-08
COL11A1	0.604654394	0.00000006
SYNC	0.604303966	6.14E-08
DHRSX-IT1	0.604240815	6.16E-08
RF00017	0.604221247	6.17E-08

RN7SKP96	0.604204499	6.18E-08
AC104389.4	0.603885086	0.000000063
SAMD9	0.603819876	6.33E-08
RGMA	0.603701896	6.38E-08
AL671277.2	0.603245353	6.56E-08
KIAA1755	0.603057774	6.64E-08
AC091180.2	0.603015647	6.66E-08
AC083843.3	0.602684034	0.000000068
DLGAP1-AS5	0.602683242	0.000000068
GJC2	0.602583372	6.84E-08
ERVFRD-1	0.602570471	6.85E-08
RHOQP3	0.602200135	7.01E-08
NME6	0.601598513	7.28E-08
AC080128.1	0.601334649	0.000000074
RGS19	0.6007821	7.66E-08
AC010619.2	0.600580712	7.76E-08
AC124045.1	0.600405379	7.85E-08
AL391422.4	0.600213029	7.94E-08
FMO5	0.600172679	7.96E-08
REV3L-IT1	0.600125153	7.98E-08
RNU1-2	0.599202743	8.46E-08
RF00017	0.59862844	8.77E-08
SRGAP3-AS3	0.598099049	9.06E-08
TBC1D8B	0.59803493	9.09E-08
ACP5	0.597976528	9.13E-08
BCL2L11	0.597953694	9.14E-08
VENTX	0.597136307	9.62E-08
AC011479.3	0.597127831	9.62E-08
C21orf62-AS1	0.596781645	9.83E-08
IL15RA	0.595770861	1.05E-07
DLEU1	0.59573358	1.05E-07
CCDC36	0.595711556	0.000000105
C10orf90	0.595603906	1.06E-07
SIRT7	0.594965465	1.10E-07
MTRNR2L6	0.594751837	1.11E-07
ARL17B	0.594488284	1.13E-07
AC016397.2	0.594422765	1.14E-07
AC011933.2	0.594228743	0.000000115
FP325331.1	0.593807697	0.000000118
AL583810.2	0.593496295	1.20E-07

HSPA2	0.593216644	1.22E-07
AC016831.4	0.593046786	1.24E-07
GLULP4	0.592736302	0.000000126
IFIH1	0.59270739	1.26E-07
PCGF2	0.592034309	1.31E-07
AC006011.2	0.591746129	1.34E-07
-	0.591469395	1.36E-07
AL359915.2	0.591093793	1.39E-07
HP	0.591084684	1.39E-07
KIAA0930	0.591018041	1.40E-07
AL365203.2	0.590918531	1.41E-07
MFAP4	0.590269482	1.46E-07
TMEM220-AS1	0.58977728	1.51E-07
WWC2	0.589761015	1.51E-07
AC099684.2	0.589510831	1.53E-07
RF00019	0.588863704	1.59E-07
PIK3R5	0.588685458	0.000000161
AC011632.1	0.588440004	1.63E-07
ZNF225	0.58819792	1.66E-07
P2RY2	0.588145037	1.66E-07
RPS15P5	0.587836031	1.69E-07
AC005702.2	0.58758517	0.000000172
AC006077.2	0.587377327	1.74E-07
AC011239.2	0.587298587	0.000000175
GTF2H2C	0.586354293	1.85E-07
TRDN	0.58590108	1.90E-07
RNU6-1138P	0.585852618	1.91E-07
AC127035.1	0.585845061	1.91E-07
AC010157.2	0.585152599	1.99E-07
RN7SL622P	0.585144535	0.000000199
NANOS1	0.584875153	2.02E-07
DNAH17	0.584643332	0.000000205
GPC4	0.583901976	2.14E-07
AC012404.1	0.58280808	2.28E-07
POT1-AS1	0.582598995	2.31E-07
TMEM150B	0.582595109	2.31E-07
SLC43A1	0.582144924	2.38E-07
AATK	0.582073656	2.39E-07
LINC02204	0.582000962	2.40E-07
NPIPB10P	0.581542196	2.46E-07

SNRK-AS1	0.581237764	2.51E-07
PLEC	0.581012615	2.54E-07
KCTD14	0.579920083	2.71E-07
RF01225	0.579277743	0.000000281
AL139246.5	0.579046937	2.85E-07
ZDHHC8P1	0.579007332	2.85E-07
RF00026	0.578886782	2.87E-07
AL353708.3	0.578723526	2.90E-07
AC092119.1	0.57823315	2.99E-07
DNAH11	0.578148286	0.0000003
TLR7	0.577910654	3.04E-07
AL158071.4	0.577753872	0.000000307
HPN-AS1	0.577585919	0.00000031
PSPN	0.577461629	3.12E-07
C7orf61	0.577308473	0.000000315
AC046158.4	0.5772395	3.16E-07
RASA4	0.576969145	3.21E-07
AC068768.1	0.576860146	3.23E-07
SASH3	0.576793623	3.25E-07
MTG1	0.576437228	3.31E-07
KIF19	0.576311352	3.34E-07
PLEKHA7	0.575379177	3.52E-07
RN7SL693P	0.575104697	3.58E-07
AL031775.2	0.574978402	3.60E-07
ASNSP6	0.574952356	3.61E-07
CD34	0.574649774	3.67E-07
ARHGEF35	0.574287777	3.75E-07
NUTM2F	0.574237627	3.76E-07
LINC02123	0.574133565	3.78E-07
TAF6L	0.574032922	3.80E-07
AC007423.1	0.573850448	3.84E-07
ICAM3	0.573825203	3.85E-07
MUC1	0.573762639	3.86E-07
ARSE	0.573539379	3.91E-07
FOXM1	0.573398338	3.94E-07
AC013391.3	0.57294783	4.05E-07
NAPSA	0.572861118	4.07E-07
AC087392.1	0.572559448	4.14E-07
LINC02199	0.571824131	4.31E-07
SCGB1B2P	0.571506272	4.39E-07

AL138688.2	0.571164909	4.48E-07
AC091133.5	0.570936972	4.54E-07
RN7SL382P	0.57059393	4.63E-07
SELPLG	0.57045241	4.66E-07
AC007881.1	0.570347032	4.69E-07
AC020741.1	0.570028635	4.78E-07
PLD5	0.569901878	4.81E-07
OR7A5	0.56945872	4.93E-07
TAP1	0.568857698	5.10E-07
TRG-AS1	0.568635817	5.17E-07
SIX2	0.567394738	5.54E-07
RN7SL377P	0.566969605	5.67E-07
LINC00499	0.566023873	0.000000598
RN7SL199P	0.566020471	5.98E-07
CCDC88B	0.565124947	6.29E-07
SPACA6P-AS	0.564901502	6.37E-07
EVC2	0.564219496	6.61E-07
TMPRSS5	0.563894922	6.73E-07
AC110285.6	0.563894697	6.73E-07
RADIL	0.563093499	7.04E-07
AC121247.2	0.5628737	7.12E-07
SLC5A3	0.562793491	7.15E-07
TNFAIP8	0.562189028	7.40E-07
ZGLP1	0.56184971	7.54E-07
ZMYND10	0.56116652	7.82E-07
KLKB1	0.560353958	0.000000818
AC112184.1	0.560229725	8.24E-07
CD180	0.560004804	8.34E-07
AC025175.1	0.559536252	8.55E-07
S100A4	0.559252731	8.69E-07
AC012184.3	0.559210771	8.71E-07
CFD	0.559178942	8.72E-07
FAM167B	0.558301782	9.15E-07
RLIMP1	0.558252214	9.17E-07
RN7SKP180	0.557906465	9.35E-07
CBX2	0.557709851	9.45E-07
AL360182.1	0.557691416	9.46E-07
LINC01485	0.557522405	9.54E-07
AL031846.2	0.55739274	9.61E-07
AC104574.2	0.556879876	9.88E-07

CCDC151	0.55653453	1.01E-06
AC007601.1	0.556427729	1.01E-06
JUND	0.556291086	1.02E-06
AC012158.1	0.556248369	1.02E-06
-	0.555793126	0.000001048
NEAT1	0.555730096	1.05E-06
ABCA8	0.55499907	1.09E-06
SLC25A30-AS1	0.554484388	1.12E-06
AC036108.3	0.554412349	1.13E-06
FLJ42393	0.553914406	1.16E-06
SGO1	0.553841791	1.16E-06
AC087072.2	0.553733796	1.17E-06
MIR5690	0.553106677	1.21E-06
SMARCE1P6	0.552955892	1.22E-06
AP001029.3	0.552771745	1.23E-06
AL121908.1	0.552026253	1.28E-06
RGS5	0.551755443	1.30E-06
SIGLEC8	0.551647702	1.31E-06
AC010997.3	0.551567672	1.31E-06
MTCO1P27	0.55135582	1.33E-06
AC010424.1	0.551129707	1.35E-06
MYO1D	0.549170349	1.49E-06
STARD10	0.548692222	1.53E-06
AC008066.1	0.548471666	1.55E-06
AC104662.1	0.548416691	1.55E-06
GEM	0.548037918	1.58E-06
GLI4	0.547640579	1.62E-06
AC003080.1	0.547629818	1.62E-06
AL583805.2	0.547509213	1.63E-06
MT1L	0.54692978	1.68E-06
TRIM22	0.546586842	1.71E-06
LRRC63	0.545533658	1.81E-06
STXBP4	0.544944248	1.86E-06
RPS10P7	0.54443409	1.91E-06
RPL3P6	0.543978207	0.000001958
CXorf67	0.543576486	2.00E-06
SERHL2	0.543513446	2.01E-06
AC008115.4	0.542532383	2.11E-06
RSBN1	0.542511585	2.11E-06
AC017007.3	0.542458065	2.12E-06

RASAL3	0.542197626	0.000002147
MIR657	0.542101511	2.16E-06
HIST1H2BJ	0.541624831	2.21E-06
RINL	0.541107079	2.27E-06
AC007950.2	0.541071735	2.28E-06
AF279873.3	0.540809278	2.31E-06
GIPR	0.540043601	2.40E-06
AC012173.1	0.539903264	2.42E-06
POLR2J4	0.539771373	2.43E-06
PABPC1P1	0.539416128	2.48E-06
MT1M	0.538664735	2.57E-06
AC146944.4	0.537915212	2.67E-06
AC020910.6	0.537774374	2.69E-06
MT1F	0.537649954	2.71E-06
SCX	0.537544536	2.72E-06
CATIP	0.537359791	2.75E-06
AC005041.3	0.537139215	2.78E-06
WFDC1	0.536763332	2.84E-06
GPR82	0.536713647	2.84E-06
AC080128.2	0.536705753	2.84E-06
PNPLA6	0.536605477	2.86E-06
MCF2L2	0.536481322	2.88E-06
SSC5D	0.536377632	0.000002891
ZNF579	0.535806367	2.98E-06
RF00432	0.535287341	3.05E-06
GAPDHP45	0.535062347	3.09E-06
HPR	0.534822395	3.13E-06
AC011510.1	0.534708031	3.15E-06
SH2D7	0.532993628	3.43E-06
STX8P1	0.532959188	3.43E-06
AL355073.2	0.531740538	0.00000365
PYY2	0.531490821	3.70E-06
BIK	0.53138849	3.71E-06
AL157712.2	0.531107432	0.000003767
AC137723.1	0.531011547	0.000003785
RNASE6	0.530664002	3.85E-06
C1QL2	0.530438815	3.89E-06
AL353732.1	0.530095634	3.96E-06
AC016831.2	0.529668454	4.05E-06
C15orf62	0.528498722	4.29E-06

DNHD1	0.528296614	4.33E-06
COX10-AS1	0.528133748	4.37E-06
MYH3	0.527420249	4.52E-06
SLC22A14	0.526996957	4.62E-06
ABCC6	0.526992017	4.62E-06
HAGLR	0.526881263	4.64E-06
GPIHBP1	0.526685652	4.69E-06
AC097724.1	0.526353646	4.76E-06
BNIPL	0.52604431	4.84E-06
CTRB1	0.525757917	4.91E-06
AL513497.1	0.525276402	5.02E-06
RNU6-2	0.524715956	5.16E-06
MIR8485	0.524643235	5.18E-06
NAGS	0.52441165	5.24E-06
AC099513.1	0.524219995	5.29E-06
WDR45P1	0.523992389	5.35E-06
GAPT	0.523718556	5.42E-06
TOP3BP1	0.523559947	5.46E-06
AC139834.1	0.523152981	5.57E-06
AC009090.4	0.523054887	5.60E-06
AC135803.1	0.522601188	5.72E-06
ADCYAP1R1	0.522220064	5.83E-06
ABCA6	0.522034541	5.88E-06
AC010463.3	0.521801642	5.95E-06
SOWAHD	0.521303792	6.09E-06
AC131934.1	0.521067371	6.16E-06
SLC25A25-AS1	0.521031065	6.17E-06
AC008737.3	0.520248559	6.41E-06
SPR	0.520145986	6.44E-06
AC105150.1	0.519885425	6.52E-06
AC090686.1	0.519237949	6.73E-06
AL049840.3	0.518001806	7.14E-06
HELZ2	0.517221875	7.41E-06
PNPT1P1	0.517178104	7.42E-06
FZD10-DT	0.517175202	7.43E-06
TNFRSF10C	0.516857876	7.54E-06
LINC02080	0.516315314	7.74E-06
AR	0.516306172	7.74E-06
P3H2	0.516264539	7.75E-06
FAM43B	0.516141651	7.80E-06

ADRA2B	0.515756296	7.94E-06
BTNL8	0.515277258	8.13E-06
AC090589.1	0.515181699	0.000008163
RPL30P14	0.515112226	8.19E-06
HIST1H2AD	0.513434774	8.86E-06
SLCO4A1-AS1	0.51296137	9.06E-06
LMF1-AS1	0.512120086	9.43E-06
LINC02188	0.511762625	9.59E-06
TRIM8	0.510329077	1.03E-05
TEKT2	0.509458419	1.07E-05
IL15	0.508806703	1.10E-05
AC026398.1	0.508381228	1.12E-05
AL031600.2	0.507818728	1.15E-05
AC092718.4	0.507796271	0.000011533
RPS3P7	0.507762485	1.16E-05
MTND3P10	0.506027212	1.25E-05
BX284668.6	0.505594904	1.28E-05
CTAGE4	0.505377652	1.29E-05
AC073508.2	0.505135838	1.30E-05
AL022097.1	0.504102087	1.37E-05
ZAP70	0.504009605	1.37E-05
SHANK2-AS1	0.503598762	1.40E-05
LCN6	0.503429442	1.41E-05
AC126755.2	0.502861219	1.45E-05
TSHR	0.502845175	1.45E-05
LINC00689	0.502088954	1.50E-05
AC010997.4	0.501775476	1.52E-05
VNN 1.00	0.500105029	1.64E-05

KEGG Pathway

Term	**P-Value**	**Benjamini**
Pathways in cancer	2.20E-06	5.40E-04
Ras signaling pathway	4.10E-06	5.40E-04
Chronic myeloid leukemia	8.20E-06	7.30E-04
Focal adhesion	1.50E-05	1.00E-03
Notch signaling pathway	1.70E-04	8.80E-03
Hippo signaling pathway	2.30E-04	1.00E-02
Proteoglycans in cancer	5.20E-04	2.00E-02
Sphingolipid signaling pathway	6.10E-04	2.00E-02

B cell receptor signaling pathway	7.30E-04	2.10E-02
Renal cell carcinoma	1.40E-03	3.60E-02
Neurotrophin signaling pathway	1.50E-03	3.60E-02
Thyroid hormone signaling pathway	2.10E-03	4.60E-02
Prostate cancer	3.60E-03	7.10E-02
PI3K-Akt signaling pathway	3.80E-03	7.10E-02
MAPK signaling pathway	4.00E-03	7.10E-02
Rap1 signaling pathway	4.70E-03	7.70E-02
T cell receptor signaling pathway	5.50E-03	8.60E-02

GO Biological Process

Term	**P-Value**	**Benjamini**
negative regulation of transcription from RNA polymerase II promoter	2.30E-16	1.00E-12
positive regulation of transcription, DNA-templated	3.50E-10	5.40E-07
transcription, DNA-templated	3.60E-10	5.40E-07
positive regulation of transcription from RNA polymerase II promoter	1.30E-09	1.40E-06
in utero embryonic development	6.10E-08	5.50E-05
regulation of transcription, DNA-templated	1.10E-06	7.90E-04
angiogenesis	7.00E-06	4.50E-03
negative regulation of transcription, DNA-templated	1.90E-05	1.10E-02
transcription from RNA polymerase II promoter	2.60E-05	1.30E-02
negative regulation of cell proliferation	4.70E-05	2.10E-02
Rho protein signal transduction	5.80E-05	2.40E-02
positive regulation of gene expression	6.70E-05	2.50E-02
negative regulation of gene expression	1.00E-04	3.60E-02
positive regulation of GTPase activity	1.10E-04	3.60E-02
regulation of actin cytoskeleton organization	1.20E-04	3.70E-02
face morphogenesis	1.30E-04	3.80E-02
cellular response to peptide hormone stimulus	1.50E-04	4.00E-02
regulation of transcription from RNA polymerase II promoter	1.60E-04	4.10E-02
positive regulation of neural precursor cell proliferation	2.00E-04	4.80E-02
signal transduction	2.70E-04	6.10E-02
Notch signaling pathway	3.10E-04	6.30E-02
positive regulation of epithelial to mesenchymal transition	3.30E-04	6.30E-02
cell differentiation	3.30E-04	6.30E-02
endocytosis	3.30E-04	6.30E-02
cellular response to vascular endothelial growth factor stimulus	4.60E-04	8.00E-02

regulation of Rho protein signal transduction	4.70E-04	8.00E-02
cytoskeleton-dependent intracellular transport	4.80E-04	8.00E-02
inner ear development	5.40E-04	8.60E-02
positive regulation of sequence-specific DNA binding transcription factor activity	6.00E-04	9.20E-02
sphingolipid biosynthetic process	6.10E-04	9.20E-02